CELLULAR PATHOMECHANISMS IN HEREDITARY SENSORY NEUROPATHY TYPE 1

Emma Rachel Wilson

UCL Institute of Neurology

&

MRC Centre for Neuromuscular Diseases

PhD Supervisors:

Professor Linda Greensmith, Professor Mary M. Reilly,

Dr Bernadett Kalmar

A Thesis submitted for the degree of Doctor of Philosophy

University College London

2017

Declaration

I, Emma R. Wilson confirm that the work presented in this Thesis is my own. Where information has been derived from other sources, I confirm that this has been indicated in the Thesis.

Abstract

Hereditary sensory neuropathy type 1 (HSN-1) is a peripheral neuropathy most frequently caused by missense mutations in the *SPTLC1* or *SPTLC2* genes, which code for two subunits of the enzyme serine palmitoyltransferase (SPT). SPT catalyzes the first and rate-limiting step of *de novo* sphingolipid synthesis. Mutations in SPT result in a change in enzyme substrate specificity, which generates two atypical products, deoxysphinganine and deoxymethylsphinganine, rather than the normal enzyme product, sphinganine. Levels of these abnormal compounds are elevated in the blood of HSN-1 patients and this is thought to cause the peripheral sensory and motor nerve damage characteristic of the disease. However, the mechanisms underlying nerve damage are largely unresolved and there remain no effective treatments. In this study, the cellular pathomechanisms that underlie the peripheral nerve damage in HSN-1 were examined using three *in vitro* models of disease.

Firstly, primary motor and sensory neurons from wildtype mice were treated with either the typical enzyme product, sphinganine, or the atypical enzyme products, deoxysphinganine and deoxymethylsphinganine. The abnormal enzyme products were found to have dose- and time- dependent neurotoxic effects in both motor and sensory neurons. In addition, functional analyses revealed that the deleterious effects of the abnormal enzyme products may be mediated, at least in part, by abnormal calcium handling and mitochondrial dysfunction. In order to further explore the disease pathomechanisms and confirm whether these deficits were also present in models that more closely resemble the genetic aspect of this disease, two additional *in vitro* models were examined. In the first of these models, a lentiviral vector was generated in order to deliver wildtype and mutant *SPTLC1* to primary motor and sensory neurons, and in the second, control and HSN-1 patient fibroblasts were obtained and examined.

The results of this Thesis suggest that alterations in mitochondrial function and cellular calcium handling may contribute to the pathomechanism of HSN-1, and may therefore represent a potential target for therapeutic development.

Acknowledgements

After such an incredible 4 years at Queen Square, it is nigh on impossible to summarise my thanks on this one page.

I am so lucky to have been supported by three fantastic supervisors: Linda, Mary and Bernadett, and I cannot thank each of them enough for their mentorship, guidance and enthusiasm for this project. Thanks also to Andrey Abramov for providing such helpful comments throughout the calcium imaging experiments.

The incredible community that is the 5th floor of the UCL Institute of Neurology, including the Greensmith, Schiavo and Fratta labs, have made every day of my PhD a joy. There are too many names to mention, but I am so grateful for the fruitful scientific discussions, the epic debates, the laughs, the pub trips, the cake and the multiple WhatsApp groups! I am especially grateful to Charlotte, my PhD buddy from day one, and Jim, whose support has been, as ever, indispensable; thank you so much for not retiring before I finished my PhD! Harriet Howard is a fantastic BSc student who also worked with me on elements of this project.

I am thankful to everyone at the MRC Centre for Neuromuscular Diseases and its support team, especially Jacky and Chris.

Thanks to my wonderful friends, who have kept me sane throughout and to Mum, Dad and Robert, who I know couldn't care less whether any letters come before or after my name, but I thank for their solidarity and unyielding support.

Finally, thanks Miss P, who as a newly qualified teacher made a 16-year-old me fall in love with biology.

I dedicate this Thesis in memory of my dear friend Modupe.

Table of Contents

List of Figures

List of Tables

List of Abbreviations

$\Delta\psi_m$	mitochondrial membrane potential
2-APB	2-aminoethoxydiphenyl borate
3-KSR	3-keto-sphinganine reductase
AAV	adeno-associated viruses
ALS	amyotrophic lateral sclerosis
AM	acetoxymethyl
AmpR	ampicillin resistance
ANOVA	analysis of variants
ATF6	activating transcription factor 6
ATP	adenosine triphosphate
BAPTA	1,2-bis(2-aminophenoxy)ethane-N,N,N′,N′-tetraacetic acid
BDNF	brain-derived neurotrophic factor
BiP	binding immunoglobulin protein
BSA	bovine serum albumin
CerS	ceramide synthase
CHO	Chinese hamster ovary
CHOP	C/EBP homologous protein
CIPN	chemotherapy-induced peripheral neuropathy
CMT	Charcot Marie Tooth
CMTNS	Charcot Marie Tooth neuropathy score
CMV	cytomegalovirus
CNS	central nervous system
CNTF	ciliary neurotrophic factor
CsA	cyclosporine A
CSF	cerebrospinal fluid
Ctip2	COUP-TF interacting protein 2
CYP4F	cytochrome P450 4F
DAPI	4',6-diamidino-2-phenylindole
DES	ceramide desaturase
DIV	days *in vitro*
DMSp	deoxymethylsphinganine
DNA	deoxyribonucleic acid
DRG	dorsal root ganglion

DSp	deoxysphinganine
EDTA	ethylenediaminetetraacetic acid
EF-1α	elongation factor 1α
EGTA	ethylene glycol-bis(β-aminoethyl ether)-N,N,N',N'-tetraacetic acid
ER	endoplasmic reticulum
ERM	ezrin-radixin-moesin
ERO1-Lα	endoplasmic oxidoreductin-1-like protein
$FADH_2$	flavin adenine dinucleotide
FCCP	carbonyl cyanide-p-trifluoromethoxyphenylhydrazone
GADD153	growth arrest and DNA damage-inducible protein
GDNF	glial cell line-derived neurotrophic factor
GFP	green fluorescent protein
GRP-78	78 kDa glucose-regulated protein
HBSS	Hanks' Balanced Salt Solution
HEK	human embryonic kidney
HIV	human immunodeficiency viruses
HMN	hereditary motor neuropathy
HRP	horseradish peroxidase
HSAN	hereditary sensory and autonomic neuropathy
HSN	hereditary sensory neuropathy
IP_3	inositol triphosphate
IRE1	inositol-requiring enzyme 1
LC-MS	liquid chromatography-mass spectrometry
LDL	low density lipoproteins
LSM	laser scanning microscope
MAM	mitochondria-associated ER membrane
MAPK	mitogen-activated protein kinases
MCV	motor nerve conduction velocity
MEF	mouse embryonic fibroblasts
MN	motor neuron
mPTP	mitochondrial permeability transition pore
NADH	nicotinamide adenine dinucleotide
NCV	nerve conduction velocity

NCX	sodium-Ca^{2+} exchanger
NMDA	N-methyl-D-aspartate
ns	not significant
ORMDL	orosomucoid-like
PBS	phosphate-buffered saline
PBST	PBS containing 0.1% Triton X-100
PDI	protein disulphide isomerase
PERK	protein kinase R (PKR)-like endoplasmic reticulum kinase
PHGDH	D-3-phosphoglycerate dehydrogenase
PLP	pyridoxal 5'-phosphate
PMCA	plasma membrane Ca^{2+}-ATPase
PNS	peripheral nervous system
PSD-95	post-synaptic density protein 95
RIPA	radioimmunoprecipitation assay
RNA	ribonucleic acid
RPM	revolutions per minute
SDS-PAGE	sodium dodecyl sulphate polyacrylamide gel electrophoresis
SEM	standard error of the mean
SERCA	sarco/endoplasmic reticulum Ca^{2+}-ATPase
SO	sphingosine
SO-kinase	sphingosine-kinase
SO1P-lyase	sphingosine-1-phosphate lyase
SOC	store-operated calcium
Sp	sphinganine
SPT	serine palmitoyltransferase
SPTLC1/2/3	serine palmitoyltransferase long chain base subunit 1/2/3
STIM	stromal interaction molecule 1
STZ `	streptozotocin
TBS	tris-buffered saline
TEMED	N,N,N′,N′-tetramethylethylenediamine
TMRM	tetramethylrhodamine methyl ester
UPR	unfolded protein response
UQCRC1	ubiquinol-cytochrome C reductase core protein 1

VLDL	very low density lipoproteins

Chapter 1. General Introduction

1.1 Inherited peripheral neuropathies

The peripheral nervous system (PNS) is composed of motor, sensory and autonomic branches and plays a critical role in the exchange of information between the central nervous system (CNS) and the limbs and organs. Inherited neuropathies are a group of rare, heterogeneic disorders, both genetically and clinically, which result in the degeneration of the peripheral nerves. These neuropathies are categorised into three main groups: hereditary motor neuropathy (HMN), hereditary sensory neuropathy (HSN) and hereditary motor and sensory neuropathy, which is more commonly known as Charcot Marie Tooth (CMT) disease (Rotthier et al., 2012). Broadly, this classification is based on clinical presentation, which can be of i) motor dysfunction, ii) mainly sensory dysfunction or iii) a combination of both motor and sensory dysfunction. However, the vast phenotypical diversity within these classifications has led to inherited neuropathy to be considered as a spectrum of disease ranging from pure motor, to predominant sensory, and with many variations in between (Rossor et al., 2013).

CMT is the most common form of inherited neuropathy, and indeed, is also the most common inherited neuromuscular disease, effecting upwards of 1 individual in every 2500 (Reilly et al., 2011; Stojkovic, 2016). First described in 1886 by the three neurologists after whom it is named, CMT is characterised by muscle wasting in the distal limbs, which spreads in the proximal direction with disease progression, alongside length dependent sensory loss (Charcot and Marie, 1886; Tooth, 1886; Rossor et al., 2013). Reduced or lost tendon reflexes also occur. Distal muscle weakness in classical CMT patients contributes to very characteristic *pes cavus,* with clawed toes, as shown in Figure 1.1 (Reilly et al., 2011).

CMT is broadly subdivided into two, the demyelinating form which is classified as CMT1 and the axonal form, CMT2. This distinction is largely made in the clinic, by measuring the median upper limb motor nerve conduction velocity

Figure 1.1

FIGURE REMOVED FOR COPYRIGHT REASONS

Figure 1.1: Distal wasting, *pes cavus* and clawed toes in a classical CMT disease patient

The lower legs (A) and feet (B) of a classical CMT1A patient, showing the very typical patterns of distal wasting, *pes cavus* and clawed toes.

Used with permission from Reilly, M. M., Murphy, S. M. & Laura, M. 2011. Charcot-Marie-Tooth Disease. *Journal of the Peripheral Nervous System*, 16, 1-14.

(MCV); thus an MCV < 38 m/s signifies CMT1, > 38 m/s is CMT2, and 25-45 m/s is classified as a third, intermediary form (CMT I, Reilly, 2007).

In contrast to the sensory and motor deficits observed in CMT, HMN involves purely motor dysfunction. These patients essentially present as CMT patients do, but without any sensory involvement (Reilly, 2007).

HSN is so named due to its predominant sensory involvement, but it should be noted that these disorders can also affect the motor and autonomic nervous systems, to varying extents. HSN is broadly divided into two groups according to mode of inheritance- the autosomal dominant inherited form (HSN-1) and the autosomal recessive inherited form (HSN-2). These classifications, however, are not absolute, and further sub-classifications on the basis of the age of onset, causative genes and symptom variability also exist in the forms of HSN-3 to 7, as well as hereditary sensory and autonomic neuropathy (HSAN) with spastic paraplegia and HSAN with diarrhoea (Auer-Grumbach, 2013; Mroczek et al., 2015).

With advances in genetic testing, the number of identified CMT genes has jumped from 30 in 2011 (Reilly et al., 2011) to more than 80 genes which are now known to be causative for the inherited neuropathies (Stojkovic, 2016). These genes implicate a wide variety of cellular pathomechanisms including, but not limited to, mitochondrial dysfunction, channel dysfunction, protein dyshomeostasis, cytoskeletal defects and axonal transport deficits (see Figure 1.2, Rossor et al., 2013). Moreover, not only can the same phenotype be caused by mutations in different genes, but the same mutation in the same gene can also cause different phenotypes (Reilly, 2007). Despite the great leaps made in the genetic toolbox, many of the underlying causative genes of the inherited neuropathies remain unidentified (Rossor et al., 2013).

1.2 Hereditary Sensory Neuropathy type 1 (HSN-1)

The most common form of HSN is the autosomal, dominant HSN-1 (Houlden et al., 2006). In a region of the South West of England and prior to its formal

Figure 1.2

FIGURE REMOVED FOR COPYRIGHT REASONS

Figure 1.2: The genes and pathways implicated in the inherited peripheral neuropathies

A summary of the known genes and proposed pathways currently implicated in the inherited peripheral neuropathies.

Used with permission from Rossor, A. M., Polke, J. M., Houlden, H. & Reilly M.M. 2013. Clinical Implications of Genetic Advances in Charcot-Marie-Tooth Disease. *Nature Reviews: Neurology*, 9, 562-71.

classification, HSN-1 was referred to as ‘Clarke’s foot’, so named after a large family from which the most common British mutation is thought to have arose (Professor Mary M. Reilly, personal communication). Today, many of the English and Australian families carrying the HSN-1 mutation are thought to be able to be traced back to this original family and a common founder, prior to 1800 (Nicholson et al., 2001).

HSN-1 patients present with profound deficits in sensory function, notably loss of pain and temperature sensation in the distal limbs, which spreads proximally in a progressive manner. Frequently this leads to complications, including chronic skin ulcers and osteomyelitis (Figure 1.3). Complications such as infections are worsened by characteristic slow wound healing and can thus result in amputation. Loss of sensation is accompanied by characteristic and spontaneous lancinating, burning pains. Notably, patients have preserved vibration and joint position sensation, reflecting the histopathological findings that small sensory axons are affected to a greater extent than large axons. In addition, patients suffer from variable, but often severe, motor involvement and, as the disease progresses, muscle atrophy in distal limbs also occurs. There is a large variability in the clinical presentation of HSN-1, with age of onset usually occurring between the second to the fifth decades of life (Houlden et al., 2006; Reilly, 2007; Davidson et al., 2012; Rotthier et al., 2012; Auer-Grumbach, 2013).

Most commonly, HSN-1 is caused by autosomal dominant mutations in the ubiquitously expressed serine palmitoyltransferase long chain base subunit 1 (*SPTLC1*) gene (9q22.1-22.3, Nicholson et al., 1996; Dawkins et al., 2001). HSN-1 caused by mutations in *SPTLC1* is sub-classified as HSN-1A. *SPTLC1* encodes one of the three major subunits of the enzyme serine palmitoyltransferase (SPT, Buede et al., 1991; Hanada et al., 1997; Weiss and Stoffel, 1997). To date, seven disease-causing missense mutations in *SPTLC1* have been identified: C133R, C133W, C133Y, V144D, S331F, S331Y and A352V (Duan and Merrill, 2015; Mroczek et al., 2015). Seven HSN-1-causing mutations have also been identified in the *SPTLC2* gene (14q24.3), which encodes the second subunit of SPT. HSN-1 caused by mutations in *SPTLC2* is sub-classified as HSN-1C. The known mutations are A182P, R183W, V359M, G382V, S384F, T409M and I504F

Figure 1.3

FIGURE REMOVED FOR COPYRIGHT REASONS

Figure 1.3: Typical ulcerated hands in a HSN-1 patient

HSN-1 patients present with loss of sensation, which can result in injuries such as the severe ulcers seen here, frequently worsened by characteristic slow wound healing. This patient has HSN-1 secondary to a *SPLTC1* mutation.

Used with permission from Reilly, M. M. 2007. Sorting out the Inherited Neuropathies. *Practical Neurology*, 7, 93-105.

(Duan and Merrill, 2015; Mroczek et al., 2015; Suriyanarayanan et al., 2016). Interestingly, to date, no disease-causing mutations have been found in the third, *SPTLC3* encoded, subunit of SPT, despite extensive mutation screening (Rotthier et al., 2010). Clinically, patients with mutations in *SPTLC1* or *SPTLC2* are phenotypically indistinguishable and mutations in both genes have been proposed to cause HSN-1 via the same mechanism of sphingolipid metabolism dysregulation (Rotthier et al., 2012).

1.3 Serine palmitoyltransferase (SPT)

SPT is a pyridoxal 5'-phosphate (PLP)-dependent α-oxoamine synthase located on the outer membrane of the endoplasmic reticulum (ER, Hanada, 2003). It catalyzes the first and rate-limiting step committing substrates to *de novo* sphingolipid synthesis (Buede et al., 1991; Hanada et al., 1997; Weiss and Stoffel, 1997). The enzyme is ubiquitously expressed and its activity has been detected in all tissues tested in rat, including brain, dorsal root ganglia, lung, liver, heart, kidney and muscle as well as in human brain and muscle (Merrill et al., 1985; Bejaoui et al., 2001). SPT is formed by SPTLC1 with one other of the subunits SPTLC2 or SPTLC3, in turn associated with a third smaller subunit, one of either ssSPTa or ssSPTb. It is the SPTLC2 and SPTLC3 subunits that contain the pyridoxal phosphate binding domain motifs, but SPTLC1 must also be present for the enzyme to be catalytically active. Moreover, it has been suggested that enzymatic activity is negligible in the absence of one of the small subunits (ssSPTa or ssSPTb, Han et al., 2009; Gable et al., 2010). The combination of the subunits comprising SPT determines the acyl-co-enzyme A (CoA) substrate, thus SPTLC1/SPTLC2/ssSPTa demonstrates a clear preference for palmitoyl-CoA, whereas other combinations utilise lauroyl-CoA, myristoyl-CoA or stearoyl-CoA preferentially, consequentially resulting in varying carbon-chain length products in the range of C_{12} to C_{18} (Han et al., 2009; Hornemann et al., 2009; Gable et al., 2010; Lowther et al., 2012; Duan and Merrill, 2015).

The condensation of L-serine with palmitoyl-CoA by SPT forms 3-keto-sphinganine, which is rapidly reduced to sphinganine (Figure 1.4). Sphinganine is then acylated by ceramide synthase (CerS) to form dihydroceramide and

subsequently desaturated by ceramide desaturase (DES) to form ceramide. Ceramide represents a central point from which sphingolipid metabolism can branch out in four directions to form ceramide-1-phosphate, sphingomyelin, glycosphingolipids or indeed, as shown in Figure 1.4, ceramidase can generate sphingosine. Sphingosine is the precursor for the key signalling molecule sphingosine-1-phosphate. From this point in the pathway sphingosine-1-phosphate can be broken down irreversibly by sphingosine-1-phosphate lyase (SO1P-lyase), this being the only exit point for complete sphingolipid breakdown (Airola and Hannun, 2013).

1.4 Sphingolipids

Sphingolipids are defined as any lipid containing the common sphingoid backbone. As described above, this backbone is derived from the condensation of an amino acid (such as serine) and a fatty acid (such as palmitoyl-CoA). Prior to the late 1980s it was largely believed that sphingolipids primarily served the cell as a structural component of the plasma membrane, together with phospholipids and cholesterol. However it is now recognized that sphingolipids and their derivatives play an important signal-mediating role in the cell (Gulbins and Petrache, 2013). In the form of sphingosine-1-phosphate, sphingolipids are found at relatively high concentrations in circulation compared to within tissue (~1 μM in plasma and 100 nM in lymph) where they act upon a broad spectrum of organs. In particular, sphingosine-1-phosphate is involved in vascular development, lymphocyte trafficking and neurogenesis (Proia and Hla, 2015). Sphingolipids also form a major component of lipid rafts. These specialised compartments of the plasma membrane serve as sites for enhanced protein-protein interaction and subsequent signal transduction from the extracellular to the intracellular environments (Simons and Ikonen, 1997; Simons and Toomre, 2000). Mutations in various enzymes within sphingolipid metabolic pathways have been associated with neurodegeneration, as seen frequently in the class

Figure 1.4

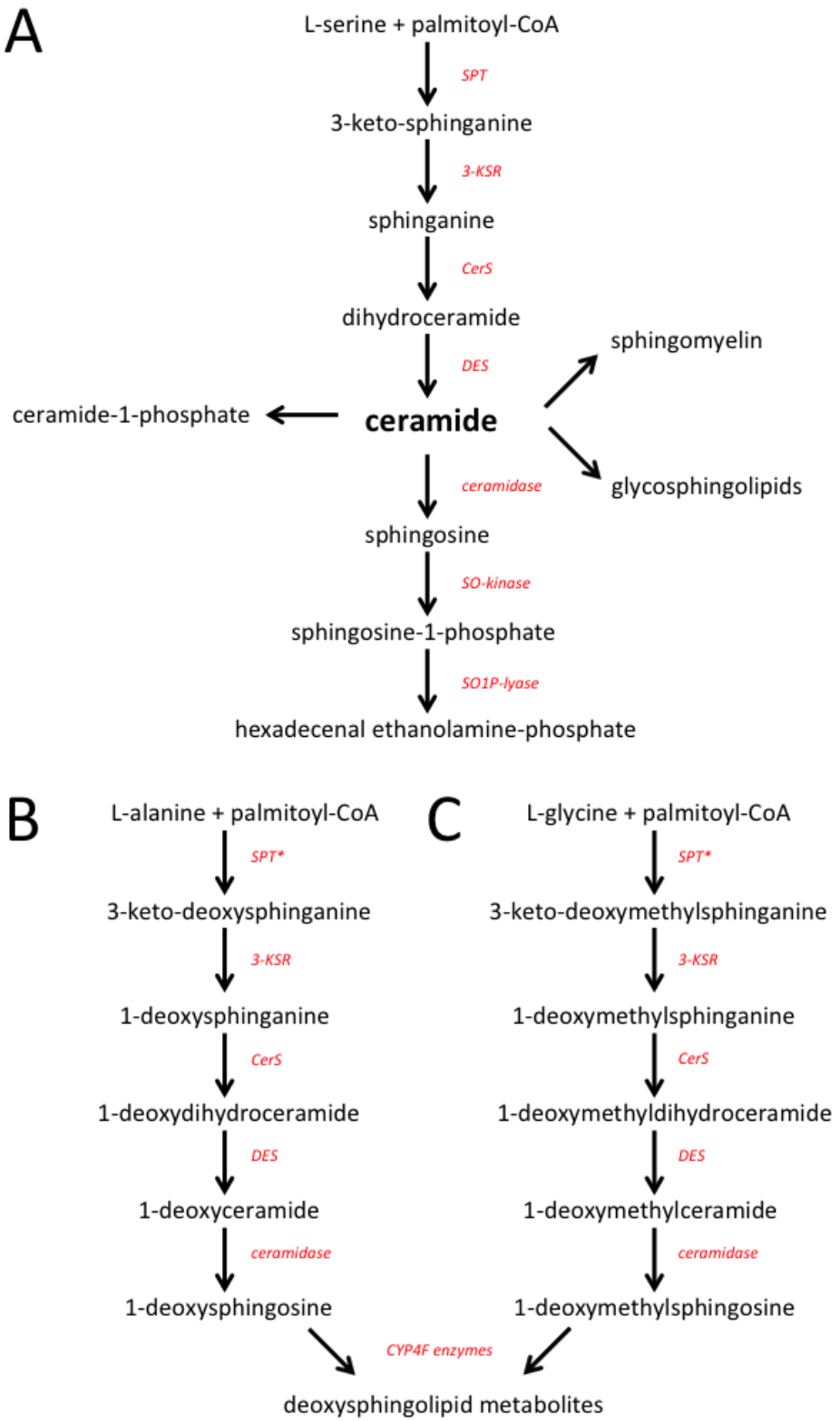
A
L-serine + palmitoyl-CoA
SPT
3-keto-sphinganine
3-KSR
sphinganine
CerS
dihydroceramide
DES
sphingomyelin
ceramide-1-phosphate
ceramide
glycosphingolipids
ceramidase
sphingosine
SO-kinase
sphingosine-1-phosphate
SO1P-lyase
hexadecenal ethanolamine-phosphate
B
L-alanine + palmitoyl-CoA
SPT*
3-keto-deoxysphinganine
3-KSR
1-deoxysphinganine
CerS
1-deoxydihydroceramide
DES
1-deoxyceramide
ceramidase
1-deoxysphingosine
C
L-glycine + palmitoyl-CoA
SPT*
3-keto-deoxymethylsphinganine
3-KSR
1-deoxymethylsphinganine
CerS
1-deoxymethyldihydroceramide
DES
1-deoxymethylceramide
ceramidase
1-deoxymethylsphingosine
CYP4F enzymes
deoxysphingolipid metabolites

Figure 1.4: The *de novo* sphingolipid synthesis pathway in mammalian cells

A Serine palmitoyltransferase (SPT) catalyzes the initial step of L-serine and palmitoyl-coenzyme A condensation to form 3-keto-sphinganine. 3-keto-sphinganine is reduced to sphinganine by 3-keto-sphinganine reductase (3-KSR*)*. Sphinganine is acylated by ceramide synthase (CerS) and subsequently desaturated by ceramide desaturase (DES) to form ceramide. Ceramide is used for the formation of the complex sphingolipids necessary for normal cell function. The degradation of ceramide is by the enzymes ceramidase, sphingosine-kinase (SO-kinase) and sphingosine-1-phosphate lyase (SO1P-lyase), in turn. **B** and **C** show the intermediate products of the same pathway when mutant SPT (as indicated by an asterix) preferentially binds L-alanine (B) or L-glycine (C), instead of the normal L-serine substrate. Formation of deoxy- species means that normal downstream complex sphingolipids cannot be synthesized. Deoxysphingosines are proposed to be hydroxylated and desaturated into deoxysphingolipid metabolites by the cytochrome P450 4F (CYP4F) subfamily of enzymes.

of diseases called the sphingolipidoses, which includes Tay-Sachs disease and Niemann-Pick disease, amongst others (Kolter and Sandhoff, 2006).

1.5 Enzyme promiscuity in HSN-1

Although the dominantly inherited nature of HSN-1 initially suggested that haploinsufficiency may be a possible disease mechanism, it is now widely accepted that HSN-1-causing mutations result in a toxic gain-of-function. HSN-1 mutations have been found to cause a shift in SPT substrate specificity, so that alanine or glycine is preferentially utilised instead of serine, as the native enzyme uses. This abnormal reaction ultimately produces atypical deoxysphingoid bases (Zitomer et al., 2009; Gable et al., 2010; Penno et al., 2010). Structural modelling of SPT indeed suggests that the HSN-1-causing mutations affect the geometry of the active site thus could alter the enzyme's substrate selectivity (Yard et al., 2007; Bode et al., 2016). The enzymatic product of the reaction when SPT binds alanine is deoxysphinganine, whereas reactions using glycine result in the production of deoxymethylsphinganine (Figure 1.4). Similarly to sphinganine, these deoxy- metabolites are also acylated, forming deoxydihydroceramide and deoxymethyldihydroceramide (Humpf et al., 1998; Zitomer et al., 2009). The deoxydihydroceramides are then converted to deoxyceramides. However, whilst typical dihydroceramide is converted to ceramide via the introduction of a 4,5-*trans* double bond, deoxydihydroceramide is converted to deoxyceramide by the introduction of a 14,15-*cis* double bond. As ceramides are converted to sphingosine, deoxyceramides are converted to deoxysphingosine, but these aberrant metabolites lack the C_1 hydroxyl group essential for sphingosine-1-phosphate lyase mediated degradation as seen in the typical sphingolipid pathway (Michel et al., 1997; Alecu et al., 2016a; Steiner et al., 2016). Whilst deoxysphingosines cannot be metabolised to the full range of canonical complex sphingolipids, since they lack the C1-hydroxyl group of typical sphingosine, Alecu et al. (2016a) showed the generation of eight new deoxysphingolipid metabolites formed by hydroxylation and desaturation reactions, mediated, at least in part, by the cytochrome P450 4F (CYP4F) enzyme subfamily. Notably, metabolism of the deoxysphingolipids was reported to be much slower than of typical sphingolipids (Alecu et al., 2016a).

Elevated levels of 1-deoxysphingoid bases have been detected in plasma of transgenic mice expressing mutant *SPTLC1,* patient lymphoblasts and plasma from HSN-1 patients (Penno et al., 2010; Garofalo et al., 2011; Rotthier et al., 2011; Auer-Grumbach et al., 2013; Murphy et al., 2013; Suriyanarayanan et al., 2016). In patients from a cohort at the National Hospital for Neurology and Neurosurgery (United Kingdom), blood plasma levels of deoxysphingoid bases ranged between 0.18 – 2.88 μM (Dr Umaiyal Kugathasan, personal communication). The levels of plasma deoxysphingoid bases, which are mainly transported on very low density and low density lipoproteins (VLDL and LDL), are reported to correlate with disease severity, indeed providing further evidence of their causality (Bertea et al., 2010; Penno et al., 2010). It is interesting that although the native enzyme does utilise alanine to some extent to generate deoxysphinganine, so that low levels of deoxysphingoid bases can be detected in the blood plasma of healthy subjects, deoxymethylsphingoid bases are not measurable, suggesting the native enzyme does not interact with glycine (Penno et al., 2010; Rotthier et al., 2011). Indeed, cells deprived of L-serine were also shown to generate elevated deoxysphingoid bases (Esaki et al., 2015).

All *SPTLC1* and *SPTLC2* mutations are thought to cause HSN-1 by dysregulation of sphingolipid synthesis and eight of the mutations identified to date have indeed been shown to be associated with increased deoxysphingoid base synthesis (in *SPTLC1*: C133W, C133Y, S331F, S331Y and in *SPTLC2*: G382V, I504F, S384F and A182P). In addition to aberrant deoxysphingoid base generation, three of the mutants (*SPTLC1*$^{S331F/Y}$ and *SPTLC2*^{I504F}) generate increased sphingosine levels, which may contribute to the more severe HSN-1 phenotype seen in these patients. Whereas the majority of the identified mutations are clustered around the active site and PLP-binding domain, the mutations associated with severe HSN-1 are found on the surface of SPT (Bode et al., 2016).

1.6 Diabetic neuropathy

As well as the inherited neuropathies, origins of peripheral neuropathies can also be diabetic, inflammatory or otherwise acquired. Diabetic neuropathy is a

common complication of both type 1 and type 2 *diabetes mellitus* and stands as the most common cause of peripheral neuropathy in the Western world (Callaghan et al., 2012).

Clinically, diabetic neuropathy is very similar to HSN-1. As with HSN-1, diabetic neuropathy is length-dependent and axonal, with loss of sensation beginning in the distal limbs. The loss of sensation is accompanied by elements of motor dysfunction and these patients can also experience neuropathic pain (Callaghan et al., 2012).

Deoxysphingoid bases have been found to be significantly elevated in the blood plasma of patients with metabolic syndrome and type 2 diabetes, which could indeed be due to the decreased serum serine levels which have also been reported, causing SPT to utilise alanine and glycine as alternate substrates and, in turn, generate deoxy- products (Bertea et al., 2010; Othman et al., 2012). Indeed, L-serine deficiency *in vitro* has been shown to produce elevated levels of deoxysphingolipids (Esaki et al., 2015). In humans, intake of glucose has been associated with acute elevation in blood deoxysphingoid base levels (Khan and Hornemann, 2017). In a longitudinal study it was shown that out of 339 at-risk patients, those with the highest plasma deoxysphingoid base levels at baseline, were most likely to go on to develop type 2 diabetes (Othman et al., 2015b). Thus, deoxysphingoid base levels have been proposed as predictive biomarkers for the development of type 2 diabetes. Interestingly, although plasma levels of deoxysphingoid bases were elevated in type 2 diabetics with distal sensorimotor polyneuropathy, they did not correlate with the clinical course (Dohrn et al., 2015).

Increased levels of deoxysphingoid bases were also found in the plasma and liver of a rat model of type 2 diabetes, the streptozotocin (STZ) injected rat, and in the plasma of the leptin-deficient *ob/ob* mouse (Othman et al., 2012; Zuellig et al., 2014). In the STZ rat, nerve conduction velocities (NCVs) were found to inversely correlate with plasma deoxysphingoid base concentrations (Othman et al., 2014).

Overall, deoxysphingoid base levels were not elevated in type 1 diabetic patients compared to healthy controls, although there is suggestion in one pilot study that

deoxyceramide levels (specifically deoxy-C24-ceramide) may be elevated in type 1 diabetic patients who report neuropathy, compared to type 1 diabetic patients who do not report neuropathy (Wei et al., 2014; Hammad et al., 2016).

In an *in vitro* system, deoxysphingoid bases indeed demonstrated dose-dependent cytotoxicity in insulin-producing pancreatic β-cells (Zuellig et al., 2014).

It was found that by targeting triglyceride levels in diabetic patients using fenofibrate, deoxysphingoid base levels could also be reduced (Othman et al., 2015a). With evidence in the STZ rat showing that lowering plasma deoxysphingoid base levels improves neuropathy (Othman et al., 2014), this presents a potential therapeutic strategy for diabetic neuropathy.

1.7 Chemotherapy-induced peripheral neuropathy (CIPN)

One of the major side effects of chemotherapy drugs, such as paclitaxel and cisplatin, is peripheral neuropathy affecting the sensory, motor and autonomic systems to varying extents. It was shown *in vitro* that paclitaxel upregulated SPT protein levels and activity, which in turn resulted in elevated levels of deoxysphingoid bases. Moreover, 27 breast cancer patients who were treated with paclitaxel chemotherapy were found to have an association between the levels of deoxysphingolipids and incidence and severity of neuropathy (Kramer et al., 2015).

1.8 Deoxysphinganine as a chemotherapeutic agent

Deoxysphinganine is also known as spisulosine or as ES-285, so named during phase I clinical trials for advanced solid cancerous tumours. In these trials neurotoxicity was reported and included one case of peripheral motor and sensory neuropathy associated with pain, which was thought to contribute to this individual's death (Schöffski et al., 2011). ES-285 was declared to have limited anti-tumour activity and the trials were subsequently discontinued (Baird et al., 2009; Schöffski et al., 2011; Massard et al., 2012).

1.9 Mouse models of HSN-1

A transgenic mouse model of HSN-1 has been developed, which ubiquitously overexpresses wildtype SPT (*SPTLC1^{WT}*) and the most common HSN-1 causing mutant SPT (*SPTLC1^{C133W}*) sourced from *cricetulus griseus* (Chinese hamster) (McCampbell et al., 2005). As in human HSN-1 patients, SPTLC1^{C133W} transgenic mice displayed elevated levels of deoxysphingoid bases in their blood plasma. In line with humans, SPTLC1^{WT} mice do also show some, but much lower, concentrations of deoxysphingoid bases in their plasma, whereas no deoxymethylsphingoid bases are detected whatsoever. Deoxysphingoid bases were also elevated in the sciatic nerve and to some extent in the spinal cord, testes and liver of SPTLC1^{C133W} mice, but not in the brain, which is of note when it is considered that HSN-1 does not affect the central nervous system (Eichler et al., 2009; Garofalo et al., 2011).

Unlike HSN-1 patients the SPTLC1^{C133W} mice did not acquire ulcerations and their gait was reported as normal. At 10 months, these mice responded no differently to their wildtype counterparts to noxious mechanical or temperature stimuli, as determined using the Von Frey, pinprick and cold acetone tests and in fact showed quicker responses to hot plate testing. The mice also performed equally well in rotarod tests using the accelerating rod paradigm (McCampbell et al., 2005). However, by 14 months these mice no longer display signs of hyperpathia and have developed deficits in mechanical (Von Frey) and thermo-sensitivity (acetone and hot plate), yet compared to SPTLC1^{WT} mice, there remains no difference in rotarod performance (Eichler et al., 2009). Histological examination revealed loss of small unmyelinated axons and a decrease in the diameter of myelinated axons in the sciatic nerve alongside neuronal stress in the dorsal root ganglia (McCampbell et al., 2005; Eichler et al., 2009).

In contradiction to what is observed in patients, SPTLC1^{C133W} mice displayed decreased fertility. Additionally, the mutant mice had some autonomic disturbances, such as decreased neurite innervation to the pancreas, and decreased gastrointestinal muscle activity (McCampbell et al., 2005; Eichler et al., 2009).

Double transgenic mice have also been generated, expressing both the wildtype and mutant *SPTLC1*. In these double transgenics, some deficits present in mutant mice were restored, including latency to paw withdrawal in the hot plate test and the Von Frey threshold (Eichler et al., 2009). The authors suggest that this may be due to heterodimerization of SPTLC2 with $SPTLC1^{WT}$ preferentially to $SPTLC1^{C133W}$. In addition, double transgenic mice showed much-reduced deoxysphingoid base levels in the blood plasma, sciatic nerve and other tissues examined. Heterozygous *SPTLC1* or *SPTLC2* knock-out mice showed no evidence of neuropathy, in further support of the hypothesis that HSN-1 is not a disease of haploinsufficency (Hojjati et al., 2005; Eichler et al., 2009).

1.10 *Drosophila Melanogaster* model of HSN-1

A *drosophila melanogaster* model of HSN-1 has also been generated, by expressing $SPTLC1^{WT}$ and $SPTLC1^{C129W}$ (the analogous amino acid position to C133 in humans). Mutant transgenic flies displayed a defective nociceptive response when compared to wildtype flies, as characterised by barrel rolling escape behaviour in response to noxious heat (Oswald et al., 2015). In line with HSN-1 patients and the HSN-1 mouse model, elevated levels of deoxysphingoid bases were detected in $SPTLC1^{C129W}$ flies, which could be exacerbated by an alanine enriched diet. Mutant transgenic *drosophila* displayed reduced survival and supplementing the diet of mutant transgenic *drosophila* with alanine, the substrate utilised by SPT to form deoxysphinganine, caused a further drastic reduction in fly survival that was not observed in wildtype transgenics. The $SPTLC1^{C129W}$ mutation also causes deficits in the development of dendritic arborisation in sensory neurons and may cause a trafficking defect, manifesting as an ER to Golgi apparatus block. These defects were rescued by co-expression of Rab1, an effector of ER-Golgi trafficking (Oswald et al., 2015).

1.11 *In vitro* models of HSN-1

In addition to these *in vivo* models, a number of *in vitro* models have been used in a bid to elucidate the underlying pathomechanisms causing peripheral nerve damage in HSN-1.

In an avian *in vitro* model, extracellular application of deoxysphingoid bases was shown to be toxic to primary sensory (dorsal root ganglion; DRG) neurons and motor neurons, causing a dose-dependent decrease in neurite branching (Penno et al., 2010). Other reported toxic effects included reduction of neurite outgrowth, retraction of existing neurites and disturbed actin-neurofilament interactions (Penno et al., 2010). In addition, preliminary work from our own laboratory indicates that external application of deoxysphinganine and deoxymethylsphinganine to mammalian DRG neurons in culture also causes decreased neurite arborisation (Kugathasan et al., 2015).

In contrast, a study of DRG cells dissected from mice overexpressing *SPTLC1*^{C133W} and grown *in vitro*, reported increased neurite length, increased neuronal branching and elevated expression of neuronal growth cone proteins (Jun et al., 2015). These conflicting reports on neurite outgrowth may well highlight the differences between intracellular deoxysphingoid base generation, as modelled by Jun et al. (2015), and circulating deoxysphingoid bases at high concentrations, as modelled by Penno et al. (2010). It is yet to be established which of these, if either, is the key underlying cause of nerve damage.

In *in vitro* work designed to explore the therapeutic potential of deoxysphinganine for cancer, it was found to cause disassembly of actin fibres in cell lines (Cuadros et al., 2000) and to be toxic to mouse neuroblastoma cell lines, causing caspase-dependent apoptosis (Salcedo et al., 2007).

However, despite the morphological changes described in cells treated with deoxysphinganines and in cells harbouring HSN-1-causing mutations, the molecular mechanisms by which the accumulation of these neurotoxic deoxysphingoid bases cause neurodegeneration remains unclear.

It has been shown that growth arrest and DNA damage-inducible protein (GADD153, also known as C/EBP-homologous protein, CHOP), which is a marker for ER stress and the unfolded protein response (UPR), is elevated in cells expressing HSN-1 mutations and also in cells treated with deoxysphinganine, presenting a possible candidate pathway to consider for the

neurotoxic mechanism of these deoxysphingoid bases (Gable et al., 2010). A downregulation of ER stress proteins binding immunoglobulin protein (BiP, also known as 78 kDa glucose-regulated protein, GRP-78) and endoplasmic oxidoreductin-1-like protein (ERO1-Lα) was reported in patient lymphoblasts harbouring the C133W and V144D *SPTLC1* mutations, indeed further implicating potential ER involvement in HSN-1 pathology (Myers et al., 2014).

Further findings in patient lymphoblasts have suggested that mitochondrial changes may also play a role in HSN-1 pathology. An upregulation of the electron transport chain protein ubiquinol-cytochrome C reductase core protein 1 (UQCRC1) was reported in patient lymphoblasts expressing the *SPTLC1*^{V144D} mutation, in addition to a decrease in expression of the immunoglobulin protein (Stimpson et al., 2015). Moreover, ultrastructural analysis using electron microscopy revealed gross morphological changes in patient lymphoblast mitochondria, including swelling, abnormal cristae and increased wrapping of the mitochondria in rough ER (Myers et al., 2014).

Studies carried out in mammalian cortical neurons gave the first suggestion that channels and receptors at the plasma membrane may play a role in HSN-1 and that there is an interaction between deoxysphinganine and N-methyl-D-aspartate (NMDA) receptor signalling (Guntert et al., 2016).

Accumulation of lipid droplets has been reported in patient lymphoblasts and was also seen in macrophages in the peripheral nerves of the *SPTLC1*^{C133W} overexpressing mice (Eichler et al., 2009; Marshall et al., 2014; Myers et al., 2014). Moreover, a pattern of deoxysphingoid base generation and lipid droplet accumulation was also observed in cells lacking *de novo* synthesis of L-serine (D-3-phosphoglycerate dehydrogenase, PHGDH, deficient cells, Esaki et al., 2015).

A critical discovery was that of Alecu et al. (2016b) who described for the first time the sub-cellular localization of deoxy- metabolites. In mouse embryonic fibroblasts, deoxysphingolipids were tracked and found to primarily localize in the

mitochondria, disrupting mitochondrial integrity, and subsequently accumulate in the ER, causing ER stress (Alecu et al., 2016b).

Co-treatment of mammalian cortical neurons and mouse embryonic fibroblasts with deoxysphinganine and fumonisin B1, which inhibits ceramide synthase (CerS), rescued some elements of toxicity, suggesting that it is deoxysphingolipid metabolites downstream of deoxysphinganine which are neurotoxic, rather than deoxysphinganine itself (Alecu et al., 2016b; Guntert et al., 2016).

1.12 Therapeutic strategies in HSN-1

At present, there is no effective treatment available for HSN-1 and patients can only be provided with supportive care (Scherer, 2011; Rotthier et al., 2012). One of the most promising treatment rationales is that of oral serine supplementation, in a bid to shift mutant enzyme substrate specificity back to serine and thus reduce the generation of deoxysphingoid bases from alanine or glycine precursors. A pilot trial in both a transgenic mouse model and in 14 HSN-1 patients presented early evidence for serine's deoxysphingoid base-lowering effects (Garofalo et al., 2011). Serine supplementation lowered blood plasma deoxysphingoid base concentrations in the *SPTLC1*^{C133W} overexpressing mouse model, and showed tendencies towards improved performances on the rotarod and Von Frey tests, when compared to non-treated counterparts. HSN-1 patients treated with serine showed a reduction of plasma deoxysphingoid base levels and reported some improved peripheral sensation (Garofalo et al., 2011). In addition, serine supplementation was found to lower plasma deoxysphingoid base levels and improve physiological outcomes in the STZ rat diabetic model, as well as have a positive effect on the HSN-1 *drosophila* model's survival (Othman et al., 2014; Oswald et al., 2015). These studies provide further evidence to support the idea that deoxysphingoid bases or their downstream metabolites cause HSN-1 pathology and thus, reducing deoxysphingolipid levels may be favourable to patient outcomes, although the latter is yet to be confirmed in a full clinical trial.

1.13 Aims of this Thesis

The overarching aim of this Thesis is to investigate the underlying pathomechanisms causing HSN-1 using *in vitro* models, in a bid to highlight potential targets for therapy development.

The underlying pathomechanism of HSN-1 remains unclear and little work has been done in appropriate *in vitro* mammalian neuronal systems. Furthermore, it is unclear how deoxysphingoid bases cause cellular damage, for example whether intracellular accumulation of deoxysphingolipids damage the cell or whether the toxic effect is mediated by the systemic circulation of deoxysphingolipid species.

To this end, this Thesis uses three *in vitro* models of HSN-1:

i) Primary mouse motor and sensory neurons treated with deoxysphingoid bases
ii) Primary mouse motor and sensory neurons virally transduced with *SPTLC1*^{WT} and *SPTLC1*^{C133W}
iii) Patient-derived fibroblasts

Ultimately, this Thesis aims to highlight potential targets for therapeutic intervention in HSN-1.

Chapter 2. Materials and Methods

2.1 Primary mixed motor neuron cultures

For primary mixed motor neuron (MN) cultures, the ventral spinal cord was dissected from 12.5-13.5 day old wildtype mouse embryos (C57BL/6J or C57BL/6J × SJL, Charles River Laboratories), based on the protocol outlined by Henderson et al. (1995).

Briefly, pregnant females were euthanized with an intraperitoneal injection of pentobarbital sodium (200 mg/ml, Merial) and subsequent cervical dislocation (as confirmation of death) as outlined by Schedule 1 procedures in the Animals Scientific Procedures Act, 1986. A laparotomy was performed and the uterus removed. Embryos were removed from the amniotic sacs and transferred to chilled Hanks' Balanced Salt Solution (HBSS, Ca^{2+} and Mg^{2+} free) containing penicillin/ streptomycin (100 units per ml/ 100 µg per ml). After removal of the head, the neural tube was separated from the rest of the embryo under a light dissection microscope, by the delicate removal of skin on the back of the embryo and teasing of the neural tube away from the body. The meninges were removed, and the dorsal horn cut away from the ventral horn.

Ventral horns were pooled and digested in trypsin (0.025%) in HBSS (Ca^{2+} and Mg^{2+} free) for 10 min at 37°C. The tissue was then triturated four times in DNase I (0.1 mg/ml, Sigma-Aldrich) in 0.4% bovine serum albumin (BSA, Sigma-Aldrich) in Leibovitz's L15 medium. Supernatant was collected and the remaining pellet triturated ten times in DNase I (0.02 mg/ml) in 0.4% BSA in Leibovitz's L15 medium. Supernatants from both rounds of trituration were combined and centrifuged with a 1 ml BSA cushion (4% in Leibovitz's L15 medium) at 380 × *g* for 5 min in order to pellet cells. The supernatant was discarded and the cell pellet re-suspended in supplemented neurobasal medium containing 2% B27 supplement, 0.5 mM GlutaMAX, 25 µM 2-mercaptoethanol, 2% horse serum, 0.1 ng/ml murine glial cell line-derived neurotrophic factor (GDNF, Peprotech), 0.5 ng/ml human or rat ciliary neurotrophic factor (CNTF, Peprotech), 0.1 ng/ml human brain-derived neurotrophic factor (BDNF, Peprotech) and penicillin/

streptomycin (50 units per ml/ 50 µg per ml). Cell number was estimated using a haemocytometer. Only bright, round cells were deemed healthy and counted.

Cells were plated onto 24-well plates (VWR) with glass coverslips (13 mm, VWR) at a cell density of 5×10^4 cells per well for immunocytochemistry. For live-cell imaging cells were plated onto glass bottom dishes (35 mm petri dish with 14 mm microwell, MatTek Corporation) at a cell density of 1×10^5 cells per well or 8-well µ-slides (Ibidi) at a cell density of 3×10^4 cells per well. For western blot, cells were plated onto 6-well plates (VWR) at a cell density of 2×10^5 cells per well. All culture dishes were pre-coated overnight with poly-L-ornithine (3 µg/ml, Sigma-Aldrich) followed by laminin (5 µg/ml, Sigma-Aldrich) for 2 h, prior to seeding cells.

These mixed ventral horn cultures were maintained in supplemented neurobasal medium as above, under standard culture conditions (37ºC, 5% CO_2). All above reagents were sourced from ThermoFisher Scientific unless otherwise specified.

2.2 Primary mixed dorsal root ganglion cultures

For primary DRG cultures, dorsal root ganglia were harvested from either 12.5-13.5 day old wildtype mouse embryos or 3-8 day old wildtype mouse pups (C57BL/6J or C57BL/6J × SJL, Charles River Laboratories). It is stated in the Results when embryonic DRG cultures are used, otherwise it should be assumed that dorsal root ganglia were obtained post-natally.

2.2.1 Embryonic DRG cultures

For embryonic DRG cultures, the spinal cord was removed from embryos as described above in Section 2.1 for primary MN cultures. This revealed dorsal root ganglia left in the embryo body, which were extracted into HBSS containing penicillin/ streptomycin (100 units per ml/ 100 µg per ml).

2.2.2 Post-natal DRG cultures

For post-natal cultures, dorsal root ganglia were extracted according to the dissection protocol outlined by Sleigh et al. (2016).

Briefly, the mouse pups were euthanized with an intraperitoneal injection of pentobarbital sodium (200 mg/ml) and as confirmation of death the carotid artery was severed, as outlined by Schedule 1 procedures in the Animals Scientific Procedures Act, 1986. The pelt was removed to allow the entire spinal column to be excised from the main body. Fat, muscle or other tissue was cleaned from the spinal column and it was cut into equal halves, and then halved again into hemi-halves along the midline, revealing the spinal cord. After removal of the spinal cord the dorsal root ganglia were extracted under a light dissection microscope into sterile HBSS (Ca^{2+} and Mg^{2+} free) supplemented with penicillin/ streptomycin (100 units per ml/ 100 µg per ml).

2.2.3 Dissociation of dorsal root ganglia

Embryonic or post-natal dissected ganglia were then incubated in pre-warmed HBSS (Ca^{2+} and Mg^{2+} free) containing 20 units/ml of papain (Sigma-Aldrich) at 37°C for 10 min with gentle rotation. Papain solution was then removed and, ganglia were re-suspended in pre-warmed HBSS containing collagenase type II (0.1%) and dispase (1.5 units/ml) at 37°C for 45 min with gentle rotation. After removal of the papain solution, dorsal root ganglia were gently triturated in order to dissociate them into a cell suspension. For immunocytochemistry, cells were plated onto 24-well plates with 13 mm glass coverslips. For western blot, cells were plated onto 6-well plates and for live cell imaging cells were plated onto glass bottom dishes (35 mm petri dish with 14 mm microwell) or 8 well µ-slides. All dishes were pre-coated with poly-D-lysine (100 µg/ml, Sigma-Aldrich) and laminin (5 µg/ml). Mixed DRG cultures were cultured in neurobasal medium supplemented with B27 supplement (2%), fetal calf serum (1%), 2 mM GlutaMAX, mouse nerve growth factor (50 ng/ml, Promega) and penicillin/ streptomycin (50 units per ml/ 50 µg per ml).

DRG cells were incubated under standard culture conditions (37 °C, 5% CO_2). All reagents above were obtained from ThermoFisher Scientific unless otherwise specified.

2.3 Fibroblast cultures

Control and patient fibroblasts were obtained from the MRC Centre for Neuromuscular Diseases Biobank London under the ethics approval 09/H0716/61. Gender and age of the fibroblast donors are detailed in Tables 1 and 2. Fibroblasts were maintained in T75 flasks in DMEM with GlutaMAX, further supplemented with 10% fetal calf serum and penicillin/streptomycin (50 units per ml/ 50 µg per ml) and kept at 37°C and 5% CO_2 (all reagents obtained from ThermoFisher Scientific). For passaging, cells were washed with phosphate-buffered saline (PBS) and then incubated with 0.05% trypsin/ ethylenediaminetetraacetic acid (EDTA, ThermoFisher Scientific). Fibroblast stocks were kept in 90% fetal calf serum and 10% DMSO and frozen overnight at -80°C before transfer to liquid nitrogen for long term storage.

2.4 Drug treatments

2.4.1 Sphingolipid treatments

Metabolites of SPT enzyme products (Avanti Polar Lipids) were dissolved in ethanol as stock solutions (1 mM). Cells at different stages after plating were either left untreated or treated with sphinganine (Sp), deoxysphinganine (DSp), deoxymethylsphinganine (DMSp) or ethanol (as a vehicle control), at final concentrations ranging from 0.1 µM to 2 µM. The duration of treatment ranged from 2 h to 6 days, as described in the Results.

2.4.2 Cyclosporine A treatment

To investigate the effect of mitochondrial permeability pore (mPTP) opening on cell survival, some sphinganine treated cultures were co-treated with the mPTP blocker cyclosporine A (CsA; Sigma-Aldrich). CsA was dissolved in ethanol as a stock solution (5 mM) and added to cultures to a final concentration of 1 µM, at the same time point as sphinganine addition.

Table 1

Code used	Age at biopsy	Gender
Control E1	25	Male
Control E2	37	Male
Control E5	20	Female
Control E6	25	Female
Control E7	38	Male
Control E8	39	Female

Table 1: Control fibroblasts

Age at biopsy and gender of donors of control fibroblasts used in this study.

Table 2

Code used	Age at biopsy	Gender	Diagnosis	Severity
Patient 1	27	Male	HSN-1A *SPTLC1*p.C133W	Severe (CMTNS2 = 21)
Patient 2	30	Female	HSN-1A *SPTLC1*p.C133W	Mild (CMTNS2 = 4)
Patient 3	21	Female	HSN-1A *SPTLC1*p.C133W	Mild (CMTNS2 = 8)
Patient 4	30	Female	HSN-1A *SPTLC1*p.C133W	Moderate (CMTNS2 = 13)
Patient 5	37	Male	HSN-1A *SPTLC1*p.C133W	Severe (CMTNS2 = 21)
Patient 6	43	Male	HSN-1A *SPTLC1*p.C133W	Moderate (CMTNS2 = 16)

Table 2: Patient fibroblasts

Age at biopsy, gender and diagnosis of donors of patient fibroblasts used in this study. CMTNS2 = Charcot Marie Tooth neuropathy score version 2 (Murphy et al., 2011).

2.4.3 Amino acid supplementation

In some instances, the supplemented neurobasal medium listed above was further supplemented with L-alanine (Sigma-Aldrich). 500 mM stock solutions for L-alanine were made up in PBS and added to the MN or DRG culture media as appropriate and to the final concentration stated in the Results. Amino acid supplementation began at the point of passaging (fibroblasts) or viral transduction (see below) and continued to the experiment end point.

2.5 Viral vector generation and delivery

Wildtype and mutant (p.C133W/c.399T>G) human *SPTLC1* gene sequences flanked with the EcoRI and EcoRV restriction sites in pUC57 plasmids with ampicillin resistance (AmpR) were purchased from Genewiz. These plasmids were amplified in One Shot TOP10 competent *Escherichia coli* (*E. coli*, ThermoFisher Scientific) on ampicillin containing agar plates (imMedia Growth Medium Ampicillin Agar, ThermoFisher Scientific) at 37°C overnight. DNA was extracted using the HiSpeed Plasmid Maxi Kit (Qiagen) according to manufacturer's instructions.

The laboratory had previously generated the viral transfer vector pCDH1-MCS1-EF1-copGFP (Systems Biosciences) containing the *HSPB1* gene with a C-terminus V5 epitope (Kalmar et al., 2017). Separate restriction digests using 1 µg of each of the *SPTLC1* containing plasmids and the *HSPB1* viral vector were performed with high fidelity restriction enzymes EcoRI-HF and EcoRV-HF and CutSmart Buffer (New England Biolabs), under the following conditions:

37°C	60 min
65°C	20 min
4°C	∞

Blue juice gel loading buffer (ThermoFisher Scientific) was added to the restriction products and they were run on a 1% agarose gel, alongside a 1 kb DNA ladder (Promega). The digested genes of interest and linearized transfer vector backbone were cut out from the gel under ultra violet light. The DNA was

extracted from the excised gel fragments using the Monarch DNA Gel Extraction Kit (New England Biolabs) according to manufacturer's instructions.

The genes of interest were then ligated into the digested transfer vector backbone using T4 DNA Ligase and T4 DNA Ligase Reaction Buffer (New England Biolabs) under the following conditions:

16°C	16 h
65°C	10 min
4°C	∞

Ligated plasmids and an empty control plasmid were amplified in One Shot TOP10 competent *E. coli* on ampicillin containing agar plates at 37°C overnight. DNA was extracted using the QIAprep Spin Miniprep Kit (Qiagen) according to manufacturer's instructions. Figure 2.1 shows a diagrammatic representation of the viral transfer vector.

The genes of interest sequences were checked throughout the cloning process by Sanger Sequencing (Source BioScience; Figure 2.2) using the sequencing primers listed in Table 3.

The plasmids containing packaging (pMDLg/pRRE and pRSV-Rev) and envelope (pMD2.G) genes to generate lentiviral particles were obtained from Addgene. These plasmids, making up this third generation lentiviral system, were amplified in *E. coli* overnight at 37°C and DNA extracted using the QIAprep Spin Miniprep Kit (Qiagen) according to manufacturer's instructions. The transfer, packaging and envelope plasmids were transfected into human embryonic kidney (HEK) 293T cells using lipofectamine 2000 reagent (ThermoFisher Scientific) and opti-MEM (ThermoFisher Scientific). HEK293T cells were maintained in T75 flasks in Dulbecco's Modified Eagle Medium (DMEM) with GlutaMAX, further supplemented with 10% fetal calf serum and penicillin/streptomycin (50 units per ml/ 50 µg per ml) and kept at 37°C and 5% CO_2 (all reagents obtained from ThermoFisher Scientific). For passaging, cells were washed with PBS and then incubated with 0.05% trypsin/EDTA (ThermoFisher Scientific). In preparation for

Figure 2.1

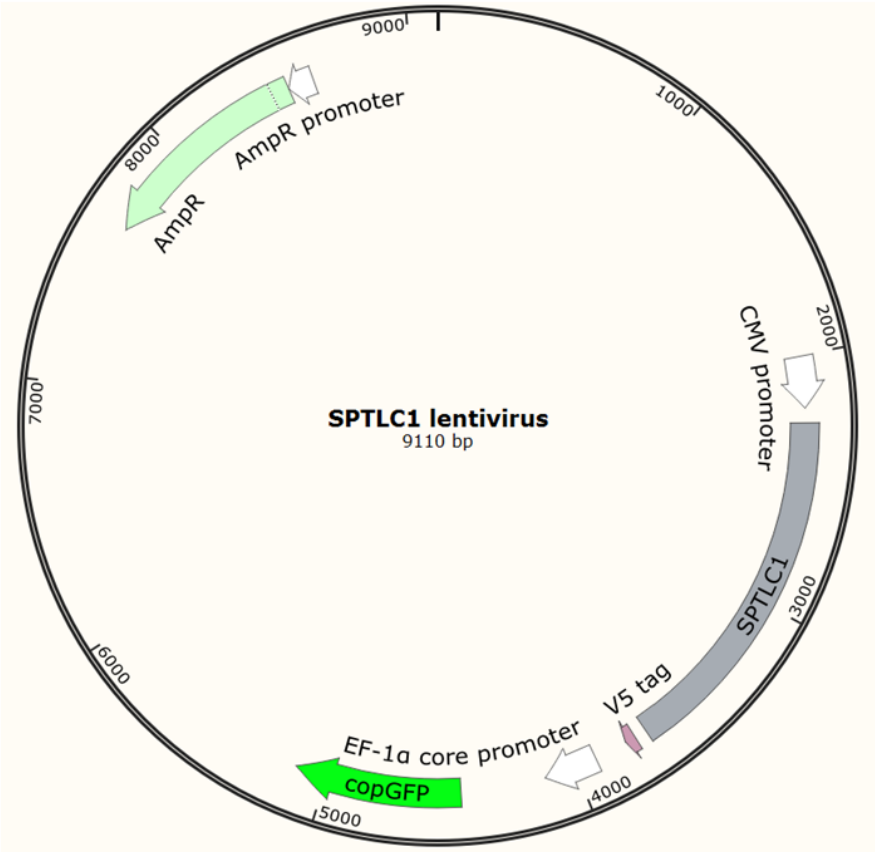

Figure 2.1: Diagrammatic representation of the viral transfer vector

Diagrammatic representation of the viral transfer vector used to generate *SPTLC1*^{WT} and *SPTLC1*^{C133W} expressing viral particles. The human cytomegalovirus (CMV) promoter allows the transcription of SPTLC1 with a V5 C-terminus epitope. Green fluorescent protein (from the copepod *Pontellina plumata*, copGFP) expression is driven by the elongation factor 1α (EF-1α) core promoter. The vector also expresses the gene for ampicillin resistance (AmpR).

Figure 2.2

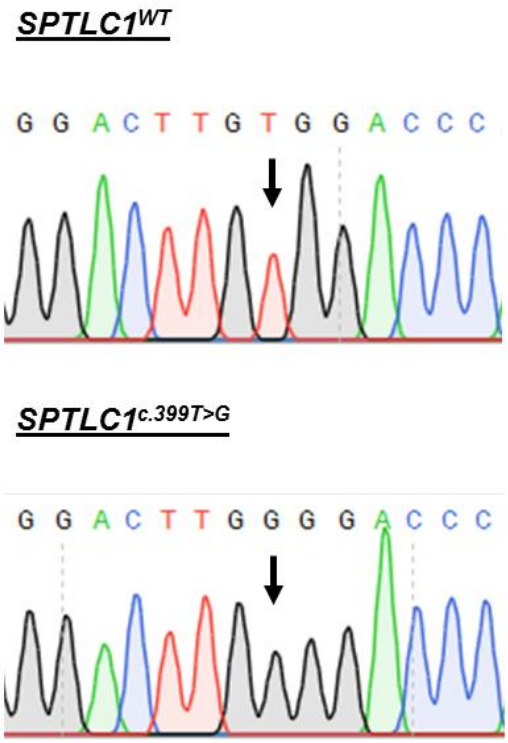

Figure 2.2: Example sequencing trace

Sequencing primers were used to confirm *SPTLC1*^{WT} and *SPTLC1*^{C133W} sequences throughout the cloning process. The above Figure shows example traces of *SPTLC1*^{WT} and *SPTLC1*^{C133W} sequences, as determined using Sanger Sequencing (Source BioScience).

Table 3

Primer name	Primer sequence
pCMV forward (Source BioScience)	5’ GAG CTC GTT TAG TGA ACC GTC 3’
Fseq1	5’ ATG GCG ACC GCC ACG GAG 3’
Fseq4	5’ TCA GCT TCG TTA CCT CCC CT 3’
Fseq6	5’ TGA CAT GGC TGA CCT CGA 3’

Table 3: Sequencing primers

The sequencing primers used to confirm *SPTLC1*^{WT} and *SPTLC1*^{C133W} sequences throughout the cloning process are detailed in the above table.

transfection HEK293T cells were grown to 60% confluency in 10 cm round dishes. After 1 day the lipofectamine and opti-MEM medium was replaced with the supplemented DMEM as above.

Lentiviral particles were harvested by collecting the cell media 2 and 3 days after the transfection. Harvests were centrifuged at 3600 × *g* for 15 min at 4°C in order to pellet any cell debris and the virus-containing supernatant filtered through a 0.45 µm filter. Filtered supernatants were subsequently centrifuged at 47000 × *g* for 2.5 h at 4°C. This supernatant was discarded and the pellets were each re-suspended in 150 µl PBS. The lentivirus was aliquoted and stored at -80°C. Multiple freeze-thaw cycles were avoided in order to maintain the integrity of the lentiviral particles.

The viral vector was applied to MN or DRG cultures after 1 day *in vitro* (DIV) at the concentrations stated in the Results. Virus containing media was changed for fresh, virus-free, media a further 24 h later. In some instances viral transduced cultures were co-treated with L-alanine as outlined above.

2.6 Western blot

For western blots primary MNs were grown to 5-6 DIV and treated with deoxysphinganines for 2 or 24 h before protein extraction. For virus treated primary cultures, primary MNs or DRG neurons were treated at 1 DIV with the viruses at the concentrations indicated in the Results, the virus was washed off a further 24 h later and protein was extracted at 6-7 DIV. Protein extraction from fibroblasts was performed 7 days after splitting.

Cells were washed once with ice cold PBS and protein was extracted from cells using radioimmunoprecipitation assay (RIPA) buffer (50 mM Tris (pH 7.5), 150 mM NaCl, 1% IGEPAL CA-630 (Sigma-Aldrich), 0.5% sodium deoxycholate, 0.5% sodium dodecyl sulphate, 1 mM EDTA, 1 mM ethylene glycol-bis(β-aminoethyl ether)-N,N,N',N'-tetraacetic acid (EGTA), Halt protease and phosphatase inhibitor cocktail (ThermoFisher Scientific)).

The Bio-Rad *DC* Protein Assay (Bio-Rad Laboratories) was used to estimate the concentration of protein per sample, according to manufacturer's instructions. Briefly, BSA protein standards (Sigma-Aldrich) were prepared in order to make a protein concentration gradient: 0.0, 0.125, 0.25, 0.5, 0.75, 1.0, 1.5, 2.0 mg/ml. 5 µl of each the standards and the samples were added to a 96-well plate (ThermoFisher Scientific) in triplicate. Bio-Rad *DC* Protein Assay reagents were mixed as per manufacturer's instructions and added to the wells. Plates were incubated at room temperature for 15 min and the absorbance measured at 750 nm on a spectrophotometer, allowing protein concentrations to be estimated based on absorbance relative to the standards. Samples were diluted in Laemmlli Sample Buffer (Bio-Rad Laboratories) containing 10% 2-mercaptoethanol and the protein-buffer mixtures boiled to 95°C for 10 min before being stored at -20°C or -80°C (for longer term storage).

Chambers for western blot (ThermoFisher Scientific or Bio-Rad Laboratories) were assembled according to manufacturer's instructions. Pre-cast NuPAGE 4-12% Bis-Tris Midi protein gels (1.0 mm, ThermoFisher Scientific) or 10% polyacrylamide gels were used. To make the 10% polyacrylamide gel, resolving gel containing ProtoGel Resolving Buffer (National Diagnostics), 10% acrylamide (Sigma-Aldrich), 0.1% ammonium persulphate (ThermoFisher Scientific), 0.001% N,N,N′,N′-tetramethylethylenediamine (TEMED, Sigma-Aldrich) and distilled water was poured into the chambers, covered with a layer of water-saturated butanol and allowed to polymerise for 1 h at room temperature. After 1 h, the butanol was washed off with distilled water and stacking gel containing Protogel Stacking Buffer (National Diagnostics), 5% acrylamide, 0.05% ammonium persulphate and 0.001% TEMED poured over the resolving buffer. Combs were inserted and the stacking gel left to polymerise for 20 min at room temperature. Approximately 5-10 µg per sample of protein, alongside a molecular weight marker (BioRad), were separated by sodium dodecyl sulphate polyacrylamide gel electrophoresis (SDS-PAGE) in MOPS or MES SDS running buffer (ThermoFisher Scientific) or tris glycine SDS-PAGE buffer (National Diagnostics), at 160 V for 60-90 min.

Gels were then placed on a nitrocellulose membrane (Amersham Protran 0.45 µm, GE Healthcare Life Sciences), sandwiched by filter paper and sponges assembled in a transfer bracket and immersed in transfer buffer with 20% methanol (National Diagnostics). Proteins were transferred onto the nitrocellulose membrane at 50-100 V for 1-2 h. The transfer of the proteins was confirmed by immersion of the membrane in Ponceau S solution (Sigma-Aldrich). Blots were then blocked for 1 h in tris-buffered saline (TBS) containing 0.1% Tween 20 and either 5% BSA or 5% milk. Blots were then incubated overnight at 4°C with the appropriate primary antibody, at a 1:1000 dilution in blocking solution. Table 4 describes the primary antibodies used for western blots in this Thesis.

Following overnight incubation, blots were washed three times, for 10 min in TBS containing 0.1% Tween 20. Blots were further incubated for 2 h at room temperature with horseradish peroxidase (HRP) -conjugated secondary antibodies (detailed in Table 5) in the appropriate blocking solution. Following a further three 10 min washes, blots were developed using Luminata Classico/ Crescendo western HRP Substrate (Merck Millipore) and visualized using a ChemiDoc Touch Imaging System (BioRad). Primary antibody incubation and subsequent steps were repeated for the β-actin antibody, which served as a loading control.

Blots were quantified using the ImageLab 5.2.1 software. Throughout this Thesis band density quantification is normalised to the β-actin loading control, and then made relative to the appropriate control. In Chapter 4 protein expression is made relative to the mean protein expression in untreated control cultures. In Chapter 5 protein expression is made relative to the protein expression in the second untreated control band in each western blot. In Chapter 6, protein expression is made relative to the second control band in each western blot.

Table 4

Primary antibodies used for western blot					
Antibody	**Dilution**	**Block**	**Species**	**Manufacturer/ category number**	**Predicted molecular weight (kDa)**
BiP	1:1000	BSA	Rabbit	Abcam ab21685	78
V5	1:1000	BSA	Mouse	Sigma V8012	55
SPTLC1	1:1000	Milk	Rabbit	Merck Millipore ABS1642	51
β-actin	1:30000	BSA/ milk	Mouse	Abcam ab6276	42

Table 4: Primary antibodies used for western blot

Details of the primary antibodies used for western blot in the experiments described in this Thesis. BiP = binding immunoglobulin protein.

Table 5

HRP-conjugated secondary antibodies used for western blot			
Antibody	**Dilution**	**Species**	**Manufacturer/ category number**
Anti-rabbit	1:5000	Swine	Dako P0217
Anti-mouse	1:5000-1:30000	Rabbit	Dako P0260

Table 5: Secondary antibodies used for western blot

Details of the HRP-conjugated secondary antibodies used for western blot in the experiments described in this Thesis. The anti-mouse secondary antibody was used at a dilution of 1:5000 for all primary antibodies other than the antibody against β-actin, where it was used at a 1:10000 – 1:30000 dilution.

2.7 Immunocytochemistry

For immunocytochemistry, at the end of each experiment, cells were fixed in 4% paraformaldehyde (Agar Scientific) in PBS (ThermoFisher Scientific) at room temperature for 15-20 min. Cells were subsequently washed in PBS for 5 min, three times. Prior to primary antibody labelling, cells were permeabilised in PBS containing 0.1% Triton X-100 (PBST; Sigma-Aldrich) and non-specific binding sites blocked in 5% animal serum, appropriate to the secondary antibody: normal goat serum (Vector Laboratories) or normal donkey serum (Sigma Aldrich). The cells were incubated overnight at 4°C with the appropriate primary antibody (or Alexa Fluor™ 488-conjugated phalloidin, ThermoFisher Scientific, to probe filamentous actin, F-actin) in blocking solution, as described above. The following day, the cells were washed in PBS for 5 min, three times before incubation for 2 h at room temperature, with the appropriate secondary antibody. Table 6 (primary antibodies) and Table 7 (secondary antibodies) outline the antibodies used for immunocytochemistry in the experiments described in this Thesis. Following another three 5 min PBS washes, cells were incubated for 10 min at room temperature with 4',6-diamidino-2-phenylindole (DAPI) counter-stain (1:2000, Sigma-Aldrich D9542) in order to stain nucleic acids (nuclei). Coverslips were mounted in Mowiol 40-88 mounting medium (Sigma-Aldrich) or Citifluor glycerol PBS solution (Agar Scientific).

2.8 LC-MS

Cells were harvested by washing in PBS, incubating in 0.05% trypsin/EDTA and centrifugation. Harvested cells were then washed in PBS for sphingoid base analysis using liquid chromatography-mass spectrometry (LC-MS) which was carried out by Saranya Suriyanarayanan and Professor Thorsten Hornemann at University of Zürich, Switzerland. Samples were acid- and base- hydrolysed and sphingoid base composition measured as previously described (Riley et al., 1999; Penno et al., 2010; Othman et al., 2012; Zuellig et al., 2014; Guntert et al., 2016). All measurements are normalised to the levels of 16 carbon length chain sphingosine (C16-sphingosine) in order to account for differences in cell number.

Table 6

Primary antibodies used for immunocytochemistry			
Antibody	**Dilution**	**Species**	**Manufacturer/ category number**
β-III tubulin	1:1000	Mouse	BioLegend 801201
β-III tubulin	1:500	Rabbit	BioLegend 845502
β-III tubulin	1:1000	Rabbit	BioLegend 802001
V5	1:400	Mouse	Sigma V8012
BiP	1:700	Rabbit	Abcam ab21685
PDI	1:100	Mouse	Enzo ADI-SPA-891-D
SPTLC1	1:100	Rabbit	Abcam ab84585
SPTLC1	1:200	Rabbit	Merck Millipore ABS1642
SPTLC1	1:100	Rabbit	Novus Biologicals NBP1-59643
SPTLC1	1:100	Rabbit	Santa Cruz Biotechnology sc-374143

Table 6: Primary antibodies used for immunocytochemistry

Details of the primary antibodies used for immunocytochemistry in the experiments described in this Thesis. BiP = binding immunoglobulin protein; PDI = protein disulphide isomerase.

Table 7

Secondary antibodies used for immunocytochemistry			
Antibody	**Dilution**	**Species**	**Manufacturer/ category number**
DyLight™ 405 anti-rabbit IgG (H+L)	1:500	Donkey	Jackson ImmunoResearch 711-475-152
Alexa Fluor™ 488 anti-mouse IgG (H+L)	1:1000	Goat	ThermoFisher Scientific A11001
Alexa Fluor™ 568 anti-rabbit IgG (H+L)	1:1000	Goat	ThermoFisher Scientific A11011
Alexa Fluor™ 568 anti-mouse IgG (H+L)	1:1000	Goat	ThermoFisher Scientific A11004
Alexa Fluor™ 568 anti-mouse IgG (H+L)	1:1000	Donkey	ThermoFisher Scientific A10037
Alexa Fluor™ 647 anti-rabbit IgG (H+L)	1:1000	Goat	ThermoFisher Scientific A21245

Table 7: Secondary antibodies used for immunocytochemistry

Details of the secondary antibodies used for immunocytochemistry in the experiments described in this Thesis.

2.9 Fluorescence microscopy and image analysis

Fluorescent images were taken using the 20× objective of a Leica epifluorescence light microscope and the Leica Application Suite software. For cell counts and for assessment of neurite outgrowth a minimum of five representative images measuring 655 × 491 µm were taken per condition, per experiment. Cells positive for β-III tubulin antibody were counted as neurons. Neurite outgrowth was assessed by tracing from the cell body to the tip of neurite. In the incidence of branching neurites, the longest neurite was measured and the shorter branch counted as a separate neurite.

2.10 Confocal microscopy

Confocal images were taken on Zeiss laser scanning microscope (LSM) 510, 710 or 780 inverted confocal microscopes using the LSM 5 Series software or ZEN LE Digital Imaging 2009 or 2012 software.

2.11 Electron microscopy

Control and patient fibroblasts were grown in T75 flasks to >90% confluency. Transmission electron microscopy was performed by Dr Samantha Loh and Dr Miguel Martins at University of Leicester, United Kingdom. Briefly, primary fixation was carried out overnight in 0.1 M sodium cacodylate buffer (pH 7.4) containing 2% paraformaldehyde, 2.5% glutaraldehyde and 0.1% Tween 20. Samples were post-fixed in 1% osmium tetroxide and 1% potassium ferrocyanide for 1 h at room temperature. Following fixation, samples were stained with 5% aqueous uranyl acetate overnight at room temperature and then dehydrated using a series of increasingly concentrated ethanol washes. The samples were embedded in TAAB epoxy resin (TAAB Laboratories Equipment Ltd.) and semi-thin sections stained with toluidine blue to allow for selection of areas for ultramicrotomy. Ultrathin sections were stained with lead citrate and imaged with a MegaView 3 digital camera and iTEM software (Olympus Soft Imaging Solutions GmbH) in a Jeol 100-CXII electron microscope (Jeol UK Ltd.). Mitochondrial-ER contact counts were performed by Dr Samantha Loh. For analysis of mitochondrial diameter the longest diameter per mitochondrion was taken, and the inclusion

criteria for mitochondria were clearly identifiable cristae and outer mitochondrial membrane.

2.12 Measurement of intracellular Ca^{2+} concentrations

For chronic treatment experiments, primary MN cultures were treated with Sp, DSp or DMSp after 1 DIV and live cells were imaged at 5-8 DIV. For acute treatment experiments, primary MN cultures were grown for 5-8 DIV and primary DRG cultures grown for 3-5 DIV, before being treated with deoxysphingoid bases for either 2 or 24 h prior to imaging. The cultures were then washed in recording medium (156 mM NaCl, 10 mM HEPES, 10 mM D-glucose, 3 mM KCl, 2 mM $MgSO_4$, 2 mM $CaCl_2$, 1.25 mM KH_2PO_4, pH 7.35) and then loaded with 5 µM fura-2 acetoxymethyl (fura-2 AM, Molecular Probes by Life Technologies) in the above recording medium with pluronic acid F127 (0.04%, ThermoFisher Scientific), for 30 min, at room temperature. Fura-2 is a ratiometric, intracellular Ca^{2+} indicator which is excited by two different wavelengths depending on whether it is Ca^{2+} bound or Ca^{2+} free, thus accounting for discrepancies in dye loading (Grynkiewicz et al., 1985). Fura-2 was replaced with recording medium and dye accumulation was detected optically using a widefield microscope coupled with a CCD camera, following excitation at wavelengths 340 nm and 380 nm, using the computer programme Andor iQ 1.9 Imaging. Emission was measured using a 510 nm filter and the ratio of fura-2 intensity following excitation at 340/380 nm wavelengths was used as a readout of cytoplasmic Ca^{2+} concentration.

ER Ca^{2+} concentration and mitochondrial Ca^{2+} concentration were measured using thapsigargin (10 µM, Sigma-Aldrich) and ionomycin (10 µM, Sigma-Aldrich), respectively, in Ca^{2+}-free recording medium (156 mM NaCl, 10 mM HEPES, 10 mM D-glucose, 3 mM KCl, 2 mM $MgSO_4$, 1.25 mM KH_2PO_4, 0.5 mM EGTA, pH 7.35). These compounds cause the release of Ca^{2+} from intracellular organelles into the cytosol, so that the increase in cytosolic Ca^{2+} due to mobilisation of Ca^{2+} following treatment with thapsigargin or ionomycin can be taken as an estimation of ER or mitochondrial Ca^{2+} concentration, respectively (see also Figure 4.2, Thastrup et al., 1990; Lytton et al., 1991; Hoek et al., 1995; Abramov and Duchen, 2003).

Voltage-gated Ca^{2+} channel entry was measured using a high potassium-containing recording medium (156 mM NaCl, 10 mM HEPES, 10 mM D-glucose, 135 mM KCl, 2 mM $MgSO_4$, 2 mM $CaCl_2$, 1.25 mM KH_2PO_4, pH 7.35). Store-operated Ca^{2+} channel entry was measured using thapsigargin (10 µM) in Ca^{2+}-free recording medium (as above), followed by replacement with normal recording medium (as above). 1 µM carbonyl cyanide-p-trifluoromethoxyphenylhydrazone (FCCP, Sigma-Aldrich) was introduced 2 min prior to thapsigargin treatment, as well as in the normal recording medium at the same concentration, in order to render mitochondria non-functional. In some experiments, SOC channel blockers 2-aminoethoxydiphenyl borate (2-APB, 100-200 µM, Sigma-Aldrich) and ML-9 (50-300 µM, Cayman Chemical) were incorporated into the recording media (Parekh and Putney, 2005; Bird et al., 2008; Putney, 2010). To trigger Ca^{2+} influx through glutamate receptors, N-methyl-D-aspartic acid (NMDA, 100 µM-10 mM, Sigma-Aldrich) or L-glutamic acid (100 µM-1 mM, Sigma-Aldrich) with glycine (15-300 µM, Sigma-Aldrich) were incorporated into Mg^{2+}-free recording media (156 mM NaCl, 10 mM HEPES, 10 mM D-glucose, 3 mM KCl, 2 mM $CaCl_2$, 1.25 mM KH_2PO_4, pH 7.35) (Dildy and Leslie, 1989; Jensen and Chiu, 1990).

The drugs and conditions used to manipulate intracellular Ca^{2+} handling are summarised in Table 8.

2.13 Measurement of mitochondrial membrane potential ($\Delta\psi_m$)

Primary MN cultures at 5-8 DIV or primary DRG cultures at 3-5 DIV were treated with the sphinganines for 2 h prior to live cell imaging. Primary cultures or fibroblasts were loaded with tetramethylrhodamine methyl ester (TMRM, 20 nM, ThermoFisher Scientific) in recording medium (156 mM NaCl, 10 mM HEPES, 10 mM D-glucose, 3 mM KCl, 2 mM $MgSO_4$, 2 mM $CaCl_2$, 1.25 mM KH_2PO_4, pH 7.35) with pluronic acid F127 (0.04%, ThermoFisher Scientific) for 30 min, at room temperature. Immediately before imaging cells were loaded with the live-cell labelled dye calcein blue, AM (1-10 µM, ThermoFisher Scientific). Z stack images were taken on Zeiss LSM 710 (MNs) or 780 (DRG neurons) inverted

Table 8

Drug	Target of drug	Experimental condition	Physiological measurement
Thapsigargin	SERCA pump inhibitor	Ca^{2+}-free recording medium	ER $[Ca^{2+}]$
		Apply in Ca^{2+}-free recording medium and then re-introduce Ca^{2+} to the external medium	SOC channel entry
Ionomycin	Non-selective ionophore	Apply after thapsigargin, in Ca^{2+}-free recording medium	$[Ca^{2+}]$ in mitochondrial and other intracellular stores
135 mM $[K^+]$	Plasma membrane depolarization	Normal recording medium	Voltage-gated Ca^{2+} channel entry
FCCP	Protonophore to abolish mitochondrial membrane potential	Apply FCCP throughout the experiment	To determine mitochondrial contribution
2-APB	SOC channel inhibitor	As above for SOC channel entry	SOC channel entry inhibition
ML-9	SOC channel inhibitor	As above for SOC channel entry	SOC channel entry inhibition
NMDA	NMDA receptor	Apply in Mg^{2+}-free recording medium containing glycine	NMDA receptor Ca^{2+} influx
L-glutamic acid	Glutamate receptor	Apply in Mg^{2+}-free recording medium containing glycine	Glutamate receptor Ca^{2+} influx

Table 8: Drugs used to explore intracellular Ca^{2+} handling

The table outlines the drugs used to measure physiological Ca^{2+} handling parameters.

confocal microscopes using the lasers 405 nm and 561 nm and the ZEN LE Digital Imaging 2009 and 2012 software. Z-stacks (minimum 720 × 720 pixels and 12 bit depth) were compressed to maximal intensity per pixel and thresholded using ImageJ version 1.51n. In these processed images, areas of interest for individual cells were outlined and TMRM intensity per cell soma (as a readout measure for $\Delta\psi_m$) and the total mitochondrial area per cell soma were measured. TMRM intensities are expressed as a percentage relative to the mean TMRM intensity in control cells, for each independent imaging session.

DRG culture $\Delta\psi_m$ experiments and image collection were carried out by Dr Umaiyal Kugathasan and Dr Bernadett Kalmar.

2.14 Statistical analysis

Statistical analysis was performed using the GraphPad Prism Version 6.0 software. The distribution of data was determined using Shapiro-Wilk, D'Agostino and Pearson omnibus and Kolmogorov-Smirnov normality tests. Where the data sets were too small to test for Gaussian distribution, non-parametric tests were used. Thus, statistical significance was determined by unpaired t test, One-Sample Wilcoxon Signed Rank, Mann-Whitney *U*, one-way analysis of variants (ANOVA) or Kruskal-Wallis tests, with post-hoc multiple comparison tests, as appropriate. *P* values < 0.05 (labelled with *), < 0.01 (labelled with **), < 0.001 (labelled with ***) were deemed significant.

Chapter 3. Investigating the morphological effects of exogenous deoxysphingoid bases on primary mammalian neurons

3.1 Introduction

As described in Chapter 1, deoxysphinganine (DSp) and deoxymethylsphinganine (DMSp) are the abnormal products of mutant SPT. Elevated levels of deoxysphingoid bases are measured in the blood plasma of HSN-1 patients and although numerous studies have provided evidence for deoxysphingoid base cytotoxicity, this has yet to be thoroughly examined in mammalian peripheral neurons, the cell type affected in HSN-1.

Exogenous DSp application has been shown to be cytotoxic to a number of cell lines of mouse, rat, primate and human origin (Cuadros et al., 2000; Salcedo et al., 2007; Zuellig et al., 2014; Esaki et al., 2015). Moreover, distinct cytoskeletal disruption, as visualised with phalloidin, has been described, although notably the microtubular cytoskeletal network is reported to be relatively unaffected (Cuadros et al., 2000; Zuellig et al., 2014). Interestingly, removal of DSp allowed the cytoskeleton of kidney cells to rapidly reform (Cuadros et al., 2000).

Another study examined the effect of exogenous application of DSp on primary, chick motor and sensory neurons and found that treatments of 0.5 µM and 1 µM cause a reduction in the number of neurites per cell (Penno et al., 2010). In chick sensory neurons, DSp treatment has also been shown to cause a decrease in the mean neurite length, with evidence of neurite retraction and disturbed actin-neurofilament interaction (Penno et al., 2010).

When explored in primary mammalian cortical neurons, Guntert et al. (2016) also found that DSp treatments of 0.5 µM and 2 µM caused cytotoxicity and indeed, prolonged 2 µM treatment with DSp resulted in changes in the actin cytoskeleton of these neuronal cells.

3.2 Aims of this Chapter

The studies described above suggest that exposure to deoxysphingoid bases is cytotoxic in several *in vitro* systems. The aims of this Chapter were to explore whether the deoxysphingoid bases also have a direct neurotoxic effect on mammalian sensory and motor neurons, the cell types typically affected in HSN-1.

3.3 Results

To examine whether the abnormal sphinganines have a direct neurotoxic effect on mammalian neurons, mixed primary dorsal root ganglion (DRG) cultures or mixed primary motor neuron (MN) cultures from wildtype mice were treated with the normal enzymatic product sphinganine (Sp), or the atypical sphingoid bases, deoxysphinganine (DSp) and deoxymethylsphinganine (DMSp) or a vehicle control (ethanol), at a range of concentrations and for varying treatment durations.

3.3.1 The effect of deoxysphingoid bases on mouse dorsal root ganglion survival and neurite outgrowth

The effect of DSp and DMSp on DRG neuron survival and neurite outgrowth was established as part of a collaboration with Dr Umaiyal Kugathasan, a fellow PhD student in the laboratory, who undertook the experiments summarised in Figures 3.1 and 3.2. As can be seen in Figures 3.1 and 3.2, exogenous application of DSp and DMSp causes decreased neurite arborisation and cell death in mouse DRG cultures (Kugathasan et al., 2015). Figure 3.1 A-D show that treatment with 1 µM DSp and DMSp caused a reduction in the number of DRG neurons in comparison to vehicle treated cultures or cultures treated with the normal enzyme product, Sp. The effect of DSp and DMSp on DRG neuron survival is summarised in Figure 3.1 E, which shows that with increasing DSp treatment duration (from 12-48 h) there is a corresponding decrease in DRG neuron survival. Interestingly, whilst DSp treatment caused a reduction in DRG neuron survival as early as after just 12 h following the commencement of treatment, DMSp treatment only caused a reduction in the DRG neuron survival over the longest treatment duration tested (48 h). In addition to DRG neuron survival, the neurite arborisation area was also

Figure 3.1

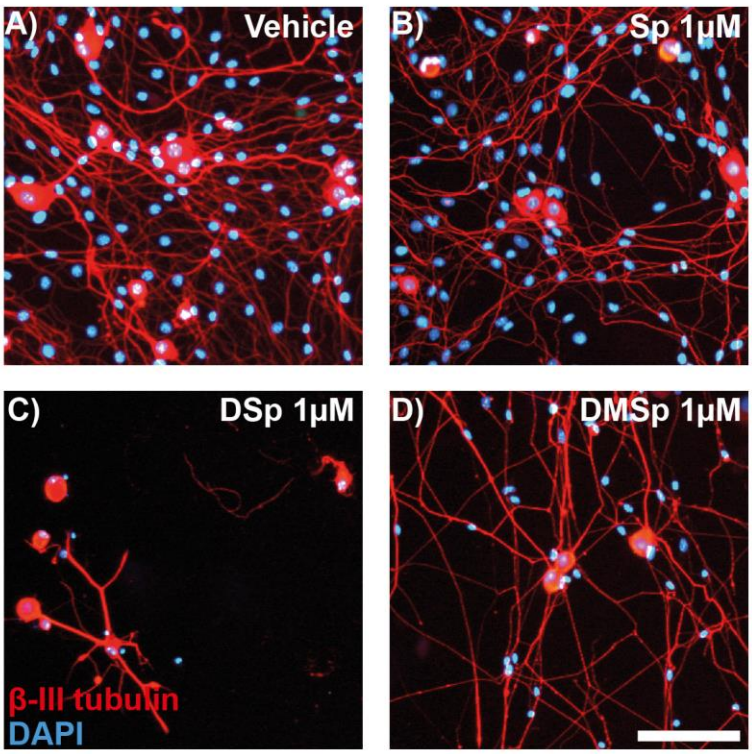

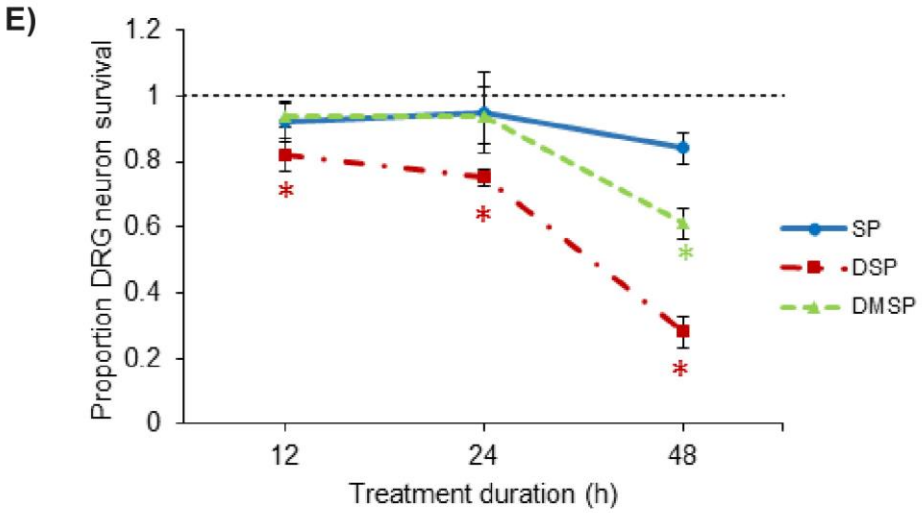

Umaiyal Kugathasan

Figure 3.1: Treatment with deoxysphingoid bases causes reduced cell survival in dorsal root ganglion cells

Dissociated dorsal root ganglia were grown for 3-4 h before being treated with sphinganines or ethanol as a vehicle control. DRG cultures were fixed and stained for analysis 12, 24 or 48 h after treatment. **A-D)** Examples of primary DRG neurons treated for 48 h with sphinganines and fixed and immunostained for DAPI (blue) and β-III tubulin (red). Scale bar = 200 μm. **E)** Quantification of DRG neuron survival following treatment with sphinganines for different durations, displayed as a proportion relative to control cultures. n = 5-6 independent experiment sets per condition. Displayed data represent the mean ± standard error of the mean (SEM). For statistical comparison, each treatment group was compared to control (dotted line) using the one-sample Wilcoxon signed rank test. *P* values * < 0.05; ** < 0.01; *** < 0.001.

(Experiments completed and analysed by Dr Umaiyal Kugathsan)

Figure 3.2

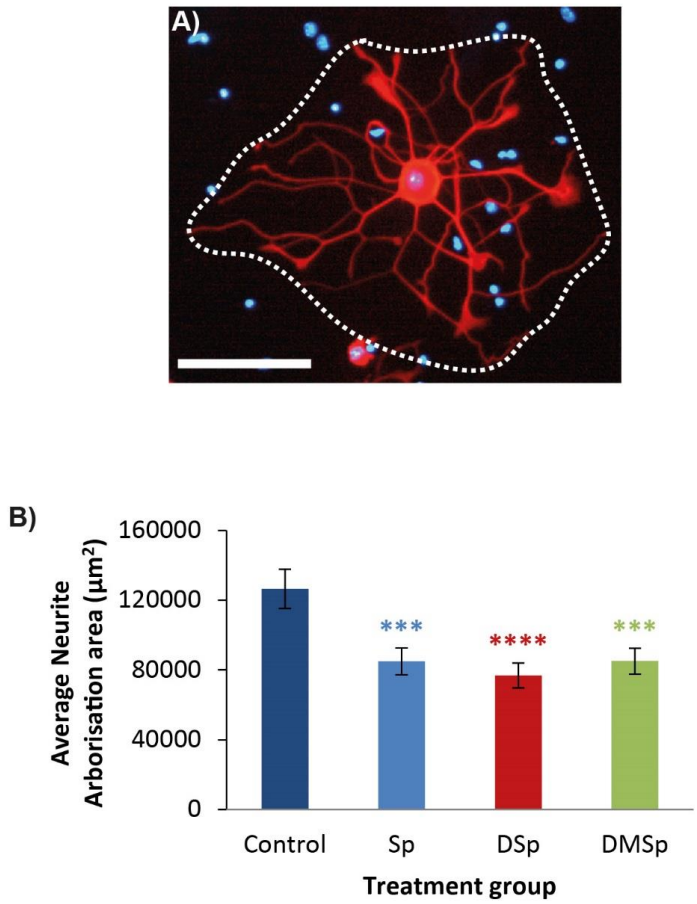

Umaiyal Kugathasan

Figure 3.2: Treatment with deoxysphingoid bases causes reduced neurite outgrowth in dorsal root ganglion cells

Dissociated dorsal root ganglia were grown for 3-4 h before being treated with sphinganines or ethanol as a vehicle control. DRG cultures were fixed and stained for analysis 12 h after treatment. **A)** The neurite arborisation area was measured as demonstrated. Scale bar = 100 µm. **B)** Quantification of neurite arborisation area following 12 h treatment with sphinganines (1 µM). n = 135-173 cells from 5 independent experiment sets per condition. Displayed data represent the mean ± SEM. For statistical comparison, each treatment group was compared to control using the Kruskal-Wallis and Dunn's multiple comparisons tests. *P* values * < 0.05; ** < 0.01; *** < 0.001; **** < 0.0001.

(Experiments completed and analysed by Dr Umaiyal Kugathsan)

assessed, as indicated in Figure 3.2 A and the results are summarised in Figure 3.2 B, which shows that treatment with all three of the possible SPT enzyme products caused a reduction in the mean neurite arborisation area when compared to the control group.

These results show that the abnormal enzyme products generated in HSN-1 are indeed toxic to mouse DRG cells *in vitro*. I therefore next examined whether the deoxysphingoid bases were also toxic to MNs, the second cell type typically affected in HSN-1.

3.3.2 The effect of the vehicle control on mouse motor neurons

To examine whether the deoxysphingoid bases were indeed toxic to mammalian MNs, I first established the effects of the ethanol vehicle control on mouse MN survival and neurite outgrowth. Survival and neurite outgrowth were assessed by immunostaining for the neuronal marker β-III tubulin and co-staining for the nuclear marker DAPI.

The results in Figure 3.3 summarise the effects of the vehicle, ethanol, on MN survival. In three different treatment models tested, outlined in the upper panels of Figure 3.3 A-C, there was no difference in MN survival between untreated cultures and those treated with ethanol vehicle control.

The effect of ethanol on the mean neurite length (Figure 3.4 B) and longest neurite length (Figure 3.4 C) of MNs was also determined in untreated and ethanol treated cultures, following the treatment paradigm shown in Figure 3.4 A. After just 24 h treatment, an increase in mean neurite length was observed in the ethanol treated cultures, from 23.0 ± 1.6 µm in the untreated neurons to 30.4 ± 1.3 µm in ethanol treated neurons ($P < 0.001$, Figure 3.4 B). Likewise, an increase in the longest neurite length from 30.3 ± 1.4 µm in untreated neurons to 47.6 ± 2.3 µm in ethanol treated neurons was observed ($P < 0.001$, Figure 3.4 C). Despite this increase in neurite length, no difference was detected between the number of neurites per neuron, as shown by the percentage of neurons with 0 neurites (Figure 3.4 D) and the percentage of neurons with 2 or more neurites

Figure 3.3

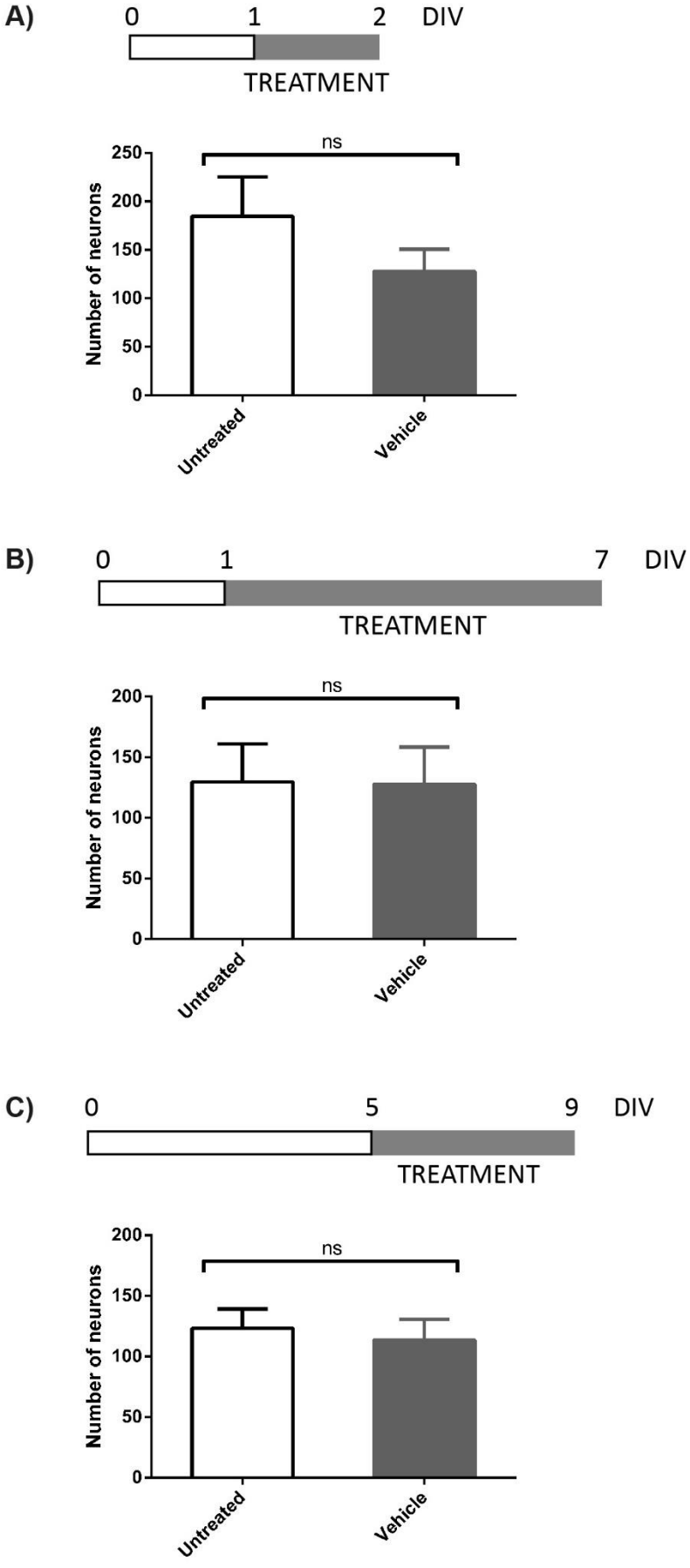
A)
0
1
2
DIV
TREATMENT
ns
Number of neurons
250
200
150
100
50
0
Untreated
Vehicle
B)
0
1
7
DIV
TREATMENT
ns
Number of neurons
200
150
100
50
0
Untreated
Vehicle
C)
0
5
9
DIV
TREATMENT
ns
Number of neurons
200
150
100
50
0
Untreated
Vehicle

Figure 3.3: The effect of an ethanol vehicle control on primary motor neuron survival

Upper panels show schematics of the treatment regimes used in the cell survival studies shown in lower panels. **A)** Dissociated MNs were grown for 24 h before treatment with an ethanol vehicle control. MNs were fixed and stained for cell survival analysis 24 h following treatment, after 2 days *in vitro* (DIV). **B)** Dissociated MNs were grown for 24 h before being treated with an ethanol vehicle control. MNs were fixed and stained for cell survival analysis after 7 DIV. **C)** Dissociated MNs were grown for 5 days before being treated with an ethanol vehicle control. MNs were fixed and stained for cell survival analysis after 9 DIV. Displayed data represent the mean ± SEM. Mann-Whitney *U* tests were used for statistical analysis. *P* values * < 0.05; ** < 0.01, *** < 0.001. ns= not significant. n = 5-10 independent experiment sets per condition.

Figure 3.4

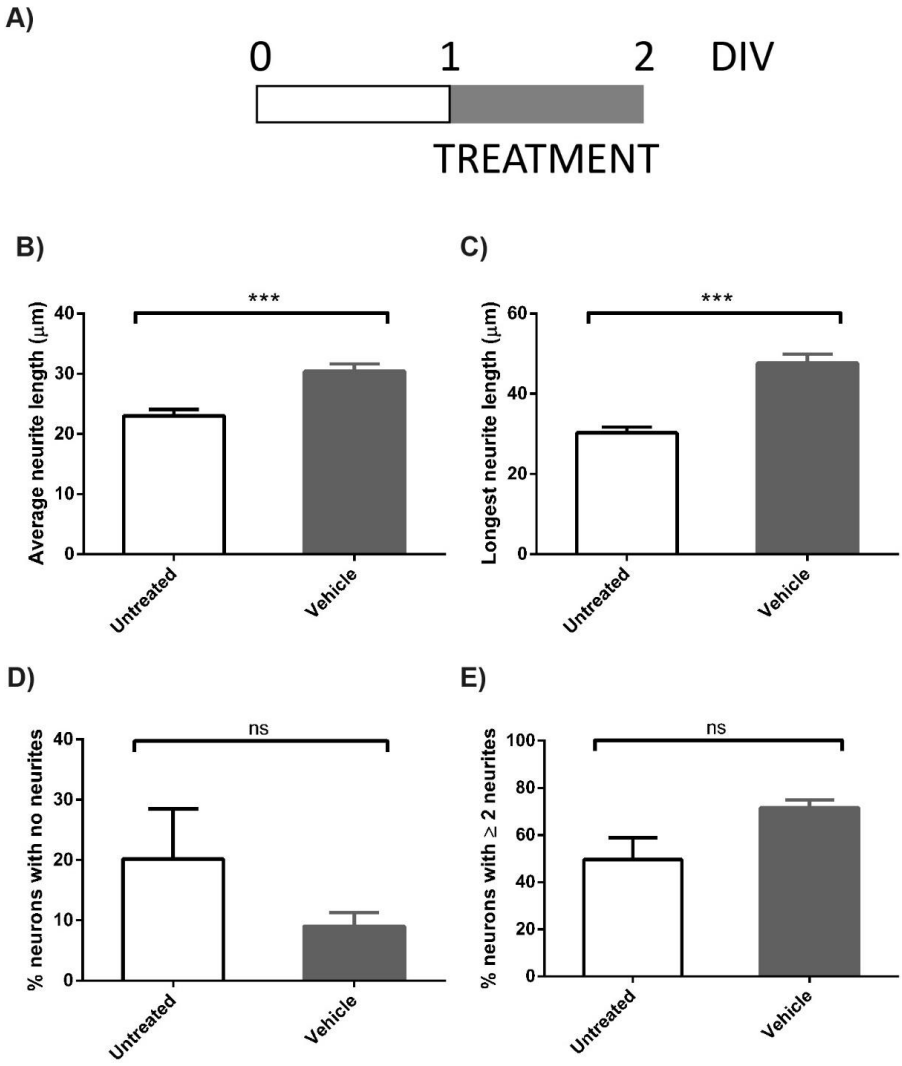

Figure 3.4: The effect of an ethanol vehicle control on neurite outgrowth in primary motor neurons

A) Schematic showing the treatment regime used in the neurite outgrowth assays shown in this Figure. **B)** Neurite length in MNs treated with ethanol. **C)** Longest neurite length in MNs treated with ethanol. **D)** The number of neurons with no neurites following ethanol treatment. **E)** The number of neurons with two or more neurites following ethanol treatment. Displayed data represent the mean ± SEM. Mann-Whitney *U* tests were used for statistical analysis and *P* values * < 0.05; ** < 0.01, *** < 0.001 determined significant. ns = not significant. n = 5-10 independent experiment sets per condition. For neurite length analysis 383-615 cells were measured per condition, from 5 independent experiment sets.

(Figure 3.4 E), in untreated cells or ethanol treated cells. Thus, although the ethanol vehicle control does not affect overall MN survival or the number of neurites per neuron, it does cause an increase in mean and mean longest neurite length, suggesting that ethanol itself may cause aberrant subcellular interactions that alter neurite growth. Thus, for all subsequent experiments other than cell survival, deoxysphinganine treatments were compared exclusively to the vehicle control, rather than the untreated group.

3.3.3 The effect of deoxysphingoid bases on mouse motor neuron survival

Previous studies have shown that the atypical deoxysphinganines have deleterious effects on immature primary chick MNs when treated within the first 24 h of plating (Penno et al., 2010). Therefore, initially the effect of treatment of immature mouse MNs with sphinganines at 1 day *in vitro* (DIV), was first examined (treatment schematic shown in Figure 3.5 A). The effect of these treatments on MN survival was assessed by immunostaining for the neuronal marker β-III tubulin and co-staining for the nuclear marker DAPI.

MN cultures were treated with either vehicle, Sp, DSp or DMSp at 1 DIV for 24 h, as indicated in the schematic in Figure 3.5 A. Typical examples of these MN cultures are shown in Figure 3.5 B-E. The effect of increasing concentrations of sphinganines on MN survival was determined by counting the number of β-III tubulin positive cells in each culture, and expressing the data as a percentage of MN survival in control cultures. As can be seen in Figure 3.5 F, in immature cultures treated at 1 DIV for only 24 h, treatment with increasing concentrations of DSp and DMSp resulted in a corresponding decrease in MN survival. Treatment with 1 µM DSp reduced MN survival to 54 ± 12% (P = 0.0137). Similarly, following 1 µM DMSp treatment MN survival was reduced to 58 ± 8% (P = 0.002). Interestingly, treatment of these immature MN cultures with the normal enzymatic product, Sp, was also found to be toxic, but only at high

Figure 3.5

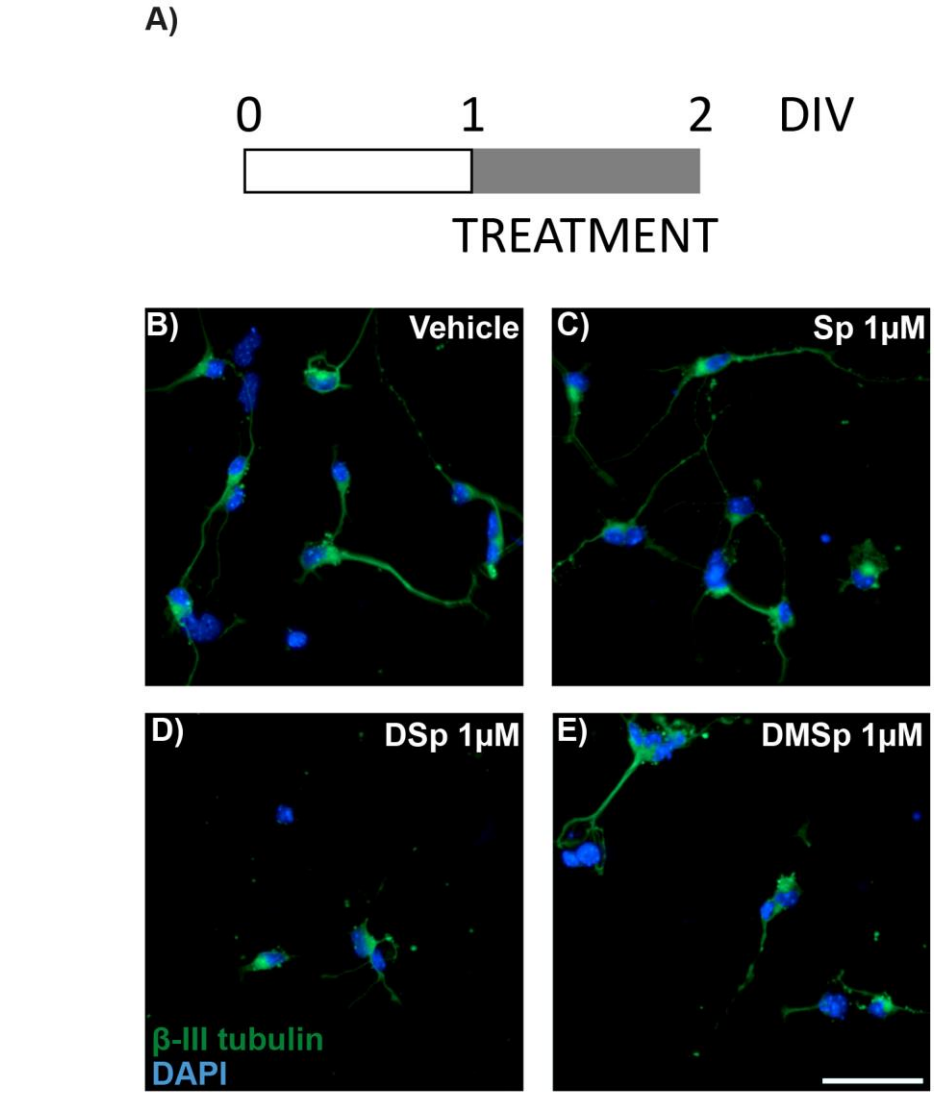
A)
0
1
2
DIV
TREATMENT
B)
Vehicle
C)
Sp 1μM
D)
DSp 1μM
E)
DMSp 1μM
β-III tubulin
DAPI
F)
Sp
DSp
DMSp
% motor neuron survival
150
100
50
0
0.1 μM
0.5 μM
1 μM
2 μM
*
*
*
**
*

Figure 3.5: 24 h treatment with deoxysphingoid bases causes a dose-dependent reduction in primary motor neuron survival

A) Schematic showing the treatment regime; dissociated MNs were grown for 24 h before being treated with sphinganines or ethanol as a vehicle control. MNs were fixed and stained for analysis 24 h following treatment, after 2 DIV. **B-E)** Examples of primary MNs treated at 24 h and fixed and immunostained at 2 DIV for DAPI (blue) and β-III tubulin (green). **F)** Quantification of MN survival following treatment with different doses of sphinganines, displayed as a percentage relative to control cultures (dotted line). Displayed data represent the mean ± SEM. For statistical comparison, each treatment group was compared to control using the one-sample Wilcoxon signed rank test. *P* values * < 0.05; ** < 0.01, *** < 0.001 were deemed significant. Scale bar = 50 µm. n = 5-11 independent experiment per condition.

concentrations, of 2 µM and above. Thus, following 24 h treatment with 2 µM Sp, 49 ± 5% of MNs survived (P = 0.0312). However, Sp treatment was less toxic than treatment with 2 µM DSp or DMSp, in which only 27 ± 15% (P = 0.0312) and 35% ± 12% (P = 0.0312) of MNs survived, respectively.

Not surprisingly, prolonged exposure of immature MNs to deoxysphinganines had even more deleterious effects on MN survival. In these experiments, cultures were treated with sphinganines at 1 DIV for 6 days, as shown by the treatment schematic in Figure 3.6 A. The representative images shown in Figure 3.6 B-E illustrate that long-term treatment with either DSp or DMSp resulted in a significant loss of MNs, as well as non-neuronal cells such as fibroblasts. As observed following 24 h treatment with deoxysphinganines (Figure 3.5), there was also a dose-dependent decrease in MN survival in response to DSp and DMSp treatment over 6 days (Figure 3.6 F). In cultures treated with 1 µM DSp, only 15 ± 9% MNs survived (P = 0.0312), and following 1 µM DMSp treatment, only 18 ± 8% of MNs survived (P = 0.0312). Prolonged treatment of immature cultures with the normal enzymatic product Sp also had a toxic effect, but again to a lesser extent than either DSp or DMSp, so that following treatment with 1 µM Sp 80 ± 8% of MNs survived (P = 0.0312).

Since MNs at 1 DIV are quite immature, the effect of sphinganine treatments in more mature MN cultures, at 5 DIV, was also examined, as illustrated by the schematic shown in Figure 3.7 A. In these experiments, the cultures were also treated for a longer period of time, for 4 days. Representative images of the cultures are shown in Figure 3.7 B-E. In these experiments, DSp and DMSp had no toxic effects on MN survival at lower concentrations (0.1-0.5 µM). However, at concentrations of 1 µM and above, DSp and DMSp were found to have toxic effects (Figure 3.7 F). Thus, following treatment with 1 µM DSp or DMSp 34 ± 9% (P = 0.0312) and 43 ± 13% (P = 0.0312) of MNs survived, respectively. However, unlike immature MNs, when these more mature MNs were treated with the typical enzyme product, Sp, there was no loss of MNs. Following treatment with 1 µM Sp, 105 ± 10% MNs survived (P = 0.8438).

Figure 3.6

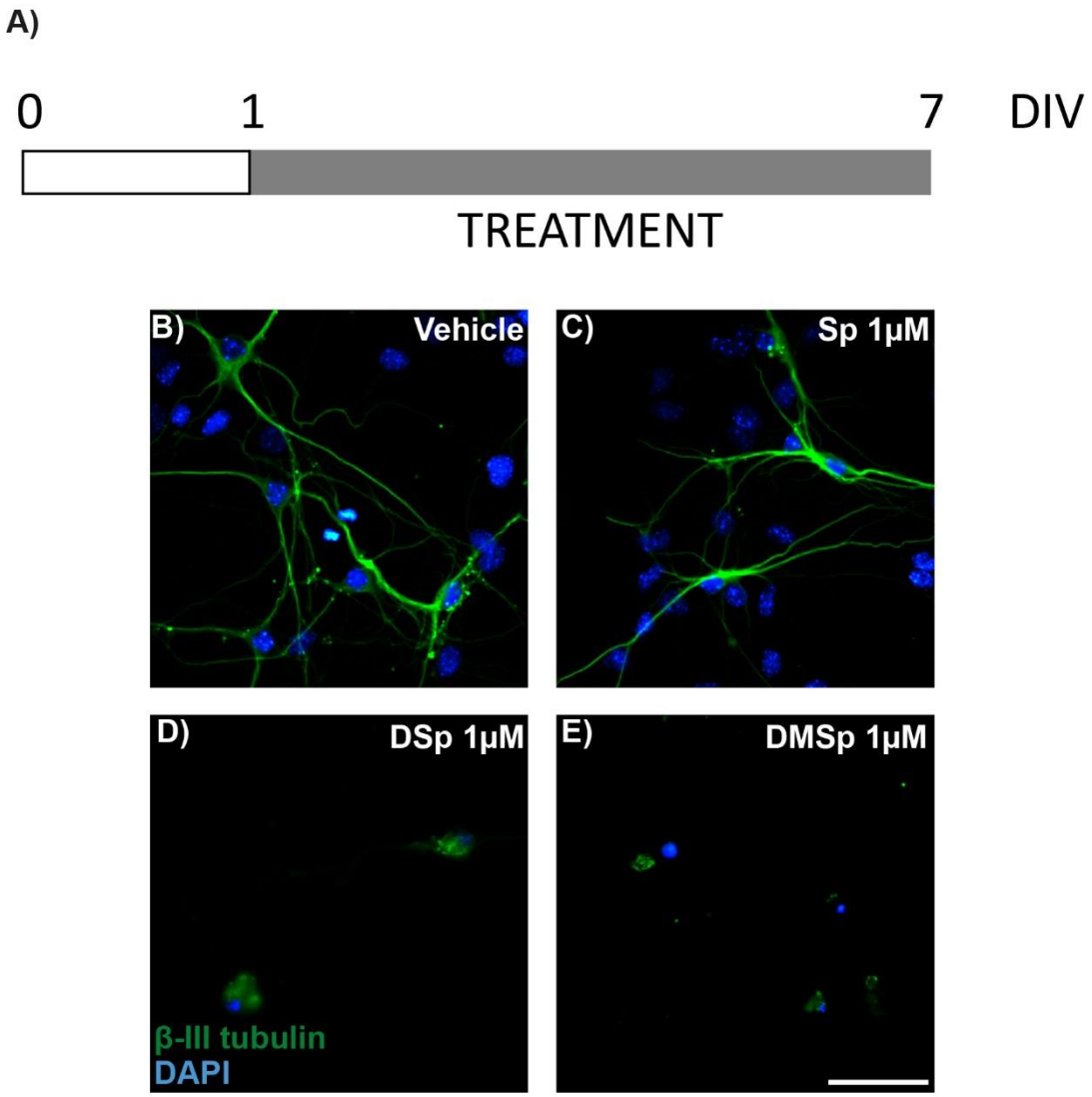
A)
0
1
7
DIV
TREATMENT
B)
Vehicle
C)
Sp 1μM
D)
DSp 1μM
E)
DMSp 1μM
β-III tubulin
DAPI
F)
Sp
DSp
DMSp
% motor neuron survival
150
100
50
0
0.1 μM
0.5 μM
1 μM
2 μM
*
*
*

Figure 3.6: Long term treatment with deoxysphingoid bases causes a dose-dependent reduction in primary motor neuron survival

A) Schematic showing the treatment regime; dissociated MNs were grown for 24 h before being treated with sphinganines or ethanol as a vehicle control. MNs were fixed and stained for analysis after 7 DIV. **B-E)** Examples for primary MNs treated at 24 h and fixed and immunostained at 7 DIV, for DAPI (blue) and β-III tubulin (green). **F)** Quantification of MN survival following treatment with different doses of sphinganines, displayed as a percentage relative to control cultures (dotted line). Displayed data represent the mean ± SEM. For statistical comparison, each treatment group was compared to control using the one-sample Wilcoxon signed rank test. *P* values * < 0.05; ** < 0.01, *** < 0.001. Scale bar = 50 µm. n = 5-7 independent experiment sets per condition.

Figure 3.7

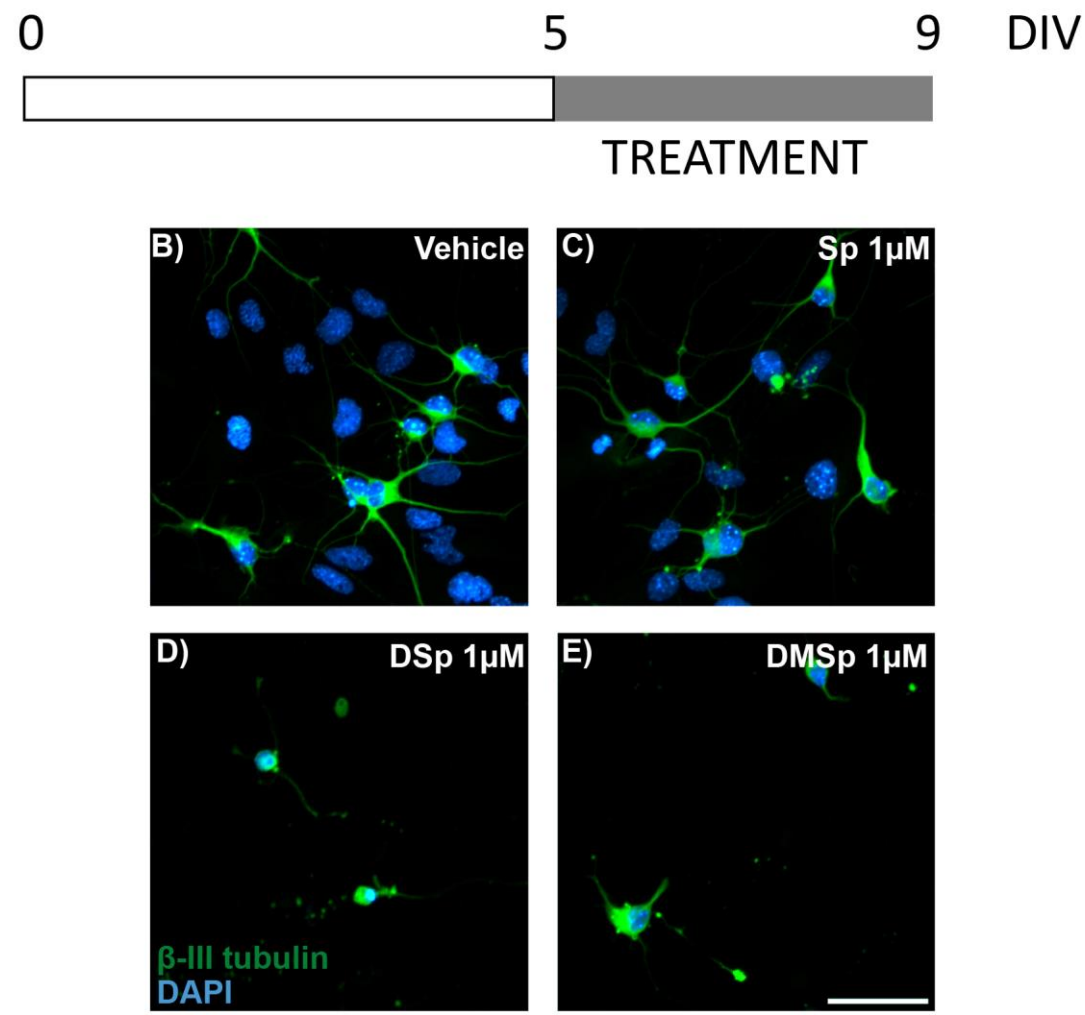
A)
0
5
9
DIV
TREATMENT
B)
Vehicle
C)
Sp 1μM
D)
DSp 1μM
E)
DMSp 1μM
β-III tubulin
DAPI
F)
Sp
DSp
DMSp
% motor neuron survival
150
100
50
0
0.1 μM
0.5 μM
1 μM
2 μM
*
*

Figure 3.7: Treatment with deoxysphingoid bases causes a dose-dependent reduction in mature primary motor neuron survival

A) Schematic showing the treatment regime; dissociated MNs were grown for 5 days before being treated with sphinganines or ethanol as a vehicle control. MNs were fixed and stained for analysis after 9 DIV. **B-E)** Examples for primary MNs treated at 5 DIV and fixed and immunostained at 9 DIV, for DAPI (blue) and β-III tubulin (green). **F)** Quantification of MN survival following treatment with different doses of sphinganines, displayed as a percentage relative to control cultures (dotted line). Displayed data represent the mean ± SEM. For statistical comparison, each treatment group was compared to control using the one-sample Wilcoxon signed rank test. *P* values * < 0.05; ** < 0.01, *** < 0.001. Scale bar = 50 µm. n = 4-6 independent experiment sets per condition.

In summary, these results show that the abnormal enzyme products DSp and DMSp, have a dose-dependent toxicity in cultured primary MNs, and even the normal enzyme product, Sp can have toxic effects on immature primary MNs, albeit only at higher concentrations.

3.3.4 The effect of deoxysphingoid bases on neurite outgrowth in primary mouse motor neurons

In addition to cell survival, the effect of DSp and DMSp on neurite outgrowth in primary MNs was also examined. Neurite length was assessed in primary mouse MNs treated with sphinganines at 1 DIV for 24 h (fixed and immunostained at 2 DIV) as shown by the schematic in Figure 3.8 A. Figure 3.8 B-E show representative images of MN cultures and that cultures treated with DSp and DMSp had less extensive neurite arborisation when compared to vehicle-treated and Sp-treated cultures. Neurite outgrowth was quantified by measuring neurite length and counting the number of neurites per neuron. The criteria for assessment is illustrated in Figure 3.8 B and the data for neurite assessment is summarised in Figure 3.9.

As shown in Figure 3.9 A, there was a decrease in the mean neurite length in MNs treated with increasing concentrations of Sp, DSp and DMSp. Indeed, treatment at a concentration as low as 0.1 µM DSp significantly decreased mean neurite length, from 30.4 ± 1.3 µm in vehicle controls (indicated by the dotted line) to 23.7 ± 1.4 µm in DSp treated cells ($P < 0.05$). DMSp was not as toxic as DSp, and there was no significant decrease in neurite length in MNs treated with 0.1 µM DMSp. However, at higher concentrations DMSp also reduced neurite length, although not as dramatically as DSp. Thus, cells treated with 1 µM DMSp had a mean neurite length of 27.2 ± 2.0 µm ($P < 0.001$), compared to 12.9 ± 1.1 µm in DSp treated cells ($P < 0.001$). Treatment with the typical enzyme product, Sp had moderate toxic effects at the highest concentration tested; treatment with 2 µM Sp resulted in a slight but significant decrease in mean MN neurite length to 28.5 ± 2.3 µm, compared to 30.4 ± 1.3 µm in the vehicle control ($P < 0.01$).

Figure 3.8

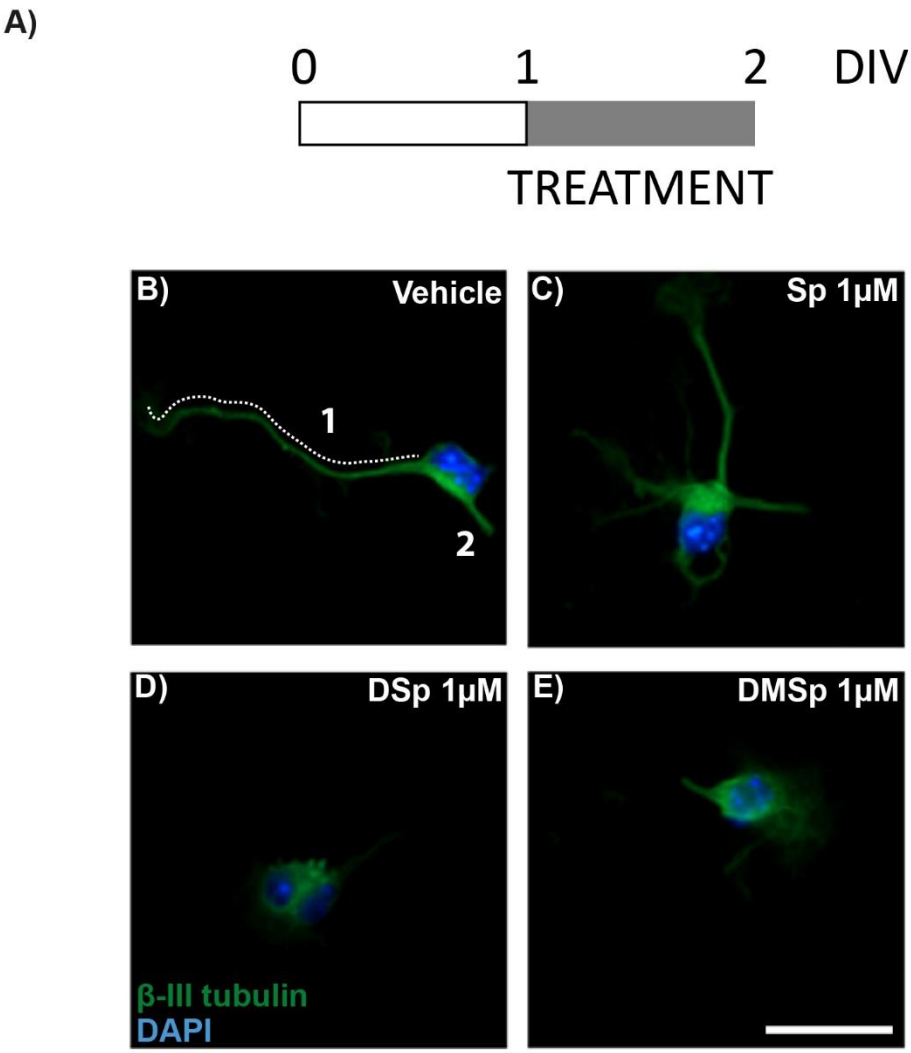

Figure 3.8: Treatment with deoxysphingoid bases causes reduced neurite outgrowth in primary motor neurons

A) Schematic showing the treatment regime; dissociated MNs were grown for 24 h before being treated with sphinganines or ethanol as a vehicle control. MNs were fixed and stained for analysis 24 h following treatment, after 2 DIV. **B-E)** Cells were stained for DAPI (blue) and β-III tubulin (green). The number of neurites per neuron was counted as indicated and neurite length was measured by tracing neurites, as indicated by the dotted line in B). Scale bar = 25 μm.

Figure 3.9

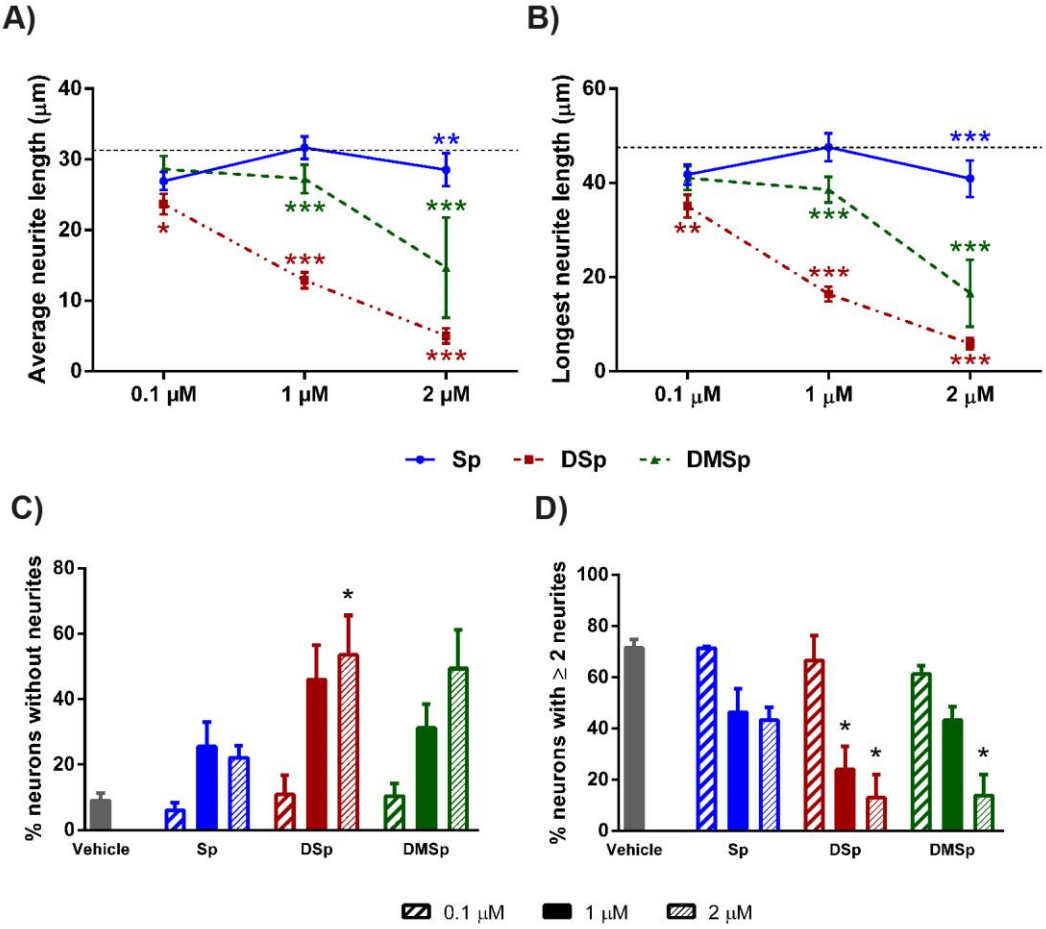
A)
B)
Average neurite length (µm)
Longest neurite length (µm)
0.1 µM
1 µM
2 µM
Sp
DSp
DMSp
C)
D)
% neurons without neurites
% neurons with ≥ 2 neurites
Vehicle
0.1 µM
1 µM
2 µM

Figure 3.9: Treatment with deoxysphingoid bases causes a dose-dependent reduction in neurite outgrowth in primary motor neurons

Primary MNs were grown for 24 h before being treated with sphinganines or an ethanol vehicle control. Cells were stained for DAPI (blue) and β-III tubulin (green). The number of neurites per neuron was counted and neurite length was measured by tracing neurites, as indicated in Figure 3.8. **A)** Neurite length in MNs following treatment with increasing concentrations of sphinganines. **B)** Longest neurite length in MNs following treatment with increasing concentrations of sphinganines. In A) and B) the black dotted line indicates the mean or mean longest neurite length of MNs treated with an ethanol vehicle control. **C)** Percentage of MNs with no neurite outgrowth following treatment with the sphinganines at a range of concentrations. **D)** Percentage of MNs with 2 or more neurites following treatment with the sphinganines at a range of concentrations. Displayed data represent the mean ± SEM. For statistical comparison, each treatment group was compared to control using the Kruskal-Wallis and Dunn's multiple comparisons tests. *P* values * < 0.05; ** < 0.01, *** < 0.001. n = 18-383 cells per condition, from 3-5 independent experiment sets.

A similar pattern was observed when the longest neurite length per MN was determined (Figure 3.9 B). DSp treatment caused the greatest reduction in longest neurite length at all concentrations tested; DMSp also reduced the length of the longest neurite, but to a lesser extent than DSp. Even Sp treatment showed a moderate, but significant, effect on the longest neurite length, at the highest concentration tested (2 µM, $P < 0.001$).

The number of neurites per MN were also counted, as an indication of neuronal maturation (Figure 3.9 C and D). Following treatment with increasing concentrations (0.1 µM – 2 µM) of DSp or DMSp, there was an increase in the number of neurons with no neurites at all and a decrease in neurons with 2 or more neurites, indicating that DSp and DMSp treatments have detrimental effects on neuron complexity. With 1 µM DSp treatment, 46 ± 10% of MNs had no neurites and 24 ± 9% of MNs had 2 or more neurites ($P < 0.05$), compared to vehicle treated cultures in which only 9 ± 2% of MNs had no neurites, and 72 ± 3% had a more complex dendritic arborisation pattern, with 2 or more neurites. DMSp was less toxic than DSp, so that in cultures treated with 1 µM DMSp 31 ± 7% of MNs had no neurites, and 43 ± 5% had 2 or more neurites. Treatment with Sp resulted in a moderate increase in the number of MNs with no neurites, (at 1 µM, 25 ± 8%) and a decrease in MNs with 2 or more neurites (at 1 µM, 46 ± 9%).

The results summarised in Figure 3.9 demonstrate that treatments with DSp and DMSp cause a dose-dependent reduction in neurite outgrowth in primary MNs, manifesting both as a decrease in neurite length and as a decrease in the number of neurite projections. In line with the cell survival studies (Figures 3.5 and 3.6), treatment with the typical SPT enzymatic product, Sp, also demonstrates toxicity, albeit to a far lesser extent than DSp and DMSp.

3.4 Discussion

The results in this Chapter show that treatments with deoxysphinganines, which are the specific products of mutant SPT, are toxic to primary mammalian DRG and MNs. Application of DSp and DMSp to primary MN cultures caused a dose-dependent decrease in cell survival in all three of the treatment paradigms tested.

Toxicity manifested as early as 24 h after treatment and, as expected, long term (6 day) treatment caused a more severe decrease in cell survival, demonstrating a duration-dependent toxicity pattern, as well as dose-dependency. Notably, toxicity was non-selective, affecting both neuronal and non-neuronal cells in these mixed cultures, despite the fact that HSN-1 is considered solely a disease of the nervous system. It has previously been suggested that *in vivo*, deoxysphingoid bases can be degraded in other tissues by the action of an unknown catabolic enzyme, which may not be expressed, or be expressed at lower levels, in neuronal tissue (Garofalo et al., 2011; Alecu et al., 2016a); this may provide explanation for the specific neuropathy-inducing effect of the deoxysphingoid bases in HSN-1 patients, despite non-selectivity in this *in vitro* system.

In the initial models tested in this study, MNs were treated at 1 DIV, in line with previous studies (Penno et al., 2010). As MNs are particularly vulnerable at this stage in culture, more mature MNs were also examined in this Chapter, whereby MNs were treated at 5 DIV, when primary cultures are generally considered mature and express key characteristics of MNs such as glutamate receptors (Van Den Bosch et al., 2000). However, even in these more mature and developed MNs, which have an extensive neuritic arborisation, DSp and DMSp were toxic at concentrations of 1 µM and above. Notably, although the typical enzymatic product, Sp, was shown to be moderately toxic in more immature MNs, these more mature MNs demonstrated resistance to Sp mediated toxicity.

Cultures treated with the vehicle, ethanol, showed no effect on cell survival in any of the three treatment paradigms tested. However, ethanol did cause an increase in neurite outgrowth, specifically neurite length, suggesting that ethanol may interact with subcellular signalling pathways. For this reason, in all following experiments in this and subsequent Chapters, sphinganine treatments were compared to the vehicle control rather than the untreated group.

Analysis of neurite length revealed that there was a dose-dependent reduction in the mean neurite length and the longest neurite length in MNs in response to treatment with all three sphinganines. In line with previous studies (Penno et al.,

2010), DSp had a more toxic effect on neurite length than DMSp, yet even treatment with the typical enzyme product, Sp, showed a small but significant decrease in neurite length when dosed at high concentrations. In this short-term treatment model, it is not possible to conclude whether the reduction in neurite length was due to retraction or to an inhibition of growth. The finding that treatment with deoxysphinganines at such an early neuronal age results in such severe toxicity suggests that in this model, deoxysphingoid bases cause an inhibition of neurite outgrowth rather than retraction of existing ones.

As a measure of neuron complexity and maturation the number of neurites per a neuron was also measured. Following treatment with deoxysphingoid bases a dose-dependent decrease in the number of neurites per MN was observed. Overall, neurite outgrowth assays suggest that DSp toxicity occurs more rapidly than DMSp, but that with time or increased concentration, DMSp may be as toxic as DSp to MNs.

Baseline plasma levels of deoxysphingoid bases in HSN-1 patients are reported to be between 0.18 and 2.88 μM in the cohort of patients at the National Hospital for Neurology and Neurosurgery (United Kingdom, Dr Umaiyal Kugathasan, personal communication). Therefore, in this study most of the experiments were conducted within this concentration range. Using these concentrations, the level of toxicity observed in this *in vitro* model of HSN-1 is significant, with over 40% of cells dying after just 1 day of treatment and yet, in patients a slowly progressing neuropathy is observed. However, although the primary embryonic MNs used in these experiments may be particularly vulnerable to toxicity, it could also be speculated that *in vivo* in patients, the protein environment in blood plasma may dampen the toxic effects of deoxsphingoid bases- indeed in blood, deoxysphingoid bases are mainly transported on LDL and VLDL and may be complexed with other proteins (Bertea et al., 2010). Alternatively, the blood plasma may act as a “dumping ground” for deoxysphingoid bases, so that the concentration measured in patients may be particularly high compared to subcellular or cerebrospinal fluid (CSF) concentrations (deoxysphingoid base concentrations have not been measured in the CSF).

3.5 Conclusions

The results of this Chapter clearly demonstrate that DSp and DMSp treatments are neurotoxic to cultured mammalian DRG neurons and MNs, manifesting as both neuronal death and decreased neurite outgrowth. In order to expand the study further and identify potential targets for therapeutic intervention, I next investigated the mechanism underlying the toxicity of the exogenously applied deoxysphingoid bases in this model of HSN-1.

Chapter 4. Exploring the pathomechanisms underlying exogenous deoxysphingoid base neurotoxicity in primary neurons

4.1 Introduction

In Chapter 3 of this Thesis it was established that exogenous application of the deoxysphingoid bases, DSp and DMSp, is toxic to primary motor and sensory neurons and causes a reduction in cell survival and a decrease in neurite outgrowth. However, the mechanisms underlying the neurotoxic effects of deoxysphingoid bases have not been fully explored, particularly in the two cell types prominently affected in HSN-1, peripheral motor and sensory neurons.

4.1.1 Proposed pathomechanisms underlying deoxysphingoid base cytotoxicity

A few studies have examined the molecular targets of deoxysphingoid bases, primarily in cell lines (Cuadros et al., 2000; Salcedo et al., 2007; Gable et al., 2010; Alecu et al., 2016b). For example, DSp has been shown to activate protein kinase C as well as caspase-dependent apoptosis via activation of caspases 3 and 12 (Salcedo et al., 2007). DSp has also been shown to cause the disassembly of actin fibres, which could be prevented by activation of the small GTP-binding protein Rho (Cuadros et al., 2000). Exogenous application of DSp to other cell lines resulted in an upregulation of the ER stress markers GADD153 (Gable et al., 2010) and spliced X-box binding protein 1 (XBP1, Alecu et al., 2016b). In addition to showing that DSp treatment of mouse embryonic fibroblasts (MEFs) causes ER stress, Alecu et al. (2016b) also showed that DSp first localises to mitochondria, and subsequently accumulates in the ER. Mitochondrial fragmentation, a reduction in cellular ATP levels, depleted oxygen consumption rate and, ultimately, a loss of mitochondrial cristae were also observed in these cells (Alecu et al., 2016b). Notably, glycolysis did not contribute to the changes in overall cellular ATP levels (Alecu et al., 2016b). In another study using MEF cells, DSp application was found to increase phosphorylated p38 mitogen-activated protein kinases (MAPK) and p21 levels (Sayano et al., 2016).

Only a few studies have examined deoxysphingoid base targets in neuronal cells (Alecu et al., 2016b; Guntert et al., 2016). Following on from their study of MEF cells described above, Alecu et al. (2016b) demonstrated that exogenous application of DSp to primary DRG cells resulted in mitochondrial swelling. In addition, DSp has been shown to not only decrease mitochondrial activity in cortical neurons, but also cause changes in numerous proteins associated with cytoskeletal dynamics (Guntert et al., 2016). This includes downregulation of Rac1 and RhoA (both members of the Rho family of GTPases) and insulin receptor substrate 53 (IRSp53, a target of Rho GTPases) and an upregulation of phosphorylated ezrin (Guntert et al., 2016). This finding is in agreement with those of Jun et al. (2015) in primary DRG cells from the SPTLC1^{C133W} transgenic mouse which showed upregulation of phosphorylated ezrin-radixin-moesin (ERM) at neuronal growth cones. Guntert et al. (2016) also found that DSp treatment resulted in an increase in cleavage of p35 to p25 and a downregulation of post-synaptic density protein 95 (PSD-95), likely to be the result of aberrant NMDA receptor activity, since there was also a downregulation of two subunits of the NMDA receptor (GluN2A and GluN2B). Furthermore, DSp application caused increased current through the NMDA receptor (Guntert et al., 2016).

Interestingly, many of these pathological effects of DSp treatment could be rescued by co-treatment with fumonisin B1, which inhibits ceramide synthase (CerS) activity, the enzyme catalysing Sp to dihydroceramide (or DSp to deoxydihydroceramide). This indicates it is a metabolite downstream of DSp and DMSp that is cytotoxic and which has aberrant intracellular activity (Alecu et al., 2016b; Guntert et al., 2016).

4.1.2 Ca^{2+} handling abnormalities and mitochondrial dysfunction in neurodegenerative diseases

Ca^{2+} plays a major and ubiquitous role in mediating signals from extracellular and intracellular sources. Ca^{2+} dyshomeostasis has been reported in two major diseases of the peripheral nervous system: neuropathic pain and diabetic polyneuropathy (Fernyhough and Calcutt, 2010), the symptoms of which clinically overlap with HSN-1. Indeed, Ca^{2+} handling abnormalities have been widely

implicated in neurodegenerative diseases in general (Pchitskaya et al., 2017). Moreover, Ca^{2+} in the ER is closely linked to ER stress and the unfolded protein response (UPR; Stutzmann and Mattson, 2011), another common hallmark of neurodegeneration (Lindholm et al., 2006; Hetz and Mollereau, 2014).

One reason that mitochondria, the major ATP generator of the cell, may be implicated in neurodegenerative disease is the high energy requirement of neuronal cells (Wallace et al., 2010). Indeed, mutations in genes directly associated with mitochondria, such as mitofusin-2 and OPA1, are causative for CMT2A and optic neuropathy type 1, respectively (Wallace et al., 2010).

Since Ca^{2+} handling, mitochondrial function and ER stress are closely interlinked (Stutzmann and Mattson, 2011) and have each been implicated in neurodegeneration as well as peripheral nerve disorders, all three of these elements of normal cell signalling were investigated in this Chapter as potential mediators of deoxysphingoid base toxicity.

4.2 Aims of this Chapter

The aims of this Chapter were to explore the principle targets of deoxysphingoid bases in primary motor and sensory neurons in a bid to uncover the underlying pathomechanisms that ultimately lead to the neuronal death reported in Chapter 3.

4.3 Results

Having established that deoxysphinganine treatments are toxic to mammalian neurons (Chapter 3, Sections 3.3.3 and 3.3.4), the potential mechanisms underlying the potent neurotoxicity of these abnormal SPT enzyme products were next explored. SPT is an ER membrane protein and it is well known that the ER plays a major role in cellular Ca^{2+} homeostasis. Since changes in intracellular Ca^{2+} levels are an important early indicator of cell stress (Trump and Berezesky, 1995; Clapham, 1995; Mattson, 2000), the ratiometric Ca^{2+} binding dye fura-2 was used to examine intracellular Ca^{2+} in primary neurons treated with the deoxysphinganines (Grynkiewicz et al., 1985). Fura-2 can be excited by two

different wavelengths depending on whether it is Ca^{2+} bound (340 nm) or Ca^{2+} free (380 nm; Grynkiewicz et al., 1985). The intensity of emitted light following excitation at each of these wavelengths allows the generation of a ratio, which is used in the following experiments as an arbitrary measure of Ca^{2+} concentration. Fura-2 ratios were measured from defined regions of interest in the soma of cells with neurite outgrowths, clearly distinguishable as the neuronal cells in the mixed cultures (see example in Figure 4.1).

4.3.1 Chronic treatment with deoxysphinganine elevates cytosolic Ca^{2+} in motor neurons

Primary MNs were grown to 1 DIV before treatment with deoxysphinganines for 4 days. This relatively long term treatment with deoxysphinganines was found to result in cell death (Chapter 3, Section 3.3.3) and this is reflected by elevated cytosolic Ca^{2+} concentrations, as can be seen in Figure 4.2 A. Thus, there was an increase in cytosolic Ca^{2+} concentration, from 0.59 $\pm$ 0.01 a.u. in vehicle treated MNs to 0.95 $\pm$ 0.08 and 0.87 $\pm$ 0.09 a.u. following 1 μM treatment with DSp or DMSp, respectively ($P < 0.001$). In keeping with the results presented in Chapter 3 (Sections 3.3.3 and 3.3.4) showing that Sp, the normal SPT enzyme product, can be toxic to immature MNs, treatment of primary MNs at 1 DIV for 4 days with Sp, also caused a small but significant elevation in mean cytosolic Ca^{2+}, to 0.66 $\pm$ 0.02 ($P < 0.05$).

Since immature MNs (1 DIV) die rapidly upon exposure to deoxysphinganines, within 24 h (Chapter 3, Section 3.3.3), it is difficult to dissect the mechanisms underlying cytotoxicity in these cells using this experimental protocol. Therefore, in the following experiments, designed to examine the mechanisms underlying deoxysphinganine neurotoxicity, more mature MNs (≥ 5 DIV) and DRG neurons (≥ 3 DIV) were examined and the treatment paradigm was more acute, shortened to just 2 h (unless otherwise stated). Importantly, mature MNs do not show the increased vulnerability to the normal enzyme product, Sp, observed in immature MNs (Chapter 3, Sections 3.3.3 and 3.3.4).

Figure 4.1

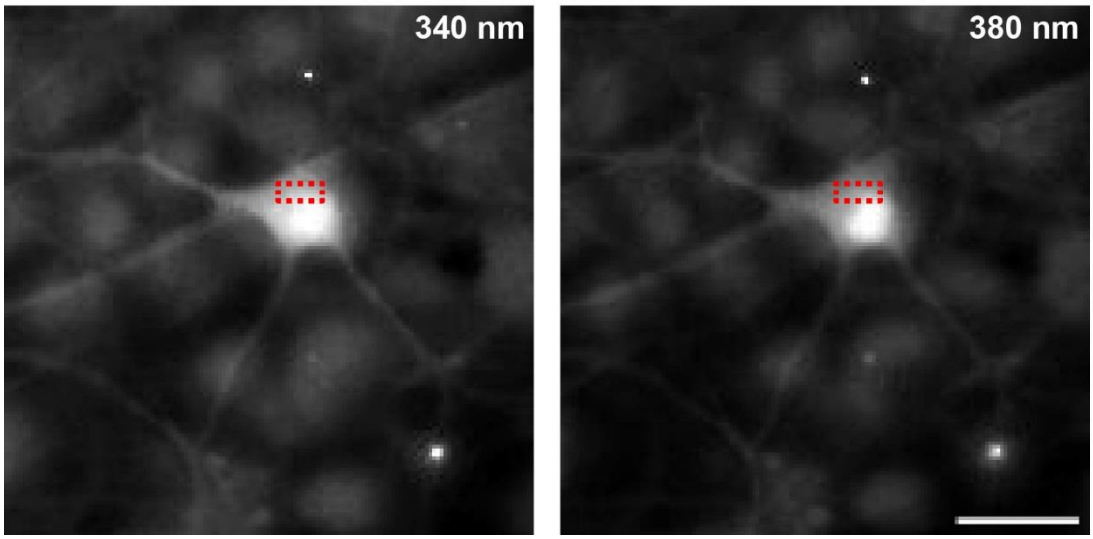

Figure 4.1: Measurement of cytosolic Ca^{2+} in primary neurons, using fura-2

Cytosolic Ca^{2+} is measured in defined regions of interest (red dotted line) in the phase-bright soma of cells with neurite outgrowths, clearly distinguishable as the neuronal cells in the mixed cultures. Fura-2 intensity is measured following excitation at 340 nm (Ca^{2+}-bound) and 380 nm (Ca^{2+}-free) wavelengths and a ratio calculated as a readout measure of cytosolic Ca^{2+} concentration. Scale bar = 20 µm.

Figure 4.2

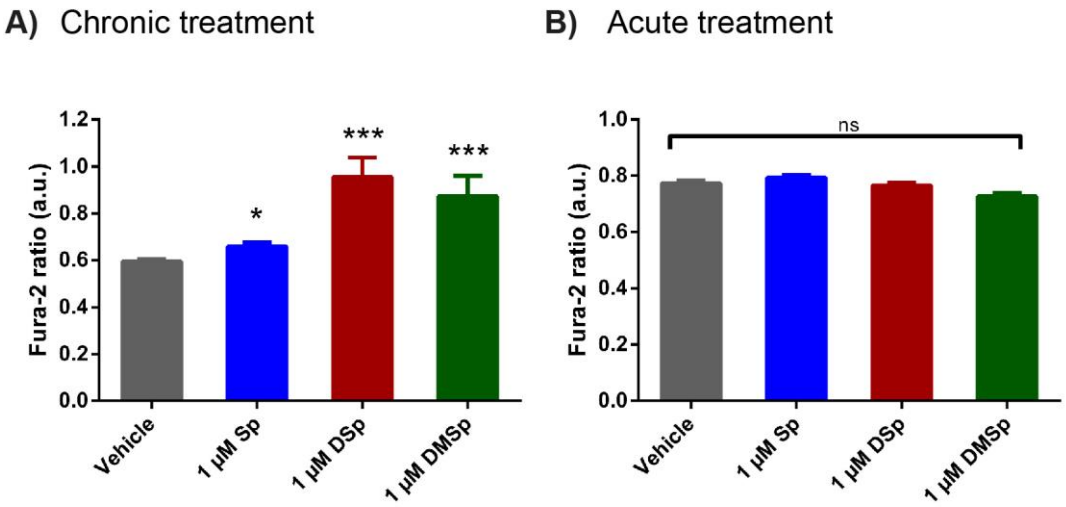

Figure 4.2: Chronic, but not acute, deoxysphinganine treatments cause elevations in cytosolic Ca^{2+} in motor neurons

Bar charts show the mean fura-2 ratio, representing cytosolic Ca^{2+} concentration. **A)** At 1 DIV, MNs were treated with either vehicle control (ethanol) or the sphinganines and imaged 4 days later, at 5 DIV. Mean ratios were established from 24-83 cells per condition, from 4-7 independent experiments. **B)** At 5-8 DIV, MNs were treated with either vehicle control or the sphinganines, 2 h prior to live cell imaging with fura-2. Mean ratios were established from 107-134 cells per condition, from 7-8 independent experiments. Error bars represent SEM. For statistical comparison, each treatment group was compared to vehicle control using the Kruskal-Wallis and Dunn's multiple comparisons tests. *P* values * < 0.05; ** < 0.01, *** < 0.001. ns = not significant.

4.3.2 Short-term treatment with deoxysphinganine does not affect cytosolic Ca^{2+} in motor neurons

Mature MNs (≥ 5 DIV) were treated acutely for 2 h with 1 µM deoxysphinganines, and the effects on baseline cytosolic Ca^{2+} levels determined, as described above. Following 2 h treatment with either DSp or DMSp, there was no significant difference in cytosolic Ca^{2+} levels (Figure 4.2 B; fura-2 ratio: 0.77 ± 0.01 in DSp treated cells and 0.73 ± 0.01 in DMSp treated cells) compared to vehicle-treated cells (ratio: 0.77 ± 0.01). These findings indicate that short-term treatment with deoxysphinganines does not alter cytosolic Ca^{2+} homeostasis and these MNs appear largely healthy.

4.3.3 Deoxysphinganines cause rapid depletion of ER Ca^{2+} in motor and sensory neurons

Although cytosolic Ca^{2+} levels were not altered by acute exposure to deoxysphinganines, it is possible that this reflects effective Ca^{2+} buffering by intracellular organelles, such as the ER and mitochondria. Therefore, the effects of deoxysphinganine treatments on ER Ca^{2+} were next examined. ER Ca^{2+} levels were determined by measuring the change in cytosolic Ca^{2+} following treatment with the sarco/endoplasmic reticulum Ca^{2+}-ATPase (SERCA) pump inhibitor, thapsigargin, which causes the ER to release Ca^{2+} into the cytosol (Thastrup et al., 1990; Lytton et al., 1991). As these experiments were performed in the absence of extracellular Ca^{2+}, the resulting change in cytosolic Ca^{2+} can be used to infer ER Ca^{2+}, as shown in a typical Ca^{2+} recording experiment shown in Figure 4.3.

In sensory DRG cultures treated for 2 h with deoxysphinganines, a dramatic reduction in ER Ca^{2+} compared to vehicle-treated DRG neurons was observed (Figure 4.4 A). DRG neurons treated with 1 µM DSp or DMSp displayed an inferred ER fura-2 ratio of 0.61 ± 0.14 and 0.46 ± 0.09, respectively, in contrast to vehicle-treated DRG neurons, which had an inferred ER fura-2 ratio of 1.50 ±

Figure 4.3

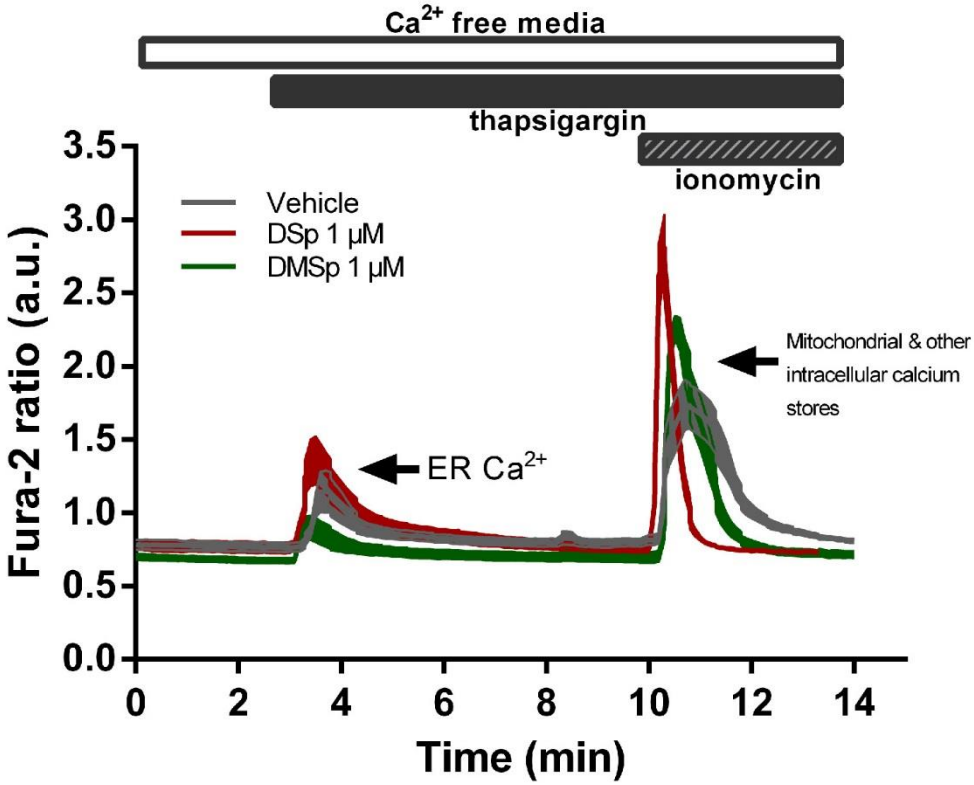

Figure 4.3: Measurement of ER and mitochondrial Ca^{2+} in primary neurons, using fura-2

A typical trace (from a motor neuron culture, mean ± SEM) indicating how thapsigargin and ionomycin were used to estimate ER and mitochondrial Ca^{2+} concentrations.

Figure 4.4

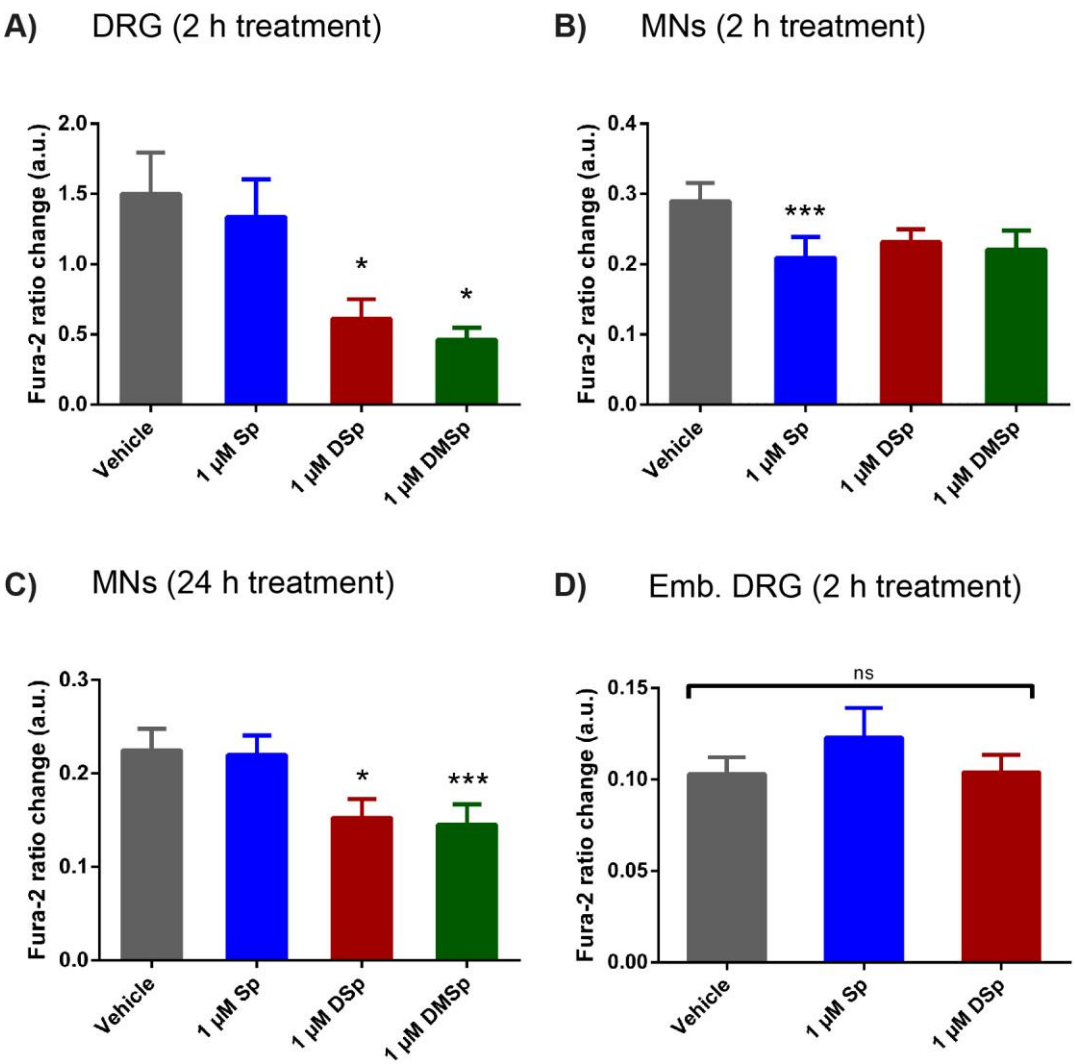
A) DRG (2 h treatment)
B) MNs (2 h treatment)
C) MNs (24 h treatment)
D) Emb. DRG (2 h treatment)
Fura-2 ratio change (a.u.)
2.0
1.5
1.0
0.5
0.0
0.4
0.3
0.2
0.1
0.15
0.10
0.05
0.00
*
***
ns
Vehicle
1 µM Sp
1 µM DSp
1 µM DMSp

Figure 4.4: Deoxysphinganines cause depletion of ER Ca^{2+} in motor and sensory neurons

Bar charts show the effect of deoxysphinganines on the mean ER Ca^{2+} levels in DRG neurons or MNs. **A)** At 3-5 DIV, DRG cultures were treated for 2 h with either vehicle control (ethanol) or the sphinganines, prior to live cell imaging. Thapsigargin was used to estimate ER Ca^{2+} and mean ER Ca^{2+} was established from 28-38 cells, from 3-4 independent experiments. **B)** At 5-8 DIV, MNs were treated with either vehicle (ethanol) or the sphinganines for 2 h, prior to live cell imaging, and as above, thapsigargin used to estimate the ER Ca^{2+}. Mean ER Ca^{2+} was established from 94-184 cells, from 11-16 independent experiments. **C)** At 6 DIV, MNs were treated with either vehicle control (ethanol) or the sphinganines for 24 h, prior to live cell imaging. Thapsigargin was used to estimate ER Ca^{2+}. Mean ER Ca^{2+} was established from 42-55 cells per condition, from 4-5 independent experiments. **D)** At 5-6 DIV, embryonic DRG cultures were treated for 2 h with either vehicle control (ethanol) or the sphinganines, prior to live cell imaging. Mean ER Ca^{2+} was established from 19-20 cells per condition, from 3 independent experiments. Error bars represent SEM. For statistical comparison, each treatment group was compared to vehicle control using the Kruskal-Wallis and Dunn's multiple comparisons tests. *P* values: * < 0.05; ** < 0.01; *** < 0.001. ns = not significant.

0.29. Intriguingly, when MN cultures were examined using the same 2 h treatment paradigm, treatment with the typical enzyme product, Sp, caused a significant decrease in ER Ca^{2+} levels, whereas the deoxysphinganines caused only non-significant reductions in ER Ca^{2+}, to 0.23 ± 0.02 and 0.22 ± 0.03 in DSp and DMSp treated cells, respectively, in comparison to 0.29 ± 0.03 in vehicle treated cells (Figure 4.4 B). However, increasing the duration of deoxysphinganine exposure from 2 h to 24 h did reveal evidence of ER Ca^{2+} depletion in MNs. Treatment of MNs with deoxysphinganines for 24 h caused a significant reduction in ER Ca^{2+}, so that in DSp and DMSp treated MNs the fura-2 ratio for ER Ca^{2+} was reduced to 0.15 ± 0.02 ($P < 0.05$ and $P < 0.01$, respectively) compared to 0.22 ± 0.02 in the vehicle treated MNs, indicative of ER stress (Figure 4.4 C).

A comparison of the results from MN and DRG cultures suggests that deoxysphinganines may induce ER stress more readily in DRG neurons than in MNs, with deoxysphinganine-induced ER stress evident in DRG neurons after 2 h treatment, yet similar depletion of ER Ca^{2+} in MNs was observed only after 24 h treatment. However, there was a clear difference between basal ER Ca^{2+} levels measured in these two cell types, so that ER Ca^{2+} was substantially higher in vehicle treated DRG neurons (1.50 ± 0.29, Figure 4.4 A) than in vehicle treated MNs (0.29 ± 0.03, Figure 4.4 B), which may allow us to detect changes in Ca^{2+} more readily in DRG neurons than in MNs. Another key difference between these two *in vitro* models is that sensory DRG neurons are harvested from wildtype mouse pups, whereas primary MNs will only survive *in vitro* if sourced from mouse embryos. Thus, ER Ca^{2+} was also explored following 2 h DSp treatment in DRG neurons harvested from mouse embryos (Figure 4.4 D). Here, no significant differences were found between DRG neurons treated with vehicle, Sp or DSp, but critically a general depletion in ER Ca^{2+} was measured in embryonic DRG neurons when compared to post-natal DRG neurons, so that in vehicle treated cultures, embryonic DRG neurons measured a very low mean ER Ca^{2+} of 0.10 ± 0.01 (Figure 4.4 D) compared to 1.50 ± 0.29 in post-natal DRG neurons (Figure 4.4 A).

4.3.4 Deoxysphinganine causes rapid ER stress in motor neurons

As well as being a major cellular store of Ca^{2+}, the ER also plays a critical role in the folding and processing of newly synthesized proteins, a process which has been shown to be Ca^{2+} dependent (Paschen and Mengesdorf, 2005). If the correct folding of proteins is perturbed, for example by a depletion of ER Ca^{2+}, an accumulation of incorrectly folded proteins can be found in the ER lumen which in turn causes the upregulation of the UPR. The UPR is characterized by a decrease in global protein synthesis and specific upregulation of ER proteins responsible for protein folding (Paschen and Mengesdorf, 2005). One such protein is the binding immunoglobulin protein (BiP), which was used in the following experiments as a marker of ER stress and the UPR (Lee, 2005).

MN cultures were grown to 5-6 DIV before being treated for 2 or 24 h with ethanol (vehicle), 1 μM Sp or 1 μM DSp. The cells were fixed and immunostained for BiP and β-III tubulin (as a pan-neuronal marker) which revealed no major changes in the localization or expression level of this UPR marker (Figure 4.5 A-F). However, western blot analysis revealed an increase in BiP expression in MN cultures treated for 2 h with DSp, compared to vehicle treated cultures or cultures treated with the normal enzyme product, Sp (Figure 4.6 A). As can be seen in the bar chart in Figure 4.6 B, there was approximately a two-fold increase in BiP expression, so that BiP expression in MN cultures treated for 2 h with DSp was 2.24 ± 0.04 compared to 1.22 ± 0.05 in vehicle treated cultures and 1.12 ± 0.15 in cultures treated with Sp for 2 h (Figure 4.6 B). Interestingly, in cultures treated for 24 h with DSp, BiP expression reduced again to levels similar to that of the vehicle treated cultures, 1.15 ± 0.39.

4.3.5 Deoxysphinganines cause rapid mitochondrial Ca^{2+} loading in motor neurons

Since mitochondria also play an important role in the regulation of intracellular Ca^{2+} in neurons, mitochondrial Ca^{2+} levels were next examined. The ratiometric dye fura-2 was used as readout measure of cytosolic Ca^{2+} and mitochondrial Ca^{2+} was then estimated using thapsigargin and the ionophore, ionomycin, in the absence of extracellular Ca^{2+}, as indicated in the experiment shown in

Figure 4.5

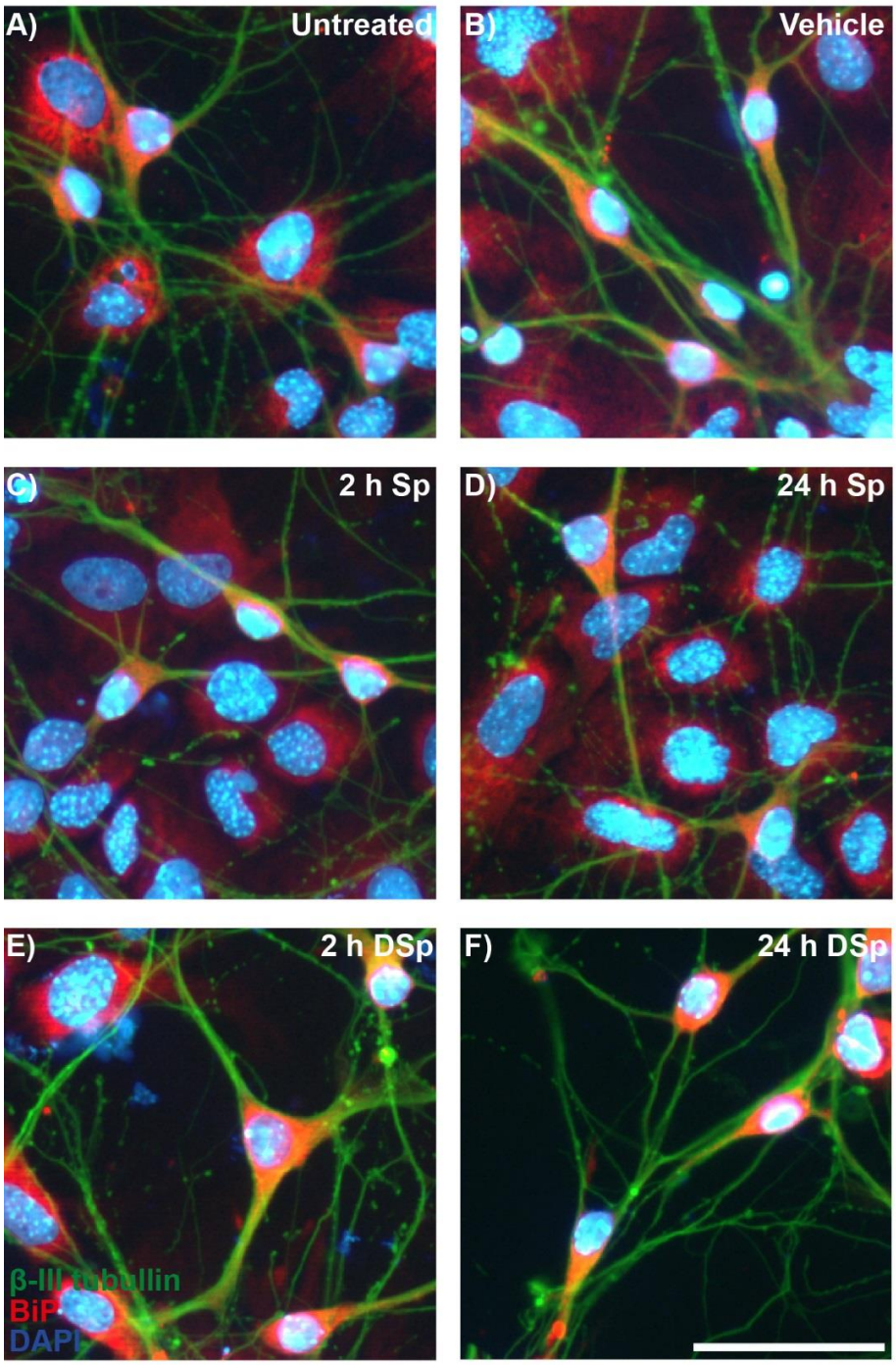

Figure 4.5: Deoxysphinganine does not cause major changes in localization of BiP in motor neurons

A-F) MN cultures were grown to 5-6 DIV before being left untreated (A), treated with an ethanol vehicle control (B), Sp for 2 h (C) or 24 h (D) or DSp for 2 h (E) or 24 h (F). Cultures were immunostained for β-III tubulin (green), BiP (red) and DAPI (blue). Scale bar = 50 µm.

Figure 4.6

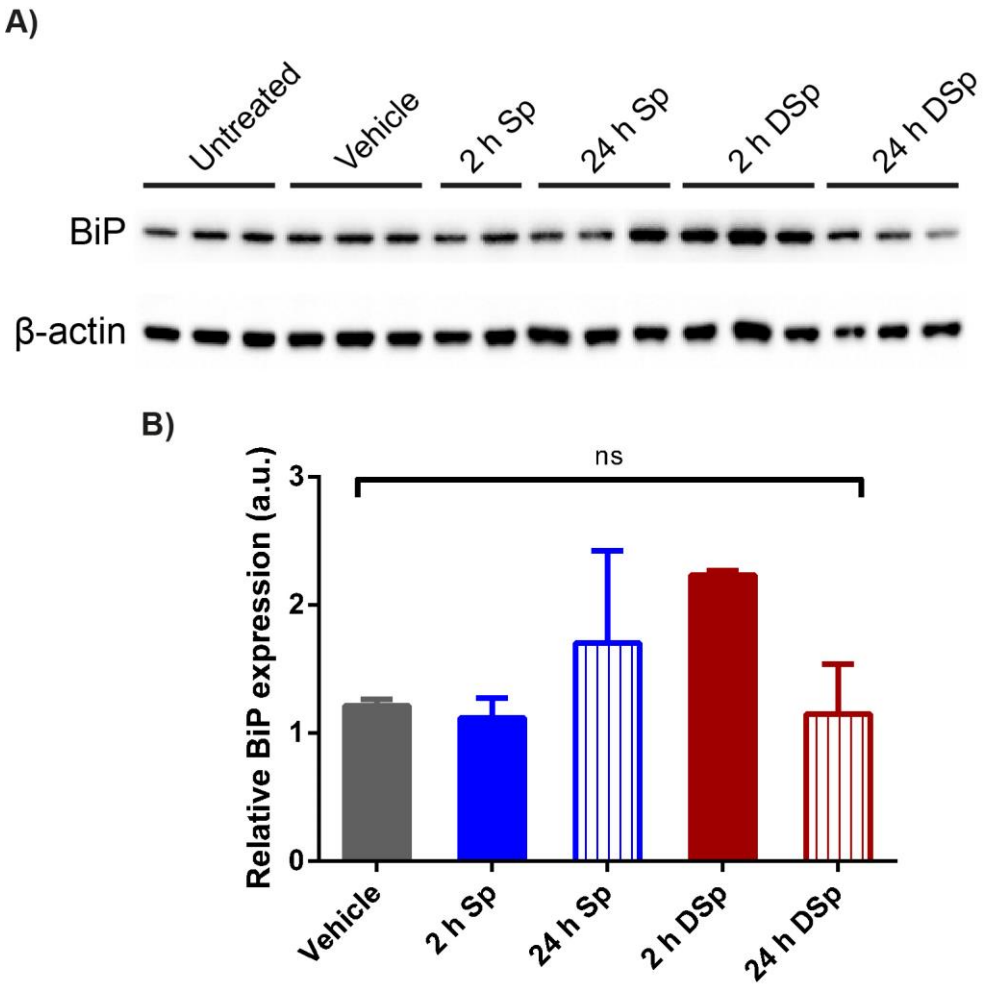

Figure 4.6: Deoxysphinganine causes rapid elevation of BiP in motor neurons

MN cultures were grown to 5-6 DIV before being either left untreated, treated with an ethanol vehicle control, Sp for 2 h or 24 h, or DSp for 2 h or 24 h. **A)** Western blot showing the expression of BiP (78 kDa) and the loading control β-actin (42 kDa) in untreated and treated MNs. **B)** The bar chart shows quantification of BiP expression, normalised to β-actin loading controls, expressed relative to mean expression measured in untreated cultures. Displayed data represent the mean ± SEM. For statistical comparison, each treatment group was compared to vehicle control using the Kruskal-Wallis and Dunn's multiple comparisons tests. *P* values: * < 0.05; ** < 0.01; *** < 0.001. ns = not significant.

Figure 4.3. This technique allows an estimation of mitochondrial Ca^{2+} to be made by calculating the difference between the fura-2 ratio before and after ionomycin addition (Hoek et al., 1995; Abramov and Duchen, 2003). However, it should be noted that although the ER contribution to the ionomycin-induced peak is largely eliminated due to advanced emptying of the ER Ca^{2+} stores with thapsigargin, it is possible that intracellular organelles distinct from the ER and the mitochondria may also provide a minor contribution of Ca^{2+}.

Treatment of DRG neurons with the sphinganines for 2 h had no effect on mitochondrial Ca^{2+} levels (Figure 4.7 A), so that in DSp-treated DRG neurons, the mean mitochondrial Ca^{2+} concentration was 1.38 ± 0.35 compared to 1.23 ± 0.19 in vehicle-treated DRG neurons. Mitochondrial Ca^{2+} was also determined in embryonic DRG, which in a similar manner to as observed in ER Ca^{2+} experiments, intrinsically displayed much lower Ca^{2+} stores, regardless of Sp or DSp treatment, so that vehicle-treated post-natal DRG neurons measured a mean mitochondrial Ca^{2+} fura-2 ratio of 1.23 ± 0.19 and vehicle-treated embryonic DRG neurons a mean mitochondrial Ca^{2+} fura-2 ratio of 0.16 ± 0.01 (Figure 4.7 A-B). Similarly, no statistically significant changes between treatment groups were revealed in embryonic DRG neurons (Figure 4.7 B).

In contrast, following 2 h treatment of MNs with the sphinganines, there was a significant elevation in mitochondrial Ca^{2+} (Figure 4.7 C). In vehicle treated MNs, the mitochondrial fura-2 ratio was 0.41 ± 0.05, but this ratio more than doubled in DSp-and DMSp-treated MNs to 1.14 ± 0.16 ($P < 0.001$) and 1.15 ± 0.14 ($P < 0.001$), respectively. A shift towards higher mitochondrial Ca^{2+} was also observed, although to a lesser extent, in Sp-treated MNs, which had a mean fura-2 ratio of 0.80 ± 0.13 ($P < 0.01$).

Intriguingly, extending the duration of exposure to deoxysphinganines to 24 h, revealed depletion of mitochondrial Ca^{2+} in deoxysphinganine treated MNs, to 0.43 ± 0.03 (not significant) and 0.35 ± 0.02 ($P < 0.05$) in DSp and DMSp treated MNs, respectively, compared to 0.50 ± 0.04 in vehicle treated MNs (Figure 4.7 D).

Figure 4.7

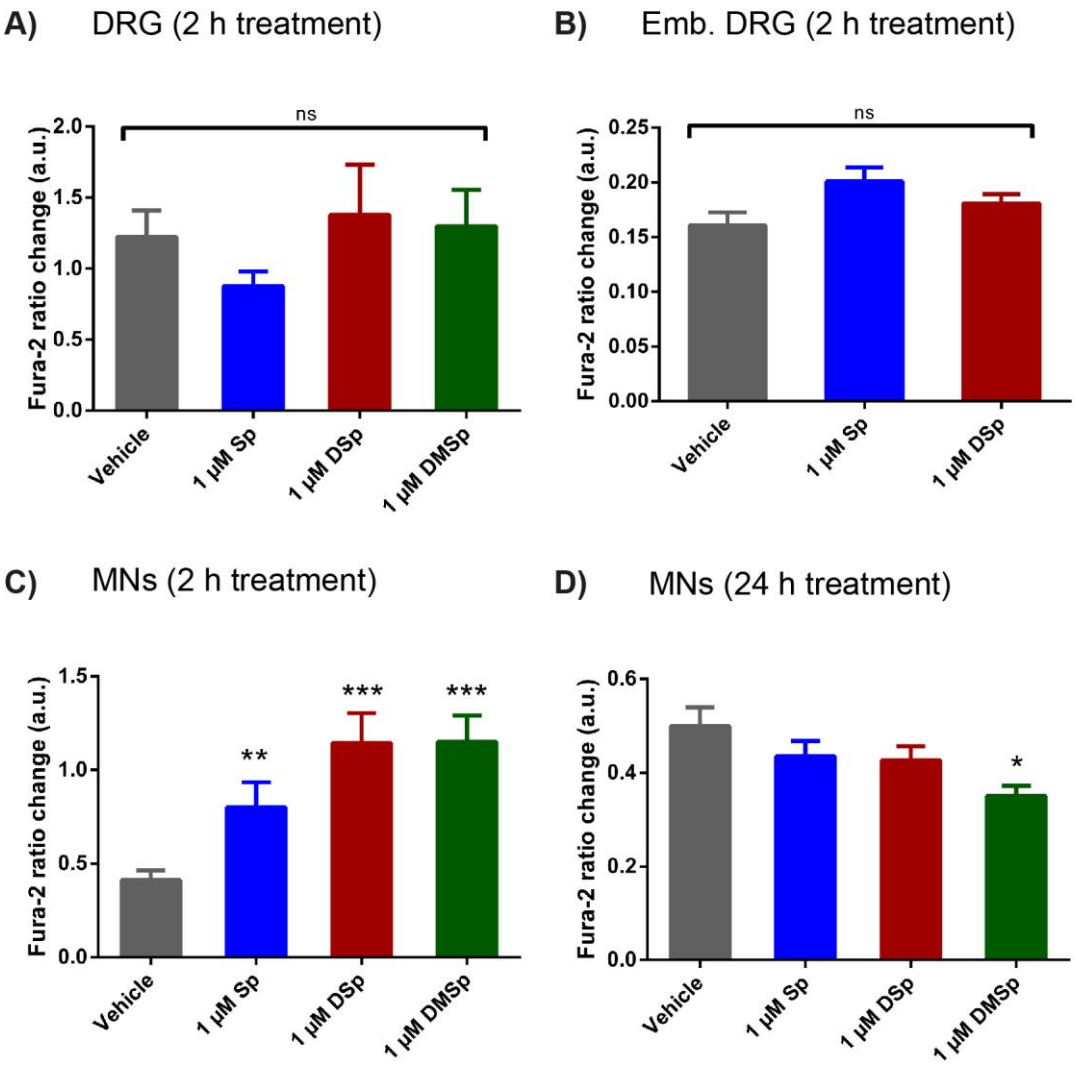
A) DRG (2 h treatment)
B) Emb. DRG (2 h treatment)
C) MNs (2 h treatment)
D) MNs (24 h treatment)
Fura-2 ratio change (a.u.)
ns
**
***
***
*
Vehicle
1 µM Sp
1 µM DSp
1 µM DMSp

Figure 4.7: Deoxysphinganines cause rapid mitochondrial Ca^{2+} loading in motor neurons

The bar charts summarise the mean mitochondrial Ca^{2+} levels in each of the experimental conditions indicated. **A)** At 3-5 DIV, DRG cultures were treated with either vehicle control (ethanol) or the sphinganines for 2 h, prior to live cell imaging. Thapsigargin and ionomycin were used to estimate mitochondrial Ca^{2+}, and mean mitochondrial Ca^{2+} was established from 32-41 cells per condition, from 4 independent experiments. **B)** At 5-6 DIV, embryonic DRG cultures were treated with either vehicle control or the sphinganines for 2 h, prior to live cell imaging. Mean mitochondrial Ca^{2+} was established from 19-20 cells per condition, from 3 independent experiments. **C)** At 5-8 DIV, MNs were treated for 2 h prior to live cell imaging. Mean mitochondrial Ca^{2+} was established from 36-44 cells per condition, from 4-5 independent experiments. **D)** At 6 DIV, MNs were treated for 24 h prior to live cell imaging. Mean mitochondrial Ca^{2+} was established from 42-59 cells per condition, from 4-5 independent experiments. Error bars represent SEM. For statistical comparison, each treatment group was compared to vehicle control using one-way ANOVA and Dunnett's multiple comparisons tests or the Kruskal-Wallis and Dunn's multiple comparisons tests. *P* values: * < 0.05; ** < 0.01; *** < 0.001. ns = not significant.

As observed with ER Ca^{2+} levels, mitochondrial Ca^{2+} levels in vehicle-treated DRG cells were substantially higher than in vehicle-treated MNs (compare Figure 4.7 A and C), but embryonic DRG neurons stored much less mitochondria Ca^{2+} than post-natal DRG neurons (Figure 4.7 B).

4.3.6 Voltage-gated Ca^{2+} channel influx at the cell membrane is unaffected in deoxysphinganine-treated motor neurons

The source of the increased mitochondrial Ca^{2+} observed following acute, 2 h treatment of MNs with the sphinganines was investigated next. Since cytosolic and ER Ca^{2+} was unaffected in MNs following this treatment paradigm (Figure 4.2 B and Figure 4.4 B), it was hypothesised that elevated mitochondrial Ca^{2+} may come from an extracellular source. First, I examined whether the elevated Ca^{2+} levels might be a consequence of changes in typical neuronal activity, such as action potential generation. Therefore the effect of deoxysphinganine treatments on voltage-gated Ca^{2+} channel entry was investigated. In these experiments, potassium was used to depolarize the plasma membrane, thus triggering the opening of voltage-gated Ca^{2+} channels. As can be seen in Figure 4.8, there was no difference in the fura-2 ratios representing voltage-gated Ca^{2+} channel entry between the vehicle control (2.11 ± 0.08), and any of the sphinganine treatments; Sp (2.11 ± 0.05), DSp (2.11 ± 0.05), DMSp (2.24 ± 0.10).

4.3.7 Deoxysphinganine causes increased store-operated Ca^{2+} (SOC) channel entry in motor neurons

I next examined whether the observed increase in mitochondrial Ca^{2+} might originate from a second class of cell membrane channels, by examining entry of Ca^{2+} through the ER-regulated, store-operated Ca^{2+} (SOC) channels. To investigate SOC channel entry, thapsigargin was used to empty Ca^{2+} from the ER, which in turn results in the opening of SOC channels on the cell membrane, in a bid to replenish the ER Ca^{2+} stores, as shown in typical experiments depicted in Figure 4.9 A and B. Thus, when the external Ca^{2+}-free medium was replaced with Ca^{2+}-containing medium, the influx of Ca^{2+} through SOC channels was

Figure 4.8

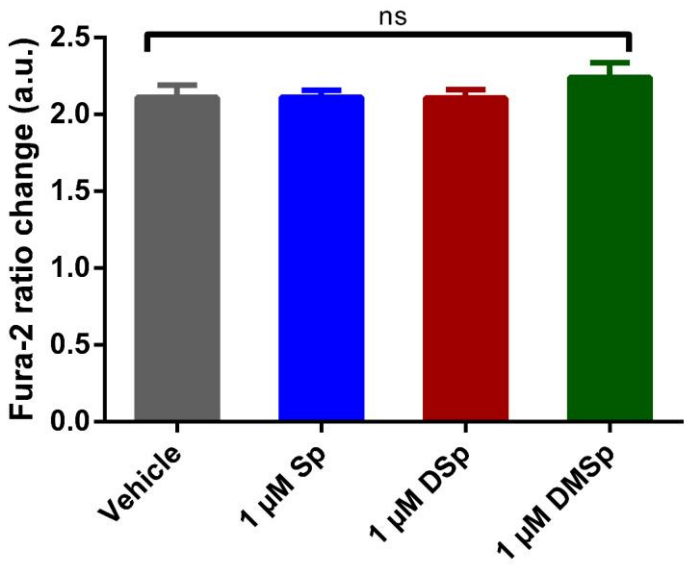

Figure 4.8: Deoxysphinganines do not affect voltage-gated Ca^{2+} channel influx in motor neurons

At 5-8 DIV, MNs were treated with vehicle control or sphinganines, 2 h prior to live cell imaging with fura-2. High potassium was used to depolarize the plasma membrane potential and trigger opening of voltage-gated Ca^{2+} channels. The bar chart shows mean voltage-gated channel Ca^{2+} entry per cell, calculated from 23-52 cells per condition, from 2-3 independent experiments. Error bars represent SEM. For statistical comparison, each treatment group was compared to vehicle control using one-way ANOVA and Dunnett's multiple comparisons tests. *P* values: * < 0.05; ** < 0.01; *** < 0.001. ns = not significant.

Figure 4.9

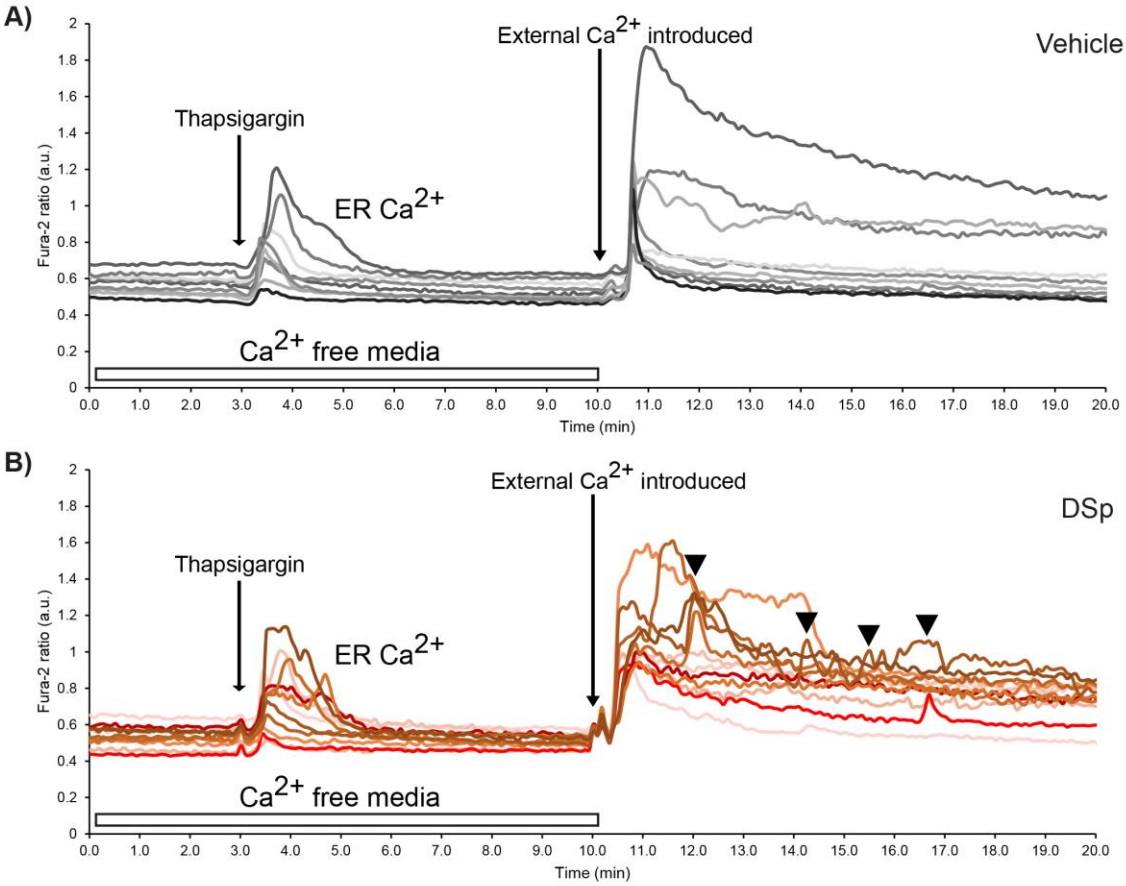

Figure 4.9: Deoxysphinganine causes dysregulation of store-operated Ca^{2+} (SOC) channels in motor neurons

At 5-8 DIV, MNs were treated with vehicle control or sphinganines, 2 h prior to live cell imaging with fura-2. **A-B)** Example traces showing SOC channel entry in vehicle (A) and DSp (B) treated cells. Each differentially shaded line represents a different MN. Arrowheads in B indicate subsequent influxes of Ca^{2+} following the initial SOC channel peak influx in the DSp-treated MNs.

measured. As can be seen in Figure 4.10 A, treatment of MNs with DSp for 2 h resulted in an increase in Ca^{2+} influx through SOC channels compared to vehicle control treated MNs, with a fura-2 ratio of 1.00 ± 0.06 and 0.67 ± 0.05, respectively ($P < 0.001$). Frequent fluctuation of fura-2 ratios in DSp-treated MNs following Ca^{2+} influx through SOC channels was also observed when compared to vehicle treated MNs (Figure 4.9 B). This may be indicative of dysregulation of these channels or other disruption at the cell membrane and, indeed, biochemical studies of the properties of deoxysphingoid bases and their derivatives propose that these compounds may have the ability to affect normal cell membrane function (Jimenez-Rojo et al., 2014).

In order to further confirm that the elevated mitochondrial Ca^{2+} observed in deoxysphinganine-treated MNs is due, at least in part, to dysfunctional SOC entry, FCCP was used to render the mitochondria dysfunctional prior to measuring SOC entry, which prevents mitochondria from contributing to changes in Ca^{2+}. FCCP is an uncoupling agent which abolishes the mitochondrial membrane potential by allowing hydrogen ions through the inner mitochondrial space before they can be used for ATP generation by complex V (Benz and McLaughlin, 1983). The results summarised in Figure 4.10 B, show that when mitochondrial function is abolished with FCCP, there is an increase in Ca^{2+} measured in the cytosol, following Ca^{2+} influx from SOC channels in both vehicle- and DSp-treated MNs. The fura-2 ratio changes from 0.67 ± 0.05 to 1.11 ±.0.13 ($P < 0.01$) in vehicle-treated MNs and from 1.00 ± 0.06 to 1.40 ± 0.11 ($P < 0.05$) in DSp-treated MNs. Thus, even in the absence of functional mitochondria, Ca^{2+} levels are elevated in DSp treated MNs compared to controls and the main source of this Ca^{2+} appears to be the extracellular space, with Ca^{2+} entry through SOC channels. This also provides further evidence that an immediate destination of Ca^{2+} which enters the cells through the SOC channels is indeed the mitochondria, since when mitochondrial buffering capacity is removed, increased Ca^{2+} is measured in the cytosol following SOC entry.

Figure 4.10

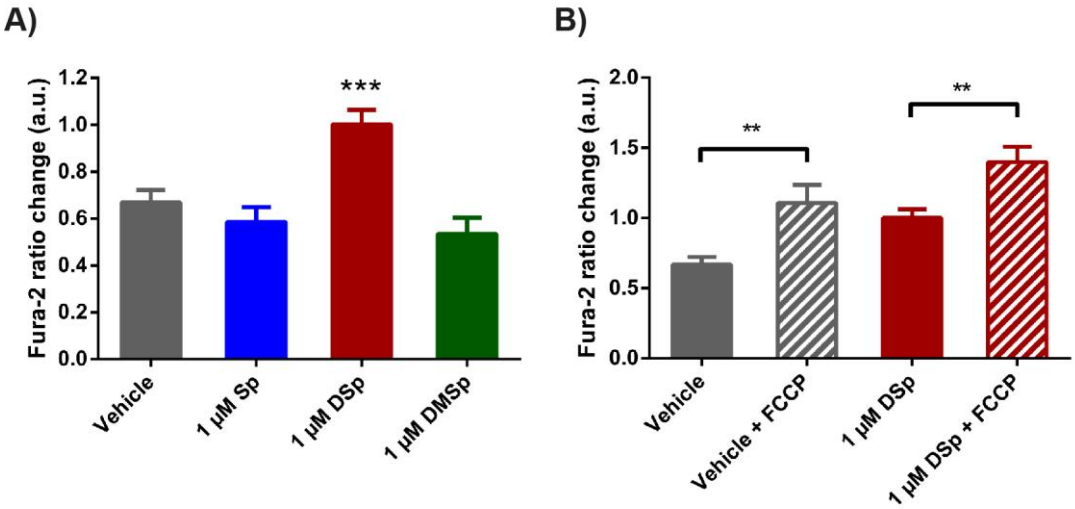

Figure 4.10: Deoxysphinganine causes elevated store-operated Ca^{2+} (SOC) channel influx in motor neurons

At 5-8 DIV, MNs were treated with vehicle control or sphinganines, 2 h prior to live cell imaging with fura-2. **A)** The bar chart shows mean Ca^{2+} entry through SOC channels, calculated from 36-97 cells per condition, from 5-9 independent experiments. **B)** SOC channel entry was measured with and without co-treatment with FCCP. The bar chart shows mean SOC channel Ca^{2+} influx, established from 38-97 cells per condition, from 4-9 independent experiments. Error bars represent SEM. For statistical comparison, each treatment group was compared to vehicle control using the Kruskal-Wallis and Dunn's multiple comparisons tests. Where indicated pairwise comparisons were made using Mann-Whitney *U* tests. *P* values: * < 0.05; ** < 0.01; *** < 0.001.

Taken together, these results suggest that a critical effect of deoxysphinganines is to alter the cell membrane, which results in dysregulation of SOC channels, which in turn affects mitochondrial Ca^{2+} levels and may contribution to disturbed ER Ca^{2+} homeostasis.

It should be noted that attempts to block SOC entry in MN cultures and HEK cells were made using 2-aminoethoxydiphenyl borate (2-APB, Parekh and Putney, 2005; Bird et al., 2008; Putney, 2010; Gemes et al., 2011) and ML-9 (Putney, 2010; Gruszczynska-Biegala et al., 2016). These proved to work inconsistently so that frequently the block was incomplete, as can be seen in the traces shown in Figure 4.11.

Previous experiments in cortical neurons have suggested that DSp may interfere with NMDA receptors (Guntert et al., 2016). Therefore, I next examined NMDA receptor Ca^{2+} influx using a similar protocol to that reported by Dildy and Leslie (1989) and Jensen and Chiu (1990). However, NMDA (co-applied with glycine) failed to trigger influx of Ca^{2+} in primary MN cultures at any of the concentrations tested (100 μM – 10 mM), as can be seen in the traces of typical experiments shown in Figure 4.12 A. Since, the NMDA receptor is a glutamate receptor, I also examined the effect of triggering a more global influx of Ca^{2+} through glutamate receptors using L-glutamic acid (100 μM – 1 mM, Jensen and Chiu, 1990). However, the results were inconsistent between cells, both within the same culture and between different cultures, as can be seen in the traces shown in Figure 4.12 B.

4.3.8 Deoxysphinganines cause mitochondrial dysfunction in motor and sensory neurons

Having established that short-term treatment with deoxysphinganines causes increased mitochondrial Ca^{2+} loading in MNs, I next tested whether these treatments cause a more generalized mitochondrial dysfunction. Changes in mitochondrial membrane potential ($\Delta\psi_m$) following 2 h sphinganine treatments were investigated using TMRM, a cationic dye which accumulates in mitochondria as a function of $\Delta\psi_m$, in both MN (Figure 4.13 A-D) and DRG

Figure 4.11

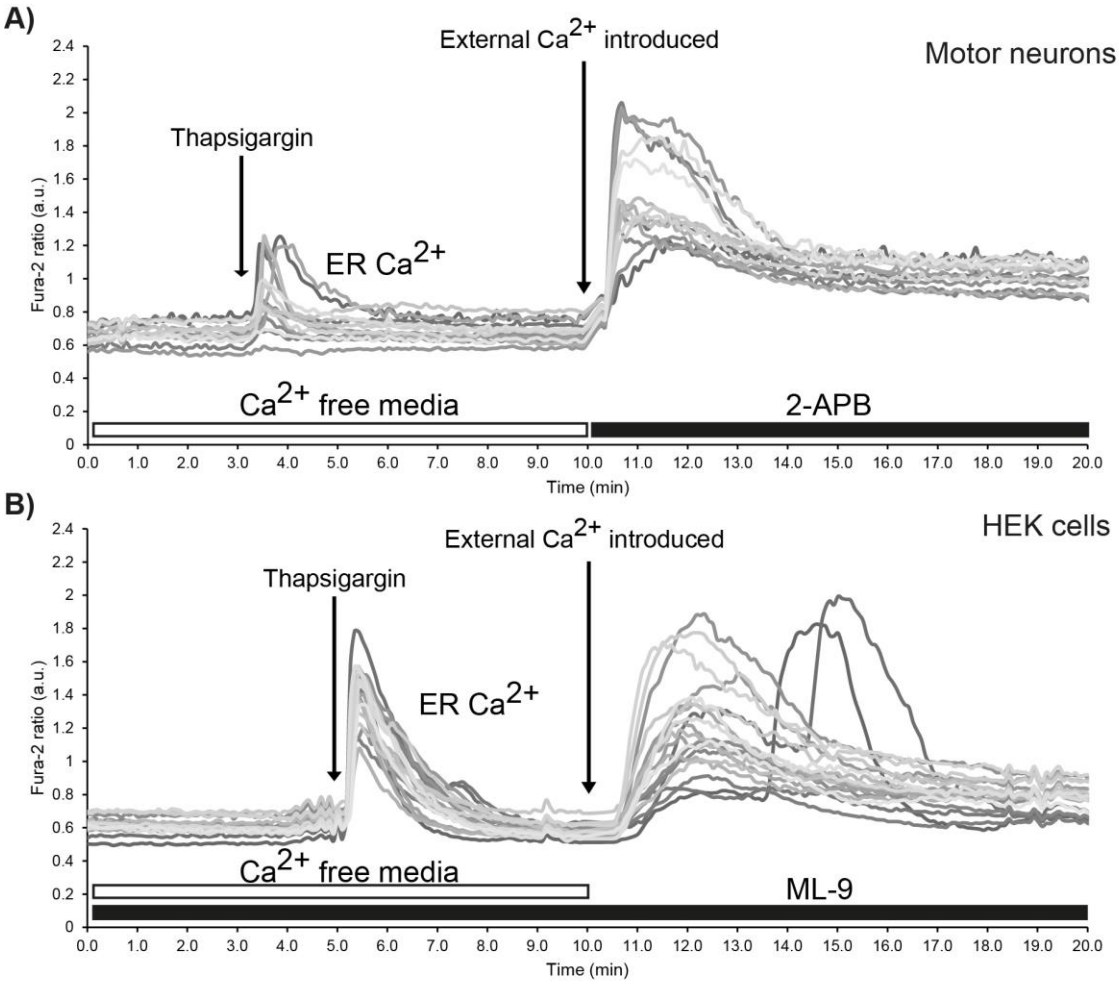

Figure 4.11: Store-operated Ca^{2+} (SOC) channel entry could not be blocked by 2-APB or ML-9

A) Primary MNs were grown to 7 DIV and loaded with fura-2 30 min before imaging. SOC channel entry was measured using thapsigargin to empty ER Ca^{2+} stores, after which Ca^{2+} was introduced to the external recording media along with 100 µM of reported SOC channel blocker 2-aminoethoxydiphenyl borate (2-APB). **B)** HEK cells were loaded with fura-2 30 min before imaging. SOC channel entry was measured as above, with 50 µM of reported SOC channel blocker ML-9 throughout the experiment. Each differentially shaded line represents a different cell.

Figure 4.12

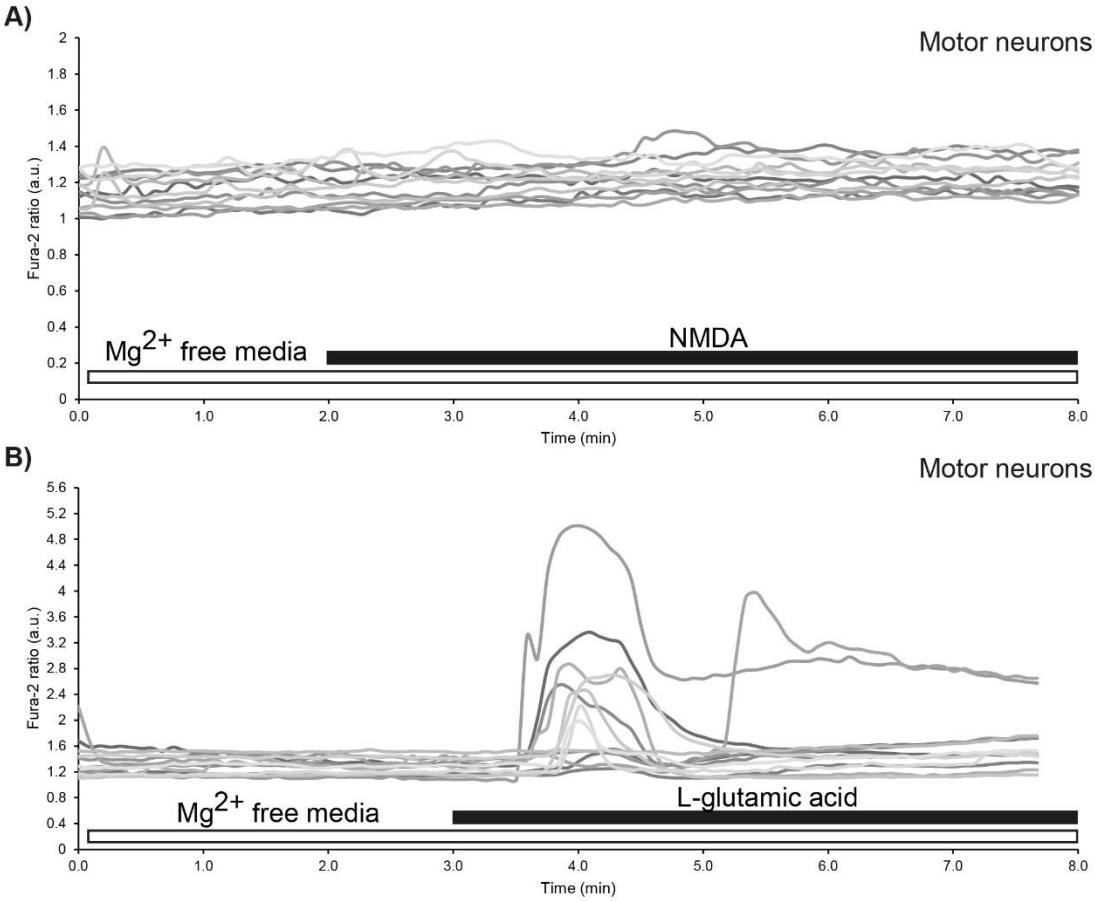

Figure 4.12: NMDA and glutamate receptor Ca^{2+} influx could not be measured in primary motor neurons

Primary MNs were grown to 15 DIV and loaded with fura-2 30 min before imaging. **A)** Cells were imaged in Mg^{2+} free media, and 250 µM NMDA and 75 µM glycine added at 2 min. **B)** Cells were imaged in Mg^{2+} free media and 250 µM L-glutamic acid and 75 µM glycine added at 3 min. Each differentially shaded line represents a different cell.

Figure 4.13

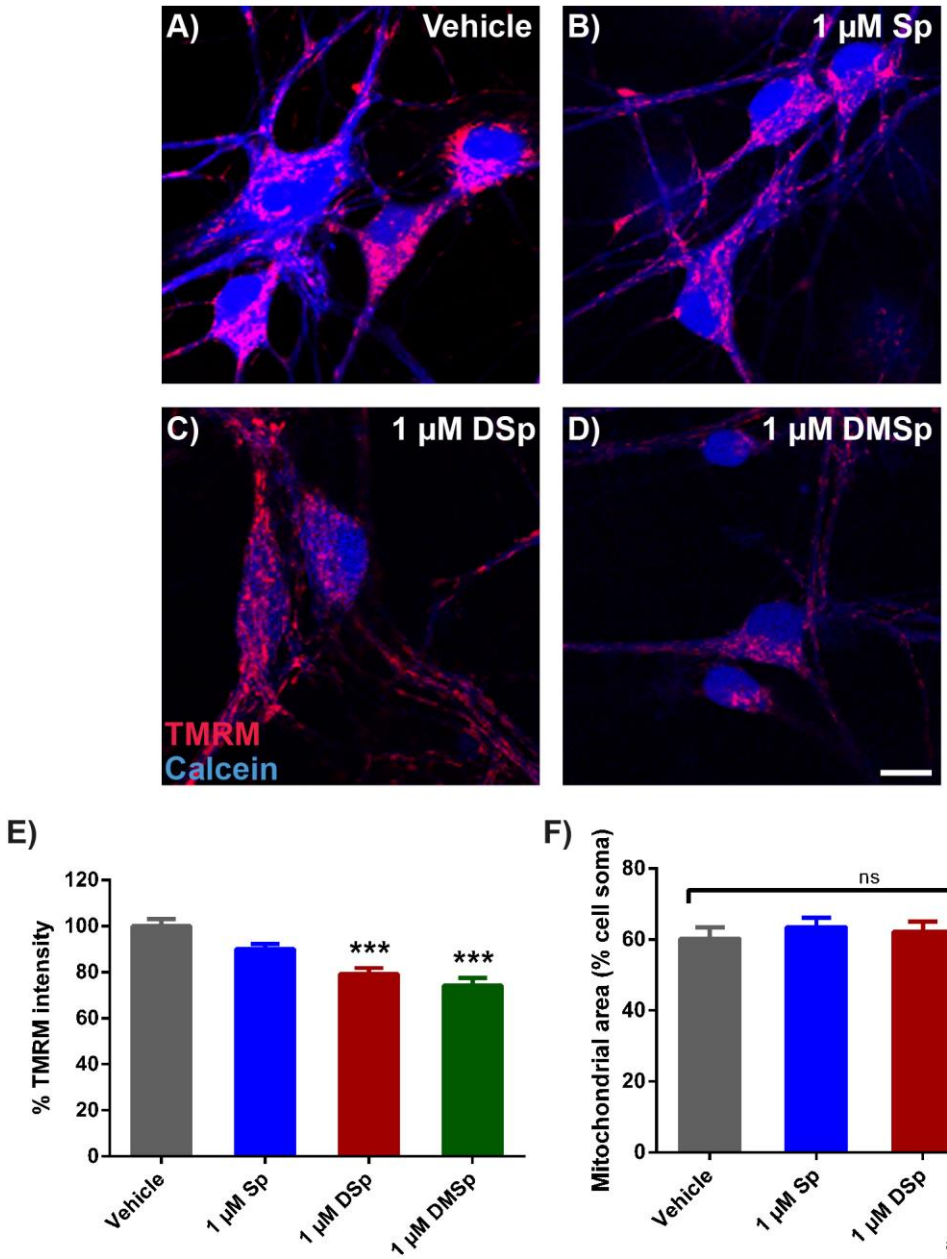
A)
Vehicle
B)
1 µM Sp
C)
1 µM DSp
D)
1 µM DMSp
TMRM
Calcein
E)
% TMRM intensity
120
100
80
60
40
20
0
***
***
Vehicle
1 µM Sp
1 µM DSp
1 µM DMSp
F)
Mitochondrial area (% cell soma)
80
60
40
20
0
ns
Vehicle
1 µM Sp
1 µM DSp
1 µM DMSp

Figure 4.13: Treatment with deoxysphinganines reduces mitochondrial membrane potential in motor neurons

A-D) At 5-8 DIV MNs were treated with sphinganines or vehicle control (ethanol) for 2 h, prior to live cell imaging. TMRM intensity is used as a readout measure for mitochondrial membrane potential and calcein is a marker of viable cells. **E)** The bar chart shows the mean TMRM fluorescent intensities per cell, measured from 26-48 MNs per condition, from 3 independent experiments and expressed as a percentage relative to control. **F)** The bar chart shows the mean total mitochondrial area per MN cell body, expressed as a percentage of the cell soma size, measured from 26-48 MNs per condition, from 3 independent experiments. Error bars represent SEM. For statistical comparison, each treatment group was compared to vehicle control using one-way ANOVA and Dunnett's multiple comparisons tests. *P* values: * < 0.05; ** < 0.01; *** < 0.001. ns = not significant. Scale bars = 10 µm.

cultures (Figure 4.14 A-D). Calcein is used in these experiments as a marker of viable cells.

Following treatment with DSp and DMSp there was a significant decrease in $\Delta\psi_m$, so that the mean TMRM intensity declined to 79 ± 2 % ($P < 0.001$) and 74 ± 3 % ($P < 0.001$) of vehicle-treated cultures, respectively (Figure 4.13 E). In this short 2 h treatment paradigm, the decrease in $\Delta\psi_m$ was not sufficient to affect the total mitochondrial area, expressed as a percentage of the cell soma size (Figure 4.13 F).

DRG neurons subject to the same treatment paradigm also displayed a reduced $\Delta\psi_m$, with DSp-treated DRG neurons having 68 ± 3 % of vehicle-treated DRG neurons TMRM intensity (Figure 4.14 E, $P < 0.001$). DMSp-treated DRG neurons also showed a decreased $\Delta\psi_m$ of 77 ± 5 % ($P < 0.001$). In these sensory DRG cells, 2 h treatment with DSp was also sufficient to cause a decrease in the mitochondrial area per cell soma, so that DSp-treated DRG neurons showed a mean mitochondrial area of 56 ± 3% compared to 70 ± 3% in vehicle-treated DRG neurons ($P < 0.01$, Figure 4.14 F).

The decrease in $\Delta\psi_m$ observed in these experiments, along with a reduced total mitochondrial area in DRG cells, following such short-term treatment with the deoxysphinganines supports the hypothesis that neuronal mitochondria are an early target of deoxysphingaine-mediated neurotoxicity.

4.3.9 Deoxysphinganine-mediated neuronal death is not rescued by blocking the mitochondrial permeability transition pore

A major pathway for cell death that occurs secondary to mitochondrial dysfunction is the opening of the mitochondrial permeability transition pore (mPTP), which opens in a bid to release mitochondrial Ca^{2+}, which in turn signals cell death via the concomitant release of cytochrome C and pro-caspases in order to trigger apoptosis (Susin et al., 1999a; Susin et al., 1999b). To explore whether the opening of the mPTP is responsible for the deoxysphinganine-mediated neuronal death observed in this study (Chapter 3, Section 3.3.3), MNs were co-

Figure 4.14

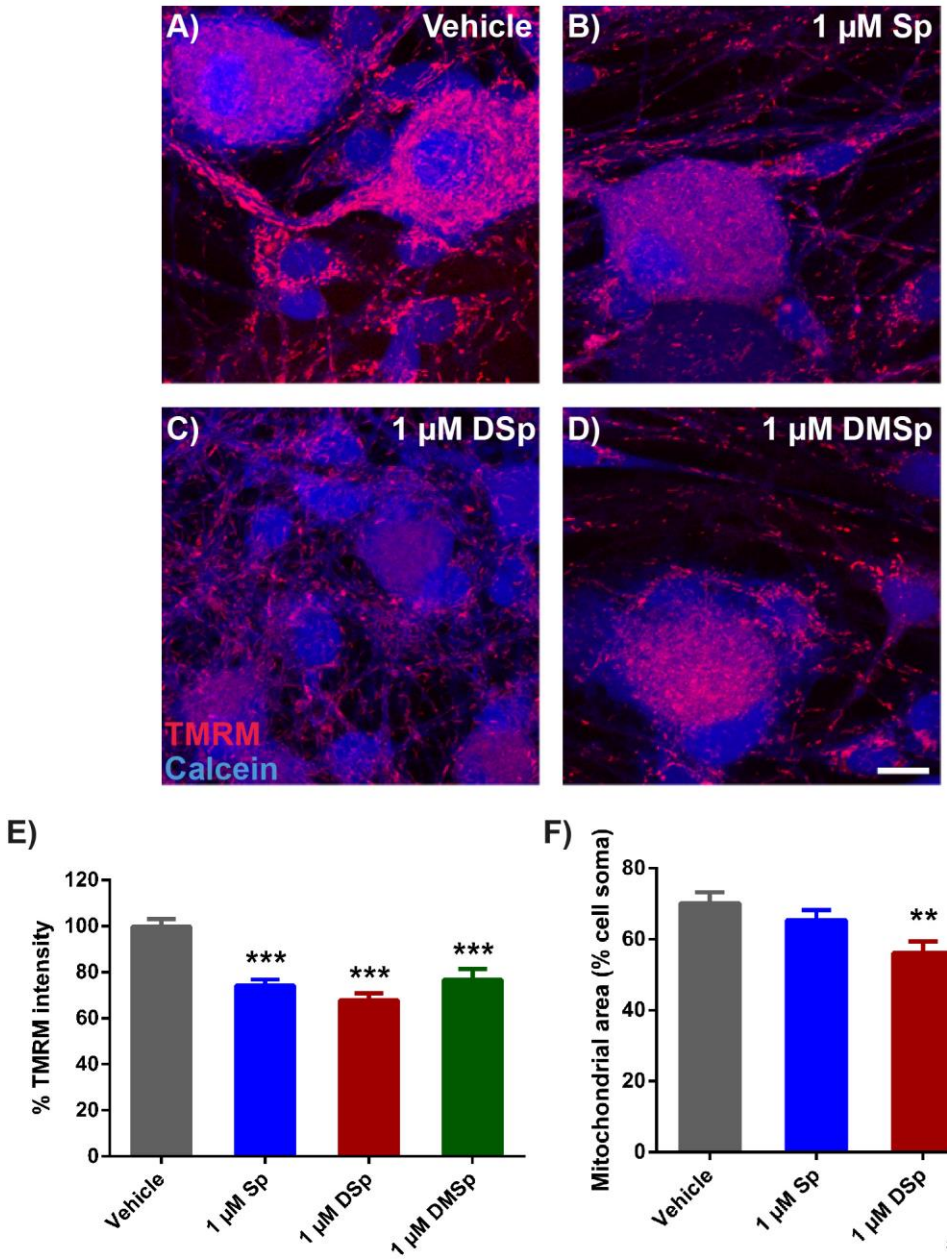
A)
Vehicle
B)
1 µM Sp
C)
1 µM DSp
D)
1 µM DMSp
TMRM
Calcein
E)
% TMRM intensity
120
100
80
60
40
20
0
***
***
***
Vehicle
1 µM Sp
1 µM DSp
1 µM DMSp
F)
Mitochondrial area (% cell soma)
80
60
40
20
0
**
Vehicle
1 µM Sp
1 µM DSp
1 µM DMSp

Figure 4.14: Treatment with deoxysphinganines reduces mitochondrial membrane potential and mitochondrial area in sensory neurons

A-D) At 3-5 DIV DRG cultures were treated with vehicle control (ethanol) or sphingaines, 2 h prior to live cell imaging. TMRM intensity is used as a readout measure for mitochondrial membrane potential and calcein is a marker of viable cells. **E)** The bar chart shows the mean TMRM fluorescent intensities per cell, measured from 29-61 cells, from 4 independent experiments and expressed as a percentage relative to control. **F)** The bar chart shows the mean total mitochondrial area per DRG cell body, expressed as a percentage of the cell soma size, measured from 29-61 cells, from 4 independent experiments. Error bars represent SEM. For statistical comparison, each treatment group was compared to vehicle control using one-way ANOVA and Dunnett's multiple comparisons tests or the Kruskal-Wallis and Dunn's multiple comparisons tests. *P* values: * < 0.05; ** < 0.01; *** < 0.001. Scale bars = 10 µm.

treated with cyclosporine A (CsA), an inhibitor of mPTP opening (Bernardi et al., 1994), alongside the sphinganines.

Immature MNs were treated with CsA (1 µM) and the sphinganines (1 µM) for 24 h, and neuronal survival was expressed as a percentage of control cultures. There was no significant difference in MN survival in cultures treated with the sphinganines alone or in addition to CsA (Figure 4.15); 54 ± 11% of MNs survived in 1 µM DSp-treated cultures, compared to 46 ± 13% in DSp + CsA-treated cultures. These results suggest that cell death caused by exogenous application of deoxysphinganines is not mediated by mitochondrial permeability transition.

4.4 Discussion

The results presented in Chapter 3, established that extracellular treatment with deoxysphingoid bases was toxic to primary neurons *in vitro.* Thus, in Chapter 4, I set out to identify the pathomechanisms underlying this toxicity.

An increase in cytosolic Ca^{2+} is a well-established indicator of cell stress leading to cell death, and indeed when primary MNs were treated with deoxysphinganines for a prolonged period there was an increase in cytosolic Ca^{2+}, corresponding to the reduced cell survival reported in Chapter 3.

However, short-term (2 h) treatment of MNs with deoxysphinganines did not result in any change in cytosolic Ca^{2+} levels, indicating that following an acute 2 h exposure to deoxysphingaines, MNs were fully functioning and not yet undergoing apoptosis. This experimental model therefore offers the opportunity to probe the underlying mechanisms of deoxysphinganine toxicity and to identify early targets of DSp and DMSp.

The ER is a key organelle for the regulation of cellular Ca^{2+} homeostasis and the SPT enzyme is located in the ER membrane; the ER is thus the site of deoxysphinganine generation *in vivo*. Typically, the ER maintains Ca^{2+} homeostasis by uptake of Ca^{2+} at SERCA pumps via ATP hydrolysis. ER Ca^{2+}

Figure 4.15

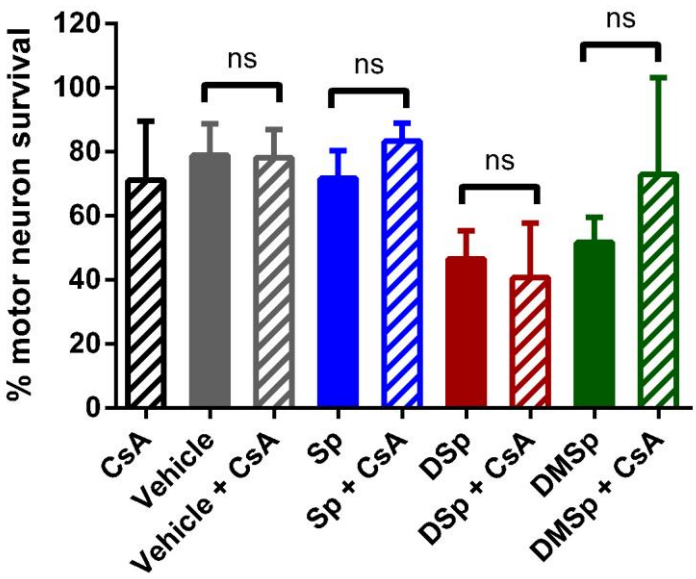

Figure 4.15: Treatment with cyclosporine A (CsA) is not sufficient to rescue deoxysphinganine mediated neuronal death

After 24 h *in vitro*, MNs were treated with either vehicle, Sp, DSp or DMSp alone or in combination with 1 µM CsA. MNs were fixed 24 h following treatment, at 2 DIV, and stained with DAPI and β-III tubulin for analysis. The bar chart shows MN survival, expressed as a percentage relative to untreated MN survival without CsA or with CsA treatment, as appropriate. N = 3-10 independent experiments per condition. Displayed data represent the mean ± SEM. Statistical analysis was performed using Mann-Whitney *U* tests. *P* values: * < 0.05; ** < 0.01; *** < 0.001. ns = not significant.

release is via inositol triphosphate (IP_3) and ryanodine receptors as well as via less well-characterized leak channels. The second messenger IP_3 is generated downstream of the activation of G-protein-coupled or tyrosine kinase-linked receptors at the plasma membrane whereas ryanodine receptor activation is in response to Ca^{2+} levels, giving rise to what is known as Ca^{2+}-induced Ca^{2+} release (Stutzmann and Mattson, 2011). Here, Ca^{2+} depletion in the ER, indicative of ER stress, was observed as early as 2 h from the start deoxysphinganine exposure in DRG cells, yet in MNs there was no measurable depletion of Ca^{2+} in the ER at this time point. However, depleted ER Ca^{2+} does become apparent at a later stage in MNs, after 24 h of treatment with the deoxysphinganines. It should be noted that ER stress is a complex phenomenon that can manifest in a multitude of ways including depletion of ER Ca^{2+}, elevation of ER Ca^{2+}, up or downregulation of proteins associated with the UPR and changes in redox state. The finding that deoxysphinganines may affect motor and sensory neurons differentially, or at least the effects may develop on a different time scale, reflects the clinical manifestation of the disease, where typically, HSN-1 patients present with sensory deficits in advance of motor deficits (Reilly, 2007). Indeed, Salcedo et al. (2007) even reported differing effects of DSp between two different cell lines, suggesting cell-specific effects or cell type vulnerability in response to deoxysphingoid bases.

Intriguingly, MNs initially appeared to store less Ca^{2+} in ER and mitochondria than sensory neurons. However, further investigation using DRG neurons sourced from embryos revealed that the differences in intracellular Ca^{2+} stores may be a result of the maturity of the cells at the point of harvesting; embryonic DRG neurons had similarly low intracellular Ca^{2+} stores as MNs. The relatively low baseline Ca^{2+} levels may thus mask any subtle ER Ca^{2+} depletion caused by the deoxysphinganines in these cells types. Indeed, protein analysis for the ER stress marker BiP, revealed that just 2 h treatment with DSp in MNs was sufficient to induce ER stress. However, after 24 h BiP appeared to deplete again to levels comparable to controls, suggesting BiP upregulation is an early response to DSp.

Mitochondria also play a major role in buffering cellular Ca^{2+} and mitochondrial abnormalities have been reported in several studies in HSN-1 patient

lymphoblasts (Myers et al., 2014; Stimpson et al., 2015) as well as in cortical neurons treated with DSp (Guntert et al., 2016). Ca^{2+} uptake into mitochondria is via the mitochondrial Ca^{2+} uniporter, driven by the electrochemical gradient present across the inner mitochondrial membrane. Ca^{2+} is typically removed from mitochondria by the Na^{+}/Ca^{2+} exchanger, although in certain conditions Ca^{2+} can also exit mitochondria via the mPTP (Verkhratsky and Petersen, 1998). Moreover, the mitochondrial outer membrane associates with the ER, where SPT localizes, via the mitochondria-associated ER membrane (MAM, Csordas et al., 2006). The MAM is known to play an important role in intermembrane transport of phospholipids as well as a potential role in the transport of ceramide (Hayashi et al., 2009), a downstream component of the *de novo* sphingolipid synthesis pathway, the pathway specifically affected by HSN-1-causing mutations. In this Chapter, the results show that 2 h treatment with the sphinganines caused a shift towards elevated mitochondrial Ca^{2+} in MNs, but not in sensory neurons. However, after 24 h treatment, mitochondrial Ca^{2+} levels returned to similar, if not lower levels as found in control cultures. It could be speculated that elevated mitochondrial Ca^{2+} is a very early event in deoxysphinganine-mediated toxicity, which precedes depletion of ER Ca^{2+} (seen only after 24 h treatment in MNs), and thus the 2 h treatment model used in these experiments is not sufficiently short to capture changes in mitochondrial Ca^{2+} in DRG cells, in which depletion of ER Ca^{2+} is evident much earlier than in MNs. Indeed, the proposal that mitochondrial Ca^{2+} levels may be affected in advance of ER Ca^{2+} levels mirrors a recent study that tracked deoxysphinagnines to the mitochondria within 5 min of application, and at later time points, also to the ER (Alecu et al., 2016b).

Extracellular treatment of MNs with deoxysphinganines leads to a rapid loading of Ca^{2+} into mitochondria, while cytosolic Ca^{2+} and ER Ca^{2+} are both unaffected following short-term (2 h) treatment. Thus, the most obvious source of Ca^{2+} is the extracellular space through specific cationic channels: voltage-gated channels, second messenger-operated channels, receptor-operated channels, store-operated channels, or under some conditions, the reversal of the sodium-Ca^{2+} exchanger (NCX; Parekh and Putney, 2005). In this Chapter, two major groups of cationic channels that could be responsible were examined; activity-dependant voltage-gated ion channels and the SOC channels that are regulated by the ER,

causing the opening of these channels upon Ca^{2+} store depletion. In order to test what activity is involved in the Ca^{2+} entry to the cells, high potassium medium was used to cause the cell membrane to depolarize, thus triggering the opening of the voltage-gated Ca^{2+} channels. Influx of Ca^{2+} through the voltage-gated Ca^{2+} channels was measured after 2 h treatment with sphinganines, and no difference was detected between the control and any of the treatment groups, indicating that the deoxysphinganines do not directly interfere with this element of normal neuronal activity, at least not at this early phase.

Another source of extracellular Ca^{2+} is via the SOC channels. The primary role of these channels is to replenish ER Ca^{2+} stocks. Another major destination of Ca^{2+} influx through these channels is mitochondria (Malli et al., 2003) and thus, it is possible that the Ca^{2+} influx induced by opening of SOC channels immediately loads into mitochondria. 2 h treatment with DSp caused a highly significant increase in Ca^{2+} influx through SOC channels. Not only was an increase in the amount of Ca^{2+} entry from the extracellular space in DSp-treated cells observed, but also a characteristic fluctuation of Ca^{2+} levels, instead of the relatively smooth decline of Ca^{2+} entry observed in control cells after the initial Ca^{2+} influx. Moreover, when mitochondrial Ca^{2+} uptake was abolished with FCCP an increase in SOC channel influx into the cytosol in both control and DSp-treated cells was observed. Thus, a major destination of Ca^{2+} flowing through the SOC channels is indeed mitochondria, but in the absence of mitochondrial buffering, Ca^{2+} remains in the cytosol. Taken together, these findings suggest that the source of elevated mitochondrial Ca^{2+} in DSp-treated neurons is, at least in part, dysfunctional SOC channels. Interestingly, dysregulation of SOC channels has also been implicated in another inherited peripheral neuropathy, CMT disease secondary to Ganglioside Induced Differentiation Associated Protein 1 (*GDAP1*) mutations (Pla-Martin et al., 2013; Barneo-Munoz et al., 2015) as well as in hereditary spastic paraplegia secondary to Atlastin 1 (*ATL1*) mutations (Li et al., 2017). Moreover SOC channel entry has also been implicated in other neurodegenerative disorders including Parkinson's disease, Alzheimer's disease and Huntington's disease (Pchitskaya et al., 2017).

Attempts were made to block SOC channel entry using two compounds, 2-APB and ML-9, but proved inconsistent. Indeed, the pharmacology of 2-APB as a SOC channel blocker is complicated, with higher concentrations reported to block SOC channel Ca^{2+} influx and lower concentrations to enhance it (Putney, 2010). SOC entry has not been widely explored in MNs and it is proposed that the relative composition of the Orai subunits (1, 2 or 3) making up the channel may affect the effectivity of the 2-APB block, with 2-APB being most effective against Orai1 (Putney, 2010). Thus, the lack of SOC channel block reported here may be reflective of a MN SOC channel comprised predominantly of Orai2/3 subunits, however this is not something which has been specifically explored in the literature. Although it is widely accepted that Orai1 is a pore-forming subunit of SOC channels, far less is known about Orai2 and Orai3 (Putney et al., 2016). ML-9 blocks SOC entry via targeting the stromal interaction molecule 1 (STIM1) which signals from the empty ER store to the plasma membrane (Putney, 2010). There are two other forms of STIM protein, STIM2, and a long splice variant of STIM1, STIM1L, which may be able to compensate for ML-9 induced STIM1 block (Putney et al., 2016).

Since evidence in the literature suggested DSp may interfere with normal NMDA receptor signalling (Guntert et al., 2016) attempts were also made to investigate NMDA, and a more general glutamate receptor dependent, Ca^{2+} influx. NMDA and L-glutamic acid failed to consistently trigger Ca^{2+} influx in primary MNs in the experimental protocols used in this Chapter, which may be reflective of the relatively immature age of the animal from which these MNs are sourced from (embryonic day 12.5-13.5) and the short amount of time these cells can be grown in culture. Indeed, electrophysiology may present a more appropriate approach to further explore whether deoxysphingoid bases have an effect on glutamate receptors.

Elevated mitochondrial Ca^{2+} levels are damaging to mitochondria and usually result in cell stress and, if the Ca^{2+} loading persists, can lead to apoptosis. In the results shown in this Chapter, elevated mitochondrial Ca^{2+} in MNs was observed, alongside a reduction in mitochondrial membrane potential, which was displayed in both MNs and DRG neurons, even after only 2 h of treatment with

deoxysphinganines. In addition to a depletion of mitochondrial membrane potential, 2 h DSp treatment was also sufficient to cause a decrease in the total mitochondrial area in DRG cells, but not in MNs. Indeed this provides further evidence that MNs and DRG neurons may respond differently to DSp or DMSp toxicity or within different time frames, as is reflected in the clinical progression of HSN-1 in patients, where sensory function is affected earlier than motor.

Mitochondrial Ca^{2+} loading, as well as loss of mitochondrial membrane potential, are known to cause opening of the mPTP in a bid to remove excess Ca^{2+} (Szabo and Zoratti, 1992; Norenberg and Rao, 2007). However, co-treatment with an mPTP blocker, CsA, did not alleviate deoxysphinganine-mediated neuronal death. Therefore, the elevation in mitochondrial Ca^{2+} observed may represent a transient change occurring rapidly in response to exogenous deoxysphinganine application. Thus cell death as a result of deoxysphinganine application appears here to be independent of mPTP-mediated apoptosis. Indeed this in agreement with studies by Salcedo et al. (2007) who found that DSp application to a cell line did not result in translocation of cytochrome C from mitochondria to the cytoplasm, a common feature of mitochondria-induced apoptosis. An upregulation of caspases 3 and 12 were reported and it was thus suggested that DSp may trigger ER-stress induced apoptosis (Salcedo et al., 2007).

DSp, but not DMSp, treatment caused elevated SOC entry in cultured MNs as well as depleted mitochondrial membrane potential and total mitochondrial area in DRG neurons. This suggests that there may be some functional differences in how DSp and DMSp toxicity manifests, and indeed this may provide reason for the readier manifestation of DSp toxicity, when compared to DMSp as seen in Chapter 3 (Section 3.3.4).

In the experiments displayed in this Chapter, the widely-used dye fura-2 was used to measure intracellular Ca^{2+}. Other dyes with a high affinity for Ca^{2+} can be used for *in vitro* imaging, including the single-wavelength dyes calcium green-1, fluo-3, fluo-4 and oregon green 488 BAPTA (Paredes et al., 2008). The ratiometric nature of fura-2 boasts advantage over single-wavelength dyes as it can account for loading discrepancies between cells, dye leakage or photo-bleaching during

imaging. Indo-1 is another ratiometric Ca^{2+} dye, which rather than being excited by two different wavelengths of light (as is fura-2), is excited by a single wavelength of light but emits lights at two wavelengths depending on its Ca^{2+} bound or unbound state. Indo-1 does however exhibit photo-instability, making it more suitable for flow cytometry than live cell imaging (Paredes et al., 2008). Other single wavelength dyes include Ca^{2+} yellow, Ca^{2+} orange, Ca^{2+} crimson, X-rhod and rhod-2, but these dyes have a tendency to compartmentalise (Paredes et al., 2008). X-rhod and rhod-2 have been reported to localize specifically to mitochondria and thus can be used as a readout measure of mitochondrial Ca^{2+} concentration, but this technique is not without controversy (Fonteriz et al., 2010). Moreover, genetically encoded Ca^{2+} indicators exist, which can be used to monitor Ca^{2+} levels specifically in organelles (Paredes et al., 2008). Due to the transfection-resistant nature of primary motor and DRG neurons genetically encoded Ca^{2+} indicators were not used in this study.

4.5 Conclusions

The results in this Chapter demonstrate that ER and mitochondrial dysfunction may play early roles in deoxysphinganine-induced neurotoxicity in HSN-1, well before any neuronal death occurs. Depleted ER Ca^{2+} and enhanced mitochondrial Ca^{2+} loading, together with a reduction in mitochondrial membrane potential, occur rapidly after treatment with deoxysphinganines in cultured neurons. Moreover, early mitochondrial Ca^{2+} loading may be a result of dysregulation of SOC channels located on the cell membrane. As these abnormalities occur at a very early stage, when morphologically these cells appear normal and no cell loss has occurred, it is likely that the observed Ca^{2+} and mitochondrial changes are part of the primary mechanism leading to the eventual neuronal death reported in Chapter 3. However, it remains to be established whether intracellular generation of deoxysphingoid bases targets similar pathways to those identified in this Chapter following extracellular application of deoxysphinganines to primary neurons in culture. In the following Chapter I set out to establish a model of HSN-1 in which neurons would be induced to intrinsically generate deoxysphingoid bases.

Chapter 5. Establishing a neuronal model of mutant *SPTLC1* HSN-1

5.1 Introduction

The experiments presented in Chapters 3 and 4 examined the effects of exogenous application of the aberrant products of the mutant SPT enzyme (DSp and DMSp) on primary motor and sensory cells. The results suggest that the deoxysphingoid bases produced in HSN-1 may cause abnormal cellular interactions that ultimately lead to cytotoxicity and peripheral nerve damage. However, in these experiments the abnormal sphinganines were applied exogenously, which does not directly model HSN-1, a genetic disease in which the mutation results in the intrinsic production of abnormal sphingoid bases. Therefore in this Chapter, in order to further understand the role of the mutant SPTLC1 protein itself in the neuronal populations involved in HSN-1, a lentiviral delivery system was exploited to establish a model system that more closely resembles HSN-1. Lentiviral vectors are suitable for genetic manipulation in primary neurons, including MNs, which can survive this method of gene transfer (Kalmar et al., 2017). As well as providing a further tool in which to probe the underlying HSN-1 cellular pathology, development of genetic models of HSN-1 also have the potential to provide appropriate *in vitro* systems to test potential therapeutic strategies, such as serine supplementation and gene-editing.

5.1.1 Existing genetic models of HSN-1

5.1.1.1 SPTLC1^{C133W} transgenic mouse model

In contrast to studies which examine the effects of exogenous application of the mutant enzyme products on various cells types (discussed in the Introductions to Chapters 3 and 4) a study by Jun et al. (2015) used the SPTLC1^{C133W} transgenic mouse to further explore the mechanisms that may underlie peripheral nerve damage in HSN-1. This mouse was developed by inserting extra copies of wildtype and mutant *SPTLC1* genes driven by a chicken β-actin promoter. The resulting mouse model expresses extra gene copies in all cells, including neurons. Using primary DRG cultures established from this overexpression mouse model, Jun et al. (2015) found that *SPTLC1^{C133W}* sensory neurons

displayed increased neurite length and branching, as well as elevated expression of phosphorylated ezrin-radixin-moesin (ERM) at the neuronal growth cone. The ERM family of proteins are regulators of actin-dependent growth-cone mobility (Ramesh, 2004). However, this is somewhat in contrast to other studies (Penno et al., 2010), as well as results presented in Chapter 3, which show that application of the abnormal products of mutant SPT cause reduced neurite outgrowth in primary neurons. These findings suggest that multiple and potentially conflicting pathways may contribute to HSN-1 pathogenesis *in vivo*.

5.1.1.2 Genetically modified mammalian cell line

The Chinese hamster ovary (CHO) cell line deficient in endogenous SPT (CHO-LyB) and genetically modified to express either wildtype SPT or the C133W mutant form of the enzyme has also been used to examine HSN-1 pathogenesis. This model results in a transient expression of the transgene with variable copy numbers among cells in culture. Analysis of these genetically modified mammalian cells revealed increased expression of the ER stress marker GADD153 when the cells were supplemented with alanine, the substrate which is utilised by SPT to form DSp (Gable et al., 2010).

5.1.1.3 Patient lymphoblasts

Patient-derived lymphoblasts have provided another tool which has been used to explore underlying pathomechanisms in HSN-1. Lymphoblast cultures, obtained from patient blood lymphocytes, can be transformed by sub-culturing to obtain large quantities of cells. Electron microscopy of HSN-1 lymphoblasts has revealed structural abnormalities, including swollen mitochondria with abnormal cristae and membrane breaks, in patient cells expressing $SPTLC1^{C133W}$ and $SPTLC1^{V144D}$ (Myers et al., 2014). As well these structural changes, levels of key mitochondrial protein, UQCRC1, and the Ig kappa chain C protein, have also been reported to be altered (Stimpson et al., 2015). In addition to mitochondrial modifications, patient lymphoblasts also display reduced levels of the ER proteins BiP and ERO1-Lα, suggesting ER homeostasis may be perturbed by the *SPTLC1* mutation (Myers et al., 2014). Moreover, electron and confocal microscopy has

revealed increased lipid droplet accumulation in patient-derived cells compared to controls (Marshall et al., 2014; Myers et al., 2014).

5.1.2 Viral vectors for gene delivery

Neurons are generally resistant to non-viral means of genetic transfer but have been successfully transduced using viral vectors (Davidson and Breakefield, 2003; Kalmar et al., 2017). Viruses are naturally occurring vehicles which can be manipulated for the experimental transfer of genetic material both *in vivo* and *in vitro*. Several vectors exist capable of such transfer of genetic material, with the three major groups being i) adenoviruses, ii) adeno-associated viruses (AAV) and iii) retroviruses (Walther and Stein, 2000; Bouard et al., 2009).

Both adenoviruses and AAV deliver genetic material as DNA, either in double or single stranded form, respectively (Walther and Stein, 2000). AAV tend to be smaller vectors, transferring up to 4.5 kb of genetic information, whereas adenoviruses have the capacity to transfer large amounts of DNA, up to 36 kb (Davidson and Breakefield, 2003; Choudhury et al., 2017). Both these vectors, which enter cells via endocytosis, possess the ability to transduce mitotic and post-mitotic cells, such as neurons (Choudhury et al., 2017). Since adenoviruses and recombinant AAV do not insert their genetic cargo into the genome, the expression of the transferred genetic material is at risk of being somewhat transient (Vannucci et al., 2013). Moreover, successful AAV transduction often requires additional helper genes, such as those from the adenovirus (Kay et al., 2001). As the transgene is not inserted into the genome of the host, this viral delivery is advantageous for *in vivo* uses as it proves safe to use. However, in models using cell lines it results in variable expression as adenoviruses are replication incompetent and therefore the transgene is lost in daughter cells.

Retroviruses are a family of viruses containing an RNA genome, which is reverse transcribed in successfully transduced cells to form DNA, which in turn inserts into the host genome (Walther and Stein, 2000; Bouard et al., 2009). Unlike adenoviruses and AAV, retroviruses enter cells via direct envelope fusion with the cell plasma membrane (Choudhury et al., 2017). Although retroviruses in

general are not able to transduce non-dividing cells, lentiviruses, a subdivision of the retrovirus family, are capable of gene transfer to both mitotic and non-mitotic cells (Davidson and Breakefield, 2003; Vannucci et al., 2013). Lentiviral vectors are typically derived from human immunodeficiency viruses (HIV) and can carry 7-8 kb of genetic information, boast limited toxicity and due to insertion into the host genome, long term gene expression (Kay et al., 2001; Davidson and Breakefield, 2003). Therefore, lentiviruses are ideal to use in non-dividing neuronal cells *in vitro*, due to their ability to achieve high fidelity, stable expression even in cells such as MNs, which are cells typically difficult to transfect.

Thus, although a number of *in vitro* and *in vivo* models of HSN-1 have been developed and studied in a bid to elucidate pathomechanisms of HSN-1, most of these models either used non-neuronal cells, such as lymphoblasts or, if using neurons, these were in the context of huge over-expression of the gene of interest. Therefore, in this Chapter, I undertook a series of experiments aimed to develop a motor and sensory neuronal model of HSN-1 that expresses the mutant gene at a low level. Thus, the *SPTLC1*^{WT} and *SPTLC1*^{C133W} genes were packaged into 3rd generation lentiviral vectors, using a backbone which had been previously shown to effectively transduce primary mammalian MNs (Kalmar et al., 2017).

5.2 Aims of this Chapter

The primary aim of the experiments described in this Chapter was to generate an *in vitro* neuronal model of HSN-1, whereby the wildtype and mutant enzymes are expressed at low levels in primary motor and sensory neurons. In addition, using this model I aimed to investigate whether expression of mutant *SPTLC1* in motor and sensory neurons results in similar levels of toxicity as observed in neurons treated with the aberrant SPT enzyme products in the experiments described in Chapter 3 (Sections 3.3.3 and 3.3.4). By measuring the sphingoid base profile in neurons expressing *SPTLC1* mutations it is also possible to confirm whether the gene product enzyme is functional and to establish the level of abnormal deoxysphingoid bases in these engineered cells. Comparison of the results obtained in the genetic expression model with those from the exogenously

treated model can answer a crucial question concerning the HSN-1 pathomechanism, namely whether it is the intracellular presence of the *SPTLC1* point mutation, or the systemic circulation of abnormal deoxysphingoid bases that underlies HSN-1 peripheral nerve damage. Finally, in this Chapter I aim to examine if any of the pathomechanisms identified in neurons treated with abnormal deoxysphinganines, presented in Chapter 4, are also apparent in neurons expressing HSN-1 causing mutations.

5.3 Results

Cultures of primary motor or DRG neurons were grown for 1 DIV, after which they were transfected with either an empty lentiviral vector, a lentiviral vector carrying human *SPTLC1*^{WT} (*SPTLC1*^{WT}) or a lentiviral vector carrying *SPTLC1*^{C133W}. The cells were incubated with the virus for 24 h and the media then replaced with standard neuronal culture media (see Materials and Methods, Chapter 2, Section 2.5). The effect of the transduction was then examined after 7-9 DIV.

5.3.1 Wildtype and mutant *SPTLC1*-carrying lentiviral vectors successfully transduce primary neurons

Primary MNs were transduced with virus at dilutions of either 1:250 or 1:100. As can be seen in Figure 5.1 A-D, the lentiviral vector successfully transduced primary MNs, as determined by the expression of green fluorescent protein (GFP). GFP is expressed in the lentiviral vector backbone from a promoter which is independent of *SPTLC1*, and was therefore used as a marker of successful viral transduction. The number of GFP$^+$ neurons was calculated for each culture and expressed as percentage of the total number of β-III tubulin$^+$ neurons present. The results shown in Figure 5.1 E summarise the results and show that there were no significant differences in transduction efficiency between the three lentiviruses. Thus, when applied at a dilution of 1:250, the empty lentiviral vector transduced 39 ± 11% of neurons, the *SPTLC1*^{WT} vector transduced 54 ± 4% of neurons and the *SPTLC1*^{C133W} vector transduced 47 ± 24% of neurons. Increasing the viral vector dilution to 1:100 had no significant effect on the transduction efficiency, so that *SPTLC1*^{WT} vector applied at 1:100 transduced 46% of neurons, compared to 54 ± 4% when applied at a dilution of 1:250.

Figure 5.1

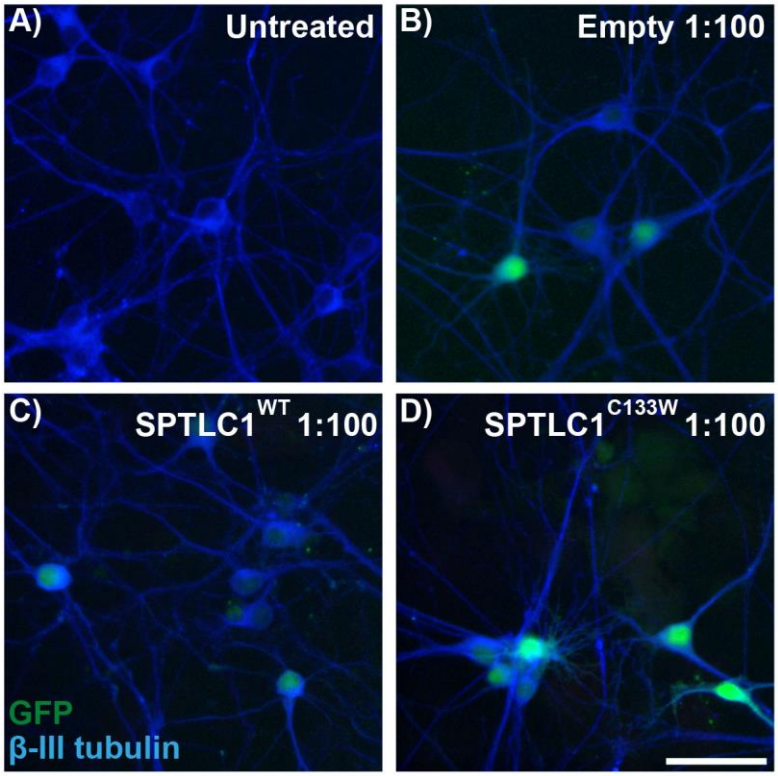
A)
Untreated
B)
Empty 1:100
C)
SPTLC1WT 1:100
D)
SPTLC1C133W 1:100
GFP
β-III tubulin

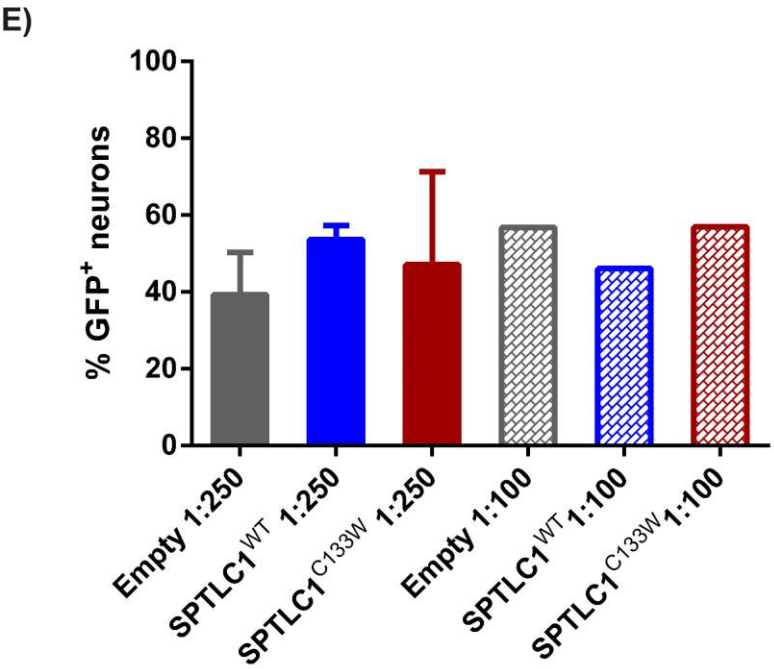
E)
% GFP+ neurons
100
80
60
40
20
0
Empty 1:250
SPTLC1WT 1:250
SPTLC1C133W 1:250
Empty 1:100
SPTLC1WT 1:100
SPTLC1C133W 1:100

Figure 5.1: Wildtype and mutant *SPTLC1*-carrying lentiviral vectors successfully transduce primary motor neurons

At 1 DIV primary MNs were transduced with a lentiviral vector. 24 h later, the cells were washed and subsequently, at 7 DIV, fixed and stained for β-III tubulin (blue). Successfully transduced cells express GFP (green). **A-D)** Example images of MNs either left untreated (A), transduced with an empty lentiviral vector (B), or a vector containing $SPTLC1^{WT}$ (C) or $SPTLC1^{C133W}$ (D). Scale bar = 50 µm. **E)** Bar chart showing quantification of the percentage of GFP^{+} neurons following transduction with empty vector, $SPTLC1^{WT}$ or $SPTLC1^{C133W}$, at final virus dilutions of 1:250 and 1:100. N = 1-2 independent experiments per condition. Displayed data represent the mean ± SEM.

5.3.2 Wildtype and mutant *SPTLC1* are expressed in transduced motor and sensory neuronal cultures

These results show that primary MNs were successfully transduced with the control and *SPTLC1*-containing vectors. I therefore next determined whether the genes of interest were being translated at the protein level in motor and sensory cultures. The V5 epitope tag was cloned into the viral vector immediately downstream of *SPTLC1* and is thus driven from the same promoter as *SPTLC1*. Western blot analysis of V5 expression in both MN cultures (Figure 5.2 A) and DRG cultures (Figure 5.2 B) transduced with $SPTLC1^{WT}$ or $SPTLC1^{C133W}$ (at a dilution of 1:250), showed bands at the molecular weight consistent of a small V5 epitope tag fused to the SPTLC1 protein. V5 expression was absent in untreated cultures or cultures transduced with the empty vector. As expected, when the dilution of virus was increased from 1:1000 to 1:250, there was a corresponding increase in V5 expression, as shown in Figure 5.3 A and quantified in Figure 5.3 B. When cells were transduced with $SPTLC1^{WT}$, V5 expression (relative to the background signal measured in untreated cultures) increased from 5.1 times (1:1000) to 6.8 times (1:500) to 12.0 times (1:250). Likewise, in cultures transduced with $SPTLC1^{C133W}$ V5 expression relative to untreated cultures increased from 3.6 times (1:1000) to 4.8 times (1:500) and 8.4 times (1:250).

The expression of transduced *SPTLC1* was also confirmed by probing the western blots with an antibody against SPTLC1 itself. In both MN (Figure 5.4 A) and DRG cultures (Figure 5.4 B) transduced with $SPTLC1^{WT}$ or $SPTLC1^{C133W}$, a doublet was observed, whereby the lower band represents endogenous mouse SPTLC1 and the upper (heavier) band shows transduced SPTLC1 fused to the V5 tag, which migrates slower by SDS-PAGE due to its higher molecular weight

Figure 5.2

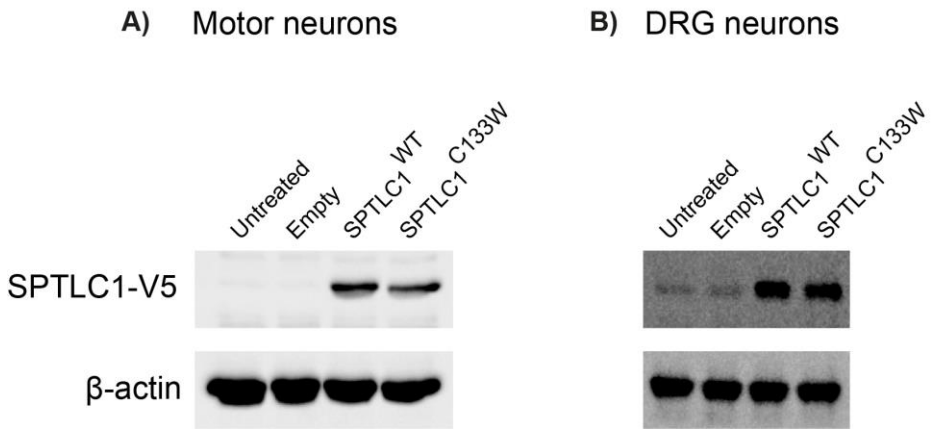

Figure 5.2: The SPTLC1-V5 fusion protein is expressed in transduced primary motor and DRG neurons

Primary MNs or DRG neurons were grown for 1 DIV before being transduced with a lentiviral vector, which was washed off after 24 h. Cultures were grown until 7 DIV before protein extraction and analysis. **A)** Western blot showing expression of the SPTLC1-V5 fusion protein (55 kDa) along with the loading control β-actin (42 kDa), in MNs transduced with virus at final dilutions of 1:250. **B)** Western blot showing expression of the SPTLC1-V5 fusion protein along with the loading control β-actin, in DRG cultures transduced with virus at final concentrations of 1:250.

Figure 5.3

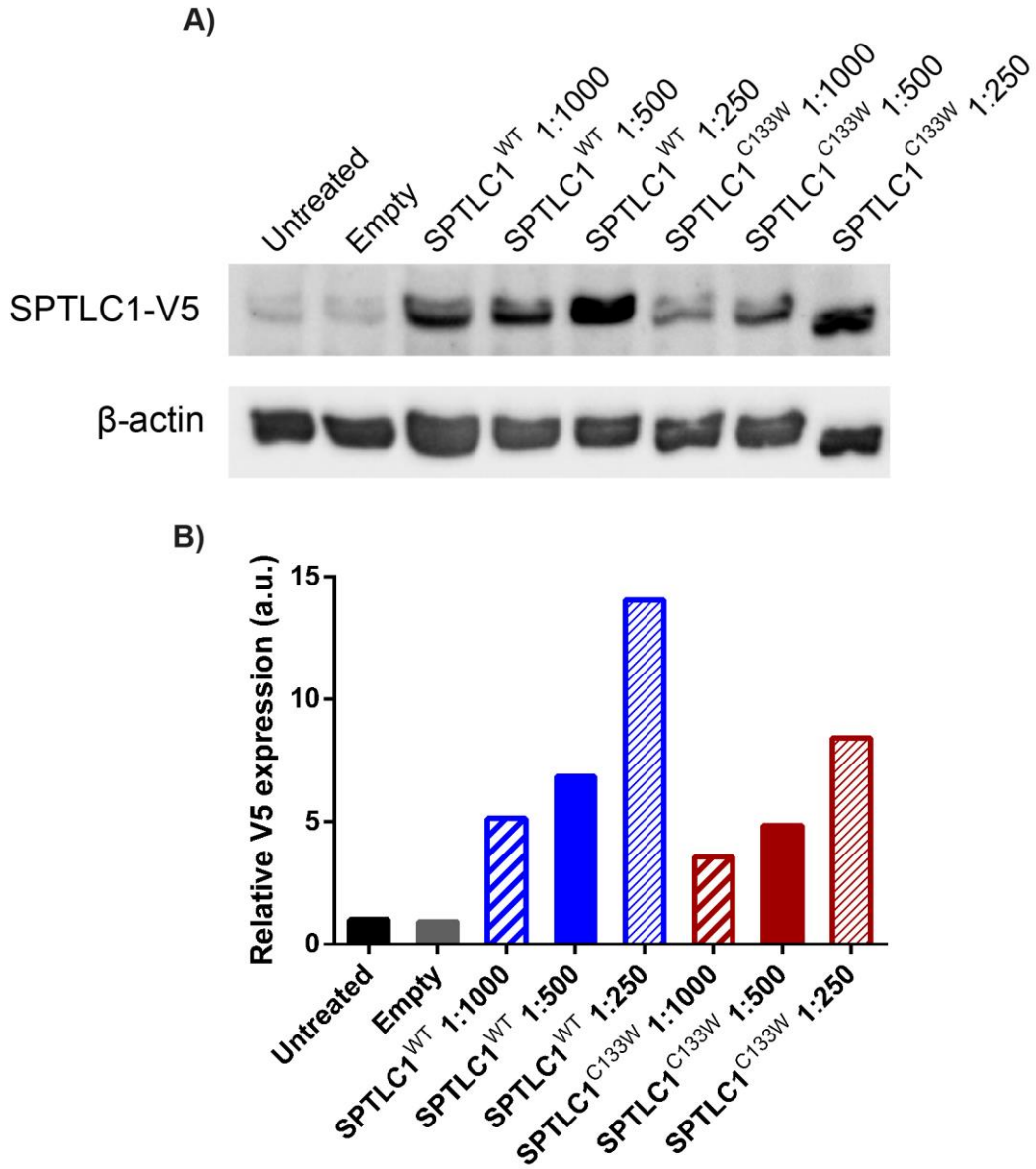

Figure 5.3: The SPTLC1-V5 fusion protein is expressed in a dose-dependent manner in primary motor neurons

Primary MNs were grown for 1 DIV before being transduced with a lentiviral vector, which was washed off after 24 h. Cultures were grown until 7 DIV before protein extraction and analysis. **A**) Western blot showing expression of the SPTLC1-V5 fusion protein (55 kDa) and the loading control β-actin (42 kDa), in MNs transduced with virus at final dilutions ranging from 1:1000-1:250. **B**) Bar chart showing quantification of SPTLC1-V5 expression normalised to β-actin loading controls, all relative to expression measured in untreated cultures.

Figure 5.4

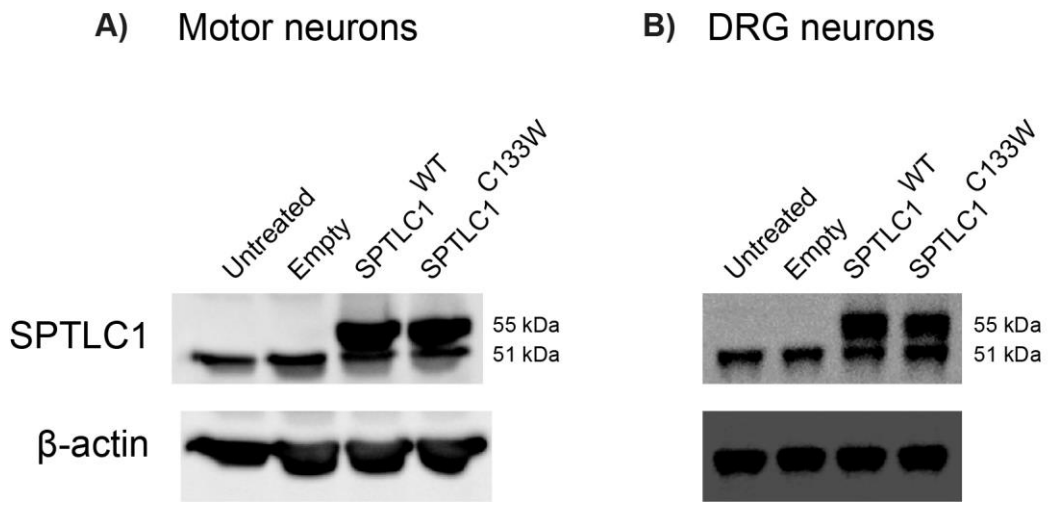

Figure 5.4: Endogenous and virally induced SPTLC1 is expressed in transduced primary motor and DRG neurons

Primary MNs or DRG neurons were grown for 1 DIV before being transduced with a lentiviral vector, which was washed off after 24 h. Cultures were grown until 7 DIV before protein extraction and analysis. **A)** Western blot showing the expression of SPTLC1 protein (endogenous protein at 51 and transduced protein at 55 kDa) and of loading control β-actin (42 kDa). **B)** Western blot showing the expression of SPTLC1 protein and of loading control β-actin in DRG cultures. In both blots A-B, the lower band represents endogenous SPTLC1 protein and the upper band represents transduced SPTLC1 protein, which runs slower than endogenous SPTLC1 due to the addition of a V5 epitope tag.

(addition of approximately 4 kDa). In comparison, in untreated cultures and cultures transduced with empty vector, only the lower band, representing endogenous mouse SPTLC1, is present. As can be seen in Figure 5.5 A, transduction with both *SPTLC1*^{WT} and *SPTLC1*^{C133W} vectors at dilutions of 1:1000 and 1:500 reduced the expression of endogenous mouse SPTLC1. As quantified in Figure 5.5 B expression of SPTLC1^{WT} (1:500, relative to endogenous SPTLC1 expression in untreated cultures) caused a reduction in endogenous SPTLC1 from 1.25 in the empty treated cultures to 0.57. Similarly, expression of SPTLC1^{C133W} (1:500) caused a reduction in endogenous SPTLC1 to 0.52.

The results summarised in Figures 5.1 – 5.5 indeed confirm that the generated lentiviral vectors successfully transduce primary neuronal cultures and moreover, that both wildtype and mutant SPTLC1 are expressed in motor and DRG cultures.

5.3.3 GFP and V5 vector markers are not consistently co-expressed in all transduced cells

The lentiviral constructs used in these experiments contain two markers, derived from different promoters. GFP expression is driven by an elongation factor 1α (EF-1α) promoter and is used as a marker of successful transduction; the V5 epitope tag is cloned directly downstream of *SPTLC1,* the expression of which is driven by a human cytomegalovirus (CMV) promoter. Immunostaining with antibodies raised against the V5 tag showed that when transduced with either *SPTLC1*^{WT} or *SPTLC1*^{C133W}*,* the GFP^{+} cells did not always correspond with the V5^{+} cells (Figure 5.6). The filled arrow heads in Figure 5.6 highlight neurons which are positive for both GFP and V5, whilst the long arrows indicate neurons positive for GFP, but not V5; empty arrow heads indicate non-neuronal cells positive for V5, but not GFP. Furthermore, although V5 was expressed in both neurons and non-neuronal cells in the mixed cultures, GFP was far more frequently expressed exclusively in neurons. As it is not possible to visualize the V5 tag in live cells, this is a problem for live-cell imaging experiments. The results shown in Figure 5.6 suggest that although the GFP marker is suitable for identification of successfully transduced neurons, GFP expression is not sufficient to confirm co-expression of the *SPTLC1* transgene.

Figure 5.5

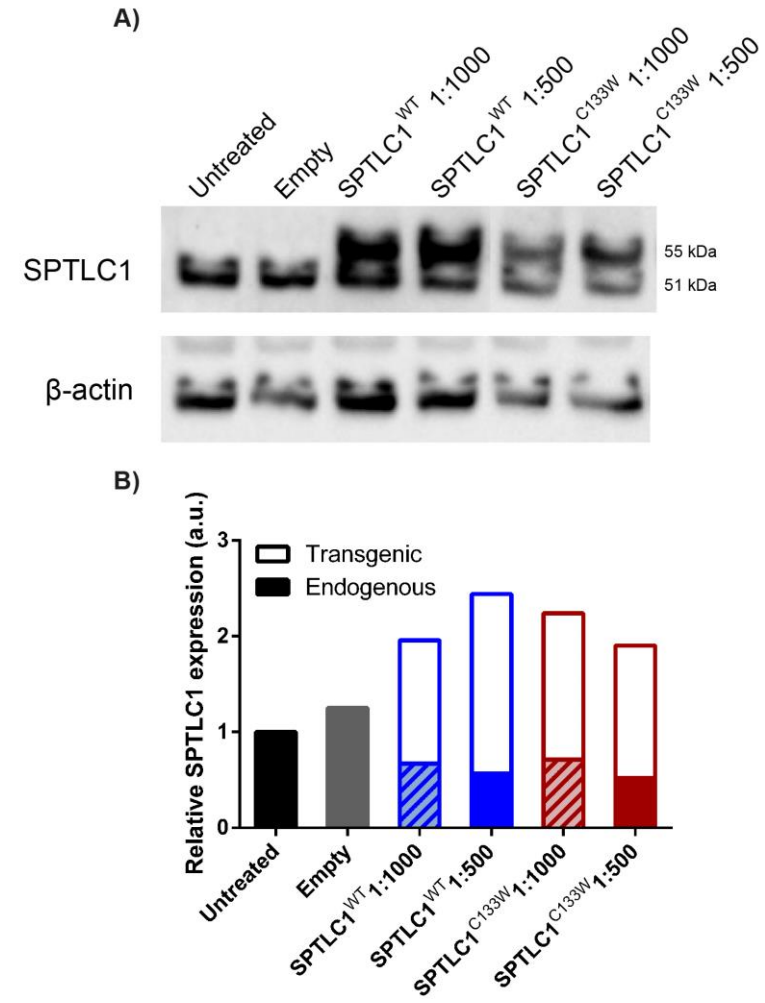

Figure 5.5: Virally induced SPTLC1 downregulates endogenous SPTLC1 in transduced primary motor neurons

Primary MNs were grown for 1 DIV before being transduced with lentiviral vector, which was washed off after 24 h. Cultures were grown until 7 DIV before protein extraction and analysis. **A)** Western blot showing the expression of SPTLC1 protein (51 and 55 kDa) and of loading control β-actin (42 kDa) in MNs transduced with virus at final dilutions ranging from 1:1000-1:500. The lower band represents endogenous SPTLC1 protein and the upper band represents transduced SPTLC1 protein, which runs slower than endogenous SPTLC1 due to the addition of a V5 epitope tag. **B)** Bar chart showing quantification of endogenous and transduced SPTLC1 expression normalised to β-actin loading controls, all relative to total SPTLC1 expression measured in the untreated culture.

Figure 5.6

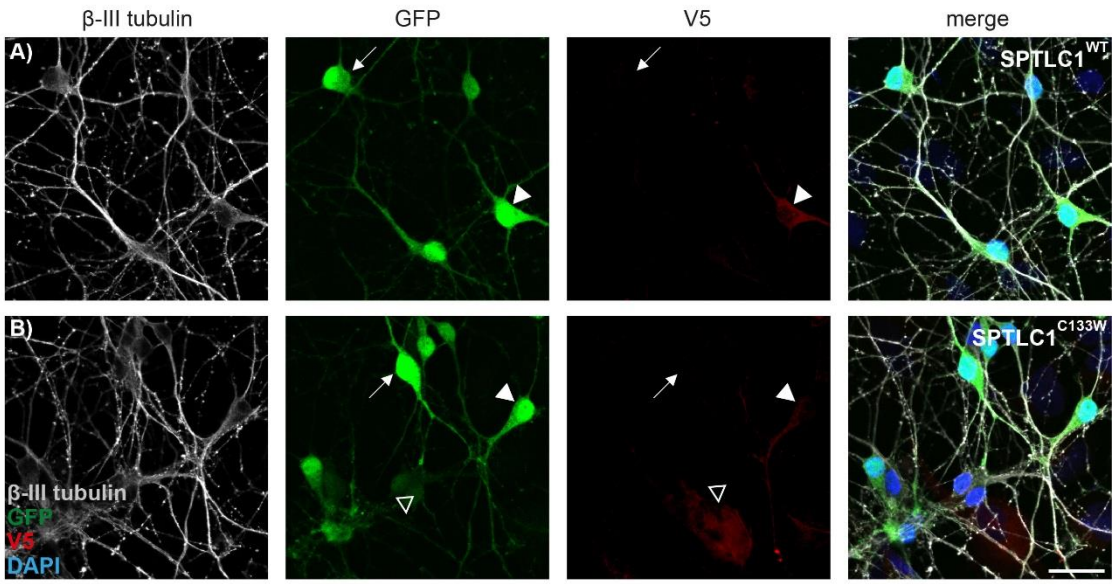

Figure 5.6: GFP$^+$ and V5$^+$ cells do not correspond

Primary MNs were grown for 1 DIV before being transduced with lentiviral vectors at final dilutions of 1:250, which was washed off after 24 h. MNs were grown until 7 DIV and fixed and stained for DAPI (blue), V5 (red) and β-III tubulin (grey). **A)** MNs transduced with SPTLC1^{WT}. **B)** MNs transduced with SPTLC1^{C133W}. Arrows indicate cells positive for GFP but negative for V5. Filled arrow heads indicate neurons simultaneously positive for GFP and V5. Empty arrow heads indicate non-neuronal cells positive for V5 but negative for GFP. Scale bar = 25 µm.

5.3.4 Motor neurons expressing *SPTLC1^{C133W}* produce a functional enzyme which generates deoxysphingoid bases

The results show that lentiviral vectors can be used to successfully transfect primary neuronal cultures with wildtype and mutant *SPTLC1*. Therefore, I next examined whether virally induced SPTLC1 was able to form an active heterotrimer with the mouse SPTLC2 and the third small subunit (ssSPTa/b) to form an enzymatically active SPT complex. The C133W mutation in the SPTLC1 subunit is known to preferentially utilise L-alanine over L-serine for condensation with palmitoyl-CoA and subsequently generate neurotoxic DSp (Zitomer et al., 2009; Gable et al., 2010; Penno et al., 2010). Thus, to test if primary MN cultures expressing *SPTLC1^{C133W}* were generating the aberrant deoxysphingoid bases shown in Chapter 3 to cause neurotoxicity, cells were collected and analyzed for lipid composition using liquid chromatography-mass spectrometry (LC-MS). These experiments were carried out in collaboration with Saranya Suriyanarayanan and Professor Thorsten Hornemann at University of Zürich, Switzerland.

At 1 DIV, MN cultures were treated with empty, *SPTLC1^{WT}* or *SPTLC1^{C133W}* lentiviral vectors (1:100). This was washed off at 2 DIV and the cells collected for analysis at 9 DIV. This protocol enabled the transgenic SPTLC1 protein 7 days to form enzymatically active complexes. In some wells, cells were supplemented with L-alanine which was added to the typical MN culture media at a concentration of 20 mM, from the point of viral transduction until the end of the experiment. Cells were then harvested, washed in PBS and processed for LC-MS to measure the sphingoid base profile in these cells. In Figures 5.7 and 5.8 all measurements are normalised to the levels of 16 carbon length chain sphingosine (C16-sphingosine) in order to account for differences in cell number.

Figure 5.7

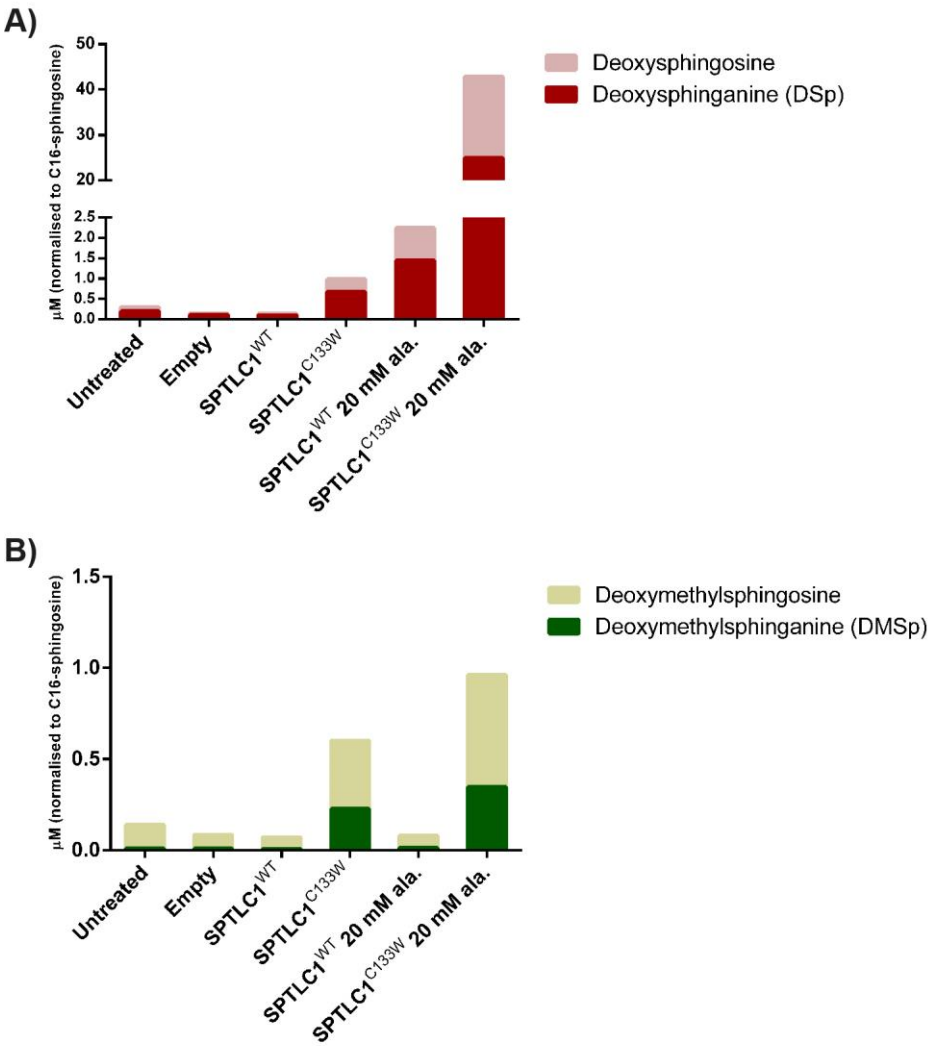

Figure 5.7: Transduced motor neuron cultures produce deoxysphingoid bases

Primary MNs were grown for 1 DIV before being transduced with lentiviral vectors (1:100), which were washed off after 24 h. Cultures were grown until 9 DIV before cells were collected for LC-MS analysis. Where indicated L-alanine supplementation was introduced at 1 DIV and continued until the end of the experiment. **A)** Levels of deoxysphinganine (dark red) and deoxysphingosine (light red) were measured in µM and normalised to the concentration of 16 carbon length chain sphingosine (C16-sphingosine). **B)** Levels of deoxymethylsphinganine (dark green) and deoxymethylsphingosine (light green) were measured and normalised to C16-sphingosine.

Figure 5.8

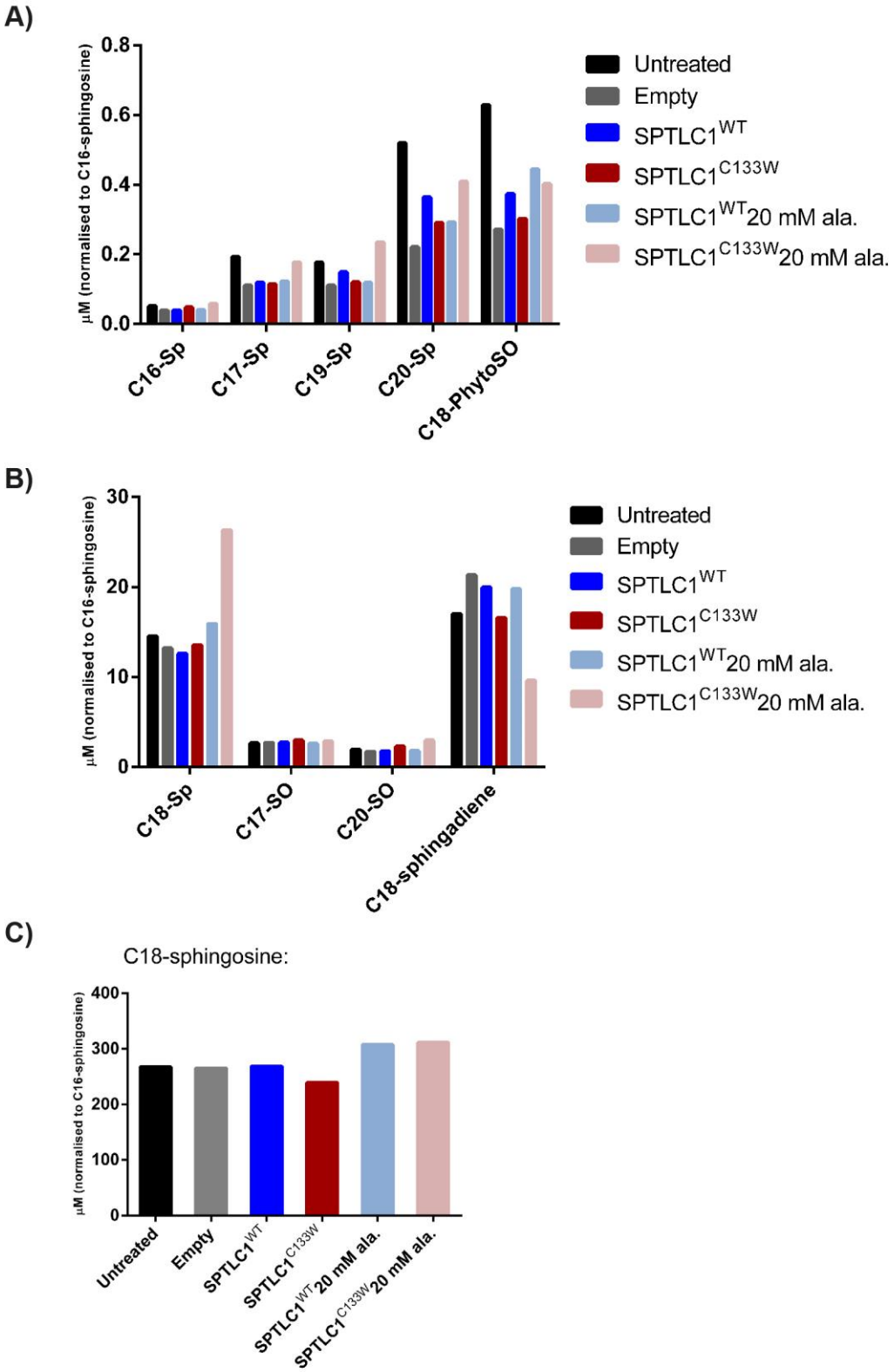
A)
µM (normalised to C16-sphingosine)
0.8
0.6
0.4
0.2
0.0
C16-Sp
C17-Sp
C19-Sp
C20-Sp
C18-PhytoSO
Untreated
Empty
SPTLC1WT
SPTLC1C133W
SPTLC1WT20 mM ala.
SPTLC1C133W20 mM ala.
B)
µM (normalised to C16-sphingosine)
30
20
10
0
C18-Sp
C17-SO
C20-SO
C18-sphingadiene
Untreated
Empty
SPTLC1WT
SPTLC1C133W
SPTLC1WT20 mM ala.
SPTLC1C133W20 mM ala.
C)
C18-sphingosine:
µM (normalised to C16-sphingosine)
400
300
200
100
0
Untreated
Empty
SPTLC1WT
SPTLC1C133W
SPTLC1WT20 mM ala.
SPTLC1C133W20 mM ala.

Figure 5.8: The typical sphingoid base profile in transduced motor neurons

Primary MNs were grown for 1 DIV before being transduced with lentiviral vectors (1:100), which were washed off after 24 h. Cultures were grown until 9 DIV before cells were collected for LC-MS analysis. Where indicated L-alanine supplementation was introduced at 1 DIV and continued until the end of the experiment. **A)** Levels of 16-20 carbon length chain sphinganine (C16-Sp, C17-Sp, C19-Sp, C20-Sp) and C18-phytosphingosine (C18-PhytoSO) were measured and normalised to C16-sphingosine. **B)** Levels of C18-Sp, C17- and C20-sphingosine (C17-SO and C20-SO) and C18-sphingadiene were measured and normalised to C16-sphingosine. **C)** Levels of C18-sphingosine were measured and normalised to C16-sphingosine.

LC-MS revealed that MN cultures transduced with *SPTLC1*^{C133W} produced both DSp and the downstream metabolite- deoxysphingosine (Figure 5.7 A). When normalised to C16-sphingosine, cultures expressing *SPTLC1*^{C133W} produced 0.67 μM of DSp and 0.31 μM of deoxysphingosine, compared to 0.10 μM DSp and 0.04 μM deoxysphingosine in cultures expressing *SPTLC1*^{WT}. Indeed, when these cultures were supplemented with 20 mM L-alanine, the precursor to the deoxysphingoid bases, a dramatic increase in the production of DSp and deoxysphingosine was seen in *SPTLC1*^{C133W} transduced cultures, with 24.91 μM DSp and 17.96 μM deoxysphingosine produced (Figure 5.7 B). L-alanine supplementation was even sufficient to cause an increase in deoxysphingoid base production in *SPTLC1*^{WT} transduced cells, to 1.44 μM DSp and 0.80 μM deoxysphingosine (Figure 5.7 A).

Deoxymethylsphinganine (DMSp) has also been shown to be elevated in HSN-1 patient plasma, although at a much lower concentration than DSp (Penno et al., 2010). In MN cultures transduced with *SPTLC1*^{C133W} 0.23 μM DMSp and 0.39 μM of downstream metabolite deoxymethylsphingosine were produced, compared to 0.01 μM DMSp and 0.06 μM deoxymethylsphingosine in *SPTLC1*^{WT} transduced MNs (Figure 5.7 C). Since deoxymethylsphingoid bases are produced from the condensation of palmitoyl-CoA with L-glycine, as expected, supplementation with 20 mM L-alanine had no major effect on the levels of deoxymethylsphingoid base production; cultures transduced with *SPTLC1*^{WT} and supplemented with 20 mM L-alanine produced 0.01 μM DMSp and 0.07 μM deoxymethylsphingosine and cultures transduced with *SPTLC1*^{C133W} and supplemented with 20 mM L-alanine produced 0.35 μM DMSp and 0.61 μM deoxymethylsphingosine.

In addition to studying the production of the abnormal deoxysphingoid bases, the profile of the typical sphingoid bases was also examined in virally transduced MN cultures (Figure 5.8). There were no major differences observed, although a trend towards elevated levels of some sphinganines was noted in cultures transduced with *SPTLC1*^{C133W} and supplemented with 20 mM L-alanine, namely C17-sphinganine (C17-Sp), C19-Sp, C20-Sp (Figure. 5.8 A) and C18-Sp (Figure 5.8 B). In contrast, production of C18-sphingadiene appeared reduced in

SPTLC1^{C133W} transduced cultures supplemented with 20 mM L-alanine (Figure 5.8 B).

The results displayed in Figures 5.7 and 5.8 show that deoxysphingoid bases are indeed produced in MN cultures transduced with human and mutant *SPTLC1*, and that levels of their production can be exacerbated with L-alanine supplementation.

5.3.5 Expression of *SPTLC1*^{C133W} has little effect on motor neuron survival, despite L-alanine supplementation

The results presented in this Chapter show that lentiviral delivery of *SPTLC1* results in the expression of a functional enzyme unit and that these transduced neurons produce abnormal deoxysphingoid bases typical of the mutant SPTLC1 containing enzyme. Since treatment of primary MN cultures with the aberrant deoxy- products of the mutant SPT enzyme caused a drastic reduction in neuronal survival (Chapter 3, Section 3.3.3), I next examined whether expression of functionally active *SPTLC1*^{C133W} also impacted on neuronal survival. Primary MNs were grown for 24 h before being treated with viral vectors at a concentration of either 1:250 or 1:100, which was washed off 24 h later. In addition to transduction with *SPTLC1*^{C133W}, some cultures were supplemented with L-alanine from the point of viral transduction to the end of the experiment, at concentrations ranging from 1 to 20 mM. L-alanine is the substrate preferentially utilised by mutant SPT and undergoes reaction with palmitoyl-CoA to form the aberrant and toxic enzyme product DSp (see Chapter 3, Sections 3.3.3 and 3.3.4 and Penno et al., 2010). Cultures were fixed and immunostained for analysis after 9 DIV and the number of neuronal cells established in each experimental condition (as described in Chapter 3, Sections 3.3.1, 3.3.2 and 3.3.3).

Figure 5.9 A-D shows representative images of MN cultures transduced with *SPTLC1*^{WT} or *SPTLC1*^{C133W} (1:100), grown in standard MN media or supplemented with 10 or 20 mM L-alanine. The number of neurons (β-III tubulin^{+}) was counted and expressed as a percentage of the number of neurons in untreated cultures (Figure 5.9 E and F). Transduction with *SPTLC1*^{C133W} (1:250)

Figure 5.9

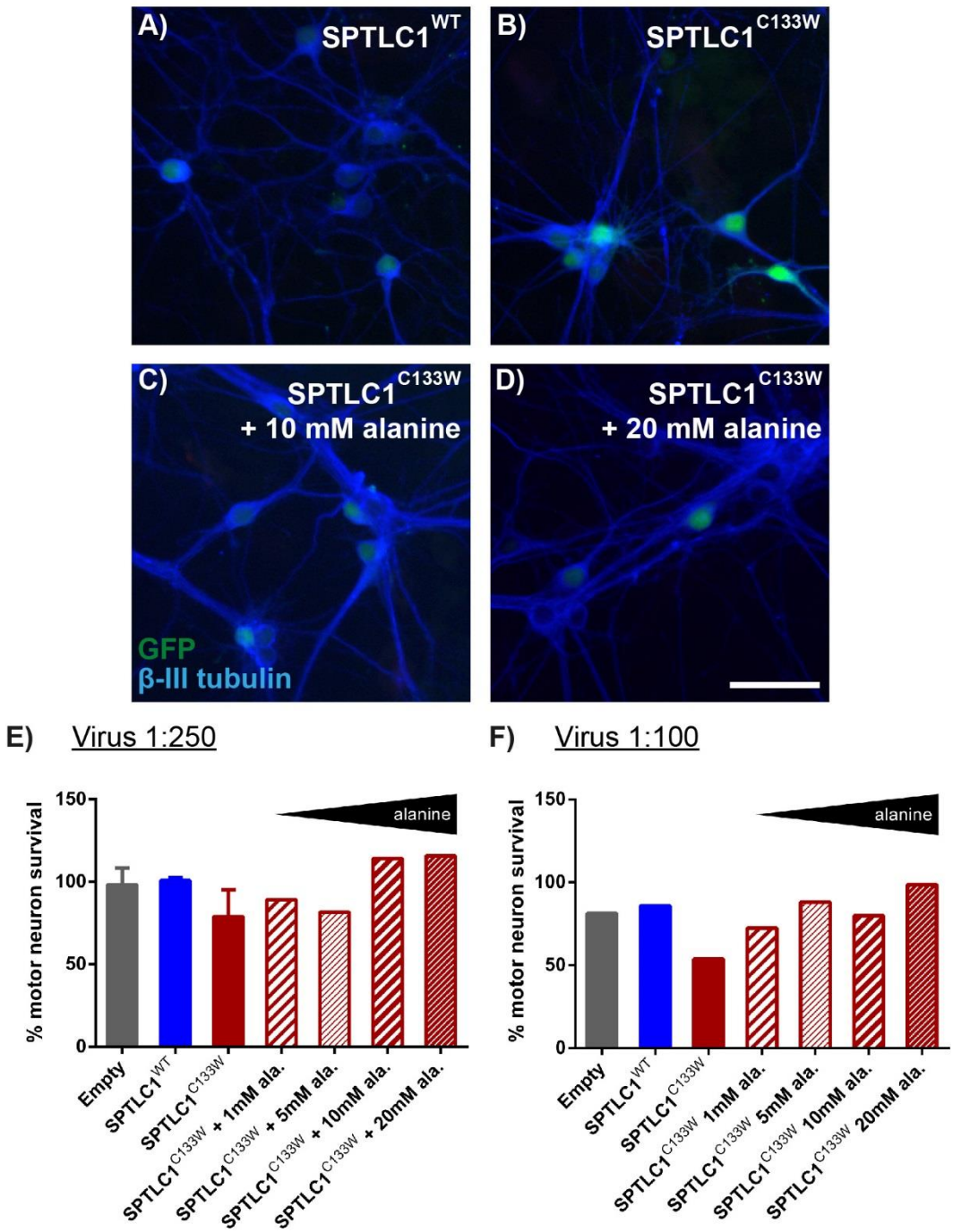
A)
SPTLC1WT
B)
SPTLC1C133W
C)
SPTLC1C133W
+ 10 mM alanine
D)
SPTLC1C133W
+ 20 mM alanine
GFP
β-III tubulin
E) Virus 1:250
F) Virus 1:100
% motor neuron survival
150
100
50
0
alanine
Empty
SPTLC1WT
SPTLC1C133W
SPTLC1C133W + 1mM ala.
SPTLC1C133W + 5mM ala.
SPTLC1C133W + 10mM ala.
SPTLC1C133W + 20mM ala.
SPTLC1C133W 1mM ala.
SPTLC1C133W 5mM ala.
SPTLC1C133W 10mM ala.
SPTLC1C133W 20mM ala.

Figure 5.9: Expression of *SPTLC1^{C133W}* has little effect on motor neuron survival, despite L-alanine supplementation

Primary MNs were grown for 1 DIV before being transduced with a lentiviral vector at final dilutions of 1:100-1:250, which was washed off after 24 h. MNs were grown until 9 DIV and fixed and stained for β-III tubulin (blue). L-alanine supplementation was introduced at 1 DIV and continued until the end of the experiment. **A-D)** Example images of MNs transduced with *SPTLC1^{WT}* (A), *SPTLC1^{C133W}* (B), or *SPTLC1^{C133W}* supplemented 10 (C) or 20 mM L-alanine (D). Scale bar = 50 µm. **E)** Bar chart showing quantification of MN survival, expressed as a percentage of untreated cultures, following transduction with empty vector, *SPTLC1^{WT}* or *SPTLC1^{C133W}* at final virus dilutions of 1:250, and supplemented with 1-20 mM L-alanine. **F)** Bar chart showing quantification of MN survival, expressed as a percentage of untreated cultures, following transduction with empty vector, *SPTLC1^{WT}* or *SPTLC1^{C133W}* at final virus dilutions of 1:100, and supplemented with 1-20 mM L-alanine. N = 1-2 independent experiments per condition. Displayed data represent the mean ± SEM.

caused a slight, but non-significant reduction in neuronal survival to 79 ± 16%, when compared to neuronal survival in the *SPTLC1*^{WT} transduced cultures of 100 ± 2% (Figure. 5.9 E). L-alanine supplementation, ranging from 1 to 20 mM, did not exacerbate this phenotype, and supplementation with both 10 and 20 mM caused an increase in neuronal survival, to 114% and 115%, respectively. Although only repeated once, when the viral dilution was increased to 1:100 a similar pattern of neuronal survival was observed (Figure 5.9 F). Neuronal survival in *SPTLC1*^{WT} transduced cultures was 86%, which reduced to 54% in *SPTLC1*^{C133W} transduced cultures, but increased to 99% in *SPTLC1*^{C133W} transduced cultures supplemented with 20 mM L-alanine.

5.3.6 Expression of *SPTLC1*^{C133W} has no effect on expression of the ER stress marker BiP in motor or DRG neurons

Treating both MN and DRG cultures with exogenous deoxysphingoid bases (abnormal SPT products) resulted in ER stress, suggesting that this may be an early pathomechanism in DSp-mediated neurotoxicity (Chapter 4, Sections 4.3.3 and 4.3.4). ER stress was therefore examined in MN and DRG cultures transduced with *SPTLC1*^{C133W}.

MN cultures were either left untreated or transduced with empty, *SPTLC1*^{WT} or *SPTLC1*^{C133W} viral vector (1:250) before analysis at 7 DIV. Immunostaining for the ER stress marker BiP did not reveal any major structural or expression level changes between MNs expressing wildtype or mutant *SPTLC1* (Figure 5.10). Western blot analysis of BiP expression in MN cultures transduced with lentiviral vectors (Figure 5.11) revealed a decrease in BiP expression across all three lentiviral vectors, although no significant changes were detected between the vectors (Figure 5.11 B). Thus, MN cultures transduced with empty vector had a relative BiP expression of 0.79 ± 0.02, cultures transduced with *SPTLC1*^{WT} a relative BiP expression of 0.63 ± 0.05 and *SPTLC1*^{C133W}, 0.64 ± 0.03, relative to untreated control cultures.

Figure 5.10

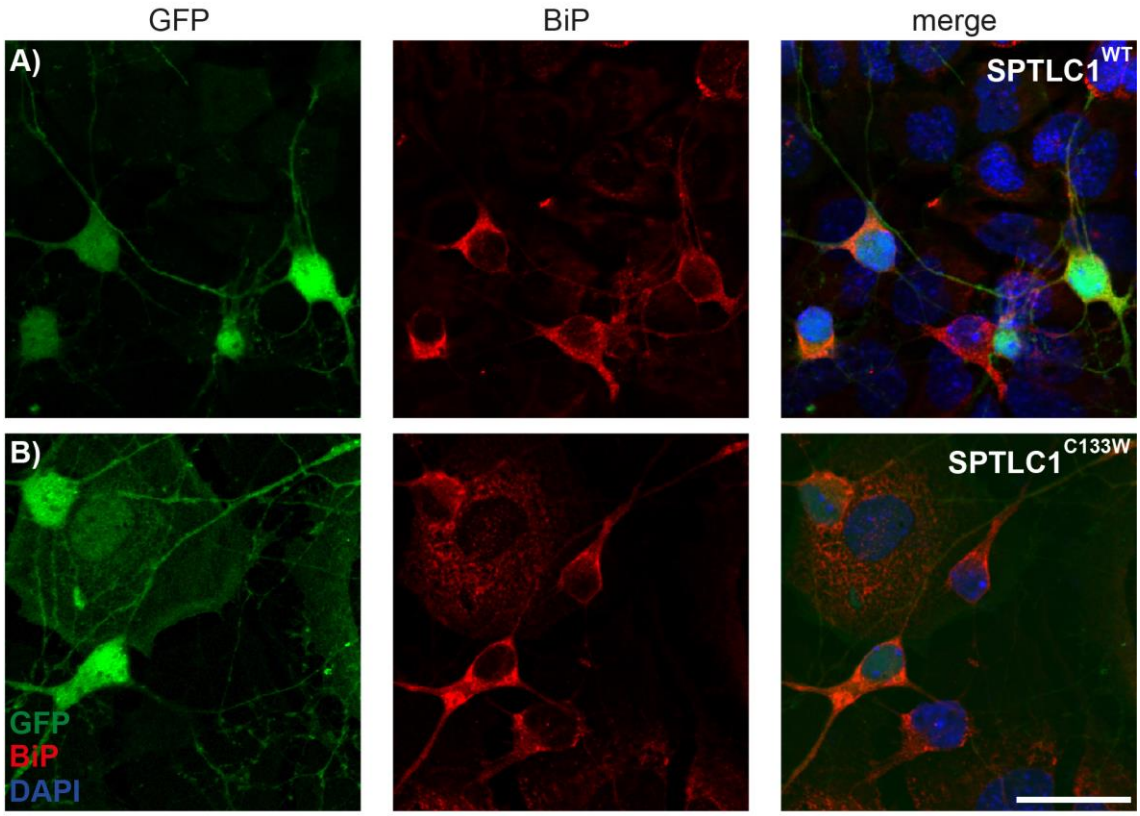

Figure 5.10: Expression of *SPTLC1^{C133W}* has no effect on expression of the ER stress marker BiP in motor neurons

Primary MNs were grown for 1 DIV before being transduced with lentiviral vectors (1:250), which were washed off after 24 h. **A)** MNs expressing SPTLC1^{WT} were grown until 7 DIV before fixation and were stained for DAPI (blue) and BiP (red). **B)** MNs expressing SPTLC1^{C133W} were grown until 7 DIV before fixation and were stained for DAPI (blue) and BiP (red). Scale bar = 25 µm.

Figure 5.11

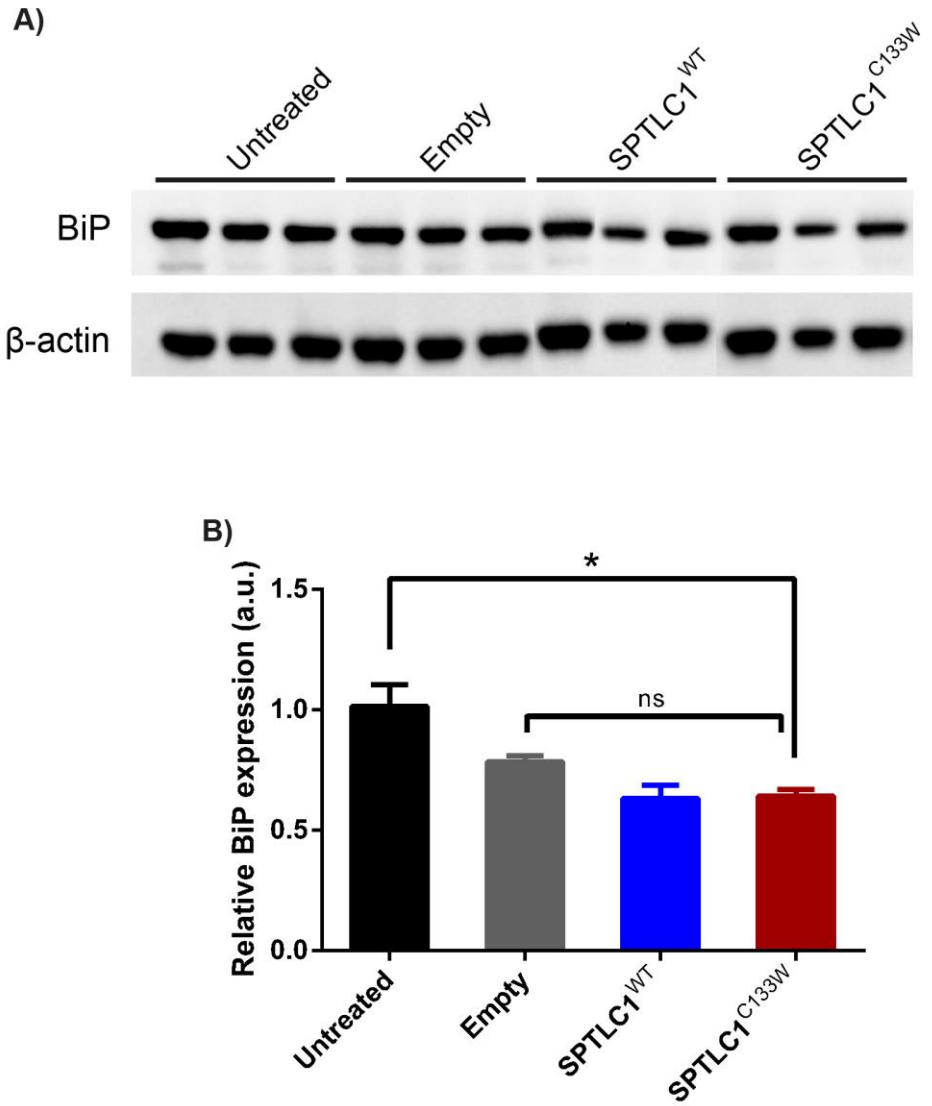

Figure 5.11: Expression of *SPTLC1^{C133W}* has no effect on expression of the ER stress marker BiP in motor neurons

Primary MNs were grown for 1 DIV before being transduced with lentiviral vectors (1:250), which were washed off after 24 h. **A)** MNs were grown to 7 DIV before protein extraction. Western blot showing the expression of BiP (78 kDa) and loading control β-actin (42 kDa) in virally transduced MNs. **B)** Bar chart showing quantification of BiP expression in MNs, normalised to β-actin loading controls, all relative to BiP expression in the second lane untreated culture. N = 3 independent experiments per condition. Displayed data represent the mean ± SEM. Kruskal-Wallis and Dunn's multiple comparisons tests were used for statistical analysis. *P* values: * < 0.05; ** < 0.01; *** < 0.001. ns = not significant.

To investigate the effects of mutant *SPTLC1* expression in sensory neurons, DRG cultures were also transduced with the same three viral vectors and analysed using immunocytochemistry (Figure 5.12) and western blot analysis (Figure 5.13) for the expression of the ER stress marker BiP. A similar pattern of global BiP depletion was observed in transduced cultures when compared to the untreated control, but with no differences between the three transduced groups (Figure 5.13 B).

Taken together, the results shown in Figures 5.9-5.13 demonstrate that neurons expressing *SPTLC1*^{C133W} do not exhibit reduced survival and do not display an overt ER stress phenotype, as described in other *in vitro* HSN-1 models.

5.4 Discussion

In this Chapter, lentiviral vectors encoding for wildtype and mutant *SPTLC1* were generated and used to successfully transduce primary motor and DRG cells. These vectors were generated so that GFP was expressed in the lentiviral backbone under a promoter that was independent of SPTLC1. Thus, the presence of GFP was used to confirm that the viral vectors were successfully infecting primary neurons. Furthermore, western blots probed for both the transduced SPTLC1 epitope tag V5 and SPTLC1 itself, confirmed that the inserted *SPTLC1* genes were translated into protein.

Expression of both wildtype and mutant human SPTLC1 caused a reduction in endogenous SPTLC1 expression, as determined by western blot. It is possible that this is due to a negative feedback loop from SPTLC1, acting on mouse *SPTLC1* transcription and/or translation. This feedback may initiate from accumulation of the protein itself, or indeed downstream metabolites within the sphingolipid pathway. There is evidence that negative feedback from downstream metabolites occurs in the sphingolipid pathway, causing inhibition of SPT via the three orosomucoid-like (ORMDL) proteins (Breslow et al., 2010; Gururaj et al., 2013; Gupta et al., 2014). The importance of this regulation, which serves to prevent the potentially toxic accumulation of sphingolipid-intermediates, is supported by the fact that ORMDL proteins are highly conserved from yeast to

Figure 5.12

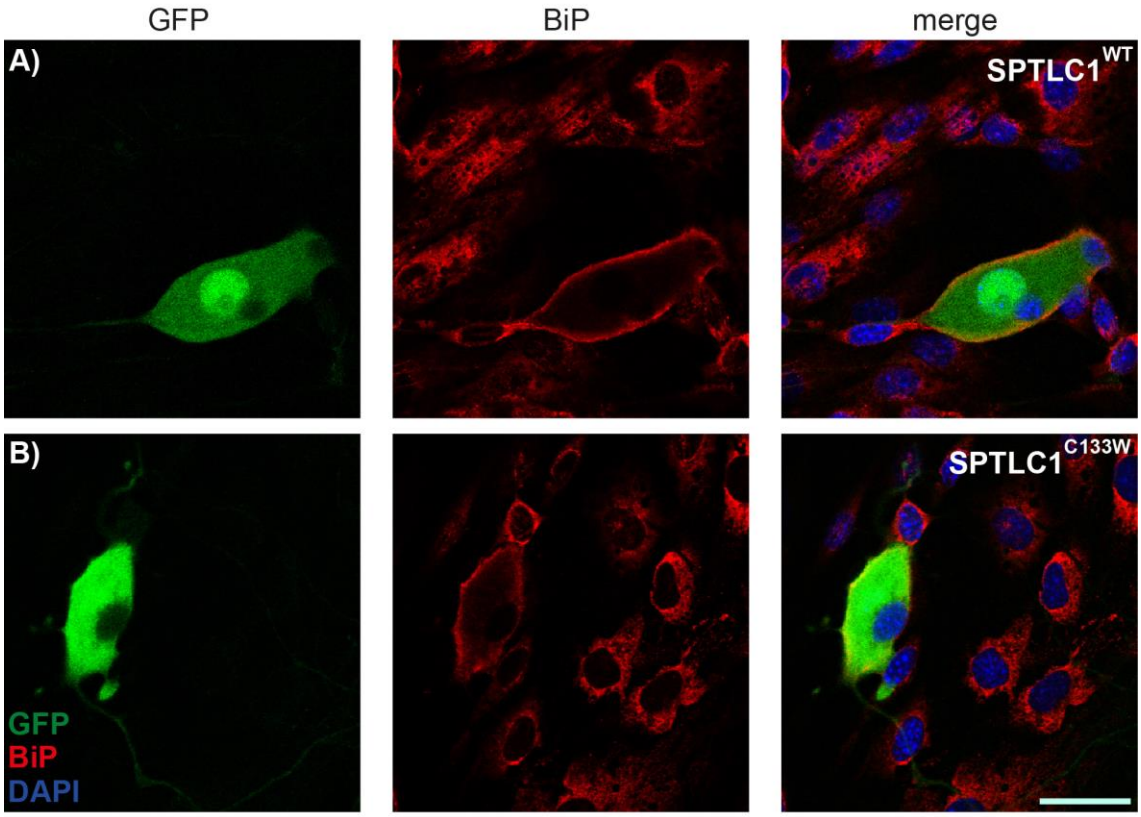

Figure 5.12: Expression of *SPTLC1^{C133W}* has no effect on expression of the ER stress marker BiP in DRG neurons

Primary DRG cultures were grown for 1 DIV before being transduced with lentiviral vectors (1:250), which were washed off after 24 h. **A)** DRG cultures expressing SPTLC1^{WT} were grown until 7 DIV before fixation and were stained for DAPI (blue) and BiP (red). **B)** DRG cultures expressing SPTLC1^{C133W} were grown until 7 DIV before fixation and were stained for DAPI (blue) and BiP (red). Scale bar = 25 µm.

Figure 5.13

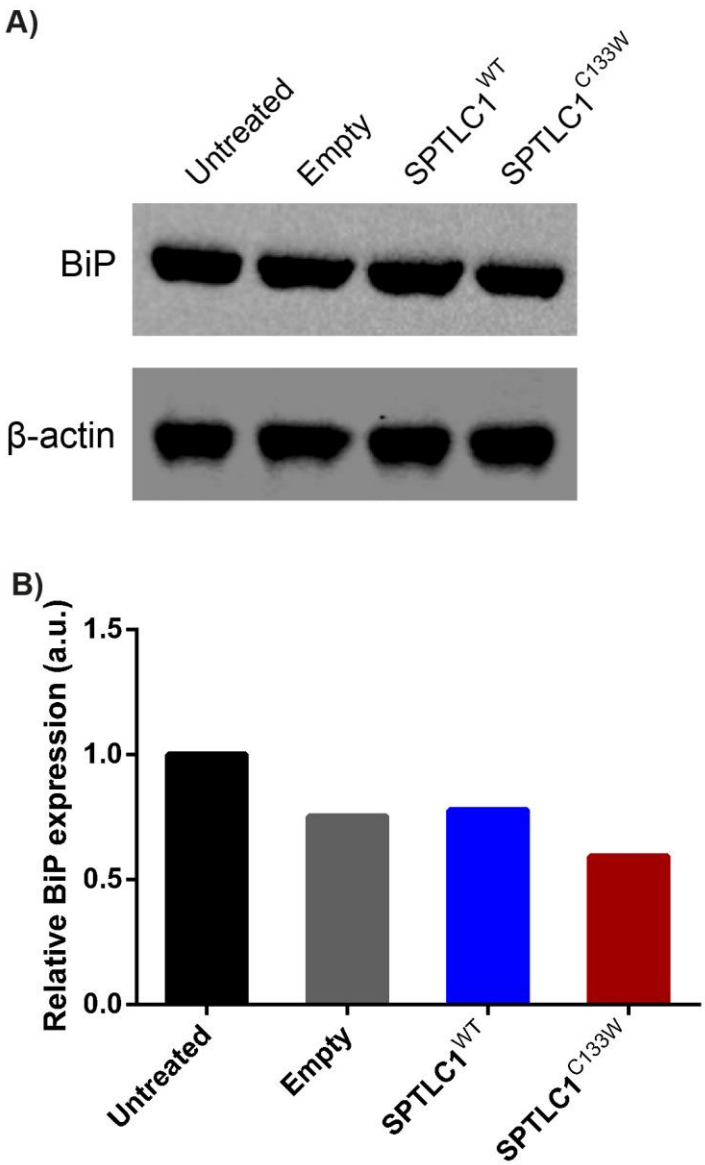

Figure 5.13: Expression of *SPTLC1^{C133W}* has no effect on expression of the ER stress marker BiP in DRG neurons

Primary DRG cultures were grown for 1 DIV before being transduced with lentiviral vectors (1:250), which were washed off after 24 h. **A)** DRG cultures were grown until 7 DIV before protein extraction. Western blot showing the expression of BiP (78 kDa) and loading control β-actin (42 kDa) in virally transduced DRG cultures. **B)** Bar chart showing quantification of BiP expression in DRG cultures, normalised to β-actin loading controls, all relative to BiP expression measured in the untreated culture.

mammal (Hanada, 2003; Breslow et al., 2010). However, less is known about *SPTLC1* regulation at the transcriptional/ translational level, although one study highlights the transcription factor COUP-TF interacting protein 2 (Ctip2) as a modulator of *SPTLC1* (and *SPTLC3*) expression during skin development in mice (Wang et al., 2013).

One surprising observation from the experiments described in this Chapter, was that many cells did not co-express both the GFP and V5 viral markers. In the viral vector used in these studies, GFP is expressed from the EF-1α promoter, whereas the V5 epitope tag, which is fused to *SPTLC1*, is expressed from the CMV promoter. It has been previously shown that both CMV and EF-1α are strong promoters, resulting in high expression of both protein products (Varma et al., 2011). A literature search did not reveal studies reporting a similar disparity between the expression levels of both transgenes in the same cell. However, it is possible that immunostaining for the V5 tag did not pick up the fusion construct which may have been buried under the much larger SPTLC1 protein conformation during protein folding or indeed that the V5 epitope tag was cleaved from SPTLC1 during protein processing. Although true differential expression of GFP and SPTLC1-V5 from the cassette seems unlikely, this could be further explored by quantitative polymerase chain reaction experiments, immunostaining with other commercially sourced antibodies raised against the V5 epitope tag, or indeed by generating a custom antibody to confirm that the SPTLC1-V5 fusion product is being produced. Interestingly, when protein lysates were denatured and run for western blot analysis, a strong and highly specific band was observed at exactly the molecular weight predicted for SPTLC1 with a V5 epitope tag, suggesting that cells in these cultures did indeed express the fusion protein at high levels.

A further observation from immunostaining experiments was that GFP was more prominently expressed in neurons, as opposed to other cells present in these mixed cultures, such as fibroblasts and glia. Previous results using a cell line, showed that the EF-1α promoter was far more efficient in inducing GFP expression than the CMV promoter (Teschendorf et al., 2002). Furthermore, a

comparison of promoter efficacy in rat cortical cultures showed that CMV-driven GFP expression was highest in astrocytes, whilst GFP expressed from EF-1α was primarily found in neurons (Tsuchiya et al., 2002). Therefore, it appears that the predominantly neuronal pattern of GFP expression observed in this study is likely to be a consequence of expression driven by the EF-1α promoter. A vector in which these two genes are under control of a single promoter may circumvent these issues, for example a bicistronic, internal ribosome entry site- (IRES-) containing vector (Martin et al., 2006).

In spite of the uncertainties about the reasons why V5 immunocytochemistry could not be used to visualize the presence of the fusion protein, western blot analysis confirmed that the fusion protein was expressed in primary neuronal cultures and at levels similar to the endogenous protein. Moreover, analysis of the lipid composition of transduced cultures confirmed that virally introduced SPTLC1 was able to form an enzymatically active heterotrimer when transduced into primary neuronal cultures. Deoxysphingoid and deoxymethylsphingoid bases were generated to a greater extent in *SPTLC1*^{C133W} expressing cells than in cells expressing *SPTLC1*^{WT}. Moreover, levels of deoxysphingoid bases were dramatically increased when *SPTLC1*^{C133W}-expressing cells were supplemented with L-alanine, the substrate preferentially utilised by mutant SPT to form deoxysphinganine (Zitomer et al., 2009; Gable et al., 2010; Penno et al., 2010).

It should be noted that lipids extracted from cells undergo acid and base hydrolysis prior to LC-MS analysis. Sphingoid bases are usually N-acylated with additional head groups, which are removed during acid and base hydrolysis. Thus, the levels of sphingoid bases measured in this study are representative of total cellular sphingoid bases, including those incorporated into downstream sphingolipids, rather than free sphingoid bases. Recent evidence has shown that although deoxysphingoid bases are not metabolized in the same manner as typical sphingoid bases, they are capable of generating a class of deoxysphingolipids (Alecu et al., 2016a). Thus, deoxysphingoid base levels reported using this technique may not be representative of true deoxysphingoid base levels in the cell cultures. Although the levels of deoxysphingoid bases

measured in transduced cultures appear to be comparable to the concentrations of DSp and DMSp shown to cause cytotoxicity in the experiments presented in Chapters 3 and 4, true deoxysphingoid base concentrations in this virally transduced model may in fact be much lower. It could therefore be hypothesised that free deoxysphingoid bases do not reach a sufficient concentration over the relatively short time these neurons are in culture (9 days) for toxicity to be revealed by cell counts or examination of the ER stress marker, BiP.

A comparison of *SPTLC1*^{WT} and *SPTLC1*^{C133W} expressing cultures revealed that the typical sphingoid base profile was largely unaffected by the mutant protein, adding further evidence to support the hypothesis that HSN-1 is not a loss-of-function disease, but rather a gain-of-function disorder resulting from the generation of abnormal deoxysphingoid bases.

As primary MN cultures treated with the abnormal deoxy- products of SPT demonstrated a significant reduction in cell survival (Chapter 3, Section 3.3.3) the effect of lentivirally delivered *SPTLC1*^{C133W} on cell survival was also examined in this Chapter. At the lower transduction dilution, the expression of the mutant enzyme did not lead to increased cytotoxicity. The use of higher concentrations of virus (1:100), which is the same condition that showed elevated deoxysphingoid base production, resulted in a 46% reduction in the survival of neurons in cultures expressing *SPTLC1*^{C133W} compared to untransduced controls. However, as this experiment was only done once (due to time limitations), further repeats are necessary to confirm whether viral transduction at 1:100 does result in neuronal death.

In a bid to shift the mutant enzyme substrate specificity from L-serine to L-alanine, and thus increase production of toxic DSp, MN cultures were supplemented with increasing doses of L-alanine (from 1-20 mM). The concentrations of L-alanine used for supplementation are well in excess of what is found in human blood plasma and CSF. In human blood plasma free alanine has been reported to be approximately 0.4 – 0.5 mM (Stein and Moore, 1954; Perry and Jones, 1961) and in human and rat CSF free alanine is in the μM range (Perry and Jones, 1961;

Therrien and Butterworth, 1991; D'Aniello et al., 2005). It has been previously shown that feeding drosophila models of HSN-1 with 10 mM alanine results in 100% cytotoxicity, manifesting in fly death (Oswald et al., 2015). In addition, in *SPTLC1*^{C133W} expressing cells, 10 mM alanine supplementation has been shown to trigger ER stress (Gable 2010). However, in the experiments described in this Chapter using murine primary MNs, although L-alanine supplementation dramatically increased the production of deoxysphingoid bases as measured by LC-MS, it modestly improved neuronal survival. In a similar manner, the studies of Jun et al. (2015), found that 10 mM L-alanine supplementation had no effect on the phenotype of DRG cells *in vitro* harvested from SPTLC1^{C133W} transgenic mice. These findings support the possibility that the main source of toxic deoxysphingoid bases found in HSN-1 patient plasma is, in fact, not those generated in neurons themselves, as examined here and by Jun et al. (2015), but is rather produced in other cell types. Moreover, these findings indicate that intracellular deoxysphingoid bases may have a different effect to extracellular deoxysphingoid bases. This supports the hypothesis that it is the systemic circulation of deoxysphingoid bases, rather than their intracellular generation, which may damage peripheral nerves in HSN-1 patients.

In addition to examining neuronal survival, I also examined the effect of transduction with mutant *SPTLC1* on the expression of the ER stress marker, BiP in neuronal cultures. Myers et al. (2014) have previously shown that in patient-derived lymphoblasts expressing the C133W mutation there was a modest, but significant reduction in BiP expression compared to healthy controls, and in lymphoblasts expressing the V144D mutation an even greater reduction in BiP expression. In the experiments described in this Chapter, in both MNs and DRG neurons, a generalized depletion of BiP expression was detected in all three of the virally transduced cultures: empty vector, *SPTLC1*^{WT}-carrying vector and *SPTLC1*^{C133W}-carrying vector. This suggests that although transduction with the lentiviral vector, or potentially expression of GFP, may cause a change in ER homeostasis, there is no SPTLC1^{C133W}-specific effect in these neurons. Alternatively, it is also possible that viral transduction itself effects cellular metabolism, possibly reducing resistance of these cells to normal metabolic stress.

Examination of the levels of deoxysphingoid bases secreted by neurons into the media may allow better comparison between the neurons in this Chapter, engineered to generate intracellular deoxysphingoid bases, and the neurons in Chapters 3 and 4, exogenously treated with deoxysphingoid bases.

5.5 Conclusions

In this Chapter, lentiviral vectors carrying *SPTLC1*^{WT} and *SPTLC1*^{C133W} were shown to successfully transduce primary motor and sensory cultures. Moreover, MN cultures expressing *SPTLC1*^{C133W} produce elevated levels of deoxysphingoid and deoxymethylsphingoid bases, the former of which can be exacerbated by supplementation with L-alanine. However, the parameters explored in this Chapter failed to reveal a significant neuropathy phenotype in transduced cultures, with no clear evidence of reduced cell survival or elevated ER stress. Although these findings may suggest that expression of mutant SPTLC1 is not the underlying trigger for HSN-1 pathology, it is also possible that intracellular accumulation of deoxysphingoid bases has a different effect to those observed when they are exogenously applied. However, very few parameters of neuronal viability were examined in this Chapter so that in order to fully understand the effect of low level overexpression of the mutant *SPTLC1*^{C133W} gene in neuronal populations on neuronal function and pathology, further research is clearly required. For example, it was not investigated whether these cells display a similar mitochondrial and ER Ca^{2+} mishandling phenotype as observed in cells treated with exogenous deoxy- and deoxymethyl- sphinganine. Further characterization of this model may indeed reveal more detail about the pathomechanism of HSN-1 and thereby provide an *in vitro* model in which to test potential therapeutics.

Chapter 6. Using patient fibroblasts to explore the pathomechanisms underlying HSN-1

6.1 Introduction

In diseases such as HSN-1, where ubiquitously expressed genes, such as *SPTLC1* and *SPTLC2*, are involved, patient cells may provide a valuable tool for exploring the underlying cause of disease. As discussed in the Introduction of Chapter 5, the only patient cells that have been previously used to explore HSN-1 pathomechanisms are patient-derived lymphoblasts (Marshall et al., 2014; Myers et al., 2014; Stimpson et al., 2015). Studies using these cells have revealed mitochondrial abnormalities, ER stress and lipid droplet accumulation as potential players in the pathogenesis of HSN-1.

In this study, six lines of fibroblasts from patients with HSN-1 secondary to the C133W mutation in *SPTLC1* were obtained in order to investigate the underlying pathomechanisms of HSN-1. The C133W mutation is the most commonly occurring HSN-1 mutation in the United Kingdom (Houlden et al., 2006). Patient fibroblasts have been used previously as an *in vitro* model of disease to unveil subcellular abnormalities in other inherited peripheral neuropathies (for example see Kennerson et al., 2010; Irobi et al., 2012; Noack et al., 2012).

Although the primary feature of HSN-1 is peripheral nerve damage, patients also report particularly slow wound healing, suggesting that abnormalities may also be present in skin fibroblasts (Auer-Grumbach, 2008). As well as expressing the *SPTLC1* mutation, skin fibroblasts from HSN-1 patients may also harbour cell damage that has accumulated over time, thereby providing the opportunity to explore any intracellular changes caused by the chronic nature of this disease. For these reasons, it was hypothesised that patient fibroblasts would provide an appropriate *in vitro* system to probe for the underlying pathways and features causing HSN-1.

6.2 Aims of this Chapter

The primary aim of this Chapter was to examine whether HSN-1 patient fibroblasts are an appropriate model of disease in which the mutant enzyme has similar functional characteristics as described in patients. Once the functional relevance of fibroblasts to HSN-1 disease was established, I aimed to test whether HSN-1 patient fibroblasts manifest any of the pathological features identified in Chapter 4 of this Thesis in primary neuronal cultures, namely mitochondrial dysfunction and ER stress. Identification of phenotypic changes in HSN-1 patient fibroblasts in comparison to controls would enable this human *in vitro* model of HSN-1 to potentially be used as a screening tool to test HSN-1 therapeutics.

6.3 Results

Throughout this Chapter, six different HSN-1 patient lines and six different healthy control lines were used. Age, gender and disease severity of the patient donors are outlined in the Materials and Methods (Chapter 2, Section 2.3).

6.3.1 SPTLC1 expression remains consistent across control and HSN-1 patient fibroblasts

Seven days after passaging, protein was extracted from six patient and five age- and sex- matched control fibroblast lines. Where indicated, L-alanine supplementation was added to typical fibroblast media from the day of passage until protein extraction. L-alanine is preferentially utilised by HSN-1 mutant SPT and results in the generation of the abnormal deoxysphingoid bases, proposed to underlie peripheral nerve damage reported in patients (see Chapter 3 and Penno et al., 2010). SPTLC1, one subunit of SPT, is a ubiquitously expressed protein and therefore as expected, western blot revealed substantial levels of SPTLC1 protein in human fibroblasts (Figure 6.1). When quantified, no differences were found in SPTLC1 expression levels between control and patient fibroblasts (Figure 6.1 B). Moreover, L-alanine supplementation had no effect on SPTLC1 expression levels in either control or patient cells (Figure 6.1 B). A relative SPTLC1 expression of 0.93 $\pm$ 0.05 and 0.92 $\pm$ 0.05 was measured in control fibroblasts without and with L-alanine supplementation, respectively,

Figure 6.1

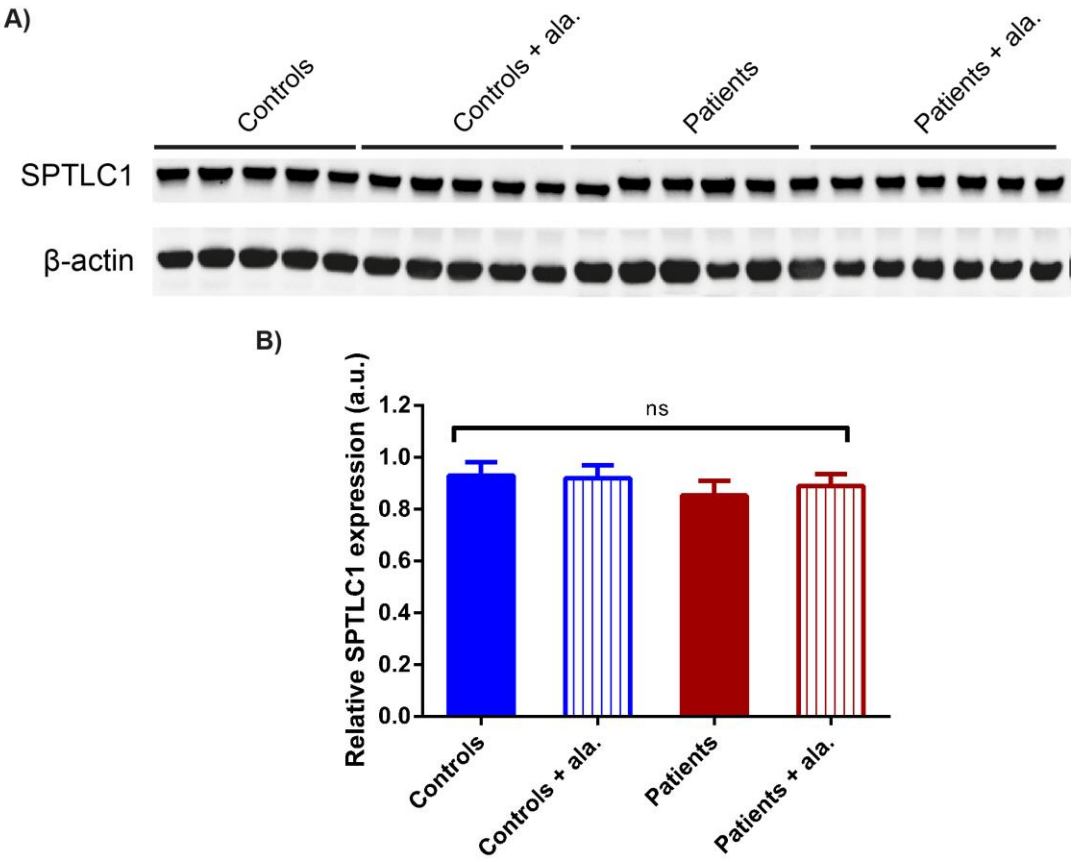

Figure 6.1: Human control and HSN-1 patient fibroblasts express SPTLC1 at equal levels

Protein was extracted from human control and HSN-1 patient fibroblasts for analysis. **A)** Western blot showing the expression of SPTLC1 protein (51 kDa) and the loading control β-actin (42 kDa) in control (n = 5) and patient (n = 6) lines, grown with and without 20 mM L-alanine (ala.) supplementation for 7 days. **B)** The bar chart shows the quantification of SPTLC1 expression normalised to β-actin loading controls, all relative to SPTLC1 expression in control. Displayed data represent the mean ± SEM. Kruskal-Wallis and Dunn's multiple comparisons tests were used for statistical comparisons. *P* values: * < 0.05; ** < 0.01; *** < 0.001. ns = not significant.

compared to 0.85 ± 0.06 and 0.89 ± 0.05 in patient fibroblasts without and with L-alanine, respectively.

Unfortunately, it was not possible to validate this finding with immunocytochemistry since none of the four anti-SPTLC1 antibodies commercially sourced appeared to effectively and/or specifically bind SPTLC1 (Figure 6.2). SPT, the heterotrimeric enzyme of which SPTLC1 forms one subunit, is an outer ER membrane protein (Hanada, 2003; Gable et al., 2010). Whilst the Novus and Millipore sourced antibodies appeared promising in initial trials (Figure 6.2 A-D), co-staining with ER marker protein disulphide isomerase (PDI) revealed a lack of colocalisation, suggesting non-specific binding of these SPTLC1 antibodies when used for immunocytochemistry (Figure 6.2 E-H).

Nevertheless, validation of SPTLC1 expression via western blot, in both control and patient fibroblasts supported continued investigation of HSN-1 using this *in vitro* system as a model of disease.

6.3.2 Mutant SPT in patient fibroblasts produces detectable levels of abnormal deoxysphingoid bases

It has been shown that SPT carrying HSN-1-causing mutations preferentially utilises L-alanine over L-serine in the condensation reaction with palmitoyl-CoA, resulting in the generation of abnormal deoxysphingoid bases, rather than typical sphingolipid precursors (Zitomer et al., 2009; Gable et al., 2010; Penno et al., 2010). Thus, it was next determined whether the patient fibroblasts carrying HSN-1-causing mutations in *SPTLC1* were indeed producing deoxysphingoid bases in this *in vitro* system.

Three lines of control and three lines of patient fibroblasts were grown to 100% confluency before the cells were collected for lipid profile analysis using LC-MS. LC-MS was carried out by Saranya Suriyanarayanan and Professor Thorsten Hornemann at University of Zürich, Switzerland, as part of a collaboration. In Figure 6.3 all measurements are normalised to the levels of 16 carbon length

Figure 6.2

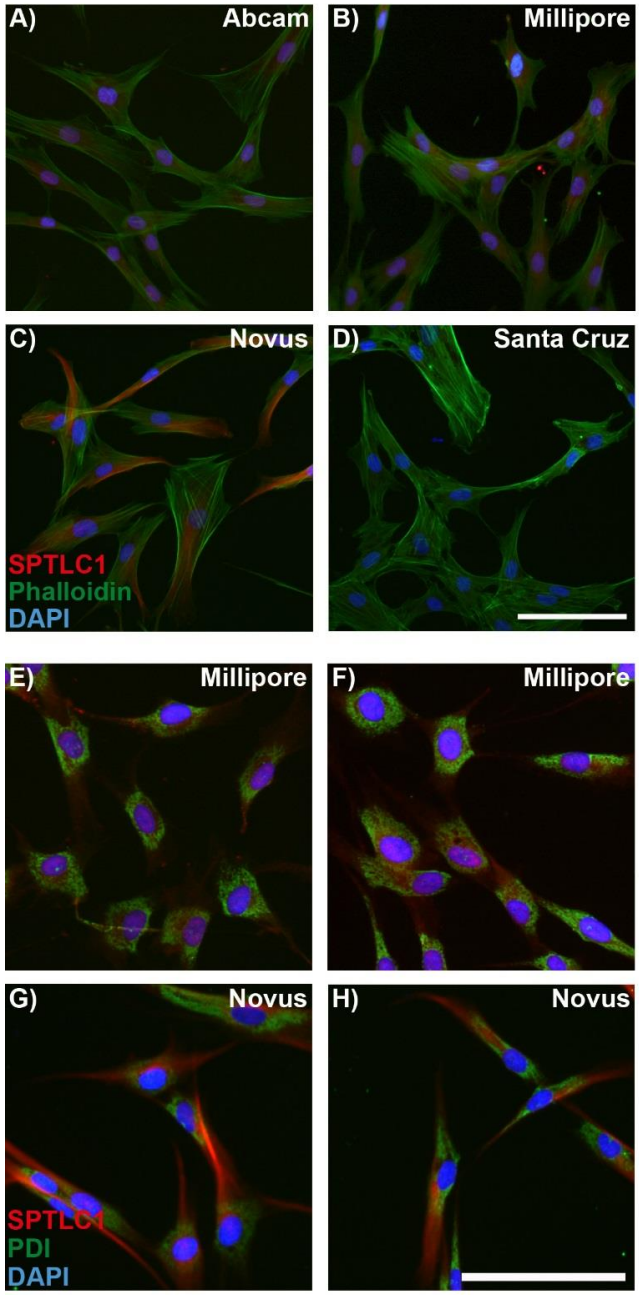

Figure 6.2: SPTLC1 antibodies did not work for immunocytochemistry

A-D) Control human fibroblasts were fixed and stained for SPTLC1 (red) and with phalloidin (green) and DAPI (blue). SPTLC1 antibodies were commercially sourced from four different companies: Abcam (A); Merck Millipore (B); Novus Biologicals (C); Santa Cruz Biotechnology (D). **E-H)** Control human fibroblasts were fixed and stained for SPTLC1 (red; Merck Millipore (E-F) or Novus Biologicals (G-H)), ER marker PDI (green) and for DAPI (blue). Scale bar = 100 µm.

Figure 6.3

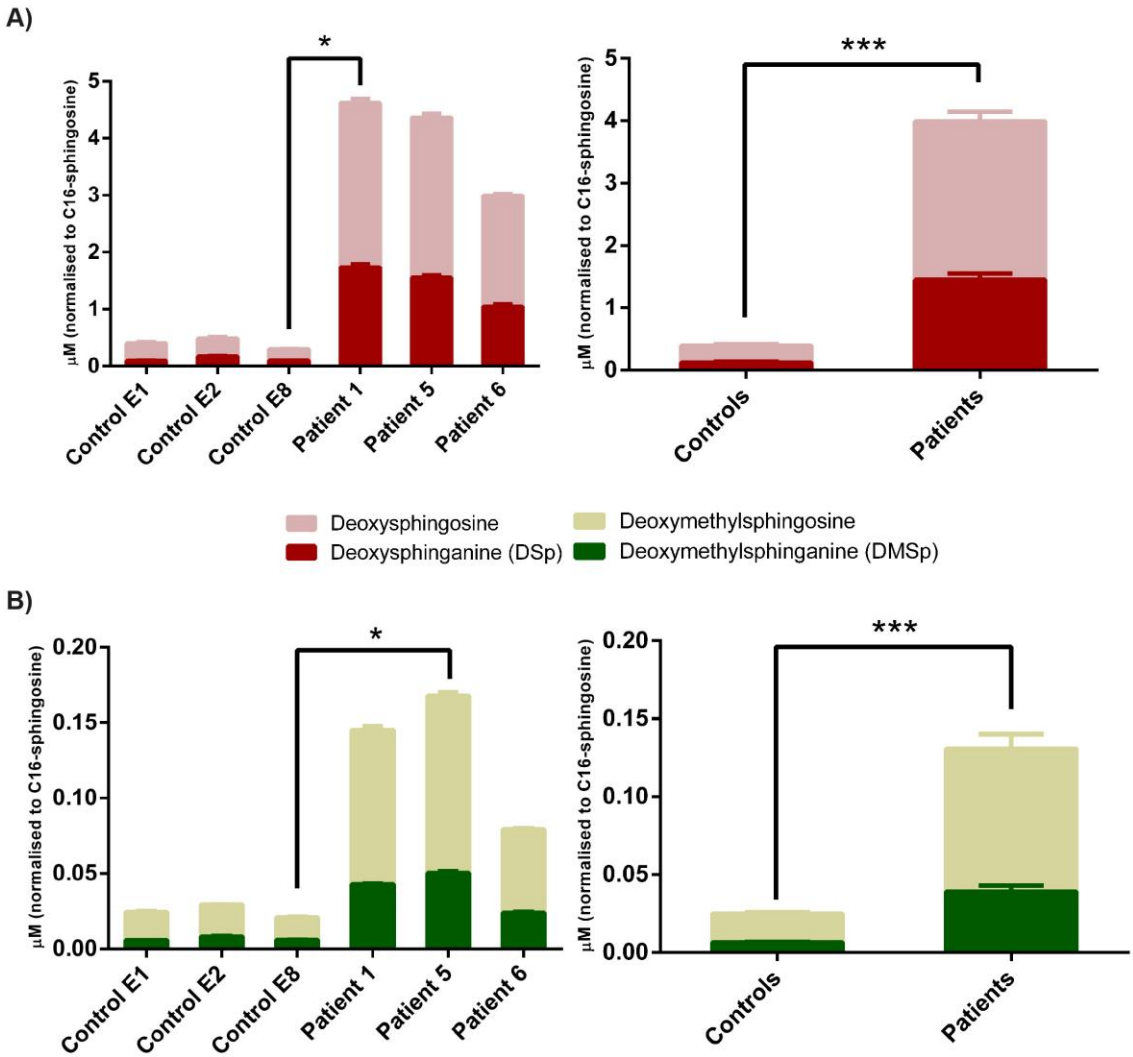

Figure 6.3: HSN-1 patient fibroblasts produce deoxysphingoid bases

Cells were collected from three control and three HSN-1 patient lines. Bar charts on the right side panels represent pooled data from the control and patient lines. **A)** Levels of deoxysphinganine (DSp, dark red) and deoxysphingosine (light red) were measured by LC-MS and normalised to the concentration of 16 carbon length chain sphingosine (C16-sphingosine). **B)** Levels of deoxymethylsphinganine (DMSp, dark green) and deoxymethylsphingosine (light green) were measured and normalised to C16-sphingosine. Displayed data represent the mean ± SEM. Statistical comparisons were made using Kruskal-Wallis with Dunn's multiple comparisons or Mann-Whitney *U* tests. *P* value * < 0.05; ** < 0.01; *** < 0.001.

chain sphingosine (C16-sphingosine) in order to account for differences in cell number.

Three control lines showed only modest generation of deoxysphinganine (DSp) and downstream metabolite deoxysphingosine. However, levels of both these deoxy- metabolites were dramatically increased in the three patient lines tested (Figure 6.3 A). Patient fibroblasts displayed DSp concentrations of 1.73 ± 0.06, 1.56 ± 0.04 and 1.05 ± 0.04 μM compared to control fibroblasts in which DSp concentrations were 0.09 ± 0.005, 0.17 ± 0.008 and 0.10 ± 0.002 μM (Figure 6.3 A). Similarly, deoxysphingosine concentrations were also elevated in patient fibroblasts, to 2.90 ± 0.06, 2.81 ± 0.07 and 1.94 ± 0.03 μM compared to 0.31 ± 0.02, 0.31 ± 0.03 and 0.20 ± 0.01 μM in controls (Figure 6.3 A). Taken together, control fibroblasts displayed a mean total deoxysphingoid base concentration of 0.40 ± 0.03 μM compared to 3.99 ± 0.26 in patient fibroblasts ($P < 0.001$, Figure 6.3 A).

Deoxymethylsphingoid bases have also been reported to be elevated in the blood of HSN-1 patients, but at much lower concentrations than DSp and deoxysphingosine (Penno et al., 2010). The patient fibroblasts examined here also displayed elevated deoxymethylsphingoid bases when compared to control lines, and as expected the concentrations measured were indeed lower than those for DSp and deoxysphingosine (Figure 6.3 B). Total deoxymethylsphingoid bases in patient cells were 0.13 ± 0.01 μM, compared to the barely detectable levels in control cells of 0.02 ± 0.001 μM ($P < 0.001$, Figure 6.3 B).

Interestingly, the deoxysphingoid and deoxymethylsphingoid base levels in patients 1 and 5 were higher than in patient 6. This correlates with disease severity reported in these patients according to the Charcot Marie Tooth neuropathy score version 2 (CMTNS2), a reliable composite score widely used clinically, including as an outcome measure in clinical trials, for CMT (Murphy et al., 2011). At the time of skin biopsy, patients 1 and 5 recorded a severe CMTNS2 of 21, whereas patient 6 was reported to have a moderate CMTNS2 of 16 (Dr Umaiyal Kugathasan, personal communication).

6.3.3 Patient fibroblasts have an altered typical sphingoid base profile

As well as examining the profile of atypical deoxysphingoid bases, the lipid profile of the canonical sphingolipid precusors was also examined (Figure 6.4). In general, it was found that patient fibroblasts displayed elevated levels of some of the sphinganines, including C16-sphinganine (C16-Sp), C17-Sp, C18-Sp and C19-Sp as well as C20-sphingosine (C20-SO, Figure 6.4 A-B). Although some sphingoid base levels remained unchanged (C20-Sp, C18-PhytoSO, C17-SO and C18-SO, Figures 6.4 A-C) levels of C18-sphingadiene were in fact depleted in patient lines (Figure 6.4 B).

The results in Figure 6.3 show that patient-derived skin fibroblasts are capable of generating deoxysphingoid bases, as measured in HSN-1 blood plasma, and thus may serve an appropriate model for further exploration of HSN-1 pathomechanisms.

6.3.4 Expression of ER stress marker, BiP, is elevated in HSN-1 patient fibroblasts supplemented with L-alanine

The results in Chapter 4, and confirmed by studies in the literature, suggest that ER stress may play a role in the pathogenesis of HSN-1 (Gable et al., 2010; Myers et al., 2014; Alecu et al., 2016b). In the present studies, the ER protein BiP was used as an indicator of ER stress. Seven days after passaging, protein was extracted from six patient and five age- and sex- matched control fibroblast lines and where indicated, 20 mM L-alanine supplementation was added to typical fibroblast media from the day of passaging until protein extraction. Western blot for BiP indicated that patient cells show a modest increase in the expression of this ER stress marker when compared to controls (Figure 6.5 A). Quantification revealed a non-significant increase in BiP expression from 0.85 ± 0.07 in controls to 1.02 ± 0.12 in patients. However, supplementation with 20 mM L-alanine demonstrated a significant increase in BiP expression from 0.66 ± 0.06 in control cells supplemented with L-alanine to 1.1 ± 0.04 in patient cells with L-alanine ($P < 0.01$).

Figure 6.4

A)

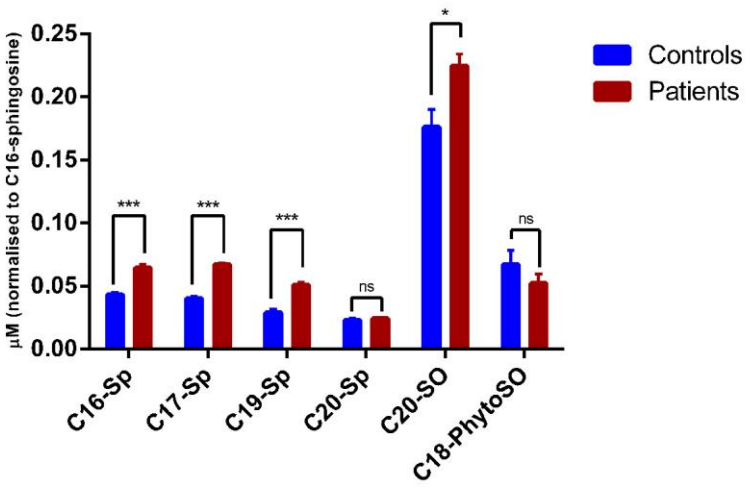

B)

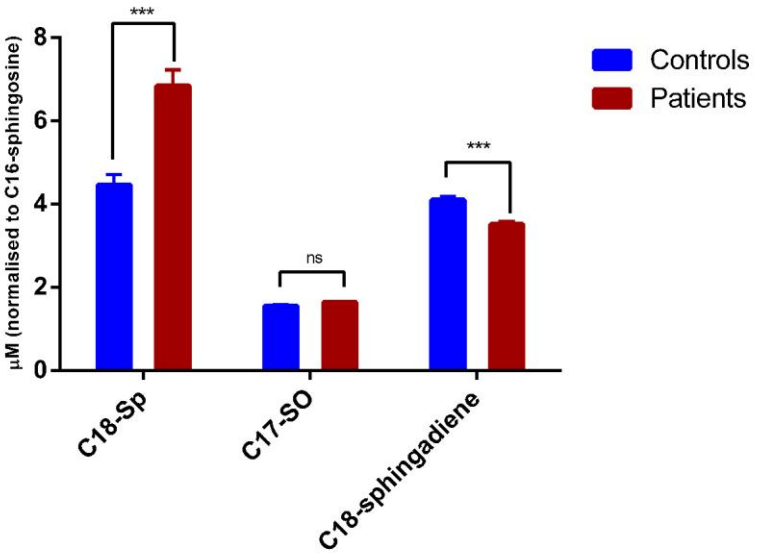

C)

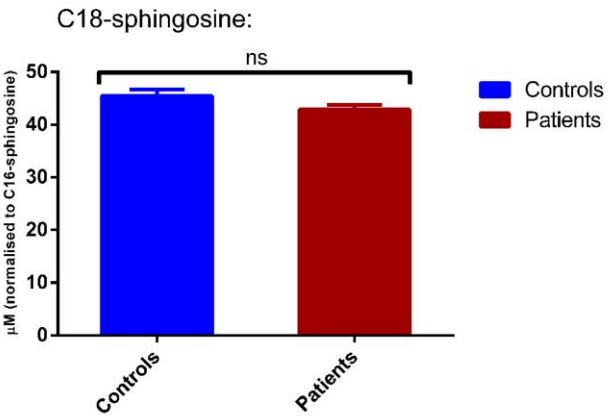

Figure 6.4: HSN-1 patient fibroblasts have an altered typical sphingoid base profile

Cells were collected from three control and three HSN-1 patient lines. **A)** Levels of 16-20 carbon length chain sphinganines (C16-Sp, C17-Sp, C19-Sp, C20-Sp), C20-sphingosine (C20-SO) and C18-phytosphingosine (C18-PhytoSO) were measured and normalised to C16-sphingosine. **B)** Levels of C18-Sp, C17-SO and C18-sphingadiene were measured and normalised to C16-sphingosine. **C)** Levels of C18-sphingosine were measured and normalised to C16-sphingosine. Displayed data represent the mean ± SEM. Statistical comparisons were made using Mann-Whitney *U* tests. *P* value * < 0.05; ** < 0.01; *** < 0.001. ns = not significant.

Figure 6.5

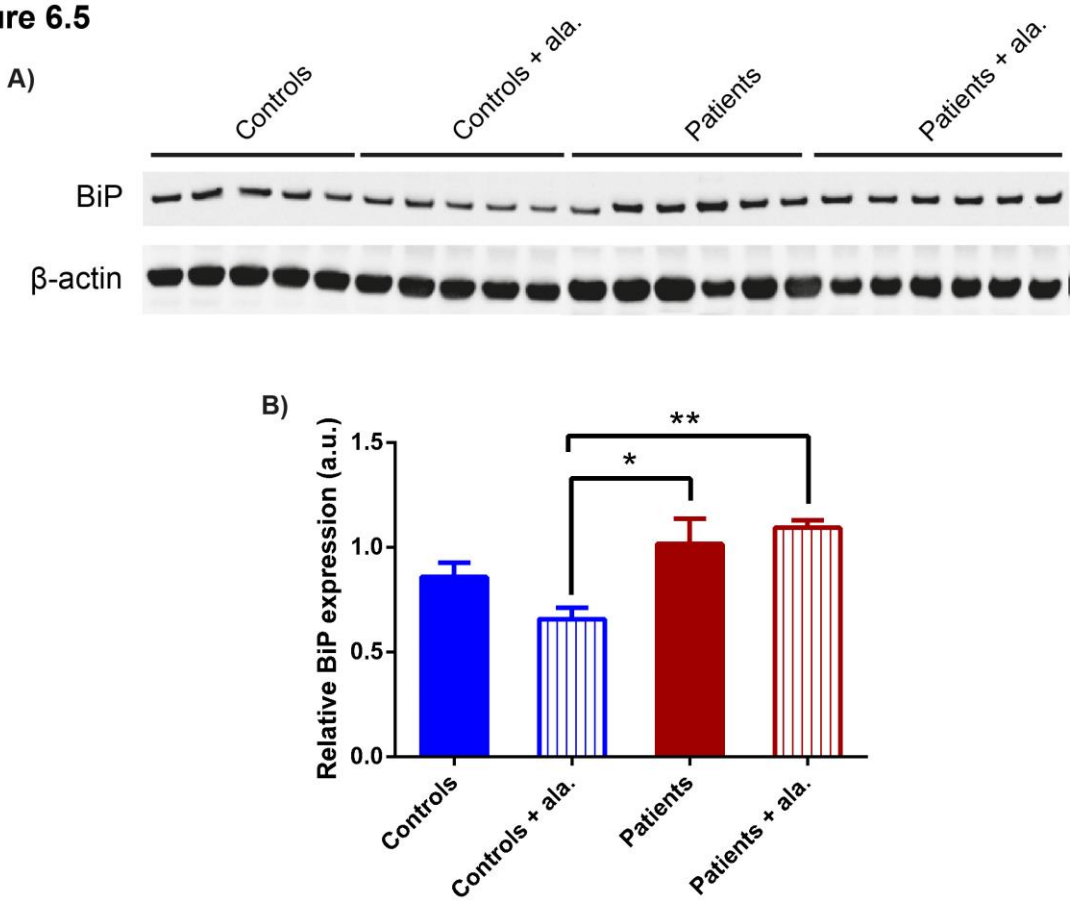

Figure 6.5: HSN-1 patient fibroblasts have increased expression of the ER stress marker BiP

Protein was extracted from human control and HSN-1 patient fibroblasts for analysis. **A)** Western blot showing the expression of the ER stress marker BiP (78 kDa) and the loading control β-actin (42 kDa) in control and patient lines, grown with and without 20 mM L-alanine (ala.) supplementation for 7 days. **B)** The bar chart shows the quantification of BiP expression normalised to β-actin loading controls, all relative to BiP expression measured in controls. Displayed data represent the mean ± SEM. Statistical comparisons were made using one-way ANOVA and Dunnett's multiple comparisons tests. *P* values: * < 0.05; ** < 0.01; *** < 0.001.

These results indicate that although patient cells may not display ER stress under typical conditions, when these cells are supplemented with L-alanine, the precursor to the neurotoxic SPT product DSp (see Chapter 3 and Penno et al., 2010), cells do exhibit increased expression of ER stress marker, BiP.

6.3.5 Patient fibroblasts maintain a normal mitochondrial membrane potential

The results presented in Chapter 4 showed that when primary mouse motor and sensory cells were treated with the abnormal deoxy- products of mutant SPT they display reduced mitochondrial membrane potential ($\Delta\psi_m$) and other mitochondrial abnormalities, such as abnormal Ca^{2+} loading. Therefore, I next examined the three patient lines confirmed as producing deoxysphingoid bases (Figure 6.3) for changes in mitochondrial function.

The fibroblasts were loaded with TMRM, a cationic dye which accumulates in mitochondria as a function of $\Delta\psi_m$ (Figure 6.6). Quantification revealed that patient fibroblasts demonstrated no differences in $\Delta\psi_m$, displaying a mean TMRM intensity 101 ± 1 % of control cells (P = 0.87, Figure 6.7 A).

6.3.6 Patient fibroblasts display decreased mitochondrial area

Using TMRM and the live cell marker calcein, the total mitochondrial area per cell was also calculated. A small but significant decrease in total mitochondrial area was revealed in patient cells, so that the mean mitochondrial area, expressed as a percentage of total cell size, was 9.7 ± 0.23% in patient cells, compared to 10.8 ± 0.33% in controls (P = 0.017, Figure 6.7 B).

Figure 6.6

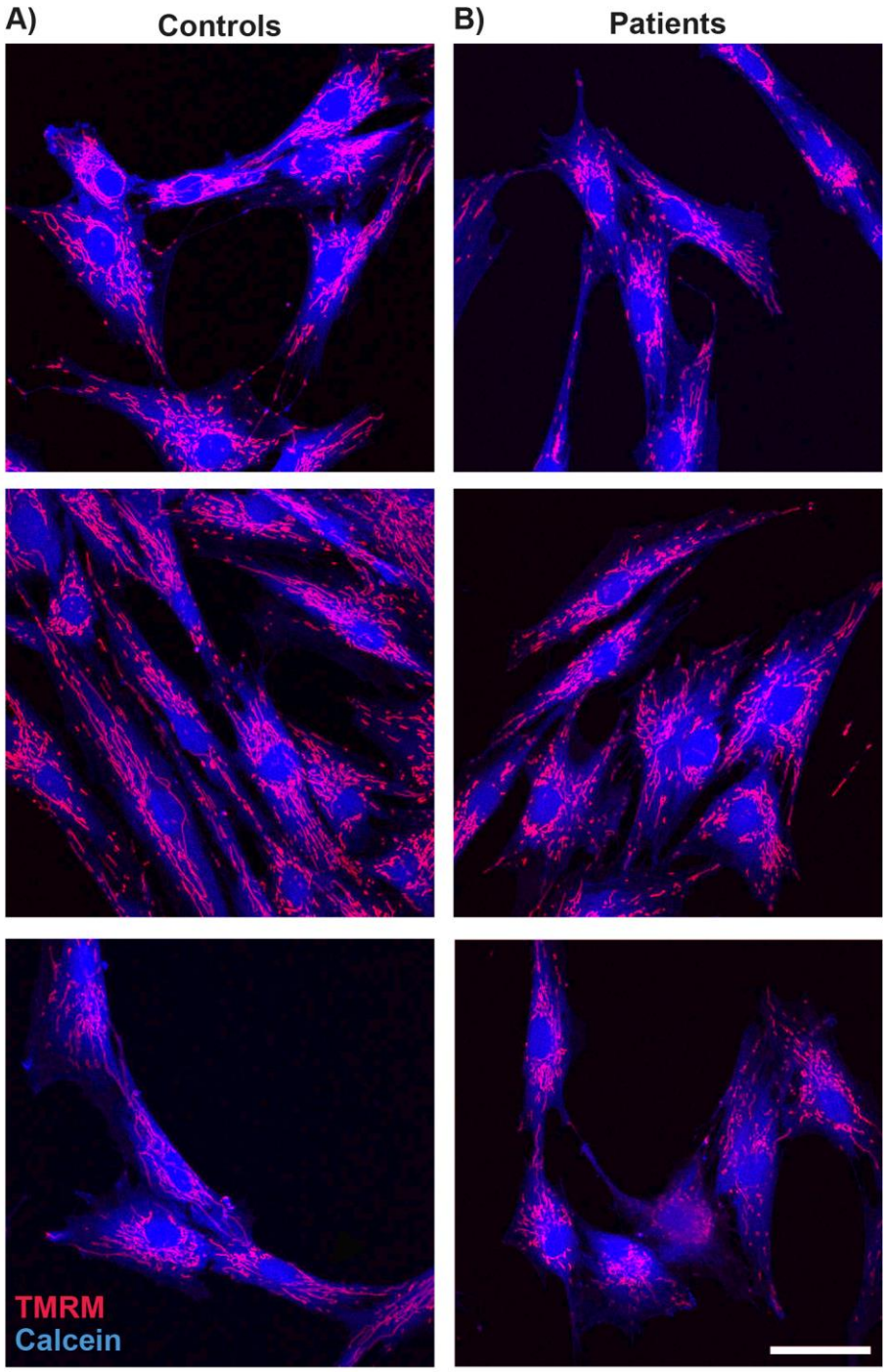

Figure 6.6: Using TMRM to explore mitochondrial function in HSN-1 patient fibroblasts

A-B) Typical images of control (A) and HSN-1 patient (B) fibroblasts loaded with TMRM and calcein. TMRM is a cationic dye which accumulates in mitochondria as a function of mitochondrial membrane potential ($\Delta\psi_m$). Calcein is used here as a marker of viable cells. Scale bar = 50 µm.

Figure 6.7

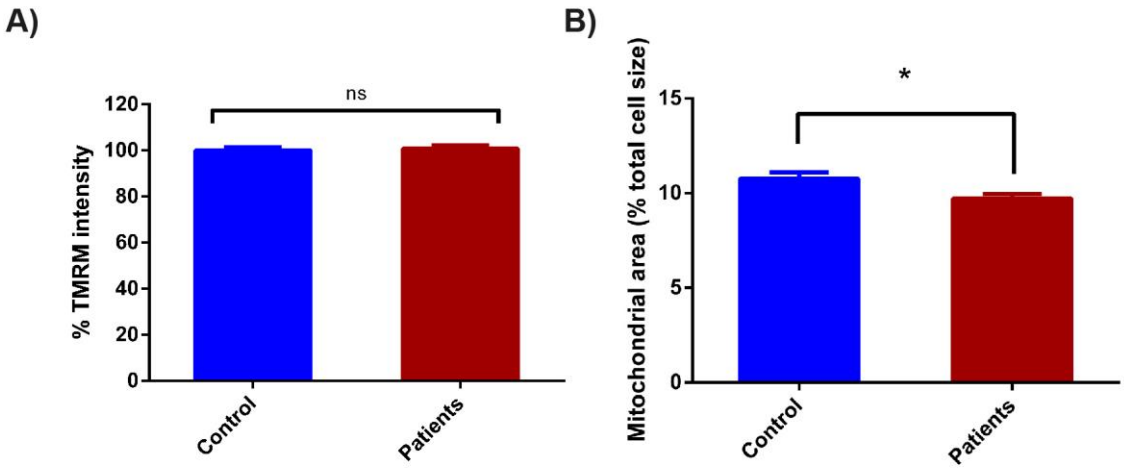

Figure 6.7: HSN-1 patient fibroblasts maintain a normal mitochondrial membrane potential, but have reduced total mitochondrial area

A) The bar chart shows the mean TMRM intensity measured from 50 control cells and 139 patient cells, from three different lines. **B)** The bar chart shows the mean total mitochondrial area per cell, expressed as a percentage of the total cell size, measured from 53 control cells and 144 patient cells, from three different lines. Error bars represent SEM. Statistical comparisons were made using the Mann-Whitney *U* or unpaired t tests. *P* values: * < 0.05; ** < 0.01; *** < 0.001. ns = not significant.

6.3.7 Mitochondrial length and mitochondrial-ER contacts are unchanged in patient fibroblasts

Structural mitochondrial abnormalities were also explored using transmission electron microscopy (Figure 6.8). Figure 6.8 A and 6.8 B show typical electron micrographs of control and patient fibroblasts, respectively. Transmission electron microscopy was performed by Dr Samantha Loh and Dr Miguel Martins at University of Leicester, United Kingdom, as part of a collaboration.

Despite an overall depletion in mitochondrial area in patient cells (Figure 6.7 B), individual mitochondrial length in patient fibroblasts was unaffected (Figure 6.9 A). The mean length of mitochondria in control fibroblasts was 674 ± 17 nm and in patients 704 ± 25 nm (P = 0.39).

In Chapter 4 of this Thesis, primary neurons treated with deoxysphingoid bases showed Ca^{2+} handling deficits, specifically in the ER and the mitochondria. For this reason, the percentage of mitochondria exhibiting mitochondrial-ER contacts (or mitochondrial-associated membrane, MAM) was also calculated from electron micrographs. The arrow heads (red) in Figure 6.8 show examples of such contacts. No significant changes were found between control and patient fibroblasts, so that the percentage of mitochondria displaying contacts with the ER was 57 ± 3% in controls and 60 ± 1% in patients (P = 0.80, Figure 6.9 B).

Ultrastructural abnormalities previously reported in patient-derived lymphoblasts, including swollen mitochondrial cristae and breakages in the mitochondrial membrane (Myers et al., 2014), were not observed in the electron micrographs of the patient fibroblasts analysed in this study.

The results shown in Figures 6.5-6.9 suggest that patient fibroblasts show only a mild pathology when compared to control fibroblasts, across the parameters tested in this Thesis. Importantly, evidence suggests that the mild pathogenic phenotype may be exacerbated by supplementation of patient cells with L-alanine, which indeed may provide a helpful tool moving forwards with this *in vitro* model.

Figure 6.8

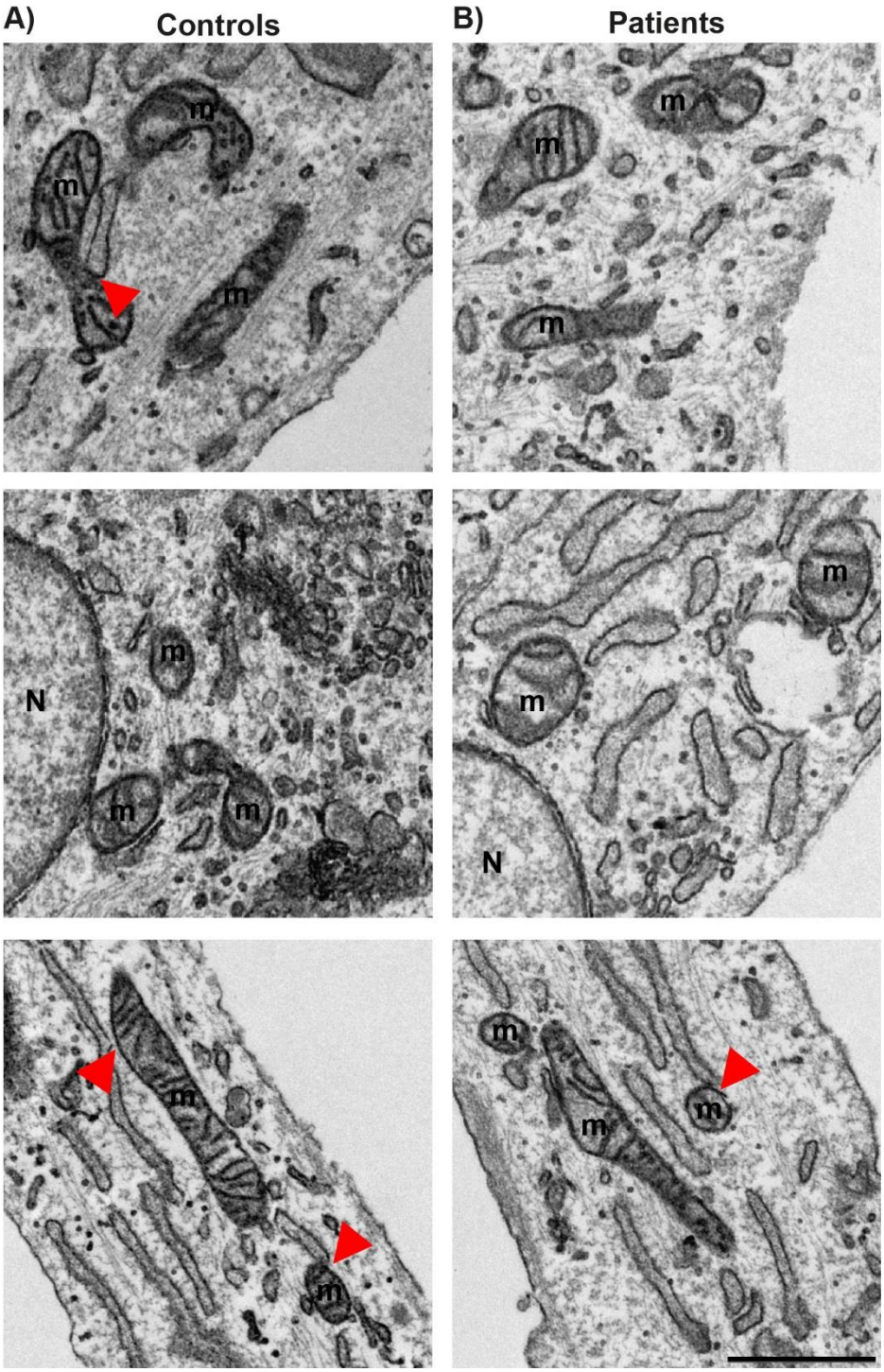

Figure 6.8: Ultrastructural analysis of HSN-1 patient fibroblasts

A-B) Typical electron microscope images of control (A) and HSN-1 patient (B) fibroblasts. Red arrow heads indicate points of mitochondrial-ER contacts. m = mitochondria. N = nucleus. Scale bar = 1 µm.

Figure 6.9

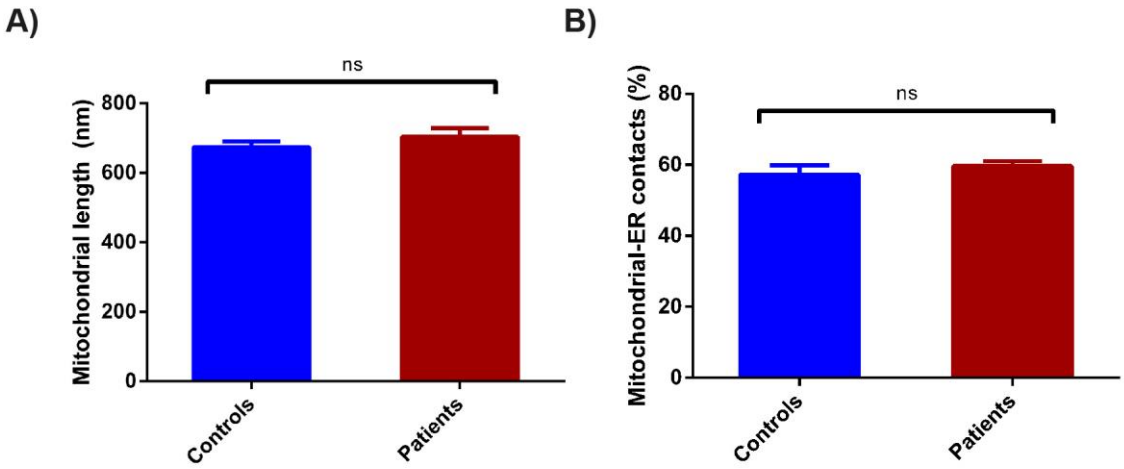

Figure 6.9: HSN-1 patient fibroblasts show no changes in mitochondrial length or mitochondrial-ER contacts

A) The bar chart shows the mean mitochondrial length quantified from 768 control mitochondria and 450 patient mitochondria, across three control lines and two patient lines. **B)** The bar chart shows the number of mitochondria with an ER contact, expressed as a percentage of number of mitochondria examined, measured from 1065 control mitochondria and 671 patient mitochondria, across three control lines and two patient lines. Error bars represent SEM. Statistical comparisons were made using the Mann-Whitney *U* test. *P* values: * < 0.05; ** < 0.01; *** < 0.001. ns = not significant.

6.4 Discussion

The results in this Chapter show than HSN-1 patient fibroblasts express SPTLC1 at constant levels which are similar to fibroblasts from healthy controls. However, when grown *in vitro*, patient cells generate far greater levels of deoxysphingoid and deoxymethylsphingoid bases than their control counterparts, as previously observed in blood samples from HSN-1 patients and in transgenic mice expressing *SPTLC1*^{C133W} mutations (Penno et al., 2010; Garofalo et al., 2011; Rotthier et al., 2011; Auer-Grumbach, 2013; Murphy et al., 2013; Suriyanarayanan et al., 2016).

Interestingly, levels of both deoxysphingoid (DSp and deoxysphingosine) and deoxymethylsphingoid (DMSp and deoxymethylsphingosine) bases correlated with the disease severity of donor patients, as determined by the CMTNS2. Deoxysphingoid base concentration and disease severity correlation has been previously noted in both HSN-1 patient-derived lymphoblasts and patient plasma (Penno et al., 2010). This finding supports the hypothesis that deoxysphingoid bases are causative for HSN-1. However, a comparison of these results with a larger pool of patient fibroblasts would provide further evidence for causality over correlation.

The variation in deoxysphingoid base levels observed in this study, despite all patients carrying an identical *SPTLC1* point mutation, suggests that other genetic or environmental factors play role in disease and may modify deoxysphingoid base levels in some patients, resulting in variable clinical manifestation. One such genetic modifier could be expression of the cytochrome P450 4F (CYP4F) enzymes which have been shown to metabolise deoxysphingoid bases to downstream deoxysphingolipids to some extent, potentially leading to non-toxic metabolites and promoting eventual removal (Alecu et al., 2016a). Indeed, Alecu et al. (2016a) propose that upregulation of such enzymes may provide a therapeutic option in HSN-1, as well as other diseases associated with elevated deoxysphingoid bases, such as type 2 diabetes.

When examining the typical sphingoid base profile, many sphinganines, of varying carbon length chains, were found at higher levels in patients than in

controls. Indeed this adds to the increasing evidence that indicates that HSN-1 is not a disease of enzymatic haploinsufficency, but rather a gain-of-function phenomenon (Hojjati et al., 2005; Eichler et al., 2009; Gable et al., 2010; Penno et al., 2010). Increased levels of C18- and C20-sphingoid bases have been previously reported in cells expressing HSN-1-causing mutations SPTLC1$^{S331F/Y}$ and SPTLC2^{I505Y}, but intriguingly not in cells expressing SPTLC1^{C133W} (Bode et al., 2016). Levels of one sphingoid base, C18-sphingadiene, were reduced in patient fibroblasts, when compared to controls. A study investigating sphingoid base profiles as potential biomarkers for *diabetes mellitus* also found a negative correlation between elevated deoxysphingoid base levels and a depletion of C18-sphingadiene (Khan and Hornemann, 2017).

As these results confirm that patient fibroblasts produce HSN-1-associated deoxysphingoid bases, this *in vitro* model was used to explore whether any of the pathomechanisms identified in Chapter 4 of this Thesis using mouse primary neurons were also present in patient cells.

Firstly ER stress was examined by looking at the expression levels of the ER stress marker BiP. A modest, but non-significant increase in BiP was detected in patient cells. Moreover, whereas L-alanine supplementation reduced BiP expression in control fibroblasts, BiP levels increased in patient lines. However, it should be noted that all changes in BiP levels were relatively small and thus these findings warrant further investigation to determine if they represent a true patient cell pathology, or are merely a result of the innate variability commonly found when using fibroblast cultures *in vitro.* Indeed, these findings are intriguing since Myers et al. (2014) reported the opposite finding in patient cells expressing SPTLC1^{C133W}. One possibility is that *SPTLC1* mutations may have different effects in different cell types; indeed HSN-1 is a disease largely of the peripheral nerves, despite the fact that *SPTLC1* (and *SPTLC2*) are ubiquitously expressed.

A number of mitochondria-associated parameters were also examined in this Chapter. Modelling mitochondrial dysfunction in neurodegenerative disease using fibroblasts should be done so with caution. Fibroblasts are proliferative cells with a different energy demand to post-mitotic neurons. Fibroblasts are highly

glycolytic, in comparison to neurons which rely primarily on oxidative phosphorylation as an ATP source. Analyses for mitochondrial membrane potential, mitochondrial length and mitochondrial-ER contacts showed that there were no differences between control and patient fibroblasts. However, overall mitochondrial area was slightly reduced in patient fibroblast lines. It should be noted that the mitochondrial dye used for $\Delta\psi_m$ and mitochondrial area analysis (TMRM) loads only into mitochondria with a $\Delta\psi_m$ and thus the mitochondrial area reported here represents an analysis of only healthy, functioning mitochondria. Indeed this is similar to what has been reported by Myers et al. (2014) in patient derived lymphoblasts, in which there was a depletion of total mitochondrial number, but no change in mitochondrial length to width ratio. It is possible that in patient cells, injured mitochondria are removed from the mitochondrial network, causing an overall depletion in mitochondrial area but largely maintaining their mitochondrial membrane potential integrity.

The MAMs are sites of ER-mitochondrial contact which play a major role in Ca^{2+} signalling and lipid metabolism. Furthermore, as increasingly reported, MAMs are also involved in processes such as ER stress and apoptosis (van Vliet et al., 2014; Krols et al., 2016). The MAM has been implicated in a number of neurodegenerative disorders including amyotrophic lateral sclerosis (ALS) and the inherited neuropathies (Krols et al., 2016). Thus, evidence from the literature, as well as results presented in Chapter 4 of this Thesis, which showed Ca^{2+} handling deficits in both the ER and mitochondria, prompted examination of ER-mitochondrial contact points (the MAM) in patient fibroblasts. However, ultrastructural analysis using EM did not reveal any changes in the number of mitochondrial-ER contact points in patient fibroblasts when compared to controls. In addition, none of the structural abnormalities reported in patient-derived lymphoblasts using EM by Myers et al. (2014) were present in the patient fibroblasts explored in this Chapter.

On one hand, the relative lack of an overt phenotype in patient fibroblasts in comparison to exogenous application of deoxysphingoid bases to primary neurons (Chapters 3 and 4) may suggest that fibroblast cells are less susceptible to these aberrant lipids than neurons. This is in keeping with the fact that,

although patients do display slow wound healing, HSN-1 is foremost a disease of the peripheral nervous system. On the other hand, the mild functional deficits seen in patient cells in this Chapter suggest that, as discussed in Chapter 5, exogenous application of deoxysphingoid bases may have a different effect to their intracellular generation.

6.5 Conclusions

In conclusion, the results presented in this Chapter demonstrate that patient fibroblasts not only express SPTLC1 at substantial levels but also produce cytotoxic deoxy- and deoxymethyl- sphingoid bases found elevated in HSN-1 patient plasma. Moreover, functional analysis revealed early indicators of moderate ER stress and potential mitochondrial abnormalities, which were exacerbated by L-alanine supplementation. These preliminary experiments suggest that further exploration of patient fibroblasts may reveal more subtle but significant mechanisms contributing to HSN-1. Moreover, these patient-derived cells could provide a model in which to test potential therapeutics including serine supplementation and gene-editing.

Chapter 7. General Discussion

HSN-1 is an inherited peripheral neuropathy which results in progressive loss of motor and sensory nerves. This neuropathy has a severe impact on the quality of life of patients, who experience common and recurrent skin wounds that are frequently infected and which can necessitate amputation (Auer-Grumbach, 2008; Rotthier et al., 2012). Moreover, these patients can become wheelchair-bound due to motor nerve degeneration and subsequent muscle wasting (Houlden et al., 2006). Unfortunately, there are no approved treatments for HSN-1 and the mechanisms by which motor and sensory nerves degenerate is yet to be fully established (Rotthier et al., 2012). To highlight potential molecular targets for the development of treatment for HSN-1, the experiments described in this Thesis aimed to uncover underlying pathomechanisms of HSN-1 using *in vitro* models.

7.1 Deoxysphingoid bases in HSN-1

HSN-1 is most commonly caused by mutations in the *SPTLC1* or *SPTLC2* genes, which encode two subunits of the enzyme serine palmitoyltransferase (SPT; Mroczek et al., 2015). It has been shown that HSN-1-causing mutations in SPT promote the enzyme to preferentially utilise L-alanine or L-glycine, over its canonical substrate L-serine, which results in the production of abnormal deoxysphingoid and deoxymethylsphingoid bases (Zitomer et al., 2009; Gable et al., 2010; Penno et al., 2010). Patients characteristically display elevated levels of deoxysphingoid and deoxymethylsphingoid bases in their blood plasma, which have been proposed to underlie peripheral nerve damage in HSN-1 (Penno et al., 2010; Garofalo et al., 2011; Rotthier et al., 2011; Auer-Grumbach et al., 2013; Murphy et al., 2013; Suriyanarayanan et al., 2016). Studies in the literature had shown these aberrant deoxy- compounds to be cytotoxic (Cuadros et al., 2000; Salcedo et al., 2007; Penno et al., 2010; Zuellig et al., 2014; Guntert et al., 2016) but work leading up to (from fellow PhD student Dr Umaiyal Kugathasan), and in Chapter 3 of this Thesis demonstrated for the first time a clear, dose-dependent toxicity when deoxysphingoid and deoxymethylsphingoid bases were applied to primary, mammalian motor and sensory neurons *in vitro*. Intriguingly, my results

also suggest that deoxysphingoid bases and deoxymethylsphingoid bases may have different molecular targets resulting in differing toxicity, with a trend towards deoxysphinganine being more toxic than deoxymethylsphinganine (Chapter 3).

A major question is whether it is the systemic circulation of deoxysphingoid bases or the intracellular generation of deoxysphingoid bases, or alternatively, both possibilities, that causes peripheral nerve damage in HSN-1. Indeed, these two models of action may represent different molecular targets. Circulating deoxysphingoid bases will first encounter cell membranes, yet deoxysphingoid bases generated within the cell may have other intracellular molecular targets in the first instance. In Chapters 3 and 4 of this Thesis, a model of circulating deoxysphingoid bases and their impact on peripheral nerves was generated. In contrast, in Chapters 5 and 6 of this Thesis, *in vitro* models more closely representing intracellular generation of deoxysphingoid bases were established and explored. Indeed, in patients manifestation of deoxysphingoid base toxicity may involve both intracellular generation and systemic circulation thus complicating the pathomechanisms leading to neuronal damage.

Sphinganine, despite being the typical enzyme product and precursor to canonical sphingolipids, also demonstrated some toxicity on primary neurons in culture, as well as other intracellular changes (Chapters 3 and 4). Overloading cells with sphinganine, and therefore its downstream metabolites, is likely to also have toxic effects that may not be related to deoxysphingoid base toxicity. Mutations in sphingosine-1-phosphate lyase (an enzyme in the sphingolipid pathway, see Figure 1.4) causes an accumulation of sphingosine-1-phosphate and have been proposed to cause CMT (Atkinson et al., 2017). Increased levels of sphingosine-1-phosphate were reported to cause a change in sphingosine-sphinganine ratio, indeed suggesting that perturbing the balance of typical sphingolipids and their precursors may itself be damaging to neurons (Atkinson et al., 2017). The HSN-1-causing mutations SPTLC1$^{S331F/Y}$ and SPTLC2^{I505Y} have been associated with increased levels of C18- and C20-sphingoid bases and an exceptionally severe HSN-1 phenotype (Bode et al., 2016). Intriguingly, the same was not reported for the SPTLC1^{C133W} mutant but this Thesis provided evidence that as well as generating deoxysphingoid bases, there may be

additional changes to the typical sphingoid base profile in SPTLC1^{C133W} patient fibroblasts (Chapter 6), indeed potentially further complicating pathogenesis *in vivo*.

7.2 ER stress in HSN-1

In agreement with other HSN-1 models in the literature (Gable et al., 2010; Myers et al., 2014; Alecu et al., 2016b), the results presented in this Thesis showed that exogenous application of the deoxysphingoid bases to mammalian motor and sensory neurons resulted in ER stress (Chapter 4). This manifested both as depletion of ER Ca^{2+} and upregulation of the UPR protein, BiP. Indeed, depletion of ER Ca^{2+} is known to cause accumulation of unfolded proteins, in turn triggering the UPR. Activation of the UPR causes the upregulation of a number of proteins, including BiP, which acts as a chaperone to eliminate misfolded proteins in the ER lumen (Paschen and Mengesdorf, 2005).

Since SPT is an ER membrane protein, the site of intracellular deoxysphingoid base generation is the ER. However, when motor and sensory neurons were engineered to express the mutant enzyme itself, as opposed to merely being treated with the abnormal products of the mutant enzyme, ER stress was not detected (Chapter 5). In a third *in vitro* model of HSN-1, patient skin-derived fibroblasts, there was an indication that low levels of ER stress may be present when the cells were supplemented with L-alanine, the substrate precursor to deoxysphingoid bases (Chapter 6). Although ER Ca^{2+} levels remain to be further explored in these two models, initial studies exploring BiP expression levels suggest that extracellularly applied deoxysphingoid bases may trigger ER stress more readily than intracellularly generated deoxysphingoid bases.

Indeed, examination of expression levels of other ER stress markers including protein kinase R (PKR)-like endoplasmic reticulum kinase (PERK), inositol-requiring enzyme 1 (IRE1), activating transcription factor 6 (ATF6) and further downstream components in these three *in vitro* models would allow further interrogation of the precise ER stress pathways involved in HSN-1. Prolonged ER stress is known to cause apoptosis, and indeed the UPR and ER stress have

been implicated in a number of other neurodegenerative disorders including Huntington's disease, Alzheimer's disease, Parkinson's disease and amyotrophic lateral sclerosis (ALS; Kim et al., 2008; Xiang et al., 2017). Targeting ER stress pathways with small molecules presents a potential therapeutic option.

7.3 Abnormal Ca^{2+} handling in HSN-1

In addition to depletion of ER Ca^{2+} in motor and sensory neurons exogenously treated with deoxysphingoid bases, other Ca^{2+} handling abnormalities were also noted, including acutely elevated mitochondrial Ca^{2+} which appears to be, at least in part, due to aberrant SOC channel activity (Chapter 4). This is not the first time deoxysphingoid base application has been shown to alter normal activity at the cell membrane, and Guntert et al. (2016) showed deoxysphinganine application to cause an increase in NMDA receptor signalling in primary cortical neurons. Biophysical examination of deoxysphingolipids has shown that they are capable of altering cell membrane function (Jimenez-Rojo et al., 2014) and thus circulating deoxysphingoid bases or deoxysphingolipids acting at peripheral nerve cell membranes presents a plausible primary target. Moreover, disturbances in normal SOC channel signalling have been reported in other CMT subtypes (Pla-Martin et al., 2013; Barneo-Munoz et al., 2015; Gonzalez-Sanchez et al., 2017) and also in other neurodegenerative diseases including hereditary spastic paraplegia, Parkinson's disease, Alzheimer's disease and Huntington's disease (Pchitskaya et al., 2017).

Mitochondrial Ca^{2+} loading was apparent only after 2 h treatment in primary motor neurons, but not present after more prolonged, 24 h, treatment or in DRG neurons (Chapter 4). It is possible that elevated mitochondrial Ca^{2+} is an acute response to increased Ca^{2+} influx through SOC channels and that the treatment paradigm used in DRG neurons was not short enough to capture these deoxysphingoid base-induced changes. Testing multiple treatment paradigms ranging from 0-2 h would allow further interrogation of this hypothesis.

Moreover, it would be important moving forwards with this study to also examine Ca^{2+} handling in the two other *in vitro* models of HSN-1 used in the Thesis which

generate deoxysphingoid bases intracellularly, since these deoxysphinganines may have different primary targets.

7.4 Mitochondrial dysfunction in HSN-1

In addition to elevated mitochondrial Ca^{2+} levels observed in in primary neurons treated with deoxysphingoid bases, there was also a decrease in mitochondrial membrane potential. This is somewhat surprising considering that mitochondrial dehydrogenases are in fact activated by Ca^{2+} ions, which would cause an increase in NADH/ $FADH_2$ generation and in turn increased electron transport chain activity, and one would assume a normal mitochondrial membrane potential (Denton, 2009). This adds further evidence to the hypothesis that elevated mitochondrial Ca^{2+} observed following treatment with the deoxysphinganines may be transient rather than a chronic state, in response to increased Ca^{2+} influx from the cell membrane.

Although the mitochondrial membrane potential was reduced in both motor and sensory neurons treated exogenously with the deoxysphinganines (Chapter 4), exploration of mitochondrial health using patient fibroblasts did not reveal similar changes, despite the fact that elevated levels of deoxysphingoid bases were being generated when compared to controls (Chapter 6). It is possible that fibroblasts can counteract deoxysphinganine-mediated subcellular changes and thus maintain mitochondrial membrane potential, whereas neurons, which are high energy demanding cells, are more vulnerable. In patients, neuronal cells are indeed the main cell type affected. It would be important moving forwards to examine the primary neurons engineered to generate deoxysphingoid bases (Chapter 5) for similar mitochondrial deficits.

Furthermore, the differences in mitochondrial membrane potential between the cell models examined in this Thesis may be a result of whether the deoxysphingoid bases are exogenously applied, or intracellularly generated. It is intriguing that in mixed cultures exogenously treated with the deoxysphinganines, a loss of both neuronal and non-neuronal cells is observed, suggesting non-cell selectivity (Chapter 3), yet in patient fibroblasts, cell distress is not overt (Chapter

6). This may suggest a different mechanism of action for extracellular and intracellular deoxysphingoid bases, rather than differences between cell types.

Interestingly, although patient fibroblasts were able to maintain a normal mitochondrial membrane potential, there was a small decrease in the total mitochondrial area. It is possible that fibroblasts can successfully remove any dysfunctional mitochondria, thus maintaining overall mitochondrial membrane potential but causing a decrease in total mitochondrial area. This may provide a reason as to why neurons are the most susceptible cell type in HSN-1.

This is not the first report of mitochondrial dysfunction or abnormalities in models of HSN-1 (Myers et al., 2014; Stimpson et al., 2015; Alecu et al., 2016b) and certainly mitochondrial involvement is widespread in neurodegenerative diseases in general (Beal, 2005; Lin and Beal, 2006).

7.5 A comparison of the three *in vitro* models of HSN-1 used in this Thesis

Throughout this Thesis, three different *in vitro* models of HSN-1 were used. Firstly, primary mammalian motor and sensory neurons were exogenously treated with deoxysphingoid bases. A second model used a viral vector to induce primary mammalian motor and sensory neurons to generate intracellular deoxysphingoid bases from transduced, mutant SPT. Thirdly, patient-derived fibroblasts were grown in culture, which were also shown to generate intracellular deoxysphingoid bases.

A major difference between these models is whether they represent systemic, circulating deoxysphingoid bases or intracellular generation of them. Indeed, phenotypes of cell death, ER stress and mitochondrial dysfunction were far more apparent in cells exogenously treated with deoxysphingoid bases. The concentrations of deoxysphinganines applied to primary neurons were based on deoxysphingoid base concentrations measured in patient plasma. However, it is possible that the concentrations that peripheral nerves are exposed to is not as high. The blood may well act as a ‘dumping ground’ for deoxysphingoid bases. Moreover, the concentrations of deoxysphingoid bases measured in patient blood

plasma is representative of total deoxysphingoid bases, including those metabolised into downstream deoxysphingolipids and those transported on LDL or VLDL, which may dampen their toxic effects *in vivo* (Bertea et al., 2010; Alecu et al., 2016a).

A restriction of all three of these models is that they can only be grown for a relatively short amount of time *in vitro*, yet HSN-1 is a chronic disease. It is possible that transduced neurons and patient fibroblasts are not grown long enough in order to accumulate deoxysphingoid bases at sufficient levels to display toxicity.

A further point to consider is whether the point mutation in SPTLC1 causes further aberrant subcellular interactions, in addition to the generation of deoxysphingoid bases. This indeed could be explored using the transduced neuronal and patient fibroblast *in vitro* models used in this Thesis.

Finally, differences between neuronal *in vitro* models and patient fibroblasts could reflect cell-specific responses either to the SPTLC1 mutation or the deoxysphingoid bases. Indeed, even motor and sensory neurons displayed different responses to exogenously applied deoxysphingoid bases (Chapters 3 and 4). The primary motor and sensory neurons used in this Thesis are derived from different aged mice, and even where both these cell types are derived from embryonic mice, these neurons may be at different stages of development, potentially contributing to differences measured *in vitro*. Motor and sensory neurons may also display differential metabolic demand and varying capacity to deal with stress.

SPTLC1 is ubiquitously expressed and although HSN-1 patients are reported to have notably slow wound healing, HSN-1 is largely considered a disease of the nervous system, which may provide reason as to why patient fibroblasts appeared largely indifferent to their control counterparts. This patient-derived material expresses *SPTLC1* at physiologically relevant levels, thus being advantageous compared to genetic overexpression models. However, with mitochondrial dysfunction highlighted as a potential player in the pathogenesis of

HSN-1, fibroblasts (a largely glycolytic cell type) may not provide the most appropriate cell type to explore the mechanisms underlying neuronal damage in this disease.

Indeed the manifestation of the HSN-1 pathology seen in patients is likely to be a complex combination of the effects of intracellular generation of deoxysphingolipids as well as their systemic circulation.

7.6 Implication of these results for HSN-1

The results presented in this Thesis demonstrate that extracellular application of deoxysphingoid bases is toxic to mammalian neurons *in vitro* and also highlights potential targets for therapeutic intervention, namely the ER, the mitochondria and the plasma membrane. Further investigation of the effect on intracellularly generated deoxysphingoid bases remains to be explored.

One promising therapeutic approach to HSN-1 is that of L-serine supplementation. L-serine is already approved as treatment for two genetic disorders which result in L-serine deficiency, namely 3-phosphoglycerate dehydrogenase deficiency and 3-phosphoserine phosphatase deficiency (de Koning, 2006). A pre-clinical trial with 14 HSN-1 patients showed evidence of L-serine ability to lower plasma deoxysphingoid bases in patients (Garofalo et al., 2011). This has since been followed up with a two-year, placebo-controlled clinical trial with 16 patients. This is yet to be published but promising data showing decreased deoxysphingoid base levels and improved CMTNS following L-serine treatment was presented at the Peripheral Nerve Society Annual Meeting 2017 (Fridman et al., 2017). Work in this Thesis demonstrates that deoxysphingoid bases are indeed toxic and thus lowering patient levels with L-serine, as described above, may well be beneficial to patient outcomes.

It should be noted that this approach may also prove beneficial for type 2 *diabetes mellitus* and diabetic neuropathy, diseases in which elevated levels of deoxysphingoid bases in patient plasma have also been reported (Bertea et al., 2010; Othman et al., 2012; Othman et al., 2014; Othman et al., 2015b). Moreover,

L-serine has been proposed to have other neuroprotective effects and a phase I clinical trial for L-serine treatment in ALS confirmed the treatment to be safe for ALS patients allowing it to be taken forward to phase II trials (Levine et al., 2017).

7.7 Limitations of this study

This Thesis uses three *in vitro* models of HSN-1. Two of these models used primary mammalian motor and sensory neurons, the cell types typically affected in HSN-1. A limitation of cells in culture, particularly primary neurons, is that they can only be grown *in vitro* for a matter of weeks, whereas HSN-1 is a chronic disease that spans life times. Moreover, much of the work in this Thesis uses primary motor neurons, a particularly challenging cell type to work with in culture which will only survive if dissected from embryonic age mice. This means that the motor neurons used in these experiments are relatively immature in comparison to the neurons affected in HSN-1 patients, who are usually teenagers or adults.

Although this Thesis uses three models to explore HSN-1, a major limitation is that these are all *in vitro*. It stands to reason that other cells within tissues may offer protective effects on peripheral neurons from HSN-1-associated deoxysphingoid base toxicity.

A mouse model of HSN-1 does exist, as discussed in Chapter 1 and in the Introduction to Chapter 5, but this model develops very late onset and very mild neuropathy (McCampbell et al., 2005; Eichler et al., 2009), which is not reflective of the usually severe, second- or third-decade onset neuropathy seen in HSN-1 patients (Houlden et al., 2006). This mouse model is an overexpression model whereby wildtype or mutant *SPTLC1* is expressed in addition to endogenous *SPTLC1*. It may be possible to generate a mouse model more closely resembling the human disease by knocking out endogenous mouse SPTLC1 in addition to expression of $SPTLC1^{C133W}$ or indeed by using other gene-editing technology to replace mouse wildtype *SPTLC1*, with a mutant form. Moreover, generation of conditional transgenic animal models may further the understanding of the source of toxicity in HSN-1. For example, comparison of animals expressing mutant *SPTLC1* only in neurons and expressing mutant *SPTLC1* only in (for example)

liver may provide answer as to whether neurotoxic deoxysphingoid bases are those generated within the nervous system tissue itself or by other organs from which deoxysphingoid bases can enter the circulation and subsequently damage peripheral nerves.

7.8 Future directions

Whilst this Thesis begins to explore pathomechanisms in HSN-1, it also triggers a number of further questions. One major question that this Thesis begins to explore is whether it is the systemic circulation of deoxysphingoid bases or their intracellular generation which causes peripheral nerve damage in HSN-1. Indeed, it would be informative to investigate how much of the intracellularly generated deoxysphingoid bases measured in patient fibroblasts and neurons engineered to express *SPTLC1* are secreted from the cells into the cell media. This would allow a more direct comparison of these models with the levels of deoxysphingoid bases exogenously applied to neurons. To further this, it would indeed be intriguing to investigate how motor and sensory neurons respond to media in which patient fibroblasts have been grown, thus containing deoxysphingoid bases generated by human cells.

A fellow PhD student in this laboratory, Dr Umaiyal Kugathsan, has used the patient fibroblasts explored in this Thesis to generate induced pluripotent stem cell-derived sensory neurons. This *in vitro* model boasts being both neuronal and human-derived. Moreover, the patient-derived nature of this system means these cells will express *SPTLC1/2* (thus are likely to generate deoxysphingoid bases) at physiological levels. Furthermore, induced pluripotent stem cell-derived neurons have the capacity to be grown *in vitro* for far longer periods of time than the primary neurons, thus have the potential to recapitulate the chronic nature of HSN-1 more effectively than the cells used in the Thesis. It would be interesting to explore the parameters highlighted in this Thesis as potential players in HSN-1 pathology in this fourth *in vitro* model (see poster abstract; Kugathasan et al., 2017).

In all, these further investigations will help to identify the most appropriate *in vitro* model(s) to use as screening tools for HSN-1 therapies.

7.9 Concluding remarks

Overall the results presented in this Thesis show that HSN-1-associated deoxysphingoid bases are toxic to motor and sensory neurons *in vitro*. Moreover, the results propose that circulating deoxysphingoid bases found in HSN-1 patients may disturb the cell membrane, affecting for example SOC channel entry. Whilst it appears that this may lead to a transient increase in mitochondrial Ca^{2+} levels, as the organelle works to maintain normal cytosolic Ca^{2+} concentrations, deoxysphingoid bases also appear to cause mitochondrial dysfunction and ER stress, which ultimately may lead to cell death and the peripheral nerve damage reported in HSN-1 patients. Work remains to be done to establish the role of intracellularly generated deoxysphingoid bases. This Thesis highlights potential targets for therapeutic intervention in HSN-1 including the cell membrane, ER stress and mitochondria.

References

Abramov, A. Y. & Duchen, M. R. 2003. Actions of Ionomycin, 4-Bra23187 and a Novel Electrogenic Ca2+ Ionophore on Mitochondria in Intact Cells. *Cell Calcium,* 33**,** 101-12.

Airola, M. V. & Hannun, Y. A. 2013. Sphingolipid Metabolism and Neutral Sphingomyelinases. *Handbook of Experimental Pharmacology***,** 57-76.

Alecu, I., Othman, A., Penno, A., Saied, E. M., Arenz, C., Von Eckardstein, A. & Hornemann, T. 2016a. Cytotoxic 1-Deoxysphingolipids Are Metabolized by a Cytochrome P450-Dependent Pathway. *Journal of Lipid Research*.

Alecu, I., Tedeschi, A., Behler, N., Wunderling, K., Lamberz, C., Lauterbach, M. A., Gaebler, A., Ernst, D., Van Veldhoven, P. P., Al-Amoudi, A., Latz, E., Othman, A., Kuerschner, L., Hornemann, T., Bradke, F., Thiele, C. & Penno, A. 2016b. Localization of 1-Deoxysphingolipids to Mitochondria Induces Mitochondrial Dysfunction. *Journal of Lipid Research*.

Atkinson, D., Nikodinovic Glumac, J., Asselbergh, B., Ermanoska, B., Blocquel, D., Steiner, R., Estrada-Cuzcano, A., Peeters, K., Ooms, T., De Vriendt, E., Yang, X. L., Hornemann, T., Milic Rasic, V. & Jordanova, A. 2017. Sphingosine 1-Phosphate Lyase Deficiency Causes Charcot-Marie-Tooth Neuropathy. *Neurology*.

Auer-Grumbach, M. 2008. Hereditary Sensory Neuropathy Type I. *Orphanet Journal of Rare Diseases,* 3**,** 7.

Auer-Grumbach, M. 2013. Hereditary Sensory and Autonomic Neuropathies. *Handbook of Clinical Neurology,* 115**,** 893-906.

Auer-Grumbach, M., Bode, H., Pieber, T. R., Schabhuttl, M., Fischer, D., Seidl, R., Graf, E., Wieland, T., Schuh, R., Vacariu, G., Grill, F., Timmerman, V., Strom, T. M. & Hornemann, T. 2013. Mutations at Ser331 in the Hsn Type I Gene Sptlc1 Are Associated with a Distinct Syndromic Phenotype. *European Journal of Medical Genetics,* 56**,** 266-9.

Baird, R. D., Kitzen, J., Clarke, P. A., Planting, A., Reade, S., Reid, A., Welsh, L., López Lázaro, L., De Las Heras, B., Judson, I. R., Kaye, S. B., Eskens, F., Workman, P., Debono, J. S. & Verweij, J. 2009. Phase I Safety, Pharmacokinetic, and Pharmacogenomic Trial of Es-285, a Novel

Marine Cytotoxic Agent, Administered to Adult Patients with Advanced Solid Tumors. *Molecular Cancer Therapeutics,* 8**,** 1430-7.

Barneo-Munoz, M., Juarez, P., Civera-Tregon, A., Yndriago, L., Pla-Martin, D., Zenker, J., Cuevas-Martin, C., Estela, A., Sanchez-Arago, M., Forteza-Vila, J., Cuezva, J. M., Chrast, R. & Palau, F. 2015. Lack of Gdap1 Induces Neuronal Calcium and Mitochondrial Defects in a Knockout Mouse Model of Charcot-Marie-Tooth Neuropathy. *PLoS Genetics,* 11**,** e1005115.

Beal, M. F. 2005. Mitochondria Take Center Stage in Aging and Neurodegeneration. *Annals of Neurology,* 58**,** 495-505.

Bejaoui, K., Wu, C., Scheffler, M. D., Haan, G., Ashby, P., Wu, L., De Jong, P. & Brown, R. H. 2001. Sptlc1 Is Mutated in Hereditary Sensory Neuropathy, Type 1. *Nature Genetics,* 27**,** 261-2.

Benz, R. & Mclaughlin, S. 1983. The Molecular Mechanism of Action of the Proton Ionophore Fccp (Carbonylcyanide P-Trifluoromethoxyphenylhydrazone). *Biophysical Journal,* 41**,** 381-98.

Bernardi, P., Broekemeier, K. M. & Pfeiffer, D. R. 1994. Recent Progress on Regulation of the Mitochondrial Permeability Transition Pore; a Cyclosporin-Sensitive Pore in the Inner Mitochondrial Membrane. *Journal of Bioenergetics and Biomembranes,* 26**,** 509-17.

Bertea, M., Rütti, M. F., Othman, A., Marti-Jaun, J., Hersberger, M., Von Eckardstein, A. & Hornemann, T. 2010. Deoxysphingoid Bases as Plasma Markers in Diabetes Mellitus. *Lipids in Health and Disease,* 9**,** 84.

Bird, G. S., Dehaven, W. I., Smyth, J. T. & Putney, J. W., Jr. 2008. Methods for Studying Store-Operated Calcium Entry. *Methods,* 46**,** 204-12.

Bode, H., Bourquin, F., Suriyanarayanan, S., Wei, Y., Alecu, I., Othman, A., Von Eckardstein, A. & Hornemann, T. 2016. Hsan1 Mutations in Serine Palmitoyltransferase Reveal a Close Structure-Function-Phenotype Relationship. *Human Molecular Genetics,* 25**,** 853-65.

Bouard, D., Alazard-Dany, D. & Cosset, F. L. 2009. Viral Vectors: From Virology to Transgene Expression. *British Journal of Pharmacology,* 157**,** 153-65.

Breslow, D. K., Collins, S. R., Bodenmiller, B., Aebersold, R., Simons, K., Shevchenko, A., Ejsing, C. S. & Weissman, J. S. 2010. Orm Family Proteins Mediate Sphingolipid Homeostasis. *Nature,* 463**,** 1048-53.

Buede, R., Rinker-Schaffer, C., Pinto, W. J., Lester, R. L. & Dickson, R. C. 1991. Cloning and Characterization of Lcb1, a Saccharomyces Gene Required for Biosynthesis of the Long-Chain Base Component of Sphingolipids. *Journal of Bacteriology,* 173**,** 4325-32.

Callaghan, B. C., Cheng, H. T., Stables, C. L., Smith, A. L. & Feldman, E. L. 2012. Diabetic Neuropathy: Clinical Manifestations and Current Treatments. *Lancet Neurology,* 11**,** 521-34.

Charcot, J. M. & Marie, P. 1886. Sur Une Forme Particuliére D'atrophie Musculaire Progressive Souvent Familial Debutant Par Les Pied Et Les Jambes Et Atteignant Plus Tard Les Mains. *Revista Medica. Ateneo Ramón y Cajal, México,* 6**,** 97-138.

Choudhury, S. R., Hudry, E., Maguire, C. A., Sena-Esteves, M., Breakefield, X. O. & Grandi, P. 2017. Viral Vectors for Therapy of Neurologic Diseases. *Neuropharmacology,* 120**,** 63-80.

Clapham, D. E. 1995. Calcium Signaling. *Cell,* 80**,** 259-68.

Csordas, G., Renken, C., Varnai, P., Walter, L., Weaver, D., Buttle, K. F., Balla, T., Mannella, C. A. & Hajnoczky, G. 2006. Structural and Functional Features and Significance of the Physical Linkage between Er and Mitochondria. *Journal of Cell Biology,* 174**,** 915-921.

Cuadros, R., Montejo De Garcini, E., Wandosell, F., Faircloth, G., Fernández-Sousa, J. M. & Avila, J. 2000. The Marine Compound Spisulosine, an Inhibitor of Cell Proliferation, Promotes the Disassembly of Actin Stress Fibers. *Cancer Letters,* 152**,** 23-9.

D'aniello, A., Fisher, G., Migliaccio, N., Cammisa, G., D'aniello, E. & Spinelli, P. 2005. Amino Acids and Transaminases Activity in Ventricular Csf and in Brain of Normal and Alzheimer Patients. *Neuroscience Letters,* 388**,** 49-53.

Davidson, B. L. & Breakefield, X. O. 2003. Viral Vectors for Gene Delivery to the Nervous System. *Nature Reviews: Neuroscience,* 4**,** 353-64.

Davidson, G., Murphy, S., Polke, J., Laura, M., Salih, M., Muntoni, F., Blake, J., Brandner, S., Davies, N., Horvath, R., Price, S., Donaghy, M., Roberts,

M., Foulds, N., Ramdharry, G., Soler, D., Lunn, M., Manji, H., Davis, M., Houlden, H. & Reilly, M. 2012. Frequency of Mutations in the Genes Associated with Hereditary Sensory and Autonomic Neuropathy in a Uk Cohort. *Journal of Neurology,* 259**,** 1673-85.

Dawkins, J. L., Hulme, D. J., Brahmbhatt, S. B., Auer-Grumbach, M. & Nicholson, G. A. 2001. Mutations in Sptlc1, Encoding Serine Palmitoyltransferase, Long Chain Base Subunit-1, Cause Hereditary Sensory Neuropathy Type I. *Nature Genetics,* 27**,** 309-12.

De Koning, T. J. 2006. Treatment with Amino Acids in Serine Deficiency Disorders. *Journal of Inherited Metabolic Disease,* 29**,** 347-51.

Denton, R. M. 2009. Regulation of Mitochondrial Dehydrogenases by Calcium Ions. *Biochimica et Biophysica Acta,* 1787**,** 1309-16.

Dildy, J. E. & Leslie, S. W. 1989. Ethanol Inhibits Nmda-Induced Increases in Free Intracellular Ca2+ in Dissociated Brain Cells. *Brain Research,* 499**,** 383-7.

Dohrn, M. F., Othman, A., Hirshman, S. K., Bode, H., Alecu, I., Fahndrich, E., Karges, W., Weis, J., Schulz, J. B., Hornemann, T. & Claeys, K. G. 2015. Elevation of Plasma 1-Deoxy-Sphingolipids in Type 2 Diabetes Mellitus: A Susceptibility to Neuropathy? *European Journal of Neurology,* 22**,** 806-14, e55.

Duan, J. & Merrill, A. H., Jr. 2015. 1-Deoxysphingolipids Encountered Exogenously and Made De Novo: Dangerous Mysteries inside an Enigma. *Journal of Biological Chemistry,* 290**,** 15380-9.

Eichler, F. S., Hornemann, T., Mccampbell, A., Kuljis, D., Penno, A., Vardeh, D., Tamrazian, E., Garofalo, K., Lee, H. J., Kini, L., Selig, M., Frosch, M., Gable, K., Von Eckardstein, A., Woolf, C. J., Guan, G., Harmon, J. M., Dunn, T. M. & Brown, R. H., Jr. 2009. Overexpression of the Wild-Type Spt1 Subunit Lowers Desoxysphingolipid Levels and Rescues the Phenotype of Hsan1. *Journal of Neuroscience,* 29**,** 14646-51.

Esaki, K., Sayano, T., Sonoda, C., Akagi, T., Suzuki, T., Ogawa, T., Okamoto, M., Yoshikawa, T., Hirabayashi, Y. & Furuya, S. 2015. L-Serine Deficiency Elicits Intracellular Accumulation of Cytotoxic Deoxysphingolipids and Lipid Body Formation. *Journal of Biological Chemistry,* 290**,** 14595-609.

Fernyhough, P. & Calcutt, N. A. 2010. Abnormal Calcium Homeostasis in Peripheral Neuropathies. *Cell Calcium,* 47**,** 130-9.

Fonteriz, R. I., De La Fuente, S., Moreno, A., Lobatón, C. D., Montero, M. & Alvarez, J. 2010. Monitoring Mitochondrial [Ca(2+)] Dynamics with Rhod-2, Ratiometric Pericam and Aequorin. *Cell Calcium,* 48**,** 61-9.

Fridman, V., Novak, P., David, W., Macklin, E. A., Mckenna-Yasek, D., Walsh, K., Oaklander, A. L., Brown, R., Hornemann, T. & Eichler, F. 2017. A Randomized, Double-Blind, Placebo-Controlled Trial Evaluating the Safety and Efficacy of L-Serine in Subjects with Hereditary Sensory and Autonomic Neuropathy Type 1 (Hsan1). PNS Annual Meeting 2017 Abstracts.

Gable, K., Gupta, S. D., Han, G., Niranjanakumari, S., Harmon, J. M. & Dunn, T. M. 2010. A Disease-Causing Mutation in the Active Site of Serine Palmitoyltransferase Causes Catalytic Promiscuity. *Journal of Biological Chemistry,* 285**,** 22846-52.

Garofalo, K., Penno, A., Schmidt, B., Lee, H., Frosch, M., Von Eckardstein, A., Brown, R., Hornemann, T. & Eichler, F. 2011. Oral L-Serine Supplementation Reduces Production of Neurotoxic Deoxysphingolipids in Mice and Humans with Hereditary Sensory Autonomic Neuropathy Type 1. *Journal of Clinical Investigation,* 121**,** 4735-4745.

Gemes, G., Bangaru, M. L., Wu, H. E., Tang, Q., Weihrauch, D., Koopmeiners, A. S., Cruikshank, J. M., Kwok, W. M. & Hogan, Q. H. 2011. Store-Operated Ca2+ Entry in Sensory Neurons: Functional Role and the Effect of Painful Nerve Injury. *Journal of Neuroscience,* 31**,** 3536-49.

Gonzalez-Sanchez, P., Pla-Martin, D., Martinez-Valero, P., Rueda, C. B., Calpena, E., Del Arco, A., Palau, F. & Satrustegui, J. 2017. Cmt-Linked Loss-of-Function Mutations in Gdap1 Impair Store-Operated Ca2+ Entry-Stimulated Respiration. *Scientific Reports,* 7**,** 42993.

Gruszczynska-Biegala, J., Sladowska, M. & Kuznicki, J. 2016. Ampa Receptors Are Involved in Store-Operated Calcium Entry and Interact with Stim Proteins in Rat Primary Cortical Neurons. *Frontiers in Cellular Neuroscience,* 10**,** 251.

Grynkiewicz, G., Poenie, M. & Tsien, R. Y. 1985. A New Generation of Ca2+ Indicators with Greatly Improved Fluorescence Properties. *Journal of Biological Chemistry,* 260**,** 3440-50.

Gulbins, E. & Petrache, I. 2013. *Sphingolipids: Basic Science and Drug Development,* Verlag Wien, Springer.

Guntert, T., Hanggi, P., Othman, A., Suriyanarayanan, S., Sonda, S., Zuellig, R. A., Hornemann, T. & Ogunshola, O. O. 2016. 1-Deoxysphingolipid-Induced Neurotoxicity Involves N-Methyl-D-Aspartate Receptor Signaling. *Neuropharmacology*.

Gupta, S. D., Gable, K., Alexaki, A., Chandris, P., Proia, R. L., Dunn, T. M. & Harmon, J. M. 2014. Expression of the Ormdls, Modulators of Serine Palmitoyltransferase, Is Regulated by Sphingolipids in Mammalian Cells. *Journal of Biological Chemistry*.

Gururaj, C., Federman, R. & Chang, A. 2013. Orm Proteins Integrate Multiple Signals to Maintain Sphingolipid Homeostasis. *Journal of Biological Chemistry,* 288**,** 20453-63.

Hammad, S. M., Baker, N. L., El Abiad, J. M., Spassieva, S. D., Pierce, J. S., Rembiesa, B., Bielawski, J., Lopes-Virella, M. F., Klein, R. L. & Investigators, D. E. G. O. 2016. Increased Plasma Levels of Select Deoxy-Ceramide and Ceramide Species Are Associated with Increased Odds of Diabetic Neuropathy in Type 1 Diabetes: A Pilot Study. *Neuromolecular Medicine*.

Han, G., Gupta, S. D., Gable, K., Niranjanakumari, S., Moitra, P., Eichler, F., Brown, R. H., Jr., Harmon, J. M. & Dunn, T. M. 2009. Identification of Small Subunits of Mammalian Serine Palmitoyltransferase That Confer Distinct Acyl-Coa Substrate Specificities. *Proceedings of the National Academy of Sciences of the United States of America,* 106**,** 8186-91.

Hanada, K. 2003. Serine Palmitoyltransferase, a Key Enzyme of Sphingolipid Metabolism. *Biochimica et Biophysica Acta,* 1632**,** 16-30.

Hanada, K., Hara, T., Nishijima, M., Kuge, O., Dickson, R. C. & Nagiec, M. M. 1997. A Mammalian Homolog of the Yeast Lcb1 Encodes a Component of Serine Palmitoyltransferase, the Enzyme Catalyzing the First Step in Sphingolipid Synthesis. *Journal of Biological Chemistry,* 272**,** 32108-14.

Hayashi, T., Rizzuto, R., Hajnoczky, G. & Su, T. P. 2009. Mam: More Than Just a Housekeeper. *Trends in Cell Biology,* 19**,** 81-88.

Henderson, C. E., Bloch-Gallego, E. & Camu, W. 1995. Purified Embryonic Motoneurons. *In:* COHEN, J. & WILKIN, G. (eds.) *Nerve Cell Cultures: A Practical Approach.* Oxford University, London.

Hetz, C. & Mollereau, B. 2014. Disturbance of Endoplasmic Reticulum Proteostasis in Neurodegenerative Diseases. *Nature Reviews: Neuroscience,* 15**,** 233-49.

Hoek, J. B., Farber, J. L., Thomas, A. P. & Wang, X. 1995. Calcium Ion-Dependent Signalling and Mitochondrial Dysfunction: Mitochondrial Calcium Uptake During Hormonal Stimulation in Intact Liver Cells and Its Implication for the Mitochondrial Permeability Transition. *Biochimica et Biophysica Acta,* 1271**,** 93-102.

Hojjati, M. R., Li, Z. & Jiang, X. C. 2005. Serine Palmitoyl-Coa Transferase (Spt) Deficiency and Sphingolipid Levels in Mice. *Biochimica et Biophysica Acta,* 1737**,** 44-51.

Hornemann, T., Penno, A., Rutti, M. F., Ernst, D., Kivrak-Pfiffner, F., Rohrer, L. & Von Eckardstein, A. 2009. The Sptlc3 Subunit of Serine Palmitoyltransferase Generates Short Chain Sphingoid Bases. *Journal of Biological Chemistry,* 284**,** 26322-30.

Houlden, H., King, R., Blake, J., Groves, M., Love, S., Woodward, C., Hammans, S., Nicoll, J., Lennox, G., O'donovan, D. G., Gabriel, C., Thomas, P. K. & Reilly, M. M. 2006. Clinical, Pathological and Genetic Characterization of Hereditary Sensory and Autonomic Neuropathy Type 1 (Hsan I). *Brain,* 129**,** 411-25.

Humpf, H. U., Schmelz, E. M., Meredith, F. I., Vesper, H., Vales, T. R., Wang, E., Menaldino, D. S., Liotta, D. C. & Merrill, A. H. 1998. Acylation of Naturally Occurring and Synthetic 1-Deoxysphinganines by Ceramide Synthase. Formation of N-Palmitoyl-Aminopentol Produces a Toxic Metabolite of Hydrolyzed Fumonisin, Ap1, and a New Category of Ceramide Synthase Inhibitor. *Journal of Biological Chemistry,* 273**,** 19060-4.

Irobi, J., Holmgren, A., De Winter, V., Asselbergh, B., Gettemans, J., Adriaensen, D., Ceuterick-De Groote, C., Van Coster, R., De Jonghe, P.

& Timmerman, V. 2012. Mutant Hspb8 Causes Protein Aggregates and a Reduced Mitochondrial Membrane Potential in Dermal Fibroblasts from Distal Hereditary Motor Neuropathy Patients. *Neuromuscular Disorders,* 22**,** 699-711.

Jensen, A. M. & Chiu, S. Y. 1990. Fluorescence Measurement of Changes in Intracellular Calcium Induced by Excitatory Amino Acids in Cultured Cortical Astrocytes. *Journal of Neuroscience,* 10**,** 1165-75.

Jimenez-Rojo, N., Sot, J., Busto, J. V., Shaw, W. A., Duan, J., Merrill, A. H., Jr., Alonso, A. & Goni, F. M. 2014. Biophysical Properties of Novel 1-Deoxy-(Dihydro)Ceramides Occurring in Mammalian Cells. *Biophysical Journal,* 107**,** 2850-9.

Jun, B. K., Chandra, A., Kuljis, D., Schmidt, B. P. & Eichler, F. S. 2015. Substrate Availability of Mutant Spt Alters Neuronal Branching and Growth Cone Dynamics in Dorsal Root Ganglia. *Journal of Neuroscience,* 35**,** 13713-9.

Kalmar, B., Innes, A., Wanisch, K., Koyen Kolaszynska, A., Pandraud, A., Kelly, G., Abramov, A. Y., Reilly, M. M., Schiavo, G. & Greensmith, L. 2017. Mitochondrial Deficits and Abnormal Mitochondrial Retrograde Axonal Transport Play a Role in the Pathogenesis of Mutant Hsp27 Induced Charcot Marie Tooth Disease. *Human Molecular Genetics*.

Kay, M. A., Glorioso, J. C. & Naldini, L. 2001. Viral Vectors for Gene Therapy: The Art of Turning Infectious Agents into Vehicles of Therapeutics. *Nature Medicine,* 7**,** 33-40.

Kennerson, M. L., Nicholson, G. A., Kaler, S. G., Kowalski, B., Mercer, J. F., Tang, J., Llanos, R. M., Chu, S., Takata, R. I., Speck-Martins, C. E., Baets, J., Almeida-Souza, L., Fischer, D., Timmerman, V., Taylor, P. E., Scherer, S. S., Ferguson, T. A., Bird, T. D., De Jonghe, P., Feely, S. M., Shy, M. E. & Garbern, J. Y. 2010. Missense Mutations in the Copper Transporter Gene Atp7a Cause X-Linked Distal Hereditary Motor Neuropathy. *American Journal of Human Genetics,* 86**,** 343-52.

Khan, A. & Hornemann, T. 2017. Correlation of the Plasma Sphingoid Base Profile with Results from Oral Glucose Tolerance Tests in Gestational Diabetes Mellitus. *EXCLI Journal,* 16**,** 497-509.

Kim, I., Xu, W. & Reed, J. C. 2008. Cell Death and Endoplasmic Reticulum Stress: Disease Relevance and Therapeutic Opportunities. *Nature Reviews Drug Discovery,* 7**,** 1013-30.

Kolter, T. & Sandhoff, K. 2006. Sphingolipid Metabolism Diseases. *Biochimica et Biophysica Acta,* 1758**,** 2057-79.

Kramer, R., Bielawski, J., Kistner-Griffin, E., Othman, A., Alecu, I., Ernst, D., Kornhauser, D., Hornemann, T. & Spassieva, S. 2015. Neurotoxic 1-Deoxysphingolipids and Paclitaxel-Induced Peripheral Neuropathy. *FASEB Journal*.

Krols, M., Van Isterdael, G., Asselbergh, B., Kremer, A., Lippens, S., Timmerman, V. & Janssens, S. 2016. Mitochondria-Associated Membranes as Hubs for Neurodegeneration. *Acta Neuropathologica,* 131**,** 505-23.

Kugathasan, U., Clark, A. J., Suriyanarayanan, S., Laurá, M., Wilson, E. R., Kalmar, B., Greensmith, L., Hornemann, T., Reilly, M. M. & Bennett, D. L. H. 2017. Human Ipsc Derived Sensory Neuron Model of Hereditary Sensory Neuropathy Type 1 (Hsn1). PNS Annual Meeting 2017 Abstracts.

Kugathasan, U., Kalmar, B., Wilson, E., Laura, M., Bennett, D., Reilly, M. M. & Greensmith, L. 2015. The Role of Deoxysphingolipid Induced Neurotoxicity in Hereditary Sensory Neuropathy Type 1 (Hsn1) Secondary to Sptlc1/2 Mutations. *Journal of the Peripheral Nervous System,* 20**,** 174-175.

Lee, A. S. 2005. The Er Chaperone and Signaling Regulator Grp78/Bip as a Monitor of Endoplasmic Reticulum Stress. *Methods,* 35**,** 373-81.

Levine, T. D., Miller, R. G., Bradley, W. G., Moore, D. H., Saperstein, D. S., Flynn, L. E., Katz, J. S., Forshew, D. A., Metcalf, J. S., Banack, S. A. & Cox, P. A. 2017. Phase I Clinical Trial of Safety of L-Serine for Als Patients. *Amyotrophic Lateral Sclerosis and Frontotemporal Degeneration,* 18**,** 107-111.

Li, J., Yan, B., Si, H., Peng, X., Zhang, S. L. & Hu, J. 2017. Atlastin Regulates Store-Operated Calcium Entry for Nerve Growth Factor-Induced Neurite Outgrowth. *Scientific Reports,* 7**,** 43490.

Lin, M. T. & Beal, M. F. 2006. Mitochondrial Dysfunction and Oxidative Stress in Neurodegenerative Diseases. *Nature,* 443**,** 787-95.

Lindholm, D., Wootz, H. & Korhonen, L. 2006. Er Stress and Neurodegenerative Diseases. *Cell Death and Differentiation,* 13**,** 385-92.

Lowther, J., Naismith, J., Dunn, T. & Campopiano, D. 2012. Structural, Mechanistic and Regulatory Studies of Serine Palmitoyltransferase. *Biochemical Society Transactions,* 40**,** 547-554.

Lytton, J., Westlin, M. & Hanley, M. R. 1991. Thapsigargin Inhibits the Sarcoplasmic or Endoplasmic Reticulum Ca-Atpase Family of Calcium Pumps. *Journal of Biological Chemistry,* 266**,** 17067-71.

Malli, R., Frieden, M., Osibow, K. & Graier, W. F. 2003. Mitochondria Efficiently Buffer Subplasmalemmal Ca2+ Elevation During Agonist Stimulation. *Journal of Biological Chemistry,* 278**,** 10807-15.

Marshall, L. L., Stimpson, S. E., Hyland, R., Coorssen, J. R. & Myers, S. J. 2014. Increased Lipid Droplet Accumulation Associated with a Peripheral Sensory Neuropathy. *Journal of Chemical Biology,* 7**,** 67-76.

Martin, P., Albagli, O., Poggi, M. C., Boulukos, K. E. & Pognonec, P. 2006. Development of a New Bicistronic Retroviral Vector with Strong Ires Activity. *BMC Biotechnology,* 6**,** 4.

Massard, C., Salazar, R., Armand, J. P., Majem, M., Deutsch, E., García, M., Oaknin, A., Fernández-García, E. M., Soto, A. & Soria, J. C. 2012. Phase I Dose-Escalating Study of Es-285 Given as a Three-Hour Intravenous Infusion Every Three Weeks in Patients with Advanced Malignant Solid Tumors. *Investigational New Drugs,* 30**,** 2318-26.

Mattson, M. P. 2000. Apoptosis in Neurodegenerative Disorders. *Nature Reviews: Molecular Cell Biology,* 1**,** 120-9.

Mccampbell, A., Truong, D., Broom, D. C., Allchorne, A., Gable, K., Cutler, R. G., Mattson, M. P., Woolf, C. J., Frosch, M. P., Harmon, J. M., Dunn, T. M. & Brown, R. H. 2005. Mutant Sptlc1 Dominantly Inhibits Serine Palmitoyltransferase Activity in Vivo and Confers an Age-Dependent Neuropathy. *Human Molecular Genetics,* 14**,** 3507-21.

Merrill, A. H., Nixon, D. W. & Williams, R. D. 1985. Activities of Serine Palmitoyltransferase (3-Ketosphinganine Synthase) in Microsomes from Different Rat Tissues. *Journal of Lipid Research,* 26**,** 617-22.

Michel, C., Van Echten-Deckert, G., Rother, J., Sandhoff, K., Wang, E. & Merrill, A. H. 1997. Characterization of Ceramide Synthesis. A Dihydroceramide Desaturase Introduces the 4,5-Trans-Double Bond of Sphingosine at the Level of Dihydroceramide. *Journal of Biological Chemistry,* 272**,** 22432-7.

Mroczek, M., Kabzinska, D. & Kochanski, A. 2015. Molecular Pathogenesis, Experimental Therapy and Genetic Counseling in Hereditary Sensory Neuropathies. *Acta Neurobiologiae Experimentalis,* 75**,** 126-43.

Murphy, S. M., Ernst, D., Wei, Y., Laurà, M., Liu, Y. T., Polke, J., Blake, J., Winer, J., Houlden, H., Hornemann, T. & Reilly, M. M. 2013. Hereditary Sensory and Autonomic Neuropathy Type 1 (Hsani) Caused by a Novel Mutation in Sptlc2. *Neurology,* 80**,** 2106-11.

Murphy, S. M., Herrmann, D. N., Mcdermott, M. P., Scherer, S. S., Shy, M. E., Reilly, M. M. & Pareyson, D. 2011. Reliability of the Cmt Neuropathy Score (Second Version) in Charcot-Marie-Tooth Disease. *Journal of the Peripheral Nervous System,* 16**,** 191-8.

Myers, S. J., Malladi, C. S., Hyland, R. A., Bautista, T., Boadle, R., Robinson, P. J. & Nicholson, G. A. 2014. Mutations in the Sptlc1 Protein Cause Mitochondrial Structural Abnormalities and Endoplasmic Reticulum Stress in Lymphoblasts. *DNA and Cell Biology,* 33**,** 399-407.

Nicholson, G. A., Dawkins, J. L., Blair, I. P., Auer-Grumbach, M., Brahmbhatt, S. B. & Hulme, D. J. 2001. Hereditary Sensory Neuropathy Type I: Haplotype Analysis Shows Founders in Southern England and Europe. *American Journal of Human Genetics,* 69**,** 655-9.

Nicholson, G. A., Dawkins, J. L., Blair, I. P., Kennerson, M. L., Gordon, M. J., Cherryson, A. K., Nash, J. & Bananis, T. 1996. The Gene for Hereditary Sensory Neuropathy Type I (Hsn-I) Maps to Chromosome 9q22.1-Q22.3. *Nature Genetics,* 13**,** 101-4.

Noack, R., Frede, S., Albrecht, P., Henke, N., Pfeiffer, A., Knoll, K., Dehmel, T., Meyer Zu Hörste, G., Stettner, M., Kieseier, B. C., Summer, H., Golz, S., Kochanski, A., Wiedau-Pazos, M., Arnold, S., Lewerenz, J. & Methner, A. 2012. Charcot-Marie-Tooth Disease Cmt4a: Gdap1 Increases Cellular Glutathione and the Mitochondrial Membrane Potential. *Human Molecular Genetics,* 21**,** 150-62.

Norenberg, M. D. & Rao, K. V. R. 2007. The Mitochondrial Permeability Transition in Neurologic Disease. *Neurochemistry International,* 50**,** 983-997.

Oswald, M. C., West, R. J., Lloyd-Evans, E. & Sweeney, S. T. 2015. Identification of Dietary Alanine Toxicity and Trafficking Dysfunction in a Drosophila Model of Hereditary Sensory and Autonomic Neuropathy Type 1. *Human Molecular Genetics,* 24**,** 6899-909.

Othman, A., Benghozi, R., Alecu, I., Wei, Y., Niesor, E., Von Eckardstein, A. & Hornemann, T. 2015a. Fenofibrate Lowers Atypical Sphingolipids in Plasma of Dyslipidemic Patients: A Novel Approach for Treating Diabetic Neuropathy? *Journal of Clinical Lipidology,* 9**,** 568-75.

Othman, A., Bianchi, R., Alecu, I., Wei, Y., Porretta-Serapiglia, C., Lombardi, R., Chiorazzi, A., Meregalli, C., Oggioni, N., Cavaletti, G., Lauria, G., Von Eckardstein, A. & Hornemann, T. 2014. Lowering Plasma 1-Deoxysphingolipids Improves Neuropathy in Diabetic Rats. *Diabetes*.

Othman, A., Rütti, M. F., Ernst, D., Saely, C. H., Rein, P., Drexel, H., Porretta-Serapiglia, C., Lauria, G., Bianchi, R., Von Eckardstein, A. & Hornemann, T. 2012. Plasma Deoxysphingolipids: A Novel Class of Biomarkers for the Metabolic Syndrome? *Diabetologia,* 55**,** 421-31.

Othman, A., Saely, C. H., Muendlein, A., Vonbank, A., Drexel, H., Von Eckardstein, A. & Hornemann, T. 2015b. Plasma 1-Deoxysphingolipids Are Predictive Biomarkers for Type 2 Diabetes Mellitus. *BMJ Open Diabetes Research and Care,* 3**,** e000073.

Paredes, R. M., Etzler, J. C., Watts, L. T., Zheng, W. & Lechleiter, J. D. 2008. Chemical Calcium Indicators. *Methods,* 46**,** 143-51.

Parekh, A. B. & Putney, J. W., Jr. 2005. Store-Operated Calcium Channels. *Physiological Reviews,* 85**,** 757-810.

Paschen, W. & Mengesdorf, T. 2005. Endoplasmic Reticulum Stress Response and Neurodegeneration. *Cell Calcium,* 38**,** 409-15.

Pchitskaya, E., Popugaeva, E. & Bezprozvanny, I. 2017. Calcium Signaling and Molecular Mechanisms Underlying Neurodegenerative Diseases. *Cell Calcium*.

Penno, A., Reilly, M. M., Houlden, H., Laurá, M., Rentsch, K., Niederkofler, V., Stoeckli, E. T., Nicholson, G., Eichler, F., Brown, R. H., Von Eckardstein,

A. & Hornemann, T. 2010. Hereditary Sensory Neuropathy Type 1 Is Caused by the Accumulation of Two Neurotoxic Sphingolipids. *Journal of Biological Chemistry,* 285**,** 11178-87.

Perry, T. L. & Jones, R. T. 1961. The Amino Acid Content of Human Cerebrospinal Fluid in Normal Individuals and in Mental Defectives. *Journal of Clinical Investigation,* 40**,** 1363-72.

Pla-Martin, D., Rueda, C. B., Estela, A., Sanchez-Piris, M., Gonzalez-Sanchez, P., Traba, J., De La Fuente, S., Scorrano, L., Renau-Piqueras, J., Alvarez, J., Satrustegui, J. & Palau, F. 2013. Silencing of the Charcot-Marie-Tooth Disease-Associated Gene Gdap1 Induces Abnormal Mitochondrial Distribution and Affects Ca2+ Homeostasis by Reducing Store-Operated Ca2+ Entry. *Neurobiology of Disease,* 55**,** 140-51.

Proia, R. L. & Hla, T. 2015. Emerging Biology of Sphingosine-1-Phosphate: Its Role in Pathogenesis and Therapy. *Journal of Clinical Investigation,* 125**,** 1379-87.

Putney, J. W. 2010. Pharmacology of Store-Operated Calcium Channels. *Molecular Interventions,* 10**,** 209-18.

Putney, J. W., Steinckwich-Besancon, N., Numaga-Tomita, T., Davis, F. M., Desai, P. N., D'agostin, D. M., Wu, S. & Bird, G. S. 2016. The Functions of Store-Operated Calcium Channels. *Biochimica et Biophysica Acta*.

Ramesh, V. 2004. Merlin and the Erm Proteins in Schwann Cells, Neurons and Growth Cones. *Nature Reviews: Neuroscience,* 5**,** 462-70.

Reilly, M. M. 2007. Sorting out the Inherited Neuropathies. *Practical Neurology,* 7**,** 93-105.

Reilly, M. M., Murphy, S. M. & Laura, M. 2011. Charcot-Marie-Tooth Disease. *Journal of the Peripheral Nervous System,* 16**,** 1-14.

Riley, R. T., Norred, W. P., Wang, E. & Merrill, A. H. 1999. Alteration in Sphingolipid Metabolism: Bioassays for Fumonisin- and Isp-I-Like Activity in Tissues, Cells and Other Matrices. *Natural Toxins,* 7**,** 407-14.

Rossor, A. M., Polke, J. M., Houlden, H. & Reilly, M. M. 2013. Clinical Implications of Genetic Advances in Charcot-Marie-Tooth Disease. *Nature Reviews: Neurology,* 9**,** 562-71.

Rotthier, A., Auer-Grumbach, M., Janssens, K., Baets, J., Penno, A., Almeida-Souza, L., Van Hoof, K., Jacobs, A., De Vriendt, E., Schlotter-Weigel, B.,

Löscher, W., Vondráček, P., Seeman, P., De Jonghe, P., Van Dijck, P., Jordanova, A., Hornemann, T. & Timmerman, V. 2010. Mutations in the Sptlc2 Subunit of Serine Palmitoyltransferase Cause Hereditary Sensory and Autonomic Neuropathy Type I. *American Journal of Human Genetics,* 87**,** 513-22.

Rotthier, A., Baets, J., Timmerman, V. & Janssens, K. 2012. Mechanisms of Disease in Hereditary Sensory and Autonomic Neuropathies. *Nature Reviews: Neurology,* 8**,** 73-85.

Rotthier, A., Penno, A., Rautenstrauss, B., Auer-Grumbach, M., Stettner, G. M., Asselbergh, B., Van Hoof, K., Sticht, H., Lévy, N., Timmerman, V., Hornemann, T. & Janssens, K. 2011. Characterization of Two Mutations in the Sptlc1 Subunit of Serine Palmitoyltransferase Associated with Hereditary Sensory and Autonomic Neuropathy Type I. *Human Mutation,* 32**,** E2211-25.

Salcedo, M., Cuevas, C., Alonso, J. L., Otero, G., Faircloth, G., Fernandez-Sousa, J. M., Avila, J. & Wandosell, F. 2007. The Marine Sphingolipid-Derived Compound Es 285 Triggers an Atypical Cell Death Pathway. *Apoptosis,* 12**,** 395-409.

Sayano, T., Kawano, Y., Kusada, W., Arimoto, Y., Esaki, K., Hamano, M., Udono, M., Katakura, Y., Ogawa, T., Kato, H., Hirabayashi, Y. & Furuya, S. 2016. Adaptive Response to L-Serine Deficiency Is Mediated by P38 Mapk Activation Via 1-Deoxysphinganine in Normal Fibroblasts. *Febs Open Bio,* 6**,** 303-316.

Scherer, S. S. 2011. The Debut of a Rational Treatment for an Inherited Neuropathy? *Journal of Clinical Investigation,* 121**,** 4624-7.

Schöffski, P., Dumez, H., Ruijter, R., Miguel-Lillo, B., Soto-Matos, A., Alfaro, V. & Giaccone, G. 2011. Spisulosine (Es-285) Given as a Weekly Three-Hour Intravenous Infusion: Results of a Phase I Dose-Escalating Study in Patients with Advanced Solid Malignancies. *Cancer Chemotherapy and Pharmacology,* 68**,** 1397-403.

Simons, K. & Ikonen, E. 1997. Functional Rafts in Cell Membranes. *Nature,* 387**,** 569-72.

Simons, K. & Toomre, D. 2000. Lipid Rafts and Signal Transduction. *Nature Reviews: Molecular Cell Biology,* 1**,** 31-9.

Sleigh, J. N., Weir, G. A. & Schiavo, G. 2016. A Simple, Step-by-Step Dissection Protocol for the Rapid Isolation of Mouse Dorsal Root Ganglia. *BMC Research Notes,* 9**,** 82.

Stein, W. H. & Moore, S. 1954. The Free Amino Acids of Human Blood Plasma. *Journal of Biological Chemistry,* 211**,** 915-26.

Steiner, R., Saied, E. M., Othman, A., Arenz, C., Maccarone, A. T., Poad, B. L., Blanksby, S. J., Von Eckardstein, A. & Hornemann, T. 2016. Elucidating the Chemical Structure of Native 1-Deoxysphingosine. *Journal of Lipid Research,* 57**,** 1194-203.

Stimpson, S. E., Coorssen, J. R. & Myers, S. J. 2015. Mitochondrial Protein Alterations in a Familial Peripheral Neuropathy Caused by the V144d Amino Acid Mutation in the Sphingolipid Protein, Sptlc1. *Journal of Chemical Biology,* 8**,** 25-35.

Stojkovic, T. 2016. Hereditary Neuropathies: An Update. *Revue Neurologique*.

Stutzmann, G. E. & Mattson, M. P. 2011. Endoplasmic Reticulum Ca(2+) Handling in Excitable Cells in Health and Disease. *Pharmacological Reviews,* 63**,** 700-27.

Suriyanarayanan, S., Auranen, M., Toppila, J., Paetau, A., Shcherbii, M., Palin, E., Wei, Y., Lohioja, T., Schlotter-Weigel, B., Schon, U., Abicht, A., Rautenstrauss, B., Tyynismaa, H., Walter, M. C., Hornemann, T. & Ylikallio, E. 2016. The Variant P.(Arg183trp) in Sptlc2 Causes Late-Onset Hereditary Sensory Neuropathy. *Neuromolecular Medicine,* 18**,** 81-90.

Susin, S. A., Lorenzo, H. K., Zamzami, N., Marzo, I., Brenner, C., Larochette, N., Prevost, M. C., Alzari, P. M. & Kroemer, G. 1999a. Mitochondrial Release of Caspase-2 and -9 During the Apoptotic Process. *Journal of Experimental Medicine,* 189**,** 381-94.

Susin, S. A., Lorenzo, H. K., Zamzami, N., Marzo, I., Snow, B. E., Brothers, G. M., Mangion, J., Jacotot, E., Costantini, P., Loeffler, M., Larochette, N., Goodlett, D. R., Aebersold, R., Siderovski, D. P., Penninger, J. M. & Kroemer, G. 1999b. Molecular Characterization of Mitochondrial Apoptosis-Inducing Factor. *Nature,* 397**,** 441-6.

Szabo, I. & Zoratti, M. 1992. The Mitochondrial Megachannel Is the Permeability Transition Pore. *Journal of Bioenergetics and Biomembranes,* 24**,** 111-117.

Teschendorf, C., Warrington, K. H., Siemann, D. W. & Muzyczka, N. 2002. Comparison of the Ef-1 Alpha and the Cmv Promoter for Engineering Stable Tumor Cell Lines Using Recombinant Adeno-Associated Virus. *Anticancer Research,* 22**,** 3325-30.

Thastrup, O., Cullen, P. J., Drobak, B. K., Hanley, M. R. & Dawson, A. P. 1990. Thapsigargin, a Tumor Promoter, Discharges Intracellular Ca2+ Stores by Specific Inhibition of the Endoplasmic Reticulum Ca2(+)-Atpase. *Proceedings of the National Academy of Sciences of the United States of America,* 87**,** 2466-70.

Therrien, G. & Butterworth, R. F. 1991. Cerebrospinal Fluid Amino Acids in Relation to Neurological Status in Experimental Portal-Systemic Encephalopathy. *Metabolic Brain Disease,* 6**,** 65-74.

Tooth, H. H. 1886. The Peroneal Type of Progressive Muscular Atrophy. *London, H.K. Lewis & Co, Ltd.*

Trump, B. F. & Berezesky, I. K. 1995. Calcium-Mediated Cell Injury and Cell Death. *FASEB Journal,* 9**,** 219-28.

Tsuchiya, R., Yoshiki, F., Kudo, Y. & Morita, M. 2002. Cell Type-Selective Expression of Green Fluorescent Protein and the Calcium Indicating Protein, Yellow Cameleon, in Rat Cortical Primary Cultures. *Brain Research,* 956**,** 221-9.

Van Den Bosch, L., Vandenberghe, W., Klaassen, H., Van Houtte, E. & Robberecht, W. 2000. Ca2+-Permeable Ampa Receptors and Selective Vulnerability of Motor Neurons. *Journal of the Neurological Sciences,* 180**,** 29-34.

Van Vliet, A. R., Verfaillie, T. & Agostinis, P. 2014. New Functions of Mitochondria Associated Membranes in Cellular Signaling. *Biochimica et Biophysica Acta,* 1843**,** 2253-62.

Vannucci, L., Lai, M., Chiuppesi, F., Ceccherini-Nelli, L. & Pistello, M. 2013. Viral Vectors: A Look Back and Ahead on Gene Transfer Technology. *New Microbiol,* 36**,** 1-22.

Varma, N., Janic, B., Ali, M., Iskander, A. & Arbab, A. 2011. Lentiviral Based Gene Transduction and Promoter Studies in Human Hematopoietic Stem Cells (Hhscs). *Journal of Stem Cells & Regenerative Medicine,* 7**,** 41-53.

Verkhratsky, A. J. & Petersen, O. H. 1998. Neuronal Calcium Stores. *Cell Calcium,* 24**,** 333-43.

Wallace, D. C., Fan, W. & Procaccio, V. 2010. Mitochondrial Energetics and Therapeutics. *Annual Review of Pathology,* 5**,** 297-348.

Walther, W. & Stein, U. 2000. Viral Vectors for Gene Transfer: A Review of Their Use in the Treatment of Human Diseases. *Drugs,* 60**,** 249-71.

Wang, Z., Kirkwood, J. S., Taylor, A. W., Stevens, J. F., Leid, M., Ganguli-Indra, G. & Indra, A. K. 2013. Transcription Factor Ctip2 Controls Epidermal Lipid Metabolism and Regulates Expression of Genes Involved in Sphingolipid Biosynthesis During Skin Development. *Journal of Investigative Dermatology,* 133**,** 668-76.

Wei, N., Pan, J., Pop-Busui, R., Othman, A., Alecu, I., Hornemann, T. & Eichler, F. S. 2014. Altered Sphingoid Base Profiles in Type 1 Compared to Type 2 Diabetes. *Lipids in Health and Disease,* 13**,** 161.

Weiss, B. & Stoffel, W. 1997. Human and Murine Serine-Palmitoyl-Coa Transferase--Cloning, Expression and Characterization of the Key Enzyme in Sphingolipid Synthesis. *European Journal of Biochemistry,* 249**,** 239-47.

Xiang, C., Wang, Y., Zhang, H. & Han, F. 2017. The Role of Endoplasmic Reticulum Stress in Neurodegenerative Disease. *Apoptosis,* 22**,** 1-26.

Yard, B. A., Carter, L. G., Johnson, K. A., Overton, I. M., Dorward, M., Liu, H., Mcmahon, S. A., Oke, M., Puech, D., Barton, G. J., Naismith, J. H. & Campopiano, D. J. 2007. The Structure of Serine Palmitoyltransferase; Gateway to Sphingolipid Biosynthesis. *Journal of Molecular Biology,* 370**,** 870-86.

Zitomer, N. C., Mitchell, T., Voss, K. A., Bondy, G. S., Pruett, S. T., Garnier-Amblard, E. C., Liebeskind, L. S., Park, H., Wang, E., Sullards, M. C., Merrill, A. H. & Riley, R. T. 2009. Ceramide Synthase Inhibition by Fumonisin B1 Causes Accumulation of 1-Deoxysphinganine: A Novel Category of Bioactive 1-Deoxysphingoid Bases and 1-Deoxydihydroceramides Biosynthesized by Mammalian Cell Lines and Animals. *Journal of Biological Chemistry,* 284**,** 4786-95.

Zuellig, R. A., Hornemann, T., Othman, A., Hehl, A. B., Bode, H., Guntert, T., Ogunshola, O. O., Saponara, E., Grabliauskaite, K., Jang, J. H.,

Ungethuem, U., Wei, Y., Von Eckardstein, A., Graf, R. & Sonda, S. 2014. Deoxysphingolipids, Novel Biomarkers for Type 2 Diabetes, Are Cytotoxic for Insulin-Producing Cells. *Diabetes,* 63**,** 1326-39.